RIVM report 500045001/2004

The Operational Priority Substances model
Description and validation of OPS-Pro 4.1

J.A. van Jaarsveld

This investigation has been performed by order of and for the account of the Ministry of Housing and Physical Planning, within the framework of project 500045, 'Model instruments Air'

RIVM, P.O. Box 1, 3720 BA Bilthoven, telephone: 31 - 30 - 274 91 11; telefax: 31 - 30 - 274 29 71

Abstract

This report describes in detail, OPS-Pro 4.1, the latest version of the Operational Priority Substances (OPS) model. OPS is a model that simulates the atmospheric process sequence of emission, dispersion, transport, chemical conversion and finally deposition. The model is set up as a universal framework supporting the modelling of a wide variety of pollutants including fine particles but the main purpose is to calculate the deposition of acidifying compounds over the Netherlands at a high spatial resolution. Previous versions of the model have been used since 1989 for all the atmospheric transport and deposition calculations in the State of the Environment reports and Environmental Outlook studies in the Netherlands.

An extensive model validation exercise was carried out using observations from the National Air Quality Monitoring Network over the past twenty years. Good agreement was found for both SO_x and NO_y species in the spatial patterns, just as in trends over the past ten years. An exception is formed by the NH_x species, which are, in general, underestimated by approximately 25%. This discrepancy has for some time been known as the 'ammonia gap'.

The total uncertainty for deposition to a nationally distributed ecosystem is estimated at 20%, 25 and 30% for SO_x, NO_y and NH_x, respectively. For a specific ecosystem (size: 500 x 500m to 5000 x 5000m), the uncertainties will be much higher: 50, 60, 100% for SO_x, NO_y and NH_x deposition, respectively. Included in these figures are the uncertainties in current emission estimates. Uncertainties in dry deposition velocities dominate the total uncertainty.

Rapport in het kort

Dit rapport beschrijft OPS-Pro 4.1, de laatste versie van het Operationele Prioritaire Stoffen (OPS) model. Het OPS model is een mechanistisch model dat op lokale en nationale schaal de atmosferische verspreiding van stoffen simuleert aan de hand van actuele meteorologische gegevens. Het model is opgezet als een universeel raamwerk waarmee de verspreiding en depositie van een breed scala aan stoffen kan worden berekend, maar het zwaartepunt ligt bij de modellering van de depositie van verzurende stoffen met een hoog ruimtelijke detail. Eerdere versies van het model worden al sinds 1989 gebruikt voor berekeningen in het kader van periodieke Milieubalansen en –verkenningen.
Een uitgebreide vergelijking van modelresultaten met metingen van het Landelijk Meetnet Luchtverontreiniging is uitgevoerd. Een goede overeenstemming in ruimtelijke verdeling wordt gevonden voor verzurende stoffen. In absolute zin komen SO_x en NO_y concentraties goed overeen met de metingen. Een uitzondering wordt gevormd door NH_x stoffen, welke in hun algemeenheid met ca. 25% worden onderschat. Dit verschil is al enige tijd bekend als het ‘ammoniakgat’. De totale onzekerheid voor depositie op een ecosysteem dat verspreid ligt over Nederland word geschat op 20, 25 en 30% voor respectievelijk SO_x, NO_y en NH_x. Voor een specifiek ecosysteem (afmeting: 500 x 500m tot 5000 x 5000m) zijn de onzekerheden veel groter: 50, 60, 100% voor respectievelijk SO_x, NO_y en NH_x. Deze onzekerheden zijn inclusief onzekerheden in de hedendaagse emissieschattingen. Onzekerheden in droge depositiesnelheden dragen verreweg het meest bij aan de grote onzekerheidsmarge bij de depositie op lokale schaal.

Preface

The first version of the Operational Priority Substances model was released to parties outside RIVM in 1989. Since then a number of improvements and extensions have been made but these versions were only available for users within RIVM. An important milestone was the addition of a graphical user interface to the model system. Given the interest showed by external parties it was felt that this was the moment to release a new model version. The current report is also intended as a background document for this release.

Another reason for a re-evaluation of the model is the fact that environmental levels of some key compounds have decreased dramatically in the past 15 years. It is not only the chemical interactions that might have changed but also the physical characteristics of pollutant producers e.g. when de-sulphurisation techniques are introduced. Finally, since eco-system specific critical load targets have replaced national deposition targets, there is a growing demand for more spatial detail in model output.

Samenvatting

Dit rapport beschrijft OPS-Pro 4.1, de laatste versie van het Operationele Prioritaire Stoffen (OPS) model. Het OPS model is een mechanistisch model dat de atmosferische processen van emissie, transport, omzetting en depositie simuleert aan de hand van actuele meteorologische gegevens. Het model is opgezet als een universeel raamwerk waarmee de verspreiding en depositie van een breed scala aan stoffen kan worden berekend, maar het zwaartepunt ligt bij de modellering van de depositie van verzurende stoffen met een hoog ruimtelijke detail. Eerdere versies van het model worden al sinds 1989 gebruikt voor berekeningen in het kader van periodieke Milieubalansen en –verkenningen. Daarnaast is het OPS model, of zijn resultaten ervan, opgenomen in diverse keten modellen.

De huidige versie van het model is vooral verbeterd op het gebied van ruimtelijke verschillen in meteorologie, landgebruik en terreinruwheid waardoor een meer lokatiegerichte droge depositie kan worden gemodelleerd. Een andere verbetering is de toevoeging van zogenaamde achtergrondconcentratiekaarten welke naast de ruimtelijke verschillen ook de verandering in de tijd in het algemene verontreinigingsniveau weergeven. Daardoor is een betere parameterisatie van chemische omzetting over de afgelopen 20 jaar mogelijk. Tenslotte is voor ammoniak uit mestaanwending de emissie afhankelijk gemaakt van meteorologische omstandigheden.

Het rapport geeft een uitgebreide vergelijking van modelresultaten met metingen van het Landelijk Meetnet Luchtverontreiniging. Deze vergelijking bestrijkt een periode van meer dan 10 jaar waardoor ook het effect van mogelijke niet-lineariteiten kan worden beoordeeld. In termen van ruimtelijke verdeling wordt een goede overeenstemming gevonden voor bijna alle verzurende stoffen. In absolute zin komen SO_x en NO_y stoffen goed overeen met de metingen voor de gehele beschouwde periode. Een uitzondering wordt gevormd door NH_x stoffen, welke in hun algemeenheid met circa 25% worden onderschat. Dit verschil is al enige tijd bekend als het ‘ammoniakgat’. Daarnaast zijn een aantal vergelijkingen uitgevoerd om de kwaliteit te beoordelen waarmee het model lokale concentraties ten gevolge van lokale bronnen kan berekenen. Hierbij wordt geconcludeerd dat het model evengoed presteert als meer gespecialiseerde modellen.

De uitkomsten van de vergelijking model en metingen zijn gebruikt om een schatting te maken van de totale onzekerheid in modeluitkomsten bij de berekening van (verzurende) depositie. Voor een ecosysteem dat verspreid ligt over Nederland komt deze onzekerheid uit op 20, 25 en 30% voor respectievelijk SO_x, NO_y en NH_x. Hierbij moet worden opgemerkt dat in het geval van NH_x er vooral sprake is van een systematische onderschatting. Voor een specifiek ecosysteem (afmeting: 500 x 500m tot 5000 x 5000m) zijn de onzekerheden veel groter: 50, 60, 100% voor respectievelijk SO_x, NO_y en NH_x. Al deze onzekerheden zijn inclusief fouten in de hedendaagse emissieschattingen. Onzekerheden in droge depositiesnelheden dragen verreweg het meest bij aan de grotere onzekerheidsmarge bij de depositie op lokale schaal.

Contents

Samenvatting **5**

Summary **10**

1. Model description **11**

1.1 Introduction *11*

1.2 Model characteristics *11*
1.2.1 Classification of trajectories 12
1.2.2 Vertical stratification 14
1.2.3 Classification with respect to the vertical structure of the boundary layer 14

1.3 References chapter 1 *16*

2. Meteorological data **17**

2.1 Meteorological areas in the OPS model *17*

2.2 Sources of primary meteorological data *18*

2.3 Processing primary data *18*
2.3.1 Calculating the potential wind speed 18
2.3.2 Spatial averaging of meteorological data 19
2.3.3 Calculation of precipitation characteristics 20
2.3.4 Determination of the snow cover indicator 20

2.4 The meteorological pre-processor *21*
2.4.1 Derivation of boundary layer parameters 21
2.4.2 Estimation of mixing heights 22
2.4.3 The wind profile 23
2.4.4 Trajectories 26
2.4.5 Summary of the meteorological data set 28

2.5 References chapter 2 *29*

3. Mathematical formulation of the model **31**

3.1 Basic equations *31*

3.2 Vertical mixing close to sources *32*
3.2.1 Local vertical dispersion 33
3.2.2 Plume rise 37
3.2.3 Inversion penetration 38

3.3 Area sources *39*
3.3.1 Horizontal dispersion for area sources 39
3.3.2 Vertical dispersion for area sources 40

3.4 References chapter 3 *42*

4. Removal processes **45**

4.1 Dry deposition *45*
4.1.1 Source depletion 47

4.2 Wet deposition *48*
4.2.1 In-cloud scavenging 48

4.2.2 Below-cloud scavenging 49
4.2.3 Local effects of in-cloud scavenging 50
4.2.4 Effects of dry and wet periods on average scavenging rates 51

4.3 Chemical transformation *52*

4.4 References chapter 4 *53*

5. Parameterisations for non-acidifying substances **55**

5.1 Emission and emission processes *55*
5.1.1 Behaviour in time 55
5.1.2 Emission speciation 57

5.2 Removal processes *58*
5.2.1 Dry deposition 58
5.2.2 Wet deposition 59
5.2.3 Chemical conversion 60

5.3 References chapter 5 *60*

6. Acidifying substances **61**

6.1 Chemical conversion *61*
6.1.1 Sulphur compounds 63
6.1.2 Nitrogen oxides 65
6.1.3 Ammonia compounds 69

6.2 Dry deposition *70*
6.2.1 Dry deposition velocities of gaseous substances 70
6.2.2 Dry deposition of NO_x 72
6.2.3 Dry deposition of acidifying aerosols 72
6.2.4 Dry deposition of NO_3^- + HNO_3 72

6.3 Wet Deposition *73*
6.3.1 SO_2 scavenging 73
6.3.2 NO_x scavenging 74
6.3.3 NH_3 scavenging 75
6.3.4 Scavenging of SO_4^{2-}, NO_3^- and NH_4^+ aerosols 75
6.3.5 Overview of wet scavenging parameters 75

6.4 Emission processes *76*
6.4.1 NH_3 emissions from land spreading 76
6.4.2 NH_3 emissions from animal housing systems 76

6.5 References chapter 6 *77*

7. Model specification **81**

7.1 Chemical characterisation of substances *81*

7.2 Emissions *81*
7.2.1 Source area 81
7.2.2 Source types 81
7.2.3 Behaviour in time 82
7.2.4 Particle-size distribution 82
7.2.5 Format of emission data files 83

7.3 Meteorological statistics *84*
7.3.1 Meteorological time-scale 84
7.3.2 Meteorological area 84

7.4 Receptor characteristics *84*
7.4.1 Receptor domain 84
7.4.2 Minimum source –receptor distance 85

7.4.3 Land-use and roughness characteristics 85
7.4.4 Selection of receptor points 86

7.5 References chapter 7 *86*

8. Model validation and uncertainty **87**

8.1 Measurements *87*

8.2 Emissions *88*

8.3 Comparison with measurements *91*
8.3.1 Estimated concentration and deposition levels due to non-anthropogenic sources 91
8.3.2 Checking the temporal behaviour 91
8.3.3 Checking the trends 97
8.3.4 Comparison of time-averaged concentrations on a point-to-point basis 98
8.3.5 Other comparisons 101
8.3.6 Comparison with single-source short-range dispersion experiments 102
8.3.7 Comparison with models for the short range 104
8.3.8 Summary and conclusions on the validation of the model 106

8.4 Quantification of the uncertainty in model results *107*

8.5 Uncertainties in concentrations and dry deposition velocities *107*
8.5.1 Effect of correlated species on error propagation 107
8.5.2 Results 110

8.6 References chapter 8 *110*

9. Comparison with previous versions of the model **113**

9.1 Model versions *113*

9.2 Comparison in the case of ammonia in the Netherlands *115*

9.3 Comparison for the case of maximum concentrations near point sources *117*

Appendix I The DEPAC dry deposition module in OPS **121**

Appendix II Suggestions for substance-specific parameter values **131**

Appendix III SO_2, NO_x and NH_3 emission data **141**

Appendix IV Prescribed concentration levels **153**

Summary

This report describes in detail, OPS-Pro 4.1, the latest version of the Operational Priority Substances (OPS) model. OPS is a model that simulates the atmospheric process sequence of emission, dispersion, transport, chemical conversion and finally deposition. The main purpose of the model is to calculate the deposition of acidifying compounds for the Netherlands as a whole using a high spatial resolution. The model is, however, set up as a universal framework supporting the modelling of other pollutants such as fine particles and persistent organic pollutants. Previous versions of the model have been used since 1989 for all the atmospheric transport and deposition calculations in the State of the Environment reports and Environmental Outlook studies in the Netherlands.

An important improvement in the present version is a better representation of spatial differences in meteorology, land use and terrain roughness, allowing more site-specific dry deposition modelling. Another improvement is the inclusion of 'background' concentration levels, varying in space and time. The trends in these background levels allow for a better parameterisation of chemical conversion and deposition across time and space. Meteorology-dependent emissions were introduced for calculating ammonia.

An extensive model validation exercise was carried out using observations from the National Air Quality Monitoring Network over the past twenty years. Good agreement was found for both SO_x and NO_y species in the spatial patterns, just as in trends over the past ten years. An exception is formed by the NH_x species, which are, in general, underestimated by approximately 25%. This discrepancy has for some time been known as the 'ammonia gap'. Furthermore, comparisons were made to test the model's ability to calculate local concentrations in relation to local sources. Concluded here is that this model performance is just as good as more dedicated short distance dispersion models.

The model validation results are used to estimate the total uncertainty in model results in calculations of acid deposition. The uncertainty for deposition to a nationally distributed ecosystem is 20%, 25 and 30% for SO_x, NO_y and NH_x, respectively. For a specific ecosystem (size: 500 x 500m to 5000 x 5000m), the uncertainties will be much higher: 50, 60, 100% for SO_x, NO_y and NH_x deposition, respectively. Included in these uncertainties are the uncertainties in current emission estimates. Uncertainties in dry deposition velocities dominate the total uncertainty.

1. Model description

1.1 Introduction

Modelling atmospheric processes has been the subject of many studies, resulting in a range of models with various complexities for specific applications. Before selecting a model or a model approach, we have to assess the intended application area carefully. In the present case the time scale (long-range with a time resolution of a season or a few months) is probably the most important boundary condition. Another important condition is the spatial scale of the receptor area, which is defined as the Netherlands with a resolution of 5 x 5 km. The emission area, however, must be at least 2000 x 2000 km to explain levels of pollutants in the Netherlands. These conditions have forced exclusion of an Eulerian model framework, simply because of the required computer capacity. Eulerian models using nested grids should, in principle, be applicable; however, operational models of this type are still under development.

The group of Lagrangian trajectory models can, in principle, meet both the time and spatial-scale requirements. An example of such a model was until recently in use by EMEP (Eliassen and Saltbones, 1983) to calculate the long-range transport and from country-to country-deposition budgets across Europe. The spatial resolution of this model is 150 x 150 km, but since the model is receptor-oriented i.e. trajectories end up in a receptor point every six hours, the spatial resolution can be increased. A more severe limitation is the use of only one layer in such models, which makes it impossible to adequately describe local-scale processes. The Langrangian EMEP model is now in a process of being replaced by an Eulerian model with a basic spatial resolution of 50 x 50 km.

An efficient method for calculating long-term averages can be found by means of arranging situations occurring in classes having similar properties and then calculating representative (short-term) concentrations for each of the classes. The average value will then follow from a summation of all concentrations, weighted with their relative frequencies. Such a method is used for the model to be described in this chapter. One of the problems that arises from this approach is the choice of a good classification scheme on the basis of relevant parameters. For short-range models a classification is usually made on the basis of wind direction, wind speed and atmospheric stability (see, for example, Calder, 1971; Runca *et al*., 1982).

The approach used for the model described here can be classified as a long- term climatological trajectory model which treats impacts of sources on a receptor independently. Because the model makes use of semi-empirical background concentration fields, it is therefore called a pseudo non-linear model. The physical background of the model concept and the derivation of the impelling meteorological parameters from routine meteorological observations will be described in this chapter. Results of meteorological parameterizations are compared with measurements wherever possible and relevant. A more general behaviour of the model and validation against measurements of pollutant concentrations will the subject of subsequent chapters.

1.2 Model characteristics

The model outlined here is a long-term Lagrangian transport and deposition model that describes relations between individual sources or source areas, and individual receptors. The model is statistical in the sense that concentration and deposition values are calculated for a number of typical situations and the long-term value is obtained by summation of these values, weighted with their relative frequencies. All relations governing the transport and deposition process are solved analytically, allowing the use of non-gridded receptors and sources, and variable grid sizes. Transport from a source to a receptor is assumed to take place in straight, well-mixed sectors of height z_i and horizontal angles of 30^0. Corrections are applied close to the source to account for height of emission and vertical dispersion; a correction for the curved

nature of real transport paths is used for larger distances. An important difference with (true) probabilistic long-term models is that this model is driven by actually observed meteorological parameters (hourly or 6-hourly synoptical).

A schematic overview of the model, consisting of two main parts, is given in Figure 1.1. These parts are:

a. A special pre-processor that calculates hourly transport trajectories arriving at a receptor on the basis of wind observations and derives secondary parameters, which define the atmospheric state along the trajectories from the observed data. This pre-processor classifies the transport trajectories into groups with similar properties and, in this way, describes the necessary statistics for the relevant period.

b. The model itself, which carries out the actual calculations on the basis of various inputs.

Each part is used separately. The pre-processor has to be run once for each period (month, season, year or a number of years) and for each receptor area. The results are placed in a database as a set of tables. The model selects its necessary climatological data from the database, depending on the area and period of interest.

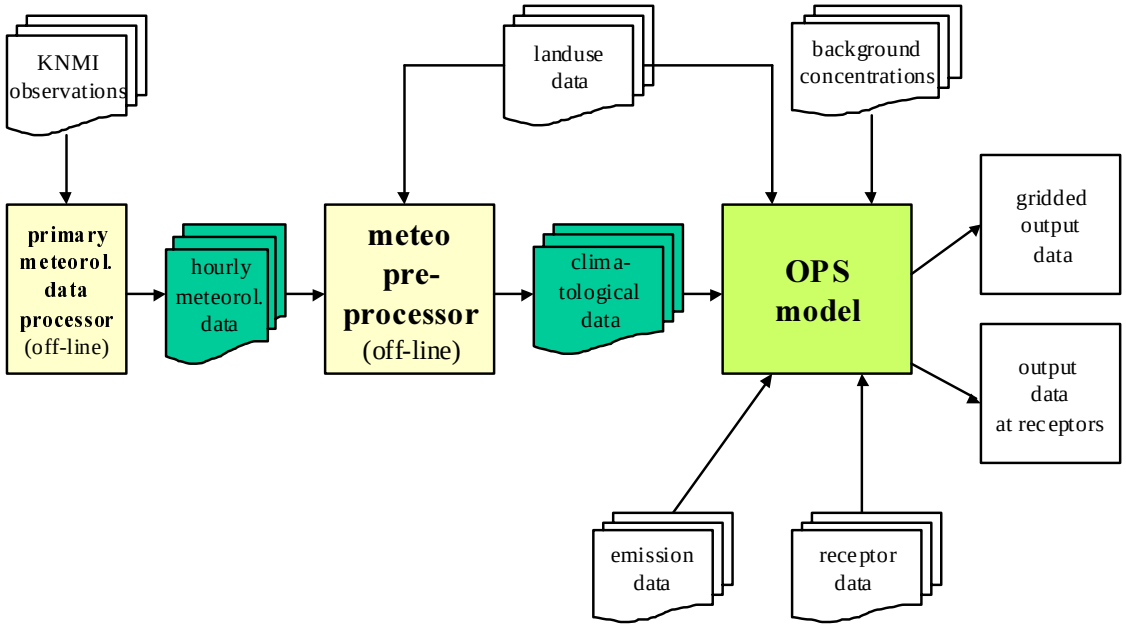

Figure 1.1 Schematic overview of the model.

The basic meteorological input consists of wind direction and wind speed at two heights, precipitation data, global radiation (or cloud cover), temperature and snow cover, all measured at one or more locations in the Netherlands. Other inputs to the model are information on receptors (coordinates, roughness length, land use) and information on sources (coordinates, emission strength, height, horizontal dimensions etceteras). The output of the model includes concentration, dry deposition and wet deposition data, listed either by receptor or in gridded form.

1.2.1 Classification of trajectories

When tracing back the path followed by an air parcel arriving at a receptor point, a trajectory as shown in Figure 1.2 is possible. The curved nature of the paths along which transport takes place makes it almost

impossible to create a 'wind rose' from a set of trajectories. Trajectories are, therefore, split into four independent parts:

1. one part representing contributions of local sources in the direction φ_1
2. one part representing contributions of sources at an intermediate distance (100 km) from the receptor in the direction φ_2
3. one part for sources at a long distance (300 km) from the receptor in the direction φ_3
4. one part for sources at a very long distance (1000 km and more) from the receptor in the direction, φ_4.

By splitting all trajectories arriving at a receptor in this way, four independent 'transport' roses can be constructed, each representing a different transport scale. Such a split-up in transport scale is preferred to a split-up in time scales because those trajectories can be directly related to the real positions of receptors and sources.

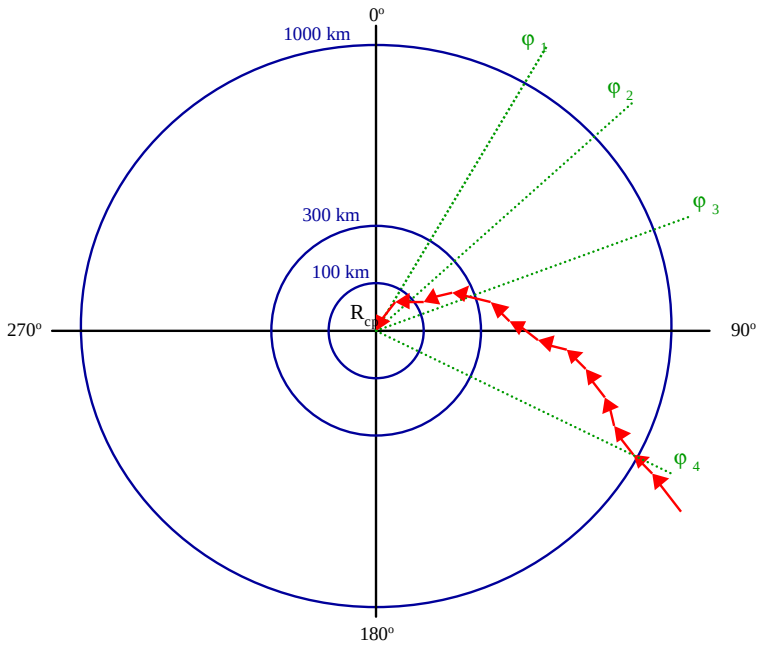

Figure 1.2 Classification of backward trajectories in terms of source–receptor distance and source– receptor direction.

The local scale represents situations where changes in meteorological conditions during transport play no important role as yet. This is usually not within 1 or 2 hours after a substance is released into the atmosphere or within 20 km from the point of release. The 1000 km trajectory represents the long-range transport of pollutants with 2-4 days transport time. For most substances the contribution of sources in this range is only 5-10 % (for Western Europe). Statistical properties of trajectories (direction, speed, height) in this range appear to be less sensitive to trajectory lengths, so the properties of these trajectories are also used for transport distances greater than 1000 km. The trajectory of 300 km long is chosen such that it covers a full diurnal cycle in meteorological parameters, of which the mixing height is the most important. The 100-km trajectory represents transport on a subdiurnal time scale as an intermediate between the local-and regional-scale transport. Within the 100 km trajectory, transitions in atmospheric stability and mixing height due to night-day transitions occur frequently.

To describe the transport from a source located in a certain wind sector, average properties for all trajectories passing the source area are introduced. An important parameter is the effective path length, fp_{eff}, which is calculated for all four distances considered. This parameter represents the ratio between the length of the (curved) path, x_{path}, followed by an air parcel and the straight source-receptor distance x_{sr}:

$fp_{eff} = x_{path} / x_{sr}$. Individual values for fp_{eff} range from 1 to 3, with a mean value for the 1000-km trajectory of 1.25. This parameter largely determines the effect of removal processes on concentrations under stagnant conditions.

1.2.2 Vertical stratification

Many meteorological parameters show a strong diurnal variation, especially in summertime. This change is caused by incoming solar radiation, which heats the earth's surface, causing convective turbulent mixing in the lower atmosphere. The variation in the mixing height ranges from about 50 m during night-time with a very stable atmosphere, to about 2000 m for days with an unstable atmosphere. The influence of the height of the mixing layer on concentrations is large, since the mixing height actually determines the mixing volume for the material released, especially for larger down-wind distances. An example of the vertical structure of the atmosphere during a three-day period, as it is perceived by this model, is given in Figure 1.3. The behaviour of plumes from high sources with respect to the mixing layer height is also shown.

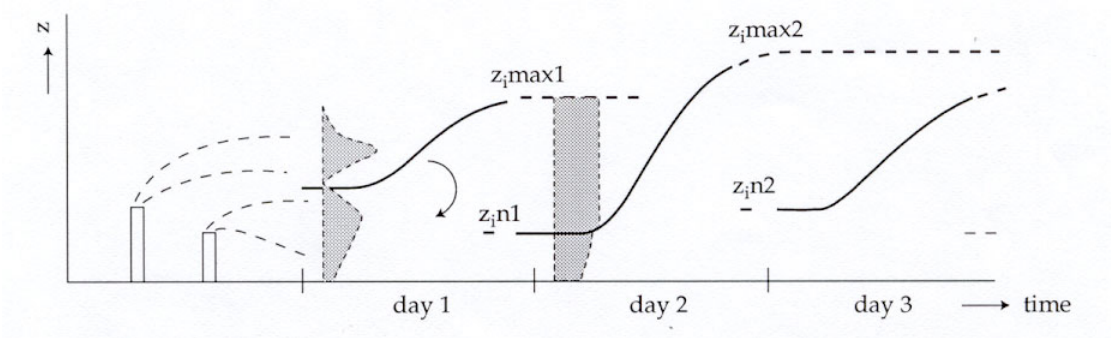

Figure 1.3 Schematic view of the vertical structure of the lower atmosphere as used in the model. The shadowed areas show the vertical concentration distributions at different transport phases.

Material released above the mixing layer in the early hours of day 1 will not reach the ground level. The vertical dimension of the plume remains small due to absence of turbulence that height and time (night). A few hours later the stable night-time situation breaks up when the sun starts to heat the surface again. The plume will then come under the influence of ground-based turbulent movements, which will rapidly mix the plume up through the growing mixing layer. In the late afternoon of day 1, the solar energy reaching the surface will diminish and the convective mixing will stop. The vertical distribution of material at that moment will be considered 'frozen' by the model; while, at the same time a ground-based inversion layer is assumed to be generated. Material under this night-time inversion layer is subject to dry deposition during the night, while material above this layer is not. In the morning of day 2 the contents of the two layers will be re-mixed when the mixing height rises above the maximum level, $z_i\,max1$, of the day before. If one considers the situation at the end of day 2, it can be said that the material released during the early hours of day 1 is mixed in a layer, $z_i\,max2$. Local low-level sources, however, will emit at that moment into a layer with height, $z_i\,n2$. In conclusion, contributions to a receptor from local sources must be calculated using local mixing heights. Contributions from sources far away must be calculated using the maximum mixing height that occurred during transport from the source to the receptor.

1.2.3 Classification with respect to the vertical structure of the boundary layer

To include the effects of different vertical stratifications in the atmosphere, mixing-height classes are used over which trajectories are distributed according to the maximum mixing height found during transport from source to receptor. The initial plume height in relation to the mixing height determines whether or

not a plume will touch the ground shortly after release. Both parameters are a function of the stability at the source site. Therefore, the chosen classification is a combination of stability at the source and maximum mixing height over the trajectory. To account for stability and mixing height effects, 3 classes for stability and 2 classes for mixing height are taken. The criteria for the classes are given in Table 1.1. The atmospheric stability is defined here on the basis of the Monin-Obukhov length (for a further definition, see section 2.4.1). The mixing-height criteria are chosen so that for the range of seasonal variations a reasonable occurrence of all classes is obtained.

Table 1.1 Criteria for the atmospheric stability, mixing height and transport distance classes

Class	Atmospheric stability	Monin-Obukhov length (m)	Trajectory: 0 km	Trajectory: 100 km	Trajectory: 300 km	Trajectory: 1000 km
			Maximum mixing height over trajectory (m)			
U1	Unstable	< 0	< 500	< 800	< 900	< 1000
U2			≥ 500	≥ 800	≥ 900	≥ 1000
N1	Neutral	> 100 and <-100	< 400	< 400	< 500	< 800
N2			≥ 400	≥ 400	≥ 500	≥ 800
S1	Stable	> 0	< 80	< 150	< 400	< 800
S2			≥ 80	≥ 150	≥ 400	≥ 800

This classification scheme for the vertical structure of the boundary layer offers the opportunity to account for source-height effects and temporary transport above an inversion layer. The scheme differs from the one used in earlier versions of the model (Van Jaarsveld, 1990), where the atmospheric stability (Pasquill classification) was determined on the basis of surface-roughness length and Monin-Obukhov length according to Golder (1972). In these earlier versions several additional boundary conditions were applied to maintain compatibility with a consensus model for long-term local-scale applications in the Netherlands, the so-called ‘National Model’ (TNO, 1976).

The development of the maximum mixing height for surface-released air pollutants as a function of down-wind distance is shown in Figure 1.4 for different initial conditions. The curves in this figure are calculated on the basis of 10-year meteorological data in the Netherlands. It can be concluded that elevated plumes (e.g. 250 m) emitted under stable conditions (classes S1 and S2) remain above the mixing layer for more than 100 km on average. This figure also shows that from the distance scales selected in section 1.2.1, mixing heights at intermediate distances can be linearly interpolated without making large errors.

Summing up the total classification scheme used: the horizontal transport from a source (area) to a receptor is determined by parameters related to one of 288 classes (4 distance scales, 12 wind direction sectors and 6 stability/mixing heights). Parameter values needed to describe source-receptor relations at actual distances and directions are obtained by linearly interpolating between the values of adjacent classes. One important disadvantage of the described classification method is that all the reactions which can taken place during transport have to be considered as independent from the absolute concentration values. This means that the method is only applicable to reactions which can be approximated as pseudo-first-order reactions.

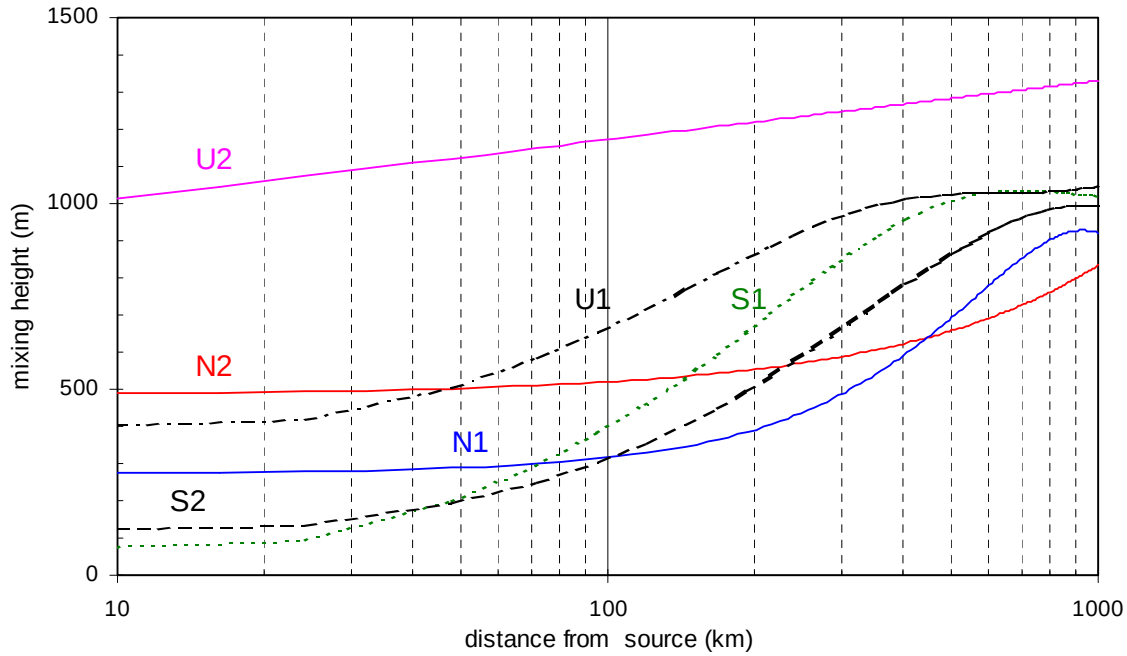

Figure 1.4 *Maximum mixing height, as experienced by an air parcel originally at ground level, as a function of down-wind distance for different stability/mixing height conditions at the moment the air parcel was released. Mixing heights are calculated as described in section 2.4.2 and averaged over a period of 10 years.*

1.3 References chapter 1

Calder K.L. (1971) A climatological model for multiple source urban air pollution. Proceedings of the 2nd Meeting of Expert Panel on Air Pollution Modelling. NATO/CCMS. p. I.1-I.33. Report no. 5.

Eliassen A. and Saltbones J. (1983) Modelling of long-range transport of sulphur over Europe: a two-year run and some model experiments. *Atmospheric Environment* **17**, 1457-1473.

Golder D. (1972) Relations among stability parameters in the surface layer. *Boundary-Layer Meteorol.* **3,** 47-58.

Runca E., Longhetto A. and Bonino G. (1982) Validation and physical parametrization of a Gaussian climatological model applied to a complex site. *Atmospheric Environment* **16**, 259-266.

TNO (1976) Modellen voor de berekening van de verspreiding van luchtverontreiniging inclusief aanbevelingen voor de waarden van parameters in het lange-termijnmodel. Staatsuitgeverij, the Hague, the Netherlands.

Van Jaarsveld J.A. (1990) An operational atmospheric transport model for priority substances; specification and instructions for use. RIVM, Bilthoven, the Netherlands. Report no. 222501002.

2. Meteorological data

Air pollution modelling relies heavily on meteorological input data. Processes such as plume rise, dilution; dispersion and long-range transport depend not only on wind speed but also on turbulence characteristics and on the wind field over the area where the pollutant is dispersed. Although parameters such as turbulence may be measured directly in the field, it is not very practical and certainly very expensive. Therefore, most model approaches make a distinction between real observations of primary data (wind, temperature, radiation etceteras) and secondary parameters (friction velocity, Monin Obukhov length, mixing height etceteras), derived from the set of primary parameters. The OPS model is designed to make use of standard and routinely available meteorological data. The parameters are wind speed and wind direction at two heights, temperature, global radiation, precipitation, snow cover and relative humidity.

2.1 Meteorological areas in the OPS model

The OPS model is intended to describe the local dispersion from specific sources but also the total influence of all relevant sources in Europe on all parts of the Netherlands. This means that - in principle - the meteorological information must be available, along with some spatial detail. For this purpose a total of six meteorological areas were chosen, mainly on the basis of the average windspeed regime over the Netherlands. The areas are shown in Figure 2.1.

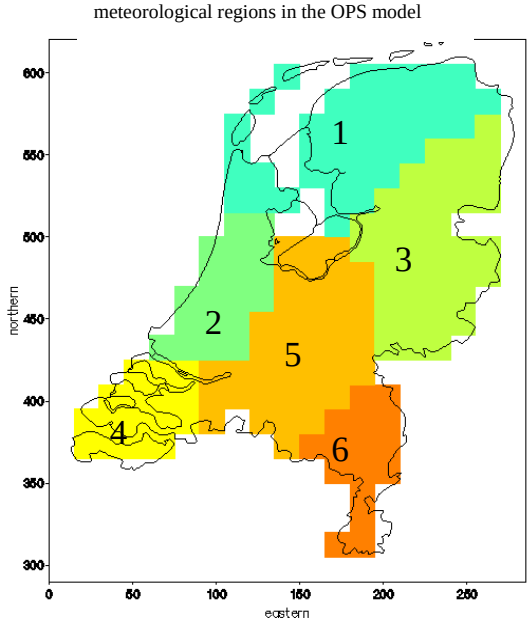

Figure 2.1. Meteorological areas in the OPS model.

All meteorological pre-processing is done individually for the six areas and saved separately. A schematic overview of this procedure is given in Figure 2.2. After this processing of the primary data a stage follows, in which secondary parameters are calculated and a climatology of similar situations (classes) is generated. Although this stage is actually called the meteorological pre-processor, it is not the first stage. When the OPS model is run, the climatological data are loaded from six files representing six areas. The OPS model itself uses some interpolation between the data of nearby areas to avoid discontinuities in output, as described in Chapter1.

The purpose of this chapter is to describe the meteorological data and the procedures used to obtain representative values for the different areas.

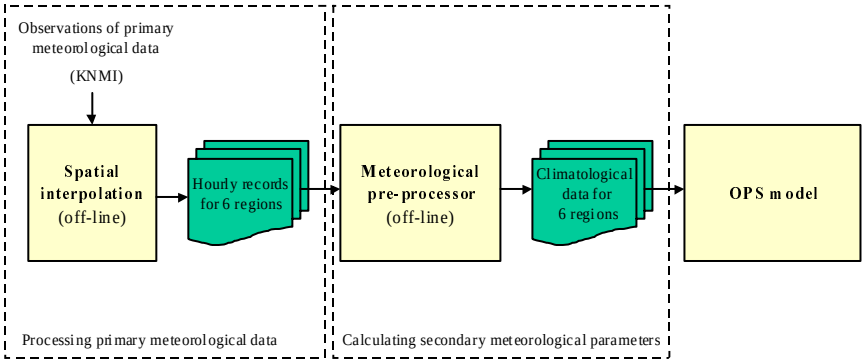

Figure 2.2 Schematic view of the OPS model with its pre-processing steps.

2.2 Sources of primary meteorological data

Since 1976 the National Air Quality Monitoring Network (LML) database has provided hourly air quality data, along with meteorological data. Up to 1993 this was mainly wind data measured in the LML network consisting of 46 sites, of which 5 were situated at the top of TV towers. In 1981 the database was expanded with data from the KNMI network on global radiation (7 –17 sites), temperature (14 sites) and precipitation data (11-14 sites). The LML meteorological observations stopped in 1993. From this point on, the wind data was replaced with observations at KNMI stations. Historical data going back to 1981 were obtained from the KNMI archives and also included in the LML database. In this way a homogeneous series of data became available, which is updated every month and currently spans a period of more than 20 years. Although earlier versions of the OPS model used wind observations from the LML network, the descriptions and data in this report apply only to the KNMI data. The positions of the selected KNMI meteorological stations are given in Figure 2.3.

2.3 Processing primary data

2.3.1 Calculating the potential wind speed

The OPS model uses spatially averaged meteorological data rather than point data. Before any form of spatial averaging can take place it is necessary that all wind data is converted to standard conditions. Not all stations have the same measuring height. Moreover, the terrain conditions are not the same for all the stations. Therefore, wind velocities are converted to a potential wind speed, defined as the wind at 10 m height and at a roughness length of 0.03 m. Because the roughness length is not the same in all wind directions, conversion is applied as a function of wind direction

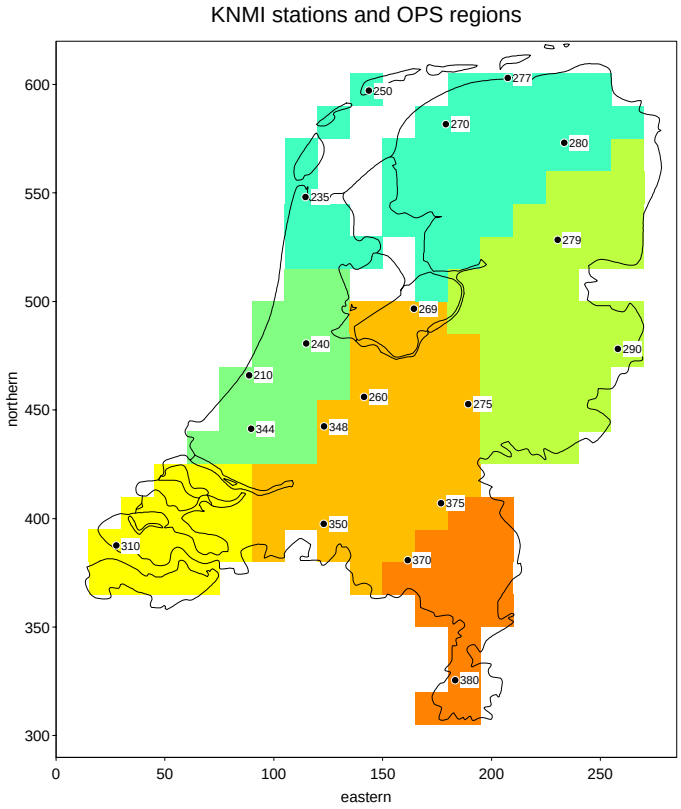

Figure 2.3 Location of KNMI stations.

2.3.2 Spatial averaging of meteorological data

In earlier approaches a number of stations were selected to be representative for a region. The major drawback of such a method is that if data sets change one has to make new selections with the risk of changing trends in the area. Also, the chance that for a given hour none of the selected stations will provide valid information is high, resulting in a high percentage of missing data. The method chosen here is first interpolating the data over the Netherlands, using all the available stations and then calculating area averages. In this way, the data are optimally used and the information of nearby stations is used automatically if local stations fail.

2.3.2.1 Wind direction

The potential wind speed in combination with the wind direction is now split into an *x* and *y* vector, and both are interpolated using a 10 x 10 km grid over the Netherlands. If the contribution of each station to each grid point is calculated, the vectors are spatially averaged to regional averages by using a mask according to Figure 2.1. The resulting wind direction per region is simply calculated by taking the arctangent of the vectors. If the observations indicate a variable wind direction, the observation is ignored. In such a case the remaining stations determine the direction of the wind in the region.

2.3.2.2 Wind speed

Spatial averaging of wind speed is done using the same interpolation procedure. Considering the use of wind speed in the model (mainly to derive turbulence parameters), the interpolation is independent of wind direction. The minimum wind speed of individual observations is set at 0.5 m/s. This takes the trigger threshold of the anemometers used into account (in the order of 0.4 m/s) to some extent, and also the fact that wind speed is given in knots or 0.5 m/s units. Ignoring situations with zero wind speed introduces a bias in the ‘average’ wind speed, and therefore will lead to larger errors in modelling than using lower limit values.

2.3.2.3 Other parameters

Interpolation of global radiation, temperature, relative humidity and precipitation probability is carried out the same way as wind speed. Precipitation intensity and snow cover are not spatially interpolated, but always apply to the Netherlands as a whole.

2.3.3 Calculation of precipitation characteristics

Precipitation events in the OPS model are described with three parameters (see section 4.2.4):

1. Precipitation probability
2. Precipitation intensity
3. The length of a rainfall period

In terms of input data, precipitation probability is required on an hourly basis, while intensity and the length of rainfall periods are required as representative values on a daily basis. The KNMI data provide - for each hour - the amount of precipitation (in 0.1 mm) and the duration within that hour (in 0.1 hour). Both the calculation of the hourly precipitation probability (in %) from the precipitation duration per hour and the calculation of the average precipitation intensity for that day are straightforward. The average length of a rainfall period requires a definition of what is considered as a contiguous rainfall period and what is not. A rainfall period starts after teh hour in which there was no precipitation. The rainfall period ends if the rainfall in a subsequent hour lasts less than 0.5 hour. The length of the period is then calculated as the sum of the duration between the starting hour and the ending hour, in which in-between hours account fully, even when the measurements indicate less than a full duration. The procedure also takes into account that precipitation periods may have started a day earlier or have not ended at the end of the day. In this way an average rainfall length is calculated for each station. A single daily and spatially averaged value is calculated from all the stations that reported precipitation that day.

2.3.4 Determination of the snow cover indicator

The presence of a snow cover is important for the calculation of dry deposition velocities in the model. If the Netherlands and a large part of Europe is covered with snow, the dry deposition will decrease dramatically and the long-range transport of pollutant may increase sharply. As such, the model focuses on the large-scale effects of snow cover and not on the local scale. The input to the model is therefore an indicator of whether most of the Netherlands (and probably western Europe) is covered with snow or not. The height of a snow layer is reported by 3-7 stations on a daily basis. The snow indicator is set at 1 if at least 80% of these stations report the presence of a snow layer.

2.4 The meteorological pre-processor

The task of the pre-processor is to calculate secondary meteorological parameters, construct backward trajectories, divide these trajectories into classes and calculate representative 'averages' for a number of corresponding parameters. Although the model system uses mixing height classes, for example, no fixed mixing heights, but averages derived from the actual hourly values, are assigned to these classes. This approach ensures a non-critical choice of class boundaries.

2.4.1 Derivation of boundary layer parameters

The calculation scheme of Beljaars and Holtslag (1990) is used for the estimation of boundary layer parameters such as surface heat flux, friction velocity and Monin-Obukhov length. Most of the routines in this scheme are based on a parameterization of day and night-time surface energy budgets as published by Holtslag and Van Ulden (1983); Van Ulden and Holtslag (1985) and Holtslag and De Bruin (1988).
The Monin-Obukhov length L is a vertical length scale, which has become very popular in estimating the stability of the atmosphere. L reflects the height to which friction forces are dominant over buoyant forces. The surface heat flux, H_0, is the vertical flux of sensible heat that is transferred by turbulence to or from the surface. This parameter determines the heating or the cooling of the lower part of the boundary layer and therefore indirectly affects the depth of the boundary layer. The friction velocity u_* determines the production of turbulent kinetic energy at the surface. The relation between L, H_0 and u_* is given by:

$$L = \frac{T \rho_a c_p u_*^3}{g H_0 \kappa} \tag{2.1}$$

where κ is the von Kármán constant, established experimentally to be about 0.40, T the absolute temperature, g the acceleration of gravity, c_p the specific heat of air, and ρ_a the air density. H_0 can be calculated from the net radiation Q^* using the surface energy budget:

$$H_0 + L E = Q^* - G_s \tag{2.2}$$

where LE is the latent heat flux and G_s the soil heat flux. The latent heat flux is modelled by De Bruin and Holtslag (1982), and Holtslag and De Bruin (1988), using a modified Priestly-Taylor model. This model is used in the routines of Beljaars and Holtslag (1990), where H_0 for a given geographical position is parameterized as a function of global radiation or cloud cover. Results of these surface energy parameterizations have been verified with experiments at the Cabauw meteorological tower. The basic equation which, according to surface-layer similarity theory, relates u_* to a vertical windspeed profile $u(z)$ is:

$$u_* = \frac{\kappa \, u(z)}{\ln(\frac{z_1}{z_0}) - \psi_m(\frac{z_1}{L}) + \psi_m(\frac{z_0}{L})} \tag{2.3}$$

where z_1 is an arbitrary height in the surface layer, z_0 the surface layer roughness length of the terrain (for a classification, see Wieringa (1981)). The functions, ψ_m, are stability correction functions for momentum, which read as follows (Paulson, 1970)

for $L < 0$:

$$\psi_m(\frac{z}{L}) = 2\ \ln\ (\frac{1+x}{2}) + \ln\ (\frac{1+x^2}{2}) - 2\ \arctan(x) + \frac{\pi}{2}$$
$$\text{with} \quad x = (1-16\ \frac{z}{L})^{1/4} \tag{2.4}$$

and for $L > 0$:

$$\psi_m(\frac{z}{L}) = -5\ \frac{z}{L} \tag{2.5}$$

Equations (2.1)-(2.5) are iteratively solved to obtain u_* and L (Beljaars and Holtslag, 1990). From Eq. (2.3) relations can be derived for windspeed profile calculations or for the translation of windspeed observations to situations with different z_0. In section 2.4.3 more details on the windspeed profile and stability correction functions are given.

2.4.2 Estimation of mixing heights

Although it was possible, in principle, to use temperature profiles from radio soundings for the determination of the mixing layer height, estimation of the mixing height on the basis of surface-layer parameters was preferred. The main reason for this is that the inversion height is usually taken at the height of the dominant temperature jump in the profile. so is valid for 'aged' pollutants, while this model needs the height of the first layer starting at the surface that effectively isolates the surface layer from higher parts of the boundary layer. Moreover, temperature profiles from radio soundings have a limited resolution in the lower boundary layer (Driedonks, 1981).

2.4.2.1 Stable and neutral conditions

Strictly speaking, the nocturnal boundary-layer height is not stationary (Nieuwstadt, 1981). Proposed prognostic models usually take the form of a relaxation process, in which the actual the actual boundary-layer height approaches a diagnostically determined equilibrium value. It turns out that the time scale of the relaxation process is very large and therefore the equilibrium value can be used as an estimator for the actual boundary-layer depth (Nieuwstadt, 1984). For this reason the direct applicability of diagnostic relationships was evaluated. A simple diagnostic relation of the form:

$$z_i = c_1 \frac{u_*}{f_c} \tag{2.6}$$

as first proposed by Delage (1974), was found to give satisfactory results for both stable and neutral atmospheric conditions. In this equation f_c is the Coriolis parameter and c_1 a proportionality coefficient. From the data set of night-time acoustic sounder observations at Cabauw (Nieuwstadt, 1981), c_1 was estimated at 0.08. Equation (2.6) was also tested using acoustic sounder observations carried out at Bilthoven in 1981 during daytime. Values for c_1 found were 0.086 during neutral atmospheric conditions and 0.092 for neutral + stable cases. For the present model Eq. (2.6) is adopted where c_1 = 0.08 for both neutral and stable cases.

2.4.2.2 Unstable conditions

Adequate diagnostic equations do not exist for the depth of the unstable atmospheric boundary layer (Van Ulden and Holtslag, 1985). It is common practice to use rate equations (Tennekes, 1973; Stull, 1983) for describing the rise of an inversion by buoyancy as well as by mechanical forces. The model adopted here is based on the model of Tennekes (1973) and describes the growth of the convective boundary layer for

a rather idealized situation. More details on this approach are given in Van Jaarsveld (1995). In Figure 2.4, model results and observations are compared as a function of time of the day for the ten-day data set of Driedonks (1981). Indeed, no systematic difference is observed in the average course of the mixed-layer height in the morning. Considering the way mixed-layer heights are used in the OPS model, namely, as averages for typical situations, one can conclude the current approach to lead to the desired results.

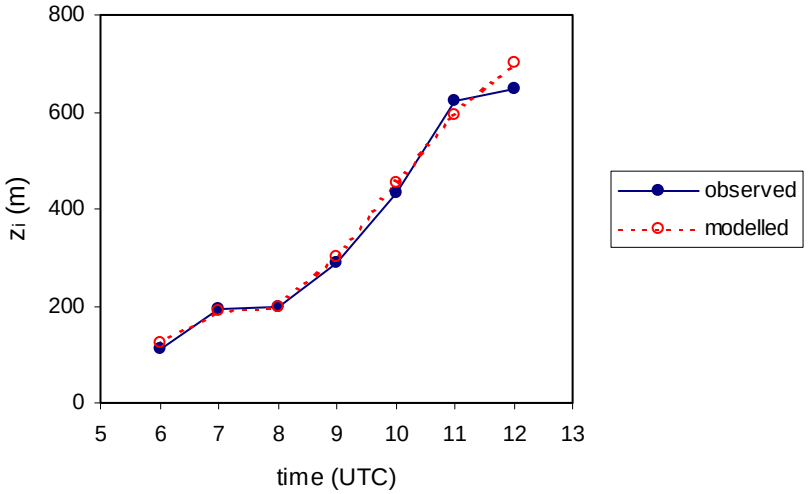

Figure 2.4 *Comparison of modelled and observed mixing-layer heights (average of ten convective days) at Cabauw.*

2.4.3 The wind profile

Pollutants are emitted at various heights in the atmosphere. Moreover, due to turbulent mixing, the effective transport height of a pollutant may change in time. Windspeed data are usually available for one or two discrete observation levels. What is needed for the description of dispersion and transport of pollutants is a relation between wind speed at different heights. It is common practice to base this relation for the lower boundary layer on Monin-Obukhov similarity theory. The following general expression for the wind speed at height z can be derived from Eq. (2.3):
where z_1 is the height at which a wind observation is available. The terms $\psi_m(z_0/L)$, present in Eq. (2.3),

$$u(z) = u(z_1)\frac{\left[\ln(\frac{z}{z_0}) - \psi_m(\frac{z}{L})\right]}{\left[\ln(\frac{z_1}{z_0}) - \psi_m(\frac{z_1}{L})\right]} \qquad (2.7)$$

have been dropped because they are comparatively small. The functions ψ_m given by Eq. (2.4) and (2.5) are, strictly speaking, only valid for the surface layer $(z_0 << z < |L|)$. However, several authors have derived correction functions describing the windspeed relation up to the top of the mixing layer (Carson and Richards, 1978; Garratt *et al.*, 1982; Holtslag, 1984; Van Ulden and Holtslag, 1985). A function which in combination with Eq. (2.7) fits the windspeed observations at the Cabauw tower in stable situations up to 200 m well is (Holtslag, 1984):

$$\psi_m(\frac{z}{L}) = -17\left[1 - \exp(-0.29\frac{z}{L})\right] \quad \text{for } L > 0 \qquad (2.8)$$

This function is used in the model instead of Eq. (2.5).

2.4.3.1 Combining wind observations

An expression similar to Eq. (2.7) can be derived from (2.3) to translate $u(z)$ measured at a location, with z_0 to $u''(z)$ representative for z_0''. The procedure is then to convert $u(z)$ to $u(z_1)$ (z_1 taken 60 m) at z_0 and then to convert $u(z_1)$ to $u''(z)$ using z_0''. The assumption in this is that the wind speed at height z_1 is not influenced by the local surface roughness. This procedure is carried out for each of the observation sites. Roughness lengths for each of the LML meteorological sites have been determined by Erisman (1990) using a relation between z_0 and the (short-term) standard deviation of wind directions given by Hanna (1981).

A representative wind speed for an area is calculated in the pre-processor by first normalizing the wind speeds at the different observational sites on the basis of an area-representative roughness length z_0m, and then averaging the roughness corrected wind speeds. A representative wind direction follows from the combined x and y vectors of the roughness-corrected wind speeds.

2.4.3.2 Observed windspeed profiles

Although the logarithmic profile appears to fit observations well, it is used in the present model mainly for extrapolation to levels lower than the observation height (10 m). For the description of (horizontally averaged) transport velocities at different heights (up to 300 m) a relation of the form:

$$u(z) = u(z_1)\left(\frac{z}{z_1}\right)^p \tag{2.9}$$

known as the power law, is used. The major advantage of this relation is that it can be easily fitted to observations. In the present case, p is derived hourly from the 10-m and 200-m observations at the Cabauw meteorological tower. The resulting p values range from 0.13 under unstable conditions (L > -30 m) to 0.45 under very stable conditions (L < 35 m).

2.4.3.3 Turning of the wind with height

The direction of the wind as a function of height is important for the description of pollutant transport especially if this is done on the basis of surface-based observations. The turning of the wind in the 20 - 200 m layer was studied by Holtslag (1984) and Van Ulden and Holtslag(1985) on the basis of observations at the Cabauw tower. The latter authors give an empirical relation for the turning angle up to 200 m:

$$A(z) = c_6\, A(z_{ref})\left[1 - \exp\left(\frac{-c_7\, z}{z_{ref}}\right)\right] \tag{2.10}$$

where $A(z)$ and $A(z_{ref})$ are the turning angles at height z and reference height z_{ref}, respectively; c_6 = 1.58 and c_7 = 1.0 are empirical coefficients. Typical values of $A(z_{ref})$ at z_{ref} = 200 m are 35, 12 and 9 degrees for stable, neutral and unstable situations, respectively.

In the OPS model a trajectory is characterized by a single direction representative for mass flow of the pollutant. This direction is taken at a height equal to half of the maximum mixing height (100-2000 m) of the trajectory. The turning angle above the 150 - 300-m layer is not known from actual observations. On the assumption that the winds become geostrophic at some level above the observation height, an analytical description of the Ekman spiral given by Businger (1982) is used:

$$U_g = G\,[\ 1 - \exp(-a_E\ z)\cos(a_E\ z)\ ] \tag{2.11}$$

$$V_g = G\,[\ \exp(-a_E\ z)\sin(a_E\ z)\,] \quad \text{with } a_E = [\ f_c\ /\ (2\ K_m)\ ]^{1/2} \tag{2.12}$$

where K_m is the (bulk) eddy viscosity of the boundary layer and U_g and V_g the respective velocity vectors in the x and y directions, with the x-axis aligned with the geostrophic wind G. From Eqs. (2.11) and (2.12) the following expression has been derived for the turning angle of the wind at height z relative to the geostrophic wind direction:

$$A_E(z) = \arctan\left[\frac{-\exp(-a_E\ z)\sin(a_E\ z)}{1 - \exp(-a_E\ z)\cos(a_E\ z)}\right] \tag{2.13}$$

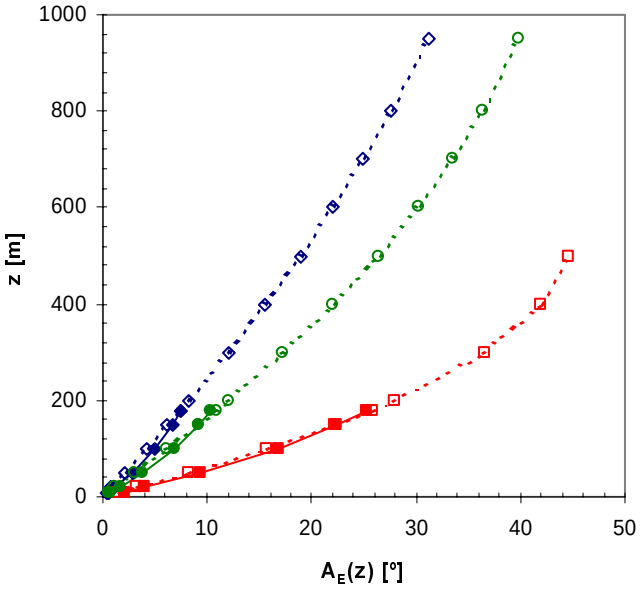

Figure 2.5 Turning of the wind direction with height (Ekman spiral) relative to the surface wind direction as a function of stability (Eq. 2.13). Results obtained using the empirical relation of Van Ulden and Holtslag (Eq. 2.10) are also plotted (solid lines). Squares: stable conditions (K_m = 1.5 $m^2\ s^{-1}$; $A(z_{ref})$ = 27^o). Circles: neutral conditions (K_m = 11 $m^2\ s^{-1}$; $A(z_{ref})$ = 11^o). Triangles: unstable conditions (K_m = 25 $m^2\ s^{-1}$; $A(z_{ref})$ = 8^o).

Although the Ekman spiral and Eqs. (2.11) and (2.12) are defined for steady-state situations with small K_m, when using higher eddy viscosity values, the resulting profiles do not appear to conflict with (mean) profiles, as observed in the lower part of the boundary layer. This is shown in Figure 2.5, where three profiles representative for stable, neutral and unstable conditions in the lower boundary layer (K_m values of 1, 10 and 50 $m^2\ s^{-1}$ resp.) are given, together with corresponding profiles, for the lower 200 m, calculated using Equation (2.10). Note that in this figure the turning angle is plotted relative to the surface wind direction ($A(z) = A_E(z) - A_E(z=0)$) instead of relative to the geostrophic wind.

For the present model the expression of Van Ulden and Holtslag (Eq. (2.10)) is used for up to 200 m; for extrapolation to higher levels Eq. (2.13) is used, with K_m values to allow the profile to fit the (observed) 10 m and 200 m directions.

2.4.4 Trajectories

Backward trajectories are constructed on the basis of hourly observations at TV towers, for which it had to be assumed that transport directions and velocities in a larger area were the same as in the Netherlands at the same time. Although this is a crude assumption, it may still give satisfactory results for longer term average calculations. The main reason for this is that long-range transport is of importance in persistent situations and those with not too low transport velocities. In these situations the observations in the Netherlands (five towers of heights between 146 and 320 m) may be expected to be representative for a much larger area.

The procedure is as follows: observed data at the towers are combined into a single x and y wind vector pair representative for a height of 200 m using the methods described in section 2.4.3. These vectors and other parameters such as mixing height are placed into shift registers, which are updated every hour. The trajectory is then determined by tracing back the height corrected wind vectors, starting at the most recent observation, until a circle around the observation point is crossed with a predefined radius (100, 300 or 1000 km, see Figure 1.2). The wind vectors are height-corrected so as to present the representative height of the mass in the trajectory, which is taken at half the maximum mixing height encountered at that stage of transport. The position where the circle is crossed, relative to the observation point, is now considered as the starting point of the backward trajectory. From this point the procedure is repeated but now in reverse, and consequently, the maximum mixing height along the trajectory takes a different course. The start and end positions of this trajectory determine the direction φ of the trajectory. Other characteristic parameters are determined by appropriately averaging hourly observations along the trajectory. Easterly directions seem to be systematically overpredicted by the method described here, while north-west directions are underpredicted. It is remarkable that for trajectories which fall fully within the observation area of the towers (e.g. 100 km), these discrepancies are also found (not shown here). Similar results were obtained by comparing these trajectories with 6-hourly 850 hPa trajectories provided by the Norwegian Meteorological Institute, although here a systematic deviation of ~ 20^0 in transport direction is found. This can be explained by the Ekman spiral (the 850 hPa trajectories are approx. 1500 m above the surface). When corrected for this systematic difference, the standard deviation between the two is of the order of 30^0.

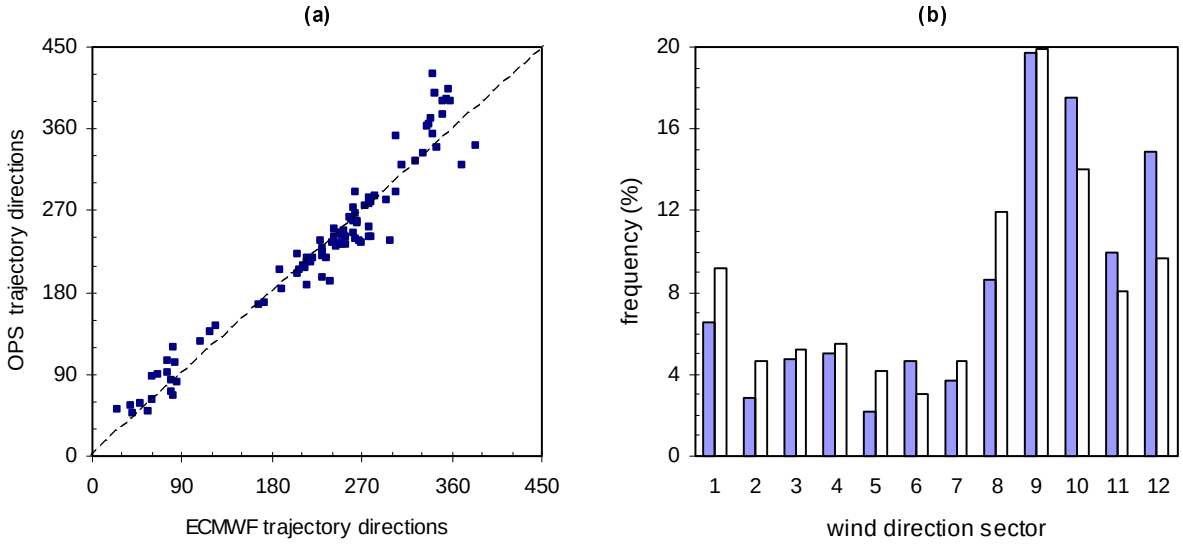

Figure 2.6 Source-receptor directions of backward trajectories derived from ECWMF wind fields versus trajectory directions derived from observations at five towers in the Netherlands. The source-receptor distance was taken as 1000 km. (a): Comparison of individual trajectories arriving at 1200 UTC, excluding trajectories with $fp_{eff} < 2$. (b): All directions grouped into 30^o sectors. Sector 1 represents 345^o - 15^o. Solid bars: ECMWF trajectories. Open bars: OPS trajectories.

In Figure 2.6a, trajectory directions calculated in this way are compared to trajectory directions derived from 3° latitude x 3° longitude resolution wind fields (1000 and 850 hPa) obtained from ECMWF (De Waal and Van Pul, 1995). The latter trajectories are calculated for an average pressure level of 960 hPa (corresponding height above surface ~ 400 m), considered as representative for the average height of transport in the mixing layer. There is hardly any systematic difference between the trajectory directions, as the total set of trajectories is compared. The standard deviation of the differences is of the order of 30° if some very curved trajectories are ignored (fp_{eff} < 2, see section 1.2.1). If directions are grouped into direction classes, then the difference may appear fairly large, as is shown in Figure 2.6b for the full set of trajectories.

Temporal isolation of pollutants from the surface due to mixing-height variations

Due to the classification of trajectories, the properties of the trajectories have to be characterized by a few parameters. In terms of mixing volumes the trajectories are defined by an average transport velocity, u_{tra}, and the maximum mixing height, $z_{i\,max}$, which has appeared during transport. In reality the mixing height that an air parcel encounters on its way to the receptor point can be lower than this height. Moreover, the parcel may be transported above the mixing layer part of the time. In such a situation the pollution in the parcel is not removed by dry deposition, a process which only occurs at the surface. To account for these effects, 'transport' dry deposition velocities ($v_{d\,tra}$) are introduced which account for the total loss of material on its way from source to receptor and are related to $z_{i\,max}$. The remaining airborne fraction F_{air} at a receptor is then proportional to (see also section 3.1.1):

$$F_{air} = \exp\left(\frac{-\,v_{d\,tra}\,x}{u\,z_{i\,\max}}\right) \tag{2.14}$$

where x is the transport distance and u the transport velocity. The procedure is to follow the air parcel and to integrate the loss of material due to dry deposition, taking into account situations where a plume is above the mixing layer or partly isolated from the surface due to ground-based inversions. Now $v_{d\,tra}$ for the trajectory can be derived from the following equations for the total cross-wind integrated dry deposited mass:

$$\sum_{t=1}^{N} \frac{M(t)}{z_i(t)}\, v_d(t) = N\,\frac{M_{rcp}}{z_{i\,\max}}\, v_{d\,tra} \tag{2.15}$$

where N is the number of (hourly) intervals, $M(t)$ the cross-wind and interval integrated mass in the actual mixing layer with height $z_i(t)$, and $v_d(t)$ the dry deposition velocity, all at time t. M_{rcp} is the remaining (cross-wind integrated, final interval) airborne mass at the receptor and $z_{i\,max}$, the maximum mixing height over the trajectory.

It is clear that the fraction of the time that pollutants spend above the mixing layer, strongly depends on the source height. Therefore the calculation of effective dry deposition velocities is carried out in the pre-processor for two characteristic source heights: a high source (unit strength, 100 m stack height and plume rise according to Briggs (1975) for a heat content of 20 MW), and a low source (35 m, no plume rise). The latter is representative for sources which always emit within the mixing layer and the former for larger point sources which emit temporarily above the mixing layer. The transport dry deposition velocities calculated in this way are used in the model in the form of correction factors to the deposition velocity at the receptor site and as such are included in the meteorological data set:

$$f_d\,(x,h) = \frac{v_{d\,tra}}{v_{d\,rcp}} \tag{2.13}$$

where x denotes the source receptor distance and h the source height. f_d has a range of 0.70 - 1.7 with a mean value of 1.2 for the elevated source. For the low source this range is 0.80 - 2.2, with a mean value of 1.4 (sulphur dioxide, 1000 km trajectories). Formally, these correction factors are substance-specific. However, only small differences are found for the usual range of dry deposition velocities. From tests it appears that transport in or above the mixing layer at night explains most of the difference between correction factors for different source heights. The correction factor for low sources is therefore used for non-buoyant plumes up to 100 m.

2.4.5 Summary of the meteorological data set

Table 2.1 gives an overview of the different parameters calculated by the pre-processor, following air parcels from source to receptor at hourly intervals in the period under consideration. Several parameters not yet discussed have been included in the table for reasons of completeness. For every trajectory, representative values for the parameters are determined using parameter-specific averaging methods. The averaging method depends on how the parameter will be used in the model. The trajectories arriving at a receptor during the period considered are distributed over a number of classes, as described in section 1.2. Average values are calculated for all class – parameter combinations using the same averaging methods. The 4 distance, 12 transport-direction, 3 stability and 2 mixing-height classes for each of the 25 parameters form, collectively, the meteorological data set for the model.

Table 2.1 Parameters calculated by the pre-processor

Parameter	Averaging method[#]	Remarks
1. transport velocity *u10*	2	calculated for $z = z_{i\,max}/2$ and converted to a reference height of 10 m
2. effective path-length fp_{eff}	1	see section 1.2.1
3. windspeed power law coeff. P	1	from 10-m and 200-m wind speed, see section 2.4.3
4. wind turning with height A	1	from 10-m and 200-m wind directions
5. global radiation Q_r	1	from measurements or derived from cloud cover
6. temperature T	1	
7. relative humidity	1	to be used for R_c parameterisations
8. sensible heat flux H_0	1	parameterisation of Beljaars and Holtslag (1990)
9. friction velocity u_*	2	derived from 10-m wind speed at default z_0
10. Monin-Obukhov length L	2	see u_*
11. mixing height $z_{i\,max}$	2	maximum mixing height over the trajectory
12. surface layer resistance R_b	2	v_d weighted (for SO_2 only), see section 4.1
13. aerodyn. resistance $R_a(4)$	2	v_d weighted, reference height 4 m, see section 4.1
14. aerodyn. resistance $R_a(50)$	2	v_d weighted, reference height 50 m, see section 4.1
15. surface resistance $(r_c\text{-}SO_2)$	2	v_d weighted, see Chapter 6
16. surface resistance $(r_c\text{-}NO_2)$	2	v_d weighted, see Chapter 6
17. surface resistance $(r_c\text{-}NH_3)$	2	v_d weighted, see Chapter 6
18. dep. corr. f_d high sources	1	see section 2.4.4
19. dep. corr. f_d low sources	1	see section 2.4.4
20. domestic heating coeff.	1	dependent on temperature below 292 K
21. rain probability P_p	1	derived from hourly or 6-hourly observations: section 4.2
22. length of precip. events τ_w	1	derived from hourly observations: section 4.2
23. precipitation intensity R_i	1	derived from hourly or 6-hourly observations: section 4.2
24. time of day at the source site	3	used to manage diurnal emission variations
25. time of day at the receptor site	3	used to describe diurnal concentration variations

[#] 1: normal averaging within classes
2: reciprocal averaging within classes
3: no averaging but classification into time-of-day groups

Table 2.2 Some statistical parameter values as a function of the atmospheric stability classes (Data based on KNMI observations over the Netherlands in the period 1990-1999)

Meteorological parameter	Unit	U1	U2	N1	N2	S1	S2	Avg#
Frequency of occurrence	%	10	22	18	17	13	20	
Wind speed at 10 m *u10*	m s^{-1}	2.5	3.9	3.9	6.9	1.3	2.6	2.9
Wind turning 10-200 m *A*	degrees	8	0	11	3	27	20	10
Temperature *T*	°C	11	16	9	8	7	8	10
Global radiation *Qr*	W m^{-2}	206	378	20	22	2	3	114
Precipitation probability R_p		0.041	0.037	0.105	0.202	0.019	0.045	0.077
Precipitation intensity R_i	mm h^{-1}	1.26	1.53	1.15	1.10	1.06	1.24	1.22
Length of prec. events τ_w	h^{-1}	1.7	1.5	2.0	2.5	1.7	1.8	2.0
Relative humidity R_h	%	83	67	88	86	92	89	83
Space heating coeff. *stc*	°C	6.6	5.4	10.0	16.2	5.7	8.0	8.7
Sensible heat flux H_0	W m^{-2}	36	80	-25	-39	-3	-19	6
Friction velocity *u**	m s^{-1}	0.28	0.43	0.36	0.68	0.53	0.18	0.19
Monin Obukhov length *OL*	m	-47	-64	196	701	6	32	44
Mixing heigth $z_{i\,max}$	m	231	888	290	540	42	146	165
Aerodynamic resistance $R_a(4)$	s m^{-1}	22	15	21	11	240	46	24
Aerodynamic resistance $R_a(50)$	s m^{-1}	34	24	45	21	862	133	47

different averaging methods , see Table 2.1

2.5 References chapter 2

Beljaars A.C.M. and Holtslag A.A.M. (1990) A software library for the calculation of surface fluxes over land and sea. *Environ. Software* **5**, 60-68.

Briggs G.A. (1975) Plume rise predictions. In: *Lectures on Air Pollution and Environmental Impact Analysis*. American. Meteorological Society, Boston MA. 59-111.

Businger J.A. (1982) Equations and concepts. In: Nieuwstadt F.T.M. and Dop H. van, editors. *Atmospheric turbulence and air pollution modelling*. D. Reidel, Dordrecht, the Netherlands.

Carson D.J. and Richards P.J.R. (1978) Modelling surface turbulent fluxes in stable conditions. *Boundary-Layer Meteorol*. **14**, 67-81.

De Bruin H.A.R. and Holtslag A.A.M. (1982) A simple parameterisation of the surface fluxes of sensible and latent heat during daytime compared with the Penman-Monteith concept. *J. Appl. Meteor.* **21**, 1610-1621.

De Waal E.S and Pul W.A.J. van (1995) Description of the RIVM trajectory model. RIVM, Bilthoven, the Netherlands. Report no. 722501001.

Delage Y. (1974) A numerical study of the nocturnal atmospheric boundary layer. *Q. J. R. Meteorol. Soc.* **100**, 351-364.

Driedonks A.G.M. (1981) Dynamics of the Well-Mixed Atmospheric Boundary Layer. [PhD thesis]. Royal Netherlands Meteorological Institute, De Bilt, the Netherlands. Scientific report W.R. 81-2.

Erisman J.W. (1990) Estimates of the roughness length at Dutch Air Quality Monitoring Network stations and on a grid basis over the Netherlands. RIVM, Bilthoven, the Netherlands. Report no. 723001003.

Garratt J.R., Wyngaard J.C. and Francey R.J. (1982) Winds in the atmospheric boundary layer - Prediction and observation. *J. Atmos. Sci*. **39**, 1307-1316.

Hanna S.R. (1981) Diurnal variation of horizontal wind direction fluctuations in complex terrain at Geysers, California. *Boundary-Layer Meteorol*. **21**, 201-213.

Holtslag A.A.M. (1984) Estimates of diabatic wind speed profiles from near surface weather observations. *Boundary-Layer Meteorol*. **29**, 225-250.

Holtslag A.A.M. and Bruin H.A.R. de (1988) Applied modelling of the nighttime surface energy balance over land. *J. Appl. Meteor*. **27**, 689-704.

Holtslag A.A.M. and Ulden A.P. van (1983) A simple scheme for daytime estimates of the surface fluxes from routine weather data. *J. Climate Appl. Meteorol*. **22**, 517-529.

Nieuwstadt F.T.M. (1981) The nocturnal boundary layer; theory and experiments [PhD thesis]. Royal Netherlands Meteorological Institute, De Bilt, the Netherlands. W.R. 81 - 1.

Nieuwstadt F.T.M. (1984) Some aspects of the turbulent stable boundary layer. *Boundary-Layer Meteorol*. **30**, 31-55.

Paulson C.A. (1970) The mathematical representation of wind speed and temperature profiles in the unstable atmospheric surface layer. *J. Appl. Meteorol*. **9**, 856-861.

Stull R.B. (1983) A heat-flux-history length scale for the nocturnal boundary layer. *Tellus* **35A**, 219-230.

Tennekes H. (1973) A model for the dynamics of the inversion above a convective boundary layer. *J. Atmos. Sci*. **30**, 558-567.

Van Jaarsveld J. A. (1995) Modelling the long-term atmospheric behaviour of pollutants on various spatial scales. Ph.D. Thesis, Utrecht University, the Netherlands

Van Ulden A.P. and Holtslag A.A.M. (1985) Estimation of atmospheric boundary layer parameters for diffusion applications. *J. Climate Appl. Meteorol*. **24**, 1196-1207.

Wieringa J. (1981) Estimation of mesoscale and local-scale roughness for atmospheric transport modelling. In: Wispelaere, C., editor. The 11th Int. Tech. Meeting on air pollution modelling and its application. Plenum Press, New York, 279-295.

3. Mathematical formulation of the model

3.1 Basic equations

The change of a mass M_p in time for a pollutant well-mixed in a layer z_i due to chemical conversion and deposition can be formulated as follows:

$$\frac{d M_p}{dt} = - k_p M_p \tag{3.1}$$

and for a secondary-formed pollutant M_s, with linear dependence on M_p:

$$\frac{d M_s}{dt} = k_c M_p - k_s M_s \tag{3.2}$$

k_p and k_s are defined as:

$$k_p = \frac{v_{d\,p}}{z_i} + k_c + \Lambda_{w\,p} \tag{3.3}$$

$$k_s = \frac{v_{d\,s}}{z_i} + \Lambda_{w\,s} \tag{3.4}$$

where v_{dp} and v_{ds} are dry deposition velocities (m s^{-1}), Λ_{wp} and Λ_{ws} wet scavenging coefficients (s^{-1}), k_c the pseudo first-order chemical reaction constant (s^{-1}), and z_i the mixing-layer height (m). Subscripts p and s refer to the primary-emitted and the secondary-formed substance respectively. Further chemical reactions involving M_s are not taken into account.
The cross-wind integrated mass flux at a distance x from the point of release for a source emitting continuously with a rate of Q_0 (g s^{-1}) can be obtained by solving Eqs. (3.1) and (3.2) after introduction of

$$Q_p(x) = Q_0 \exp\left(- k_p \frac{x}{u}\right) \tag{3.5}$$

$$Q_s(x) = Q_0 \frac{k_c}{k_p - k_s}\left[\exp\left(- k_s \frac{x}{u}\right) - \exp\left(- k_p \frac{x}{u}\right) \right] \tag{3.6}$$

a horizontal transport velocity u (m s^{-1}) ($u = x/t$):
The concentration (g m^{-3}) at a distance x is related to the mass-flux through:

$$C(x) = \frac{Q(x)}{u} D_y(x)\, D_z(x) \tag{3.7}$$

where $D_y(x)$ and $D_z(x)$ represent the lateral and vertical dispersion factor, respectively. The subscripts p and s have been dropped because this and the following expressions are equal for both the primary and

the secondary substance. If horizontal transport is assumed to take place in one out of m_s wind direction sectors, then $D_y(x)$ within this sector is given by:

$$D_y(x) = \frac{m_s}{2\ \pi\ x} \tag{3.8}$$

and $D_y(x) = 0$ outside the sector. In the case of a homogeneous vertical distribution of the pollutant in the mixing-layer z_i, $D_z(x)$ is simply:

$$D_z(x) = \frac{1}{z_i} \tag{3.9}$$

For the dry deposition flux $F_d(x)$ (g m^{-2} s^{-1}) we obtain:

$$F_d(x) = C(x)\, v_d \tag{3.10}$$

where $C(x)$ and v_d both have to be formally defined for a reference height z above the surface.
The wet deposition flux $F_w(x)$ is defined by:

$$F_w(x) = \frac{Q(x)}{u} D_y(x)\, \Lambda_w \tag{3.11}$$

Time-averaged concentration and deposition in a receptor point due to a source at a distance x and in a direction φ is calculated by:

$$\overline{C}(x,\varphi) = \sum_{s=1}^{s_c} \sum_{m=1}^{m_s} \left[\frac{Q(x,s,m)}{u(s,m)} D_y(x)\, D_z(x,s,m)\, f(s,m) \right] \tag{3.12}$$

$$\overline{F_d}(x,\varphi) = \sum_{s=1}^{s_c} \sum_{m=1}^{m_s} \left[v_d(s,m)\, C(x,s,m)\, f(s,m) \right] \tag{3.13}$$

$$\overline{F_w}(x,\varphi) = \sum_{s=1}^{s_c} \sum_{m=1}^{m_s} \left[\frac{Q(x,s,m)}{u(s,m)} D_y(x)\, \Lambda_w(s,m)\, f(s,m) \right] \tag{3.14}$$

where $f(s,m)$ is the distribution function of wind-direction classes m_s and atmospheric stability/mixing height classes s_c for the period over which the averaging has to be carried out. Note that in all the above equations x refers to the real transport path length and that v_d and Λ_w in Eqs. (3.10) and (3.11) refer to deposition parameters at the receptor site while those in Eqs. (3.3) and (3.4) refer to parameters representative for the total trajectory.

3.2 Vertical mixing close to sources

A serious limitation for models assuming instantaneous vertical mixing in the mixing-layer is that concentrations due to emissions of low-level sources will be underestimated, while the effect of sources emitting at high levels can be overestimated. In Eulerian models this problem can be solved by defining

sublayers in the mixing-layer. For one-layer Lagrangian deposition models a correction factor is defined sometimes, representing the fraction of the emission that is directly deposited within the grid cell (Eliassen and Saltbones, 1983; Janssen and Asman, 1988). In some statistical LRT models immediate vertical mixing within the boundary layer is also assumed (Smith, 1981; Venkatram *et al*., 1982). Other authors use vertical distribution functions based on the K-diffusion theory (Bolin and Persson, 1975; Sheih, 1977; Fisher, 1978).
The problem of local dispersion is solved in this model by replacing $D_z(x) = 1/z_i$ in Eq. (3.9) by a Gaussian plume formulation, in which the vertical dispersion (for z=0) is described as a function of source height, mixing height and a stability-dependent vertical dispersion coefficient σ_z:

$$D_z(x) = \frac{2}{\sqrt{2\pi}\,\sigma_z}\left(\exp\left[\frac{-(2z_i - h)^2}{2\sigma_z^2}\right] + \exp\left[\frac{-(2z_i + h)^2}{2\sigma_z^2}\right] + \exp\left[\frac{-h^2}{2\sigma_z^2}\right] \right) \qquad (3.15)$$

where h is the effective source height. Equation (3.15) was selected to describe local vertical diffusion, mainly to achieve some compatibility with the 'National Model' in the Netherlands. Equation (3.15) gives the same value as $1/z_i$ within 1.5% for the entire range of h within the mixing layer when $\sigma_z > 1.6\ z_i$, so a gradual change from limited vertical dispersion to full mixing at larger distances is automatically obtained.

3.2.1 Local vertical dispersion

For an appropriate determination of the vertical dispersion parameter the turbulent state of the atmospheric boundary layer must be assessed. Most widely used is the approach of Pasquill (1961) and Gifford (1961). The Pasquill-Gifford scheme prescribes the quantitative relation between the stability of the atmosphere and insulation in combination with wind speed. The scheme has been deduced from experiments using sources near the ground. First versions of the present model (Van Jaarsveld, 1990) also used the Pasquill-Gifford scheme for dispersion and an empirical method for estimating stability similar to the Pasquill-Turner scheme (KNMI, 1972). Vertical dispersion was described as $\sigma_z = c_{z0}\, a\, x^b$, with c_{z0} a correction factor for surface roughness and a and b stability-class-dependent dispersion coefficients taken from TNO (1976). Turbulence typing schemes such as the Pasquill-Turner one are biased toward neutral stability when convective situations actually exist (Weil and Brower, 1984).
Kretzschmar and Mertens (1984) reviewed the turbulence typing schemes and corresponding dispersion algorithms of a number of Gaussian short-range models. They found that the predicted maximum concentration and also the distance of this maximum concentration differed between the models by one order of magnitude. In the present version of the model more recent concepts of the description of turbulence and dispersion in the boundary layer have been used. In such a concept the boundary layer is divided into a number of regimes, each characterised by distinct scaling parameters (Holtslag and Nieuwstadt, 1986; Gryning *et al*., 1987). The Holtslag and Nieuwstadt scheme is adopted here in a simplified form. The regimes distinguished are (see also Figure 3.1):

a. a surface layer with a height up to 0.1 z_i,
b. a convective mixing layer ($z_i/L < -10$ and $z/z_i > 0.1$)
c. a near neutral upper layer ($0 > z_i/L > -10$ and $z/z_i > 0.1$) and
d. a second near neutral layer above a stable surface layer ($0 < z_i/L$ and $z/z_i > 0.1$).

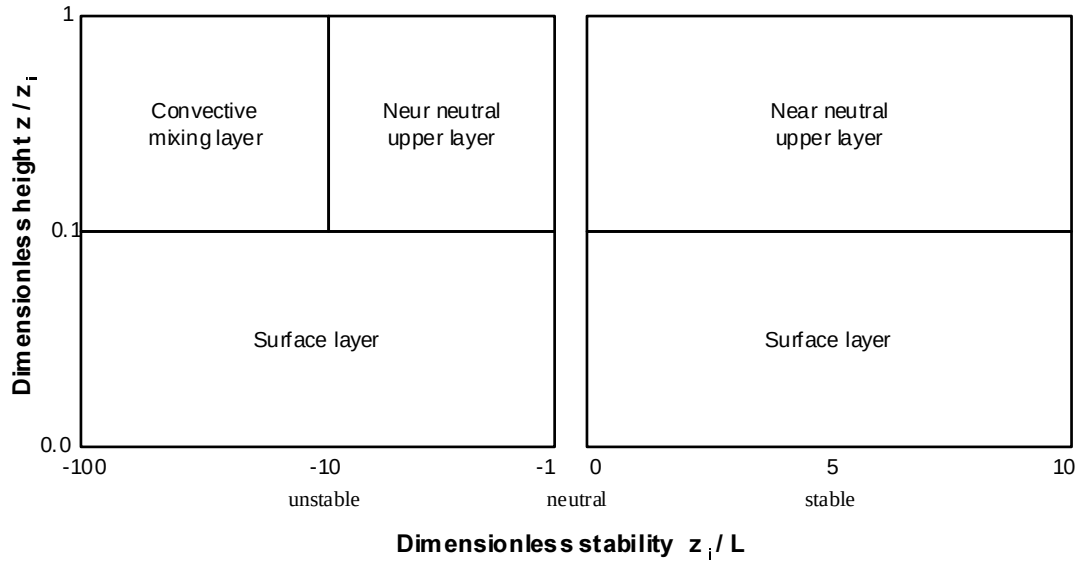

Figure 3.1 The scaling regions of the atmospheric boundary layer distinguished by the present model, and shown as function of the dimensionless height, z/z_i, and the stability parameter, z_i/L. This scheme is a simplified form of the Holtslag and Nieuwstadt scheme (1986).

a. *surface layer*

The effect of stability on the structure in this layer can be described by the Monin-Obukhov similarity theory. Nieuwstadt and Van Ulden (1978) have shown that the vertical dispersion from a ground-level source in this layer can be adequately described by K-models. The K-model can be derived from the diffusion equation (1.5) in combination with Eq. (1.6) when horizontal diffusion is neglected and a continuous cross-wind line source is assumed:

$$u \frac{\partial C}{\partial t} = \frac{\partial}{\partial z} K_z(z) \frac{\partial C}{\partial z} \tag{3.16}$$

Businger (1973) has shown that K_z can be adequately approximated by the diffusivity of heat:

$$K_z = \kappa \; u_* \; z \; / \; \psi_h(z / L) \tag{3.17}$$

where $\Psi_h(z/L)$ is the non-dimensional temperature gradient ($\Psi_h(z/L) = 0.74\ (1 - 9\ z/L)^{-1/2}$ for $L \leq 0$ and $\Psi_h(z/L) = 0.74 + 6.3\ z/L$ for $L > 0$). Note that the von Kármán constant κ in Eq. (3.17) is specified by Businger as 0.35, while for the rest of this work, κ is taken 0.4.
The K-model is usually solved numerically; however, analytical solutions for surface-layer K-models have also been given [OK?] Van Ulden, 1978). Instead of using a separate model for the surface layer, applying the K- proposed (e theory in combination with the Gaussian dispersion formulation given in Eq. (3.15) has been attempted. In fact, a Gaussian model is an analytical solution of the general diffusion equation for a continuous source in a situation with constant wind speed and diffusion, and where advection in the x direction is much more important than diffusion in this direction. Under these conditions σ_z can be related to the turbulent eddy diffusivity K_z (Pasquill, 1962):

$$\sigma_z^2 = 2\ K_z \; x / u \tag{3.18}$$

This relation suggests that σ_z increases with distance proportional to $x^{1/2}$, while dispersion experiments show that this is only so for large σ_z. This discrepancy is mainly caused by not taking into account the vertical dimensions of the plume. The larger the plume grows, the more eddies have an effect on it. This

is in fact what is suggested by the height dependence of K_z (Eq. 3.17). For (near) surface releases, u and K_z should be averaged over the plume height by integration because the centre of mass may rise above the release height. In the present case an iterative approach is followed, in which u and K_z are taken at a representative height equal to 0.67 σ_z and where u is derived from the wind speed at 10 m using the logarithmic profile of Eq. (2.3.18). In this way K_z becomes a function of x. The advantage of this approach is that effects of release height and z_0 can be explicitly taken into account, the latter through its effects on u and L. The error that is made by describing a non-Gaussian vertical distribution as Gaussian is not large.

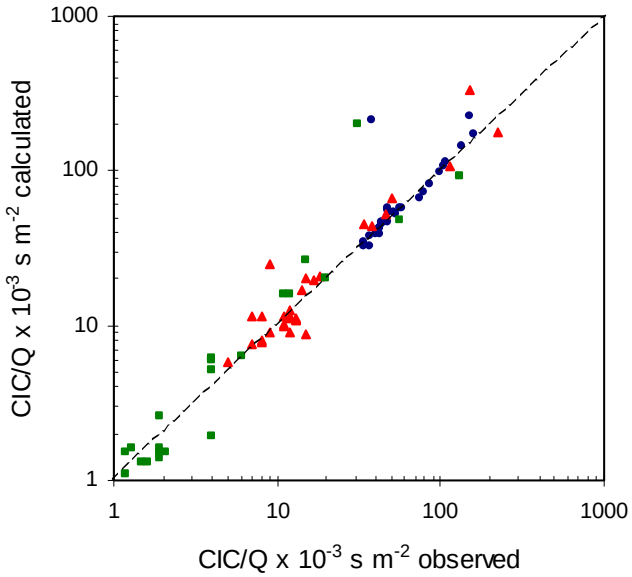

Figure 3.2 Comparison of calculated and measured cross-wind integrated concentration (CIC) divided by the source strength for three down-wind distances. Circles: 50 m. Squares: 200 m. Triangles: 800 m. The observational data, including u_* and L, are derived from the 'Prairie Grass' data by Van Ulden (1978).

The vertical diffusion from sources near the ground is tested using experimental data derived by Van Ulden (1978) from the 'Prairie Grass experiment' (Barad, 1958). Computed cross-wind integrated concentrations at distances of 50, 200 and 800 m from the source compare favourably with the observations as is shown in Figure 3.2. The comparison also indicates that the approach followed here has the same performance as the analytical scheme of Van Ulden (1978).

b. *convective mixing layer*

The dispersion process in the convective mixing layer is dominated by the asymmetric structure of turbulence (Gryning *et al*., 1987). Down draughts in this layer occupy a greater area than updraughts; therefore pollutants released from an elevated source have a higher probability of travelling downward than upward. A Gaussian dispersion approach is not suited for such cases. Several models have been proposed to describe the asymmetric behaviour e.g. the probability density function model (Misra, 1982; Venkatram, 1983; Weil and Brower, 1984) or the impingement model for buoyant sources (Venkatram, 1980b). Several advanced short-term short-range models, however, still use Gaussian dispersion for the convective mixing layer. Therefore for the present long-term model the Gaussian distribution was considered adequate.
Theoretical investigations by Deardorff (1972) and laboratory experiments by Willis and Deardorff (1974; 1978; 1981) indicate that turbulence and dispersion in a convective boundary layer are controlled by two important parameters: z_i and the convective velocity scale, w_*:

$$w_* = \left(\frac{g}{T}\frac{H_0}{\rho_a\ c_p}\ z_i\ \right)^{1/3} \tag{3.19}$$

Another aspect demonstrated by these experiments and also by large eddy simulations (Wyngaard and Brost, 1984) is that turbulent fluxes can be opposed to local concentration gradients. This phenomenon puts the applicability of eddy diffusion as a basis for dispersion description in this layer on very tenuous ground (Weil, 1985).
Several authors have proposed dispersion parameterisations on the basis of convective velocity scaling. Reviews on this subject are given by Weil (1985) and Briggs (1985). The formulation of Weil and Brower (1984) for convective to neutral cases is taken as suggested by Briggs (1985), reading:

$$\sigma_z = z_i\ X\left[\ (\sigma_{wc}\ /\ w_*)^2 + (\sigma_{wm}\ /\ w_*\ )^2\ \right]^{1/2} \tag{3.20}$$

where $X = (x/u)w_*/z_i$, and σ_{wc} and σ_{wm} are the standard deviations of the vertical velocity component due to convective activity and windshear (mechanical turbulence), respectively. For the convective limit, $\sigma_{wc}/w_* = 0.56$ (Kaimal *et al*., 1976) and the neutral limit, $\sigma_{wm} = 1.26u_*$ (Panowski *et al*., 1977). A similar formulation is used in the Danish OML model but with $\sigma_{wm} = 1.10u_*$ (Berkowicz *et al*., 1986).

c. and d. *upper near neutral layers*

The characteristics of dispersion in the near neutral upper layer have not been thoroughly investigated. Turbulence in this region is rather homogenous, enabling the use of a Gaussian plume formulation. Following Venkatram (1984) and Gryning *et al*. (1987) the estimate of the vertical spread is based on Taylor's theory, which relates σ_z to the standard deviations of the vertical wind fluctuations, σ_w. The relation can generally be written as

$$\sigma_z = \sigma_w\ t\quad f_z(\ t\ /\ \tau_L\ ) \tag{3.21}$$

where t is the travel time ($t = x/u$) and τ_L the Lagrangian time scale. A practical relation that matches the short and long time limits of statistical theory is:
Gryning *et al*. (1987) suggest time scales τ_L of 300 s for $L < 0$ and 30 s for $L > 0$. Their adopted

$$f_z\ (t\ /\ \tau_L) = (\ 1 + 0.5\ t\ /\ \tau_L\ )^{-1/2} \tag{3.22}$$

expressions for σ_w read:

$$(\sigma_w\ /\ u_*)^2 = 1.5\,[\ z/(-\kappa\ L)\ ]^{2/3}\ \exp(-2z/z_i) + (1.7 - z/z_i) \qquad (\ L \le 0\ )$$

$$(\sigma_w\ /\ u_*)^2 = 1.7(\ 1\ -\ z/z_i\ )^{3/2} \qquad (\ L \ge 0\ ) \tag{3.24}$$

The latter equation was proposed by Nieuwstadt (1984b) for horizontally homogeneous and stationary conditions. Vertical dispersion calculated for the near neutral upper layer matches those of the convective mixing layer at the boundary between the regions
($z/L = -10$) rather closely.

Comparison with observations

Computed cross-wind integrated concentrations have been compared with observations obtained in various field experiments with passive tracers. These observations, including the meteorological

parameters z_i, u_* and L, have been compiled by Gryning *et al*. (1987). The stack heights in the different experiments were 2 m, 10 m and 115 m and the downwind distance range at which concentrations were measured was
0.2 - 6.1 km. Figure 3.3 shows the results, split into the different stability regimes.

In general, the agreement is satisfactory, especially for the convective mixing layer and the near neutral upper layer. Concentrations in the surface layer seem to be underestimated for the 115-m source (lower part of the scatter diagram) and overestimated for the 2-m source (upper part of the diagram). The latter overestimation is not seen in the comparison with the Prairie Grass data (Figure 3.2).

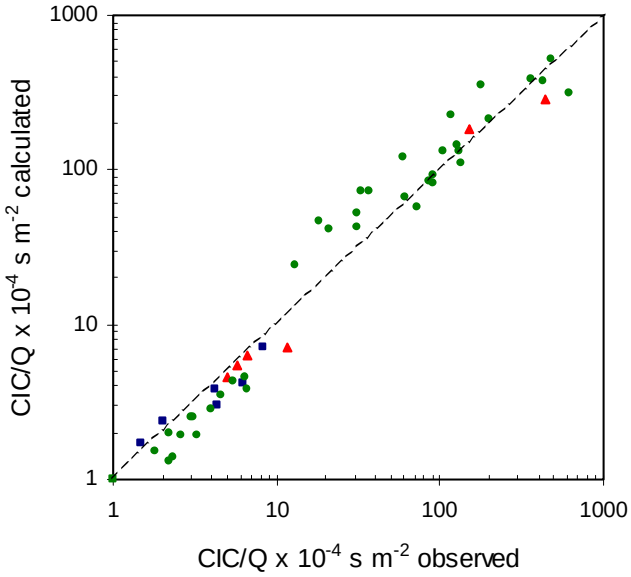

Figure 3.3 *Comparison of calculated and measured cross-wind integrated concentration (CIC) divided by the source strength. Circles: surface layer stability regime. Squares: convective mixing layer regime. Triangles: near neutral upper layer regime. Observational data from various experiments was compiled by Gryning et al. (1987).*

3.2.2 Plume rise

Many models are available for the calculation of the rise of hot effluent from stacks, e.g. final rise models as proposed by Briggs (1971, 1975) or Weil (1985). These models incorporate some of the more contemporary physics of the convective boundary layer. Two approaches have been applied in the OPS model, one based on Briggs (1971) and one based on Briggs (1975). The Briggs (1975) approach is described in Van Jaarsveld (1995). In general terms the Briggs (1971) approach is not only simpler but proved to provide better results after comparing model results with results of dispersion experiments. For this reason and because it is already applied for many years in the Dutch National Model (TNO, 1976) it is selected again for the present model.

The final plume rise Δh for convective and neutral conditions ($0 < L$ or $|L| > 50$ m) to be calculated as:

$$\Delta h = 38.8 \left(\frac{F_b}{u_{st}} \right)^{3/5} \qquad for \quad F_b \geq 55 \tag{3.25}$$

and

$$\Delta h = 21.1 \frac{F_b^{3/4}}{u_{st}} \qquad for \quad F_b > 55 \tag{3.26}$$

where u_{st} is the ambient wind speed at the stack top h_s and F_b the stack buoyancy flux. The stack buoyancy flux (in $m^4 s^{-3}$) is given by:

$$F_b = \frac{g}{\pi} V_f \left(1 - \frac{T}{T_s}\right) \qquad or \qquad F_b = 8.8\, Q_h \tag{3.27}$$

Here, V_f is the volumetric flow rate of the stack gas ($m^3 s^{-1}$), T the absolute ambient temperature at stack height and T_s the temperature of the stack gas. Qh is the heat output of the stack in MW.
For stable conditions the final rise is given by:

$$\Delta h = 2.6 \left(\frac{F_b}{s\, u_{st}}\right)^{1/3} \quad \text{with stability parameter } s = \frac{g}{T}\frac{\delta\theta}{\delta z} \tag{3.28}$$

where $\delta\theta/\delta z$ is the potential temperature gradient at stack level. $\delta\theta/\delta z$ at stack height may vary in dependence of stability in the surface layer. For lack of actual observations, an average value of 0.006 K m^{-1} is taken as representative for stable situations (TNO, 1976). Near the source the plume may not have reached its final plume rise. The initial plume rise is usually evaluated using a $x^{2/3}$ dependence. (e.g. Berkowicz et al., 1986). Under the assumption that on average the vertical rise goes faster than the (downward) vertical plume growth, the final plume rise is considered to be instantaneously reached..

3.2.3 Inversion penetration

The interaction of buoyant plumes with the top of the mixing layer can be described by models such as given by Manins (1979) or Briggs (1985). Both these relations assume a (thin) temperature inversion at z_i which can only be passed if the dissipation rate of the plume is still high enough after rising from h_s to z_i, but they differ strongly on the degree of penetration. Situations with strong (subsident) temperature inversions at low altitudes sometimes occur, leading to trapping of pollutants emitted by high stacks (Moore, 1987). Temperature jumps at z_i, with z_i as defined in section 2.3.3 are, however, rather small in most situations, especially under neutral conditions.
As described in section 2.2.3, a classification into stability and mixing-height classes has been chosen, mainly to include effects of vertical stratification on a local scale. One class (N1, local scale) includes, for example, mixing heights below 400 m, represented by a single harmonic mean height. The following simple distribution scheme has been chosen for such a situation with its ensemble mixing height:

$$f_m = \frac{z_i - (h_s + \Delta h)}{\Delta h} + c_i \qquad if \quad h_s \le z_i \tag{3.29}$$

$$f_m = \frac{z_i - (h_s + \Delta h)}{z_i} + c_i \qquad if \quad h_s > z_i \tag{3.30}$$

where f_m is the fraction of the plume in the mixing layer ($0 \le f_m \le 1$) and c_i an empirical constant representing the trapping effect. For neutral situations c_i is 0.5, indicating no trapping at all. In stable and unstable cases c_i is taken as 0.85. This distribution scheme only affects concentration in the mixing layer on a local scale. As is pointed out in section 2.2.2 plumes that are originally emitted above the mixing layer may enter the mixing layer at a later stage e.g. due to fumigation. It is assumed for these cases that plume heights do not change during transport above the mixing layer and also that vertical dimensions remain small.

3.3 Area sources

The dispersion of material from a source in the preceding sections is described for a source with no initial horizontal or vertical dimensions. In practice, however, it is seldom possible to treat all the sources in an certain area as point sources due to lack of detailed information. Also when the source is of the diffusive type e.g. ammonia evaporating from a pasture it is much more effective to treat the pasture as a single area source rather than splitting it up in numerous point sources.
When the heights of the different sources show an important variation, it is likely to include this variation in the source description as an initial vertical dispersion (Martin, 1971). For modelling concentrations inside and outside an area source, expressions like Eq. (3.15) can be applied, but both the vertical and horizontal distribution terms $D_z(x)$ and $D_y(x)$ have to be modified to introduce the special properties of the area source.

3.3.1 Horizontal dispersion for area sources

A point source will normally contribute to a receptor in only one wind sector, m, which is determined by:

$$m = \varphi \frac{m_s}{2\pi} + 1 \tag{3.32}$$

where φ is the source - receptor direction specified in radians. For area sources, however, contributions from more than one wind sector is possible. The horizontal dimension of an area source is introduced in the model by using the virtual point-source concept, where the virtual origin is put at a distance x_v upwind from the real position of the source (see Figure 3.4). This virtual distance depends on the number of wind-direction sectors which are applied in the model ($m_s = 12$):

$$x_v = \frac{m_s\, s_a}{2\pi} \tag{3.33}$$

where s_a is the diameter of the source. Replacing x by $(x + x_v)$ in Eq. (3.8) introduces the effect of the horizontal dimensions of the source into the description of the horizontal dispersion.

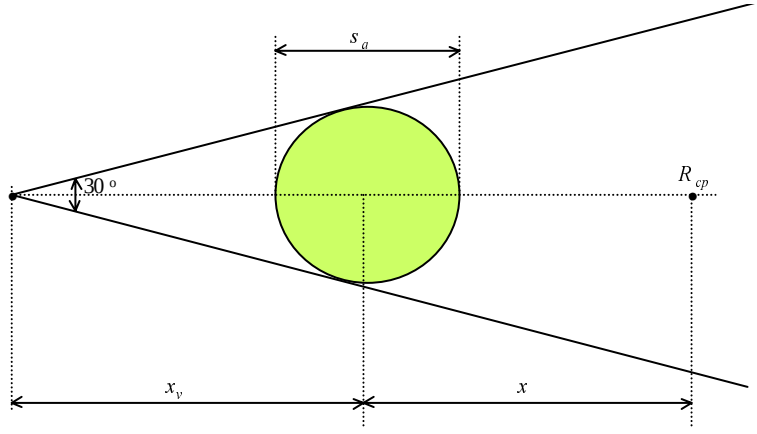

Figure 3.4 Area source represented by a virtual point source.

Another part of the problem is that an area source contributes more often to a given receptor point than a point source does. This is illustrated in Figure 3.5

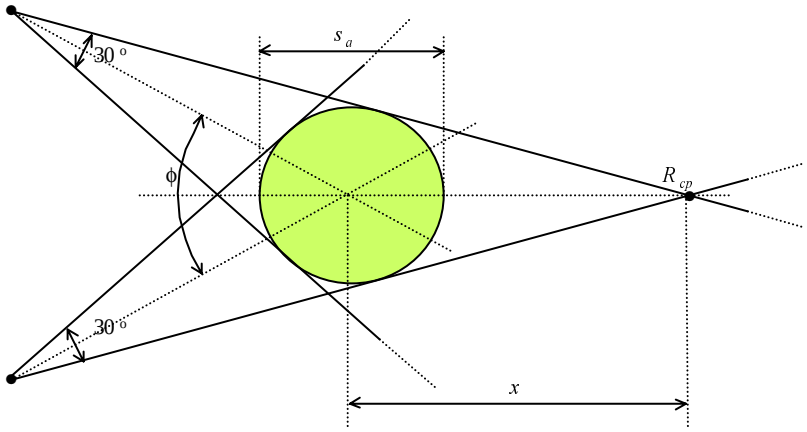

Figure 3.5 Wind directions for which an area source contributes to the concentration in a receptor point.

The wind direction angle for which influence from the area source to concentrations in a receptor point R_{cp} can be expected is indicated by ϕ. This angle can be calculated as:

$$\phi = \frac{2\pi}{m_s} + 2\ \arcsin\left(\frac{2x}{s_a}\right) \tag{3.34}$$

or in terms of contributing wind sectors n:

$$n = \frac{\phi}{\frac{2\pi}{m_s}} = 1 + \frac{m_s}{\pi}\ \arcsin\ \left(\frac{2x}{s_a}\right) \tag{3.35}$$

For very large distances ($x \rightarrow \infty$), n approaches 1, so an area source at that distance is seen as a point source. Another extreme case is when the receptor point is at the edge of the area source ($x = s_a/2$); the number of sectors then becomes: $n = 1 + m_s/2$, which means that using a classification in 12 sectors, the contributions of 7 wind-direction sectors have to be accumulated in determining an average concentration. Equation (3.35) is applied for x down to $s_a/2$. The maximum of seven contributing sectors is also applied for receptors within the area source. If the receptor is in the centre of the area source, the contribution of all sectors is taken into account, but with their total contribution reduced by a factor of 7/12.

3.3.2 Vertical dispersion for area sources

The virtual point source concept as used for the description of horizontal dispersion from sources with non-zero horizontal dimensions is in principle also suitable for the description of vertical dispersion if plumes have initial vertical dimensions. The corresponding virtual distance would then of course differ from x_v given in Eq. (3.33). The vertical plume dimension of a source with non-zero horizontal dimensions cannot be described by the virtual point source concept because $D_z(x)$ is a non-linear function of x. In the following an effective vertical dispersion parameter is derived which is used in the equation for $D_z(x)$ If one considers an area source as a source representing an infinite number of point sources, then the effective vertical distribution term at a distance x down-wind from the centre of the area source can be written as (see Figure 3.6):

$$D_z(x)\,eff = \frac{1}{r_2 - r_1} \int_{r_1}^{r_2} D_z(r)\,dr \qquad (r_1 \geq 0) \tag{3.36}$$

where $D_z(r)$ is the vertical distribution term for a point source at distance r down-wind as given by Eq. (3.15). r_1 is taken as zero when $r < s_a/2$.

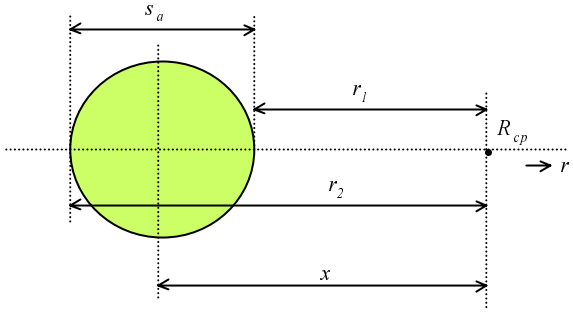

Figure 3.6 Schematic representation of an area source.

Under the condition that reflection against the top of the mixing layer is of minor importance ($z_i >> \sigma_z(r)$) and the source height is low ($\sigma_z(r) >> h$), then the above expression can be written as:

$$D_z(x)\,eff = \frac{1}{r_2 - r_1} \int_{r_1}^{r_2} \frac{2}{\sqrt{2\pi}} \frac{1}{\sigma_z(r)}\,dr \qquad (r_1 \geq 0) \tag{3.37}$$

In order to introduce a initial vertical distribution and also to express the vertical distribution in a more convenient parameter, the following form is chosen:

$$\frac{1}{\sigma_z(x)eff} = \frac{1}{r_2 - r_1} \int_{r_1}^{r_2} \frac{1}{\sigma_z(r) + \sigma_{zi}}\,dr \qquad (r_1 \geq 0) \tag{3.38}$$

where σ_{zi} represents the distribution of source heights within the area source. The vertical dispersion parameter $\sigma_z(r)$ in this model has the form $a\,r^b$. It is not possible to obtain a simple solution to the integral in Eq. (3.38) for all possible values of b. The following expression has been chosen as a practical approximation:

$$\sigma_z(x)\,eff = \left(\sigma_z(r_2) - \sigma_z(r_1)\right) \left[\ln\left(\frac{\sigma_{zi} + \sigma_z(r_2)}{\sigma_{zi} + \sigma_z(r_1)} \right) \right]^{-1} \tag{3.39}$$

Equation (3.39) is applied inside and outside the area source with a lower limit equal to s_a for r_2 and a lower limit equal to $h/8$ or 0.1 m for σ_{zi}. The resulting $\sigma_z eff$ is used in conjunction with (3.15). When $\sigma_z eff$ is compared with σ_z for a single point source as a function of down-wind distance then it appears that $\sigma_z eff$ is small and rather constant within the area source, rapidly increasing outside the area source and approaching to σ_z at a large distance.

3.4 References chapter 3

Barad M.L., editor (1958) Project Prairie Grass, a field program in diffusion.Volume 1, Geophysics Research Paper no. 59. Geophysics Research Directorate, Air Force Cambridge Research Center, Cambridge MA, USA.

Berkowicz R., Olesen H.R. and Torp U. (1986) The Danish Gaussian Air Pollution Model (OML): description, test and sensitivity analysis in view of regulatory applications. In: De Wispelaere C., Schiermeier F.A. and Gillani N.V., editors. *Air pollution modeling and its application V*. Plenum Press, New York. p. 453-482.

Bolin B., Aspling G. and Persson, C. (1974) Residence time of atmospheric pollutants as dependent on source characteristics, atmospheric diffusion processes and sink mechanisms. *Tellus* **26**, 185-195.

Briggs G.A. (1971) Some recent analyses of plume rise observation. Proceedings. 2nd Intern. Clean Air Congress, H.M. Englund and W.T. Berry (Eds.), Academic Press, New York, 1029-1032.

Briggs G.A. (1975) Plume rise predictions. In: *Lectures on Air Pollution and Environmental Impact Analysis*. American. Meteorological Society, Boston MA. 59-111.

Briggs G.A. (1985) Analytical parameterisations of diffusion: The convective boundary layer. *J. Climate Appl. Meteorol*. **24**, 1167-1186.

Businger J.A. (1973) Turbulent transfer in the atmospheric surface layer. In: Haugen D.A., editor. Workshop on Micrometeorology. AMS, Boston MA. p. 67-100.

Eliassen A. and Saltbones J. (1983) Modelling of long-range transport of sulphur over Europe: a two-year run and some model experiments. *Atmospheric Environment* **17**, 1457-1473.

Fisher B.E.A. (1978) The calculation of long term sulphur deposition in Europe. *Atmospheric Environment* **12**, 489-501.

Gifford F.A. (1961) Use of meteorological observations for estimating atmospheric dispersion. *Nuclear Safety* **2**, 47-51.

Gryning S.E., Holtslag A.A.M., Irwin J.S. and Sivertsen B. (1987) Applied dispersion modelling based on meteorological scaling parameters. *Atmospheric Environment* **22**, 79-89.

Holtslag A.A.M. and Nieuwstadt F.T.M. (1986) Scaling the atmospheric boundary layer. *Boundary-Layer Meteorol*. **36**, 201-209.

Janssen A.J. and Asman W.A.H. (1988) Effective removal parameters in long-range air pollution transport models. *Atmospheric Environment* **22**, 359-367.

Kaimal J.C., Wyngaard J.C., Haugen D.A., Cote O.R., Izumi Y., Caughey S.J. and Readings C.J. (1976) Turbulence structure in the convective boundary layer. *J. Atmos. Sci*. **33**, 2152-2169.

KNMI (1972) Klimatologische gegevens van Nederlandse stations. Frekwentietabellen van de stabiliteit van de atmosfeer. Royal Netherlands Meteorological Institute, De Bilt, the Netherlands.

Kretzschmar J.G. and Mertens I. (1984) Influence of the turbulence typing scheme upon cumulative frequency distributions of the calculated relative concentrations for different averaging times. *Atmospheric Environment* **18**, 2377-2393.

Manins P.C. (1979) Partial penetration of an elevated inversion layer by chimney plumes. *Atmospheric Environment* **13**, 733-741.

Martin D.O. (1971) An urban diffusion model for estimating long term average values of air quality. *J. Air Pollut. Control Assoc*. **21**, 16-19.

.Moore D.J. (1987) Conditions in which power stations contribute to high ground level SO2 concentrations in the U.K. *Atmospheric Environment* **21**, 1849-1855.

Nieuwstadt F.T.M. (1984b) The turbulent structure of the stable nocturnal boundary layer. *J. Atmos. Sci*. **41**, 2202-2216.

Nieuwstadt F.T.M. and Ulden A.P. van (1978) A numerical study on the vertical dispersion of passive contaminants from a continuous source in the atmospheric surface layer. *Atmospheric Environment* **12**, 2119-2124.

Panowski H.A. Tennekes H., Lenschow D.H. and Wyngaard J.C. (1977) The characteristics of turbulence velocity components in the surface layer under convective conditions. *Boundary-Layer Meteorol*. **11**, 355-361.

Pasquill F. (1961) The estimation of the dispersion of windborn material. *Meteorol. Mag*. **90**, 33-49.

Pasquill F. (1962) *Atmospheric Diffusion*. Van Nostrand, New York. p. 77.

Sheih C.M. (1977) Application of a statistical trajectory model to the simulation of sulfur pollution over northeastern United States. *Atmospheric Environment* **11**, 173-178.

Smith F.B. (1981) The significance of wet and dry synoptic regions on long-range transport of pollution and its deposition. *Atmospheric Environment* **15**, 863-873.

TNO (1976) Modellen voor de berekening van de verspreiding van luchtverontreiniging inclusief aanbevelingen voor de waarden van parameters in het lange-termijnmodel. Staatsuitgeverij, The Hague, the Netherlands.

Van Jaarsveld J.A. (1990) An operational atmospheric transport model for priority substances; specification and instructions for use. RIVM, Bilthoven, the Netherlands. Report no. 222501002.

Venkatram A. (1980b) Dispersion from an elevated source in a convective boundary layer. *Atmospheric Environment* **14**, 1-10.

Venkatram A. (1983) On dispersion in the convective boundary layer. *Atmospheric Environment* **17**, 529-533.

Venkatram A. (1984) The uncertainty in estimating dispersion in the convective boundary layer. *Atmospheric Environment* **18**, 307-310.

Venkatram A., Ley B.E. and Wong S.Y. (1982) A statistical model to estimate long-term concentrations of pollutants associated with long-range transport. *Atmospheric Environment* **16**, 249-257.

Weil J.C. (1985) Updating applied diffusion models. *J. Climate Appl. Meteorol*. **24**, 1111-1130.

Weil J.C. and Brower R.P (1984) An updated Gaussian plume model for tall stacks. *J. Air Pollut. Control Assoc*. **34**, 818-827.

Willis G.E. and Deardorff J.W. (1974) A laboratory model of the unstable planetary boundary layer. *J. Atmos. Sci*. **31**, 1297-1307.

Willis G.E. and Deardorff J.W. (1978) A laboratory study of dispersion from an elevated source within a modelled convective planetary boundary layer. *Atmospheric Environment* **12**, 1305-1311.

Willis G.E. and Deardorff J.W. (1981) A laboratory study of dispersion from a source in the middle of the convective mixed layer. *Atmospheric Environment* **15**, 109-117.

Wyngaard J.C. and Brost R.A. (1984) Top-down and bottom-up diffusion of a scalar in the convective boundary layer. *J. Atmos. Sci*. **41**, 102-112.

4. Removal processes

In this section deposition and transformation will be treated as processes both determining the life-time of pollutants in the atmosphere and having an effect on the vertical distribution of the pollutants in the lower part of the boundary layer. Specific velocities or rates for substances are discussed in Chapter 3.

4.1 Dry deposition

The vertical transport of atmospheric contaminants - either in gaseous or in particle form - to or from the underlying surface is governed by a number of processes. Some of these are determined by atmospheric properties common to all contaminants and others by specific physical and chemical properties of the gases in conjunction with properties of the surface. The vertical exchange flux F_d in this model is described as the product of a vertical velocity v_d specified for a height, z, and the difference in concentration at this height, C_a, and the surface or substrate concentration C_s:

$$F_d = v_d(z) [\ C_a(z) - C_s\ ] \tag{4.1}$$

For substances which immediately react at the surface with other substances or for substances attached to particles, C_s may be considered zero. However, for substances such as persistent organic compounds, C_s may be so high under specific conditions that the vertical flux is upward (Van Jaarsveld *et al*., 1994). In that case Eq. (4.1) describes the emission flux. For gases such as nitrogen oxide (NO) this may be the case for most ecosystems (Duyzer and Fowler, 1994). In an electrical analogue $v_d(z)$ can be represented as a contaminant conductivity, which can be expressed as the inverse of three resistances:

$$v_d(z) = [\ R_a(z) + R_b + R_c\ ]^{-1} \tag{4.2}$$

The sequence of the three resistances represents the resistances in the three stages of vertical transport, i.e. (1) for the turbulent layer, the aerodynamic resistance R_a, (2) for the layer immediately adjacent to the surface, the pseudo-laminar resistance layer R_b, and for the receptor the surface resistance R_c. The resistance R_a depends mainly on the local atmospheric turbulence, whereas R_b depends on both turbulence characteristics and molecular diffusion of the contaminant considered. Substance and receptor characteristics determine R_c, which for vegetation can be seen as the replacement resistance of a number of other resistances such as stomatal, mesophyll, cuticular and water-layer resistances (Erisman, 1992). In the case of deposition to water or bare soil, R_c represents all resistances due to diffusion and transport in the water or soil column. During pre-processing the meteorological data, hourly R_c values are calculated for SO_2 because for this component a strong relation with specific conditions such as the presence of a snow cover is assumed. In Chapter 3 more details are given on specific choices of R_c values.
Hicks *et al*. (1989) assume that the atmospheric resistance to transport of gases and small particles is similar to that of heat. Here Wesely and Hicks (1977) are followed; they approximate R_a by:

$$R_a(z) = \frac{1}{\kappa u_*} [\ \ln(\frac{z}{z_0}) - \psi_h(\frac{z}{L}) + \psi_h(\frac{z_0}{L})\ ] \tag{4.3}$$

where $\psi_h(z/L)$ is the stability correction for heat (Beljaars and Holtslag, 1990), see also section 3.2.1.
Investigations of the pseudo-laminar layer resistance show that R_b is strongly influenced by the diffusivity of the material being transferred and the rigidity of a rough surface (Garratt and Hicks, 1973; Brutsaert, 1975). The value of R_b is approximated by Wesely and Hicks (1977); Hicks *et al*. (1987):

$$R_b = \frac{2}{\kappa u_*}\left(\frac{N_{Sc}}{N_{Pr}}\right)^{\frac{2}{3}} \tag{4.4}$$

where N_{Sc} and N_{Pr} are the Schmidt and Prandtl numbers respectively. N_{Pr} is ~0.72, while N_{Sc} is defined as: $N_{Sc} = \upsilon/D_g$, with υ being the kinematic viscosity of air ($\tilde{}$0.15 x 10^{-2} m^2 s^{-1}) and D_g the molecular diffusivity in air. The pre-processor of the model calculates R_b for SO_2 only. Since the ratio of diffusion coefficients in air for different substances is proportional to the root of their molecule masses M_m, the ratio of their R_b values can be expressed as:

$$R_{b_i} = R_{b_j}\left(\frac{M_{m_i}}{M_{m_j}}\right)^{\frac{1}{3}} \tag{4.5}$$

where the subscripts $_i$ and $_j$ denote substances $_i$ and $_j$.
Through the depletion of material at the surface, a process of material redistribution within the mixing layer will be induced. This redistribution will be driven by vertical turbulent diffusion or, inversely, limited by the aerodynamic resistance of the lower part of the mixing layer. The result is that the concentration at the surface will decrease more than the average concentration in the mixing layer. Vertical concentration gradients can be very strong, especially for substances which have a low surface resistance or during stable atmospheric conditions, when $R_a(z)$ is very large. Measurements at the Cabauw meteorological tower (Van Dop *et al.*, 1980; Onderdelinden *et al*., 1984) confirm the existence of large gradients. For SO_2 under stable night-time conditions, for example, a ratio between the concentration at the 4-m level and the 100-m level of about 0.3 was found.
To take the surface effect fully into account, Horst (1977) developed a so-called surface depletion model. In this model he introduced small negative sources at the surface - representing the material lost by dry deposition - and calculated the resulting concentration profile as the sum of the contribution of the undepleted source and the contributions of the negative sources. Since the resulting concentration has to be determined numerically, the method is time consuming and as such is not suited for an analytical model as described here. The chosen approach for this model can be described as 'source depletion with surface correction'.
In a steady-state situation, the vertical deposition flux F_d in the lower boundary layer can be considered as independent of height:

$$F_d(z_2) = F_d(z_1) \tag{4.6}$$

or (assuming $C_s = 0$):

$$v_d(z_2)\,C(z_2) = v_d(z_1)\,C(z_1) \tag{4.7}$$

The concentration ratio between the two levels z_1 and z_2 can then be given as (Van Egmond and Kesseboom, 1983):

$$\frac{C(z_1)}{C(z_2)} = \frac{R_a(z_1) + R_b + R_c}{R_a(z_2) + R_b + R_c} \tag{4.8}$$

Scriven and Fisher (1975) describe the relation of v_d with height in a similar way, however, without the stability corrections which are applied for the calculation of $R_a(z)$. For situations where the gradient is not fully developed, i.e. close to a source or when stability goes from unstable to stable, it is assumed that the atmosphere is acting in analogy to an electric capacitor which is unloaded by a resistor. The first-order time constant, τ, for such a circuit can be characterised by a simple R_cC_c value, where R_c is the electrical

equivalent for the aerodynamic resistance over a layer and C_c the electrical equivalent for the height of that layer. The distance-dependent profile can now be given as:

$$\frac{C(x,z_1)}{C(x,z_2)} = 1 - \left(1 - \frac{R_a(z_1) + R_b + R_c}{R_a(z_2) + R_b + R_c}\right)\left(1 - \exp\left[\frac{-t}{\tau}\right]\right) \tag{4.9}$$

in which:

$$t = \frac{x}{u} \quad \text{and} \quad \tau = (z_2 - z_1)\,(R_a(z_2) - R_a(z_1)) \tag{4.10}$$

Since $R_a(z)$ is not a linear function of z, the time constant τ will also be height dependent. Nevertheless, for reason of simplicity, a single height of 50 m was chosen for z_2 in line with Van Egmond and (1983b). This height may be considered as an upper limit for very stable situations since the nocturnal boundary layer height in such situations is also of the order of 50 m (Nieuwstadt, 1984). Values for τ can range from minutes, in the case of unstable atmosphere, to more than 10 hours in case of stable situations. In the latter case the stationary condition is, in fact, never reached within the usual duration of a stable period.

4.1.1 Source depletion

In a source depletion model, the loss of airborne material due to deposition is accounted for by appropriately reducing the source strength as a function of down-wind distance. This is what is actually described by Eqs. (3.5) and (3.6) for the distant independent parameters u, z_i and removal rates. A more general expression for Eq. (3.5) is (dry deposition only):

$$Q(x) = Q_0 \exp\left[-\int_0^x \frac{v_d(z)}{\bar{u}} D_z(x)\,dx\right] \tag{4.11}$$

where Q_0 is the undepleted source strength at $x = 0$. As pointed out earlier, the expression $D_z(x)$ depends on the ratio σ_z/z_i, resulting in either Eq. (3.9) or (3.15). In addition, the mixing height z_i has a tendency to increase with distance, also resulting in an increasing transport velocity $\bar{u}$. Therefore, the integral in Eq. (4.11) cannot be solved analytically for the entire range of x, but has to be split in two or more parts, representing the different stages in plume development from source to receptor. For this reason three stages are distinguished:

I. Transport within an area source. The vertical dispersion within such a source is characterised by $\sigma_{z\ eff}(x)$ (Eq. 3.39). This effective vertical dispersion parameter is almost independent of the position within the area source. Therefore $D_z(x)$ is approached by:

$$D_z(x) = \frac{2}{\sqrt{2\pi}\ \sigma_{z\ eff}\left(x = \frac{s_a}{2}\right)} \tag{4.12}$$

II. The phase where the plume is not yet uniformly mixed in the mixing layer. This stage starts at $x = 0$ in case of a point source or at $x = s_a/2$ in the case of an area source. A separate description of this phase is especially important for low-level sources because of the enhanced ground-level concentrations close to the source. $D_z(x)$ is given by Eq. (3.15). When the reflection against the top of the mixing layer is neglected at this point (Eq. 3.15 is dominated by the last term anyway), $D_z(x)$ can be written as:

$$D_z(x) = \frac{2}{\sqrt{2\pi}\,\sigma_z} \exp\left[\frac{-h^2}{2\sigma_z^2}\right] \tag{4.13}$$

III. The phase where the plume is uniformly mixed in the mixing layer. This phase starts at a distance x_b from the source, where σ_z equals the (local) mixing height z_i. This distance is usually smaller than 50 km. Applying Eq. (3.9) for $D_z(x,h)$ in Eq. (4.11) results in:

$$D_z(x) = \frac{1}{z_{i\max}} \tag{4.14}$$

As is pointed out in section 2.2, the mixing height $z_{i\,max}$ is a function of the transport distance x. Transport times can be of the order of days, where several diurnal cycles in mixing height and aerodynamic resistances can occur. To compensate for these effects on the source depletion ratio, $Q(x)$ is corrected with a factor $f_d(x,h)$ (see section 2.3.4 and Eq. 2.3.27), which is determined in the meteorological pre-processor.

For the three phases of the plume various transport velocities are applied, depending on the height of the centre of the plume mass. Also the height for which v_d is specified is taken as phase-dependent. In principle v_d has to be specified for the lowest height, where the vertical concentration distribution is not yet disturbed by the dry deposition process. In phase I where the plume has a distinct Gaussian vertical shape, v_d is taken at z = 1 m. For phase III v_d is taken at z = 50 m, while for phase II v_d is linearly interpolated between the values of phases I and II. The vertical profile correction (Eq. 4.9) is started at the beginning of phase II but has most of its effects in phase III. Further details on the source depletion approach are given in Van Jaarsveld (1995).

The source depletion ratio at a (large) distance from an area source, due to dry deposition, is calculated as the product of the depletion ratios in the different stages of plume development. This depletion ratio is applied in Eq. (3.7) in combination with similar depletion ratios for wet deposition and chemical conversion.

4.2 Wet deposition

Although the wet deposition process is complex, an attempt has been made to use as simple a parameterisation as possible, which can be applied more-or-less universally for both long-range transport and more local deposition. Two main scavenging processes are distinguished in this model: below-cloud scavenging and in-cloud scavenging. Below-cloud scavenging is important for scavenging from plumes close to sources in situations where there is no interaction with clouds yet. In general, however, in-cloud processes are responsible for the highest wet deposition loads (Hales, 1978).

4.2.1 In-cloud scavenging

Natural storms are complex in their microphysical and dynamical structure and relations between concentrations in precipitation and the surrounding air are very variable (Barrie, 1992). Modelling of the precipitation process in transport models is usually done using either linear scavenging ratios or a numerical approach, including all the physical and chemical details of the process; there are hardly any solutions in between. The present model describes the in-cloud scavenging as a statistical process rather than as single events. The process is viewed as a discontinuous flow reactor in which chemicals in air entering a precipitation system are transferred to other chemicals and/or precipitation. At a large distance

from the source, where the pollutant is well vertically mixed and has also had the opportunity to penetrate into the cloud base, the scavenging coefficient of a pollutant Λ (h^{-1}) is given by:

$$\Lambda = \frac{W\ R_i}{z_i} \tag{4.15}$$

where R_i is the precipitation intensity (m h^{-1}) and W the ratio between the (initial) concentration in precipitation and the (initial) concentration in air, both on a weight/volume basis and at the ground level. This formulation, when used with an empirically determined W, integrates, in fact, all the processes in and below the cloud.

4.2.2 Below-cloud scavenging

This process is only taken into account in the first few kilometres down-wind from a source; in the further transport stage the scavenging process is treated as a in-cloud process parameterised with a bulk scavenging ratio. For short transport distances - where there is generally still no interaction between a plume and clouds - the scavenging of gases is determined by the flux of pollutant to falling raindrops (below-cloud scavenging). Local below-cloud scavenging of secondary-formed products is ignored because the contribution to total scavenging will be very low.

Reversibly soluble gases
When concentrations in air and raindrops are in (near) equilibrium during the scavenging process due to limited solubility and/or slow reactions in the drop, an expression similar to (4.20) is used; however, with a correction for the concentration in air at the ground:

$$\Lambda_b = \frac{W\ R_i}{z_i} \frac{C(z=0)}{\overline{C(z)}} \tag{4.16}$$

where $C(z)$ is the average mixed-layer concentration. W in this case could be replaced by the effective dimensionless Henry's Law constant of the gas in question. This solution ignores any vertical redistribution of plumes as is the case when the equilibrium is not instantaneous. An example of a reversibly soluble gas is SO_2. This gas is slowly converted to bisulphite (HSO_3^-) in falling raindrops and the SO_2 concentration in the drops is in (near) equilibrium with the surrounding air (Barrie, 1978). The approach followed here implies that as long as elevated SO_2 plumes do not touch the ground close to the source, they have no impact on wet deposition. This is confirmed by washout experiments (Ten Brink *et al*., 1988).

Irreversibly soluble gases
For irreversibly soluble gases the flux to falling raindrops is limited by the molecular diffusion of the gas in air and not by the flux of the species in the drop itself or the concentration of species in the drop (Levine and Schwartz, 1982). The wet deposition rate then becomes a function of the drop-size spectrum where small drops are responsible for a large fraction of the overall scavenging (Marshall and Palmer, 1948). This model uses the parameterisation of Janssen and Ten Brink (1985), who related Λ_b to the precipitation intensity using the drop-size spectrum of Best (1950):

$$\Lambda_b = \alpha_1\ D_g^{\alpha_2}\ R_i^{\alpha_3} \tag{4.17}$$

where D_g is the molecular diffusion coefficient of the species in air ($cm^2\ s^{-1}$) and α_1, α_2 and α_3 parameters depending on the drop-size distribution. For a lower limit of the drop-size distribution of 0.125 mm, α_1 has a value of 1.21, $\alpha_2 = 0.744$ and $\alpha_3 = 0.628$; D_g is expressed in $cm^2 s^{-1}$, R_i (here) in mm h^{-1} and Λ_b in h^{-1}. The below-cloud scavenging rate during precipitation for a highly soluble gas like HCl will, according to

Eq. (4.17), amount to 0.45 h^{-1} (D_g = 0.19 cm^2 s^{-1} and R_i = 1.5 mm h^{-1}). In contrast to elevated SO_2 plumes, irreversibly soluble gases such as HCl show a maximum wet deposition flux within a few hundred metres. This is also in agreement with results of the washout experiments of Ten Brink *et al*. (1988).

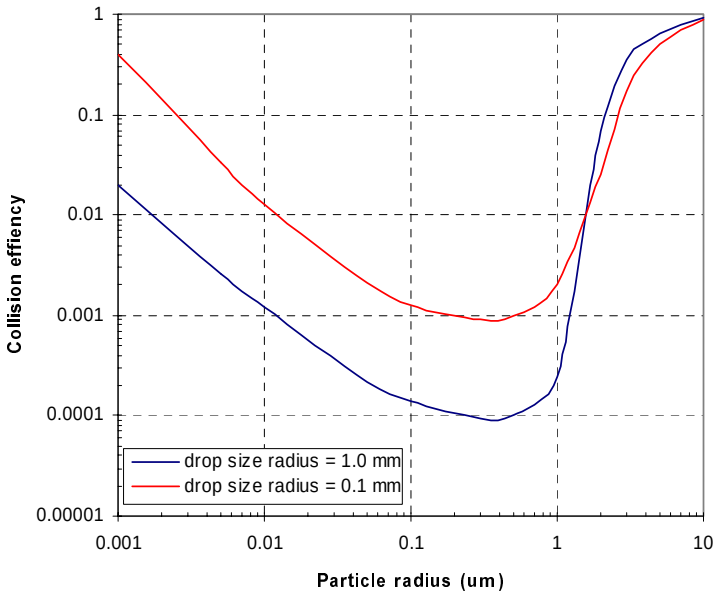

Figure 4.1 *Semi-empirical relation between the collision efficiency ε and collected particle sizes for two drop sizes (Slinn, 1983).*

Below-cloud scavenging of particles.
Wet scavenging of aerosols is an efficient process (Slinn, 1983). Falling raindrops collide with aerosol particles and collects them. Basic mechanisms are impaction, interception and Brownian motion, indicating that there is a strong dependency on particle size as well as drop size. For the below-cloud scavenging of particles an expression given by Janssen and Ten Brink (1985) has been adopted, which is similar to that of irreversibly soluble gases:

$$\Lambda_b = \alpha_4 \varepsilon R_i^{\alpha_5} \tag{4.18}$$

where α_4 and α_5 are drop-size distribution dependent parameters and ε is the particle-droplet collision efficiency, which is a function of both particle size and droplet size. For the same conditions as defined for Eq. (4.17), α_4 has a value of 1.326 and α_5 = 0.816. The ε values used have been given by Slinn (1983) as a function of droplet size and range for 1 mm droplets from unity for large particles (> 10 μm) down to 10^{-4} for particles in the 0.1-1 μm diameter range. In Figure 4.1, ε is plotted as a function of particle size and drop size using semi-empirical relations given by Slinn (1983). The ε values used in the TREND model are also derived from the Slinn relations.

4.2.3 Local effects of in-cloud scavenging

The combined below- and in-cloud scavenging rate calculated using Eq. (4.20) is usually much higher than the below-cloud scavenging rate. On the other hand, in-cloud scavenging can only have effect if the pollutant is able to penetrate clouds. Plumes from high stacks and especially those with additional plume rise will be sucked more into convective clouds then surface-based plumes. The time scale on which plumes reach the cloud base is tentatively taken as the time in which the vertical dimension of plumes

will grow equal to the difference between the effective plume height and the assumed cloud base height, where the cloud base height is taken equal to the mixing height. In addition a processing time within the cloud is assumed of the order of 0.5 hours before full in-cloud scavenging can take place. This results in the following expression, describing the gradual change from below-cloud scavenging only to a combined below- and in-cloud scavenging:

$$\Lambda_w = \Lambda\ pr + \Lambda_b\ (1 - pr) \quad \text{with} \quad pr = exp\left[- \frac{(h' + 100\ )^2}{2\ \sigma_z^2\ c_w} \right] \tag{4.19}$$

where h' and c_w are defined as:

$$\begin{aligned} &\text{point sources :} && h' = z_i - h; && c_w = 1 \\ &\text{within area sources :} && h' = z_i - h + \sigma_z\ (\frac{s_a / 2 - x}{s_a / 2} - 1\ ); && c_w = 3 \\ &\text{outside area sources :} && h' = z_i - h - \frac{s_a^3}{1600\ x^2}; && c_w = 1 \end{aligned} \tag{4.20}$$

4.2.4 Effects of dry and wet periods on average scavenging rates

The scavenging rates as defined so far refer to situations during precipitation events. What really needs describing is the wet deposition as an average for a large number of cases, including situations with no precipitation at all and situations with extended rainfall. When significant amounts of a pollutant are removed by single precipitation events then we cannot simply use a time-averaged scavenging rate but have to account for the statistical distribution of wet and dry periods (Rodhe and Grandell, 1972). Here, it is assumed that rain events occur according to a Poisson distribution. The change in airborne pollutant mass M in time due to wet deposition is then found as (Van Egmond *et al.*, 1986):

$$\frac{d\ M}{dt} = - \frac{M}{(\tau_w + \tau_d\ )} [\ 1 - \exp(-\Lambda_w\ \tau_w\ )\ ] \tag{4.21}$$

with τ_w being the average length of rainfall periods and τ_d the average length of dry periods, related to the probability of wet deposition P_p by $P_p = \tau_w/(\tau_w + \tau_d)$. The resulting effective scavenging rate is given by:

$$\Lambda_{\ w\,eff} = \frac{P_p}{\tau_w} [\ 1 - \exp(-\Lambda_w\ \tau_w\ )\ ] \tag{4.22}$$

P_p and τ_w are determined from hourly observations of rainfall amount and duration at 12 stations, where rainfall duration is measured with a 6-min resolution. In the current version of the model P_p and τ_w are used with no spatial variation. Dependency on wind direction and stability is, however, taken into account. It should be pointed out in this context that values for τ_w and P_p are derived from Eulerian rainfall statistics, while they are used for a characterisation of wet deposition in a Lagrangian reference frame. Hamrud *et al.* (1981) found little difference between Eulerian and Lagrangian statistics by following trajectories along observation sites. Because they based their conclusions on data with a 6-h resolution, it is not certain that these findings are also valid for our case with the higher time resolution. Due to lack of more information the Lagrangian (τ_w) and Eulerian (τ_{we}) lengths of rainfall periods are taken to be equal.

Monthly mean P_p values calculated from 12-year KNMI observations vary from 0.040 in August to 0.10 in December; τ_{we} values vary from 1.3 h in August to 2.5 h in March. Rodhe and Grandell (1972) found much higher τ_{we} values in Sweden: 9 h in winter and 4 h in summer. However, they based their calculations on two-hourly values of precipitation amounts. If the model is fed by 6-hourly synoptical data, then it is not possible to calculate τ_w from the data. In such a case fixed monthly values are used, derived from the above mentioned KNMI data.
A boundary condition for using Eq. (4.22) at short distances is that at $x = 0$, Λ_{weff} be equal to $P_p \Lambda_w$. The right asymptotic behaviour of Eq. (4.22) is obtained by limiting τ_w to the travel time x/u using the following expression:

$$\tau_w = \tau_{we} [\ 1 - \exp(-\frac{0.4\ \frac{x}{u}}{\tau_{we}})\ ] \qquad (4.23)$$

The approach for calculating effective deposition rates on the basis of Poisson-distributed dry and wet periods as given here is checked against average rates obtained from a so-called brute force approach in section 4.2.
This model requires as input, W at the beginning of a shower (Eq. 4.15). On the basis of Poisson distributed dry and wet periods, Van Jaarsveld and Onderdelinden (1986) have given a relation between this W and W's derived from measurements of average concentrations in air and rain:

$$W_{avg} = \frac{z_i}{R_i \tau_w} [\ 1 - \exp(-\frac{W R_i}{z_i} \tau_w)\ ] \qquad (4.24)$$

This relation sets of a clear upper limit on average scavenging ratios. Assuming z_i = 1000 m, R_i = 1.3 mm h^{-1}, τ_w = 2.7 h and $W \rightarrow \infty$, W_{avg} will be 2.8 x 10^5. Much higher W_{avg} values derived from measurements may indicate erroneous results. For substances very effectively scavenged ($W \rightarrow \infty$), Λ_{weff} will become equal to $1/(\tau_w + \tau_d)$. This means that wet deposition will be determined by the number of rain events in a certain period rather than by the amount or duration of rainfall.
It might be clear that any form of reactive scavenging in this model is based on empirical parameters derived from present situations. This is in particular the case for SO_2. Extrapolating to situations very different from those where parameters were derived can lead to significant errors in the computed wet deposition.

4.3 Chemical transformation

In the OPS model one primary and up to two secondary species are transported simultaneously. In case of sulphur and reduced nitrogen one primary (SO_2 and NH_3, respectively) and one reaction product is transported (SO_4^{2-} and NH_4^+, respectively) while for oxidised nitrogen one primary ($NO + NO_2 = NO_x$) and two reaction products (HNO_3 and NO_3^-) are transported.
No special local dispersion and deposition effects are taken into account for reaction products because these products will be formed gradually after the primary pollutant is emitted into the atmosphere. Conversion rates can be parameterised as functions of parameters such as global radiation, temperature, time of day or others included in the climatological data set created by the pre-processor (Table 2.1). It is not possible to use conversion rates in dependence of absolute species concentrations since concentration distributions of sources are calculated independently.

4.4 References chapter 4

Barrie L.A. (1978) An improved model of reversible SO_2-washout by rain. *Atmospheric Environment* **12**, 407-412.

Barrie L.A. (1992) Scavenging ratios: black magic or a useful scientific tool? In: Schwartz S.E. and Slinn W.G.N, editors. *Precipitation scavenging and atmosphere-surface exchange*, Volume 1. Hemisphere Publ. Corp., Washington. p. 403-419.

Beljaars A.C.M. and Holtslag A.A.M. (1990) A software library for the calculation of surface fluxes over land and sea. *Environ. Software* **5**, 60-68.

Duyzer J.H. and Fowler D. (1994) Modelling land atmosphere exchange of gaseous oxides of nitrogen in Europe. *Tellus* **46B**, 353-372.

Erisman J.W. (1992) Atmospheric deposition of acidifying compounds in the Netherlands. [PhD thesis]. Utrecht University, the Netherlands.

Garratt J.R. and Hicks B.B. (1973) Momentum, heat and water vapour transfer to and from natural and artificial surfaces. *Q. J. R. Meteorol. Soc.* **99**, 680-687.

Hales J.M. (1978) Wet removal of sulfur compounds from the atmosphere. *Atmospheric Environment* **12**, 389-399.

Hamrud M., Rodhe H. and Grandell J. (1981) A numerical comparison between Lagrangian and Eulerian rainfall statistics. *Tellus* **33**, 235-241.

Hicks B.B., Baldocchi D.D. Meyers T.P., Hosker Jr. R.P. and Matt D.R. (1987) A preliminary multiple resistance routine for deriving dry deposition velocities from measured quantities. *Water Air Soil Pollut*. **36**, 311-330.

Hicks B.B., Matt D.R. and McMillen R.T. (1989) A micrometeorological investigation of surface exchange of O_3, SO_2 and NO_2: a case study. *Boundary-Layer Meteorol*. **47**, 321-336.

Horst T. W. (1977) A surface depletion model for deposition from a Gaussian plume. *Atmospheric Environment* **11**, 41-46.

Janssen A.J. and Brink H.M. ten (1985) De samenstelling van neerslag onder een rookgaspluim: modellering, berekening en validatie. Netherlands Energy Research Foundation, Petten, the Netherlands. Report ECN-170.

Levine S.Z. and Schwartz S.E. (1982) In-cloud and below-cloud scavenging of nitric acid vapor. *Atmospheric Environment* **16**, 1725-1734

Marshall J.S. and Palmer M.W.M. (1948) The distribution of raindrops with size. *J. Meteorol.* **5**, 165-166.

Nieuwstadt F.T.M. (1984) Some aspects of the turbulent stable boundary layer. *Boundary-Layer Meteorol.* **30**, 31-55.

Onderdelinden D., Jaarsveld J.A. van and Egmond N.D. van (1984) Bepaling van de depositie van zwavelverbindingen in Nederland. RIVM, Bilthoven, the Netherlands. Report no. 842017001.

Rodhe H. and Grandell J. (1972) On the removal time of aerosol particles from the atmosphere by precipitation scavenging. *Tellus* **XXIV**, 442-454.

Scriven R.A. and Fisher B.E.A. (1975) The long range transport of airborne material and its removal by deposition and washout - I. General considerations. *Atmospheric Environment* **9**, 49-58.

Slinn W.G.N (1983) Predictions for particle deposition to vegetative surfaces. *Atmospheric Environment* **16**, 1785-1794.

Ten Brink H.M., Janssen A.J. and Slanina J. (1988) Plume wash-out near a coal-fired power plant: measurements and model calculations. *Atmospheric Environment* **22**, 177-187.

Van Dop H., Ridder T.B., Tonkelaar J.F. den and Egmond N.D. van (1980) Sulfur dioxide measurements on the 213 metre tower at Cabauw, the Netherlands. *Atmospheric Environment* **14**, 933-946.

Van Egmond N.D. and Kesseboom H. (1983) Mesoscale air pollution dispersion models I: Eulerian Grid Model. *Atmospheric Environment* **17**, 257-265.

Van Egmond N.D., Jaarsveld J.A. van and Onderdelinden D. (1986) The Dutch aerosol study: general overview and preliminary results. In:Lee S.D, Schneider T., Grant, L.D. and Verkerk P.J., editors. In: *Aerosols: Research, Risk Assessment and Control Strategies*. Lewis Publ., Chelsea, USA. p. 269-282.

Van Jaarsveld J.A., Aalst R.M. van and Onderdelinden D. (1986) Deposition of metals from the atmosphere into the North Sea: model calculations. RIVM, Bilthoven, the Netherlands. Report no. 842015002.

Van Jaarsveld J.A., Pul W.A.J. van and Leeuw F.A.A.M. de (1994) Modelling the long range transport and deposition of persistent organic pollutants over Europe and its surrounding marine areas. In: Gryning S.E. and Millán M.M., editors. *Air pollution modelling and its application X*. Plenum Press, New York. p. 143-155.

Van Jaarsveld J. A. (1995) Modelling the long-term atmospheric behaviour of pollutants on various spatial scales. Ph.D. Thesis, Utrecht University, the Netherlands

Wesely M.L. and Hicks, B.B. (1977) Some factors that effect the deposition rates of sulfur dioxide and similar gases on vegetation. *J. Air Pollut. Control Assoc.* **27**, 1110-1116.

5. Parameterisations for non-acidifying substances

Two substance classes, non-acidifying and acidifying, are distinguished in the OPS model. The present chapter deals with a more generic modelling approach applied for a wide range of substances. Because of the availability of more specific knowledge the acidifying substances are modelled on the basis of more specific processes, and to some extent also using interactions between substances. This group is covered in chapter 6.

5.1 Emission and emission processes

Important for the dispersion of pollutants are the meteorological conditions at the moment substances are released into the atmosphere. Systematic differences can be found for meteorological conditions, the most important being seasonal variations and diurnal cycles. Variations in emissions such as those related to diurnal cycles in traffic density may be taken into account by introducing typical daily variations. In such cases, despite still using yearly mean emission data, the model relates typical daily cycles in wind speed, temperature, radiation etceteras with the user-specified daily cycle in emissions. Although less specific than relating emission to meteorological conditions directly, this approach is believed to describe an important part of the effects.

In some cases emission rates depend on the meteorological conditions themselves, e.g. emissions due to evaporation of liquids. In such a case a correlation is likely to exist between emission rates and deposition rates (Van Jaarsveld *et al*., 2000). This type of interaction is not addressed by means of a generic approach in the OPS model. Only in the specific case of the NH_3 evaporation from field-applied manure is this process covered (see section 6.4).

5.1.1 Behaviour in time

Daily emission variations
The time-dependent emission behaviour can only be specified as a daily variation. A number of pre-defined daily variations have been included in the model, where the options are:

0 continuous in time
1 according to the (average) industrial activity for a working day
2 according to the (average) heating activity for space heating
3 according to the (average) traffic intensity.

Figure 5.1 shows the pre-defined daily emission variations incorporated into the model. The daily variation in emission is also definable by the user in the form of relative emission factors to be specified in 2-hour time steps.

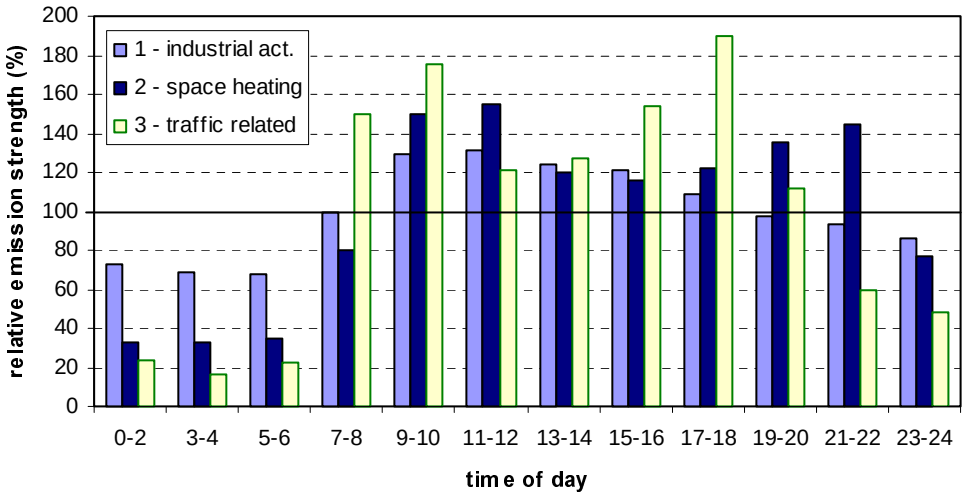

Figure 5.1 The average variation of the emission for three source types in the course of the day.

Seasonal emission variations

The OPS model supports only one type of seasonal emission variation, the variation of emission due to space heating in houses and buildings. This seasonal variation is automatically switched on if the daily variation for space heating is selected for an emission source (code 2, see previous section).The seasonal effect on space heating emissions is modelled on the basis of so called degree-day values in combination with a windspeed correction:

$$stc = (19^{o}\text{-}T_{24})\,(u_{10}/3.2)^{0.5} \qquad \text{if } T_{24} < 12\ ^{o}\text{C} \qquad (5.1)$$

in which T_{24} is the daily average outdoor temperature in ^{o}C and u_{10} the wind speed at a height of 10 m in m/s; *stc* is taken to be zero if T_{24} >= 12^{o}C. Average *stc* values are calculated with the meteorological pre-processor for each meteorological class and included in the meteorological data set. The correction of the space heating emission is carried out in OPS by first normalising *stc* with a long-term average value of *stc*.

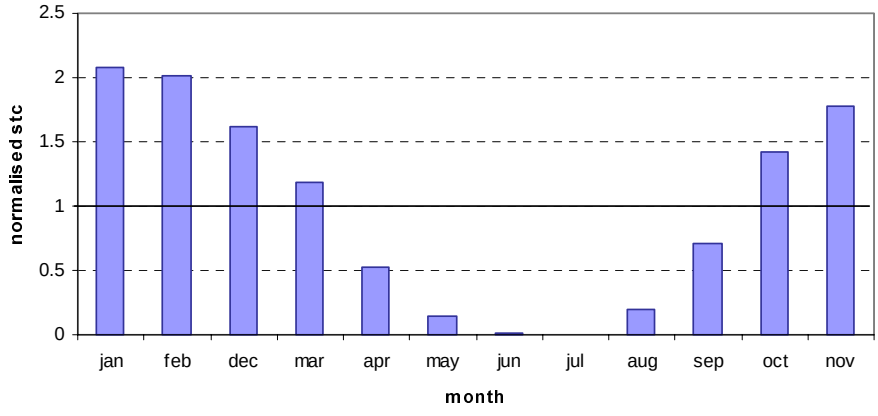

Figure 5.2 Variation in space heating emission relative to long-term average emission.

In Figure 5.2 gives the monthly variation in the normalised *stc*. These results are averages for the 1978-1991 period. Specific yearly mean values of the normalised *stc* may differ from 1, indicating warmer or colder winter seasons.

The effect of seasonal variation may be illustrated in the NO_x emission due to space heating, which is in the order of 5% of the total emissions on a yearly basis. In a specific (cold) winter month an emission of this kind may amount up to 25% of the total emission. If this is combined with the daily emission variation and the phenomenon that dispersion is low when these emissions are high (early morning and evening), the influence of variations in space heating emissions on atmospheric concentrations are clearly very significant. In order to take advantage of the different time-related variations, it is important to specify space heating and traffic-related emissions as separate source categories in the emission datafile.

5.1.2 Emission speciation

The model distinguishes two types of emissions: gaseous and particulate. In the case of gaseous emissions the rise of hot plumes is accounted for but the effect of cold and/or dense plumes (e.g. spills of liquefied gases) is not taken into account. For particulate emissions, the emission is considered to be distributed over five particle-size classes, namely:

< 0.95 µm 0.95 - 4 µm 4 - 10 µm 10 - 20 µm and >20 µm

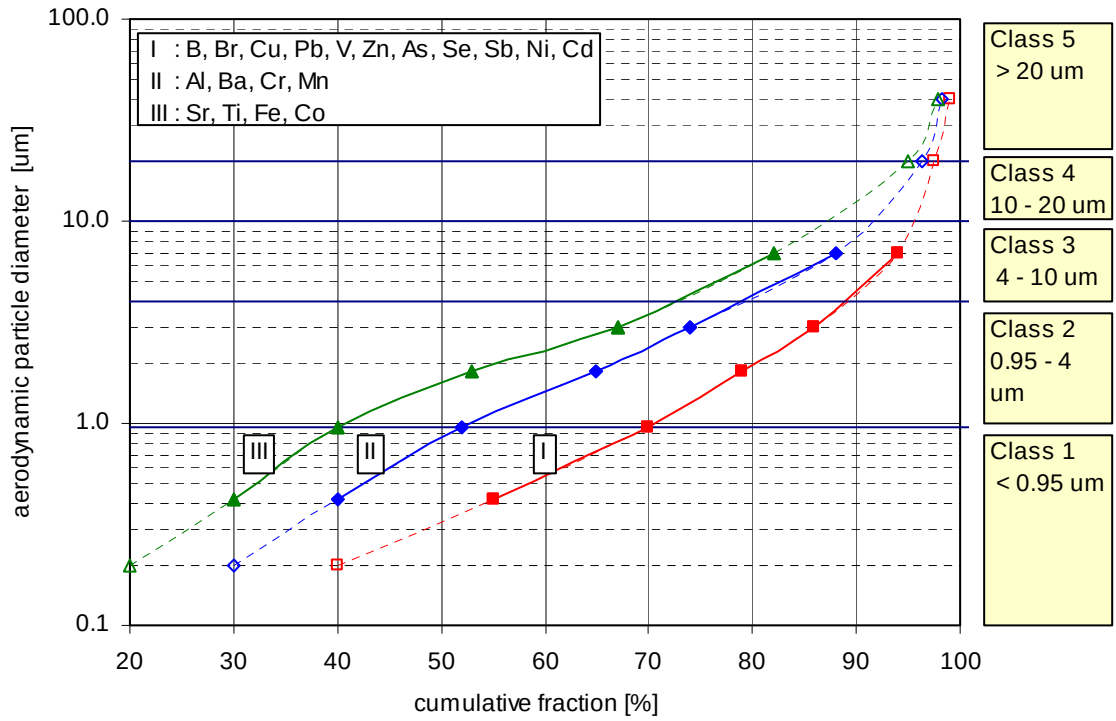

Figure 5.3 *Particle-size distributions for a number of elements measured in background concentrations, and classified into three groups (Potma et al., 1986). After log-normal extrapolation these distributions are also taken to be representative of source emissions. The particle-size classification used in the OPS model is given on the right-hand side.*

The selection of classes and class boundaries is mainly based on available field data at the time the model was developed. The model calculates concentration and deposition for these classes separately, with size-specific properties for each class. This method with discrete classes is more time consuming then methods using analytical approaches to size distribution development but more straight-forward. The user can choose from three standard particle-size distributions (see Figure 5.3 and Table 5.1), or can specify a more specific distribution over the above-mentioned classes. In calculating the concentrations and depositions for the heaviest particles (> 20 µm), allowance is made for the fact that

the sedimentation rate of these particles is not insignificant, so that plume descent occurs with distance. It is important to note that the particle size distribution must be specified for the moment that particles become airborne. Distributions measured in ambient air usually do not show the heavier particles because their atmospheric lifetime is shorter than smaller particles.

5.2 Removal processes

Loss of mass along the trajectory from source to receptor occurs in this model in three ways:

- dry deposition
- wet deposition
- conversion.

The material lost through dry and wet deposition is accumulated and included in the output, similar to the calculated concentrations. The daughter products (e.g. sulphate) formed by conversion are – in case of non-acidifying substances – ignored. For particulate pollution, the loss parameters are related to the particle-size class and incorporated in the model. The user cannot alter these parameters.

5.2.1 Dry deposition

Dry deposition is simulated in the OPS model by means of the so-called resistance model. Three resistances in series determine the deposition velocity here:

- the aerodynamic resistance (R_a)
- the laminar boundary layer resistance (R_b)
- the surface resistance (R_c).

The deposition velocity is given by:

$$v_d = (R_a + R_b + R_c)^{-1} \quad \text{[m/s]} \qquad (5.2)$$

where R_a and R_b are calculated when the meteorological statistics for a certain period/area are made, and as such form part of these statistics; R_c has to be specified by the user for the substance he/she wishes to calculate as an average over the period to be considered. As an alternative, an average deposition velocity v_d, may be input, whereby the model calculates R_c using average values of R_a and R_b. In this way, the specific R_a and R_b for a particular stability class can still be used. The average v_d, which can be entered in the above manner, has an upper limit because R_c >= 0 s/m, which means that the upper limit of v_d is in the order of 0.035 m/s.

Dry deposition of particulate substances is entirely related to the dimensions of the particles. The deposition velocities for the particle-size classes have been determined using Sehmel's model (1980). This model predicts the deposition velocity of a particle dependent on the particle size, the roughness length of the ground surface, the density of the particles and the friction velocity, u^*. The procedure yields a deposition velocity for all stability classes and particle-size classes distinguished in the OPS model. Here, the logarithmic class mean has consistently been seen as representative of all particle diameters in a class. In the class with the largest particles (> 20 μm), 40 μm was taken as representative value.

The user of the model only influences the effective deposition velocity through the distribution of the substance over the five particle-size classes. The deposition velocities concerned (weighted over the various stability classes) are given in Table 5.1.

Table 5.1. Standard particle-size distributions (see also Figure 5.3) in which the average (weighted over the various stability classes) dry deposition velocity is given for each class

Class number	1	2	3	4	5
Particle size range (μm)	<0.95	0.95-4	4-10	10-20	>20
Mass Median Diameter (μm)	0.5	2	6	15	40
Characteristic dry deposition velocities (m s^{-1}):					
v_d :	0.00065	0.0025	0.0071	0.013	0.067
Pre-defined distributions (%):					
fine (I)	70	20	5.5	2.5	2.0
medium (II)	53	28	11.5	4.2	3.3
coarse (III)	42	33	14.5	5.9	4.6

5.2.2 Wet deposition

In the OPS model, wet deposition is related to the following measured parameters and parameters incorporated into the meteo-statistics: rainfall probability, rainfall intensity and average shower duration.

Wet deposition may occur in two ways:
- washout (of readily soluble gases or particles below the cloud) and
- rainout (of substances taken up into cloud droplets).

Washout of gases readily soluble in water is entirely parameterised on a diffusion coefficient in air (*Dg* in $cm^2.m^{-1}$) to be specified by the user. Washout of sparingly soluble gases is not incorporated in this model because of its small contribution to the total wet deposition. Rainout is related to a scavenging ratio to be specified, which may have been determined for a substance either empirically from concentrations in rainwater and air or theoretically via Henry's constant. The wet deposition velocity, which is calculated from the specified scavenging ratio, limits the washout velocity calculated on the basis of a (user-specified) diffusion coefficient in air. The reason is that the last-mentioned (empirical) parameter is considered to comprise both processes. In addition to the above-mentioned wet deposition specification, a wet deposition velocity during rainfall can be specified (in % x h^{-1}) as an alternative; the model then estimates the associated *Dg* from (Durham *et al.*, 1981):

$$Dg = k\, M^{-0.5} \qquad (5.3)$$

where *M* is the molecular weight and *k* is a conversion constant (*k* = 1). However, in this way the relationship with the rainfall intensity becomes lost.

5.2.3 Chemical conversion

The conversion rate for gaseous substances can be given as a constant and/or as a variable related to the solar radiation measured in that period. This conversion rate can be specified using two parameters:

a - a constant conversion rate (in $\%.h^{-1}$).
b - a variable conversion rate, dependent on the solar radiation.

b yields a conversion rate which varies from one stability class to the other (see Table 1.1 for the classification criteria) The model calculates the conversion rate for a given class according to:

$$conv\ [\%.h^{-1}] = a\ [\%.h^{-1}] + b\ [\%.h^{-1}.W^{-1}.m^{2}] * Q_r\ [W.m^{-2}] \qquad (5.4)$$

where Q_r is the global solar radiation. The solar radiation has been incorporated in the meteo-statistics as a function of the meteorological class. Long-term average values of Q_r in the Netherlands are given in Table 5.2

Table 5.2 Average global radiation per (local) stability class

	U1	U2	N1	N2	S1	S2
Global radiation Q_r [$W\ m^{-2}$]	206	378	20	22	2	3

The maximum hourly average solar radiation is in the order of 900 W m^{-2} and the long-term average approximately 114 W m^{-2}. In view of the wind-direction dependence of the solar radiation and its variation over the day, the effective value of the conversion rate cannot be precisely determined beforehand. However, the model calculates this effective value from a mass-weighted averaging of the conversion rates of the separate classes, and emission sources, and is as such included in the model output.

In contrast with the acidifying compounds (see next chapter), the conversion process is envisaged here exclusively as a removal term. Dispersion and deposition of the daughter product are consequently not included.

5.3 References chapter 5

Durham J.L., Overton J.H.,and Aneja V.P. (1981) Influence of gaseous nitric acid on sulfate production and acidity in rain. *Atmospheric Environment* **15**, 1059-1068.

Potma C.J., Onderdelinden D. and Slanina J. (1986) Contribution from a coal fired power station to local air concentrations and deposition levels (in Dutch). PEO report NOK-LUK 3, no. 20.70-017.10, RIVM, Bilthoven.

Sehmel G.A. and Hodgson W.H. (1980) A model for predicting dry deposition of particles and gases to environmental surfaces. *AIChE Symposium Series* **86**, 218-230.

Van Jaarsveld, J.A., Bleeker, A. and Hoogervorst, N.J.P. (2000) Evaluatie ammoniakredukties met behulp van metingen en modelberekeningen. RIVM rapport 722108025, RIVM, Bilthoven.

6. Acidifying substances

Chemical conversion and dry and wet deposition were treated in the previous chapter as processes quantified by conversion rates, dry deposition velocities and scavenging ratios, respectively. These parameters, with characteristic values for each airborne substance, can, in the simplest case, have values constant in time and space. In most cases, however, dependencies on meteorological parameters such as temperature, radiation, precipitation, wind speed and direction are either known or at least anticipated. In addition, parameter values may depend on concentrations of precursors and/or other pollutants. An important environmental problem where these dependencies play a role is the so-called acidification of the natural environment through the deposition of acidifying components. In this case a number of relevant interdependencies have to be included in the model approach, otherwise the model cannot adequately describe spatial differences and/or the development in time. Another reason for a special treatment of the acidifying components is the more than average availability of experimental data on emission, conversion and deposition processes. The acidifying components include:

- sulphur compounds (SO_x): sulphur dioxide (SO_2), sulphate (SO_4^{2-})
- oxidised nitrogen compounds (NO_y): nitrogen oxides (NO and NO_2), peroxyacetyl nitrate (PAN), nitrous acid (HNO_2), nitric acid (HNO_3) and nitrate (NO_3^-)
- reduced nitrogen compounds (NH_x): ammonia (NH_3) and ammonium (NH_4^+).

The gaseous SO_2, NO and NH_3 are primary emitted pollutants, while the gaseous NO_2, PAN, HNO_2 and HNO_3 and the non-gaseous SO_4^{2-}, NO_3^- and NH_4^+ are formed from the primary pollutants in the atmosphere under influence of concentrations of, for example, ozone (O_3) or free OH-radicals. In the present study, however, the primary oxidised nitrogen pollutant is defined as the sum of NO and NO_2, further denoted as NO_x. The secondary products SO_4^{2-}, NO_3^- and NH_4^+ form mainly ammonia salts having low vapour pressures and consequently appearing as aerosols in the atmosphere (Stelson and Seinfeld, 1982a). The life cycles of the sulphur, nitrogen oxide and ammonium compounds taken into account in the model are given in Figure 6.1.

6.1 Chemical conversion

The set-up of the present model permits only a description of a reaction rate by a pseudo first-order reaction rate constant, k_c. The reaction rate is then given by:

$$\frac{d[C]}{dt} = k_c\ [C] \tag{6.1}$$

where C is the pollutant concentration; k_c is not necessarily a constant, but can also be taken as a function of time of day, radiation, temperature etceteras. Moreover, k_c may be taken as a function of a (pre-described) background concentration. In this way it is possible to introduce non-linear relationships in a basically linear transport model. The necessary relationships can be provided by chemically more detailed models.

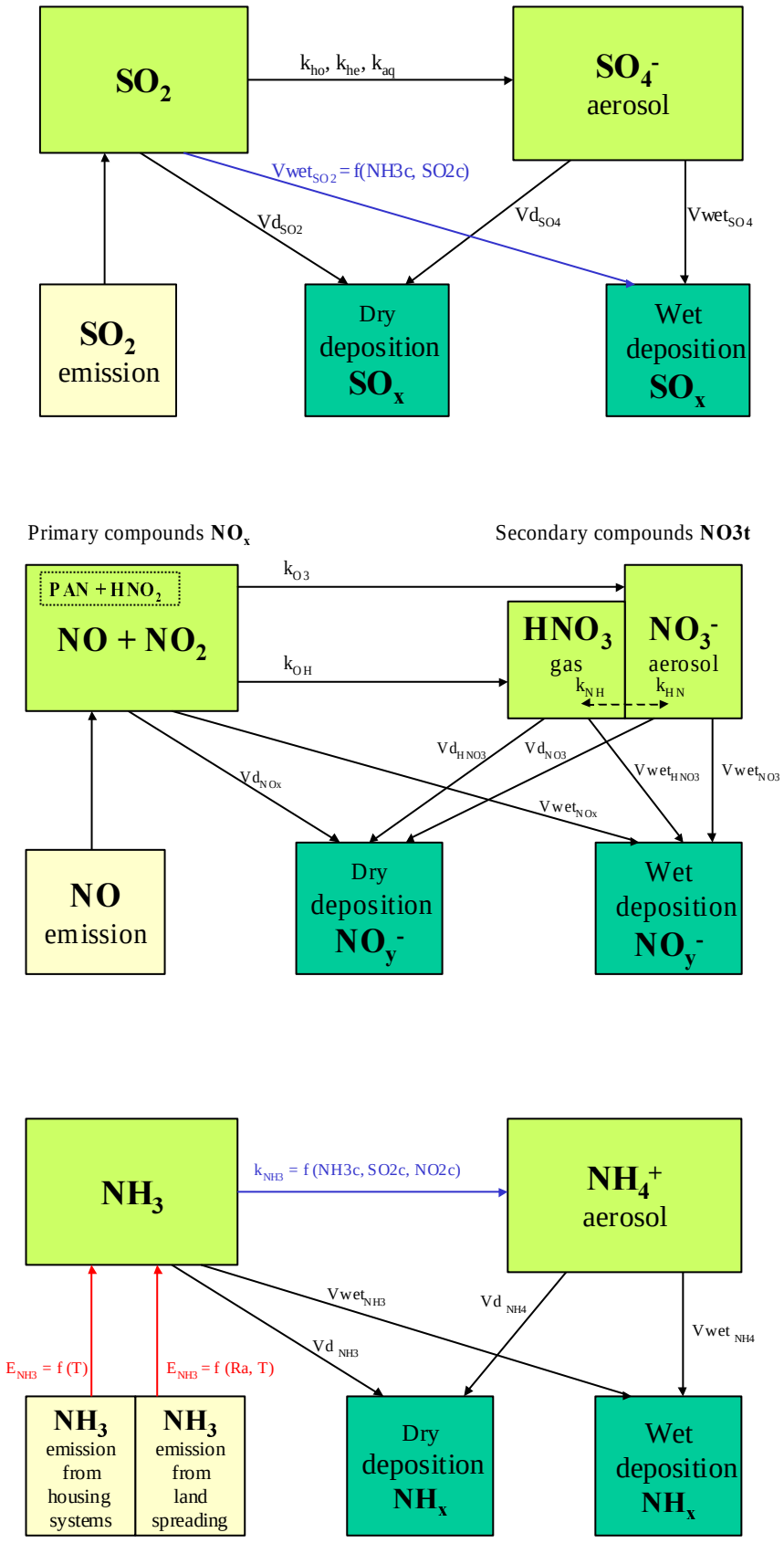

Figure 6. Emission, conversion and deposition paths of the OPS model for acidifying compounds.

6.1.1 Sulphur compounds

Combustion of fossil fuels is the main source of atmospheric SO_2 in industrialised areas. The atmospheric chemistry of sulphur can be divided into gas-phase, heterogeneous and aqueous-phase reactions. From the gas-phase reactions the most important is the oxidation by OH radicals:

$$OH + SO_2 \leftrightarrow HOSO_2 \tag{6.2}$$

Prevailing evidence indicates that the $HOSO_2$ radical ultimately leads to the formation of H_2SO_4, with regeneration of the OH radical (Stockwell and Calvert, 1983a):

$$HOSO_2 + 2H_2O \rightarrow H_2SO_4 + OH \tag{6.3}$$

Heterogeneous reactions are defined here as reactions taking place within or on solid or aqueous particles other than cloud droplets. The primary process in this kind of reactions is the adsorption of SO_2 by particles in which humidity plays an important role (Liberti *et al*., 1978). Subsequent conversion of adsorbed SO_2 into sulphate depends highly on the nature of the aerosol. Using reaction chamber experiments, Haury *et al*. (1978) show that SO_2 oxidation is catalysed through the presence of transition metals but that their results cannot be easily generalised and applied to atmospheric conditions. Möller (1980) suggests initial oxidation rates in industrial plumes larger than 1×10^{-5} s^{-1}, but only a small portion of atmospheric SO_2 will be oxidised in this way due to saturation of the particle surface. An overall average oxidation rate of 1.7×10^{-6} s^{-1} is adopted here, which is 20% higher than the value suggested by De Leeuw *et al*. (1985).

Aqueous-phase processes encompass extensive chemical transformations, many of them being oxidative in nature. In addition, there are numerous rapid equilibria in the aqueous phase. The importance of the aqueous phase transformation has been emphasised by many researchers. e.g. Möller (1980) and Lamb *et al*. (1987). Oxidation in cloud water by dissolved ozone (O_3) and hydrogen peroxide (H_2O_2) is generally indicated as the most important mechanism. Some authors suggest a dominating influence of NH_3 (pH > 5) on the oxidation of aqueous SO_2 (Stelson *et al*., 1979; Behra *et al*., 1989). This phenomenon is especially important in areas with high NH_3 emissions such as the Netherlands, which means that in the present case overall conversion rates are expected to be higher than elsewhere. An average oxidation rate in water droplets was estimated by Möller (1980) at 5.0×10^{-5} s^{-1}. A value of 4×10^{-5} s^{-1} is currently used in the OPS model.

A suitable parameterisation of aqueous-phase processes for the present model cannot be more than a bulk parameterisation i.e. considering clouds as black boxes passing by at a certain probability with SO_2 going in and sulphate aerosol coming out at a certain rate. A parameter suitable to indicating the presence of clouds would be the observed cloud cover. Since this parameter is not directly available in the meteorological data set used, the precipitation probability P_p was chosen instead. This parameter is more representative for the presence of precipitating clouds and, averaged over a longer period, might also be indicative for non-precipitating clouds.

Under European conditions , most of the H_2SO_4 will react with NH_3 to yield an NH_4^+ containing aerosol. This is a one-way reaction and the aerosol will not evaporate again:

$$NH_3 + H_2SO_4 \rightarrow (NH_4)_2SO_4 \tag{6.4}$$

and

$$NH_3 + H_2SO_4 \rightarrow (NH_4)HSO_4 \tag{6.5}$$

These reactions form the link between sulphur and ammonia in the atmosphere.

6.1.1.1 Implementation of SO_x chemistry in the model

The following rate expression for the formation of SO_4^{2-} aerosol includes contributions from the gas-phase, heterogeneous and aqueous-phase oxidation:

$$\frac{d[SO_4^{2-}]}{dt} = (k_{ho}[OH] + k_{he} + k_{aq} f_{aq} P_p)[SO_2] \quad (6.6)$$

where k_{ho}, k_{he} and k_{aq} are the respective gas-phase, heterogeneous and aqueous-phase oxidation rates and P_p the (measured) precipitation probability; f_{aq} is an empirical factor that not only accounts for the cloud presence/precipitation duration ratio but also for the fact that the aqueous-phase sulphate formed will only partly appear as sulphate aerosol. Both effects are assumed to be of equal importance (f_{aq} = 1). The OH radical concentration [molec cm^{-3}] is taken to be proportional to the global radiation Q_r [W m^{-2}] following Van Egmond and Kesseboom (1985):

$$[OH] = c_r Q_r \quad (6.7)$$

where c_r is a proportionality constant [$molec^{-1}$ cm^3 W^{-2} m^2]. Both Q_r and P_p are part of the meteorological input data set of the model. By parameterising [OH] as a function of Q_r, the diurnal and seasonal variations are automatically included for the gas-phase oxidation. Parameter values used in the model are listed in Table 6.1. A value of 7.35 x 10^3 is calculated for c_r on the basis of an average noontime OH concentration for sunny days in summer months of 1.6 x 10^6 molec cm^{-3}, as measured in Jülich (Germany) in the 1980-1983 period (Hübler *et al*., 1984; Perner *et al*., 1987). Van Egmond and Kesseboom (1985) estimated a *cr* value of 3.54 x 10^3 for the winter half year (October-April). The annual mean for the OH concentration of 0.59 x 10^6 molec cm^{-3} obtained using Eq. (6.7) falls within the range of (0.3-3) x 10^6 molec cm^{-3}, a result found a literature review by Hewitt and Harrison (1985). Total SO_2 calculated oxidation rates range from 1.7 x 10^{-6} s^{-1} on clear nights to 9.0 x 10^{-6} s^{-1} in daytime in the summer, with a yearly average rate of 6.4 x 10^{-6} s^{-1}. The EMEP (Lagrangian) model uses a sine function to describe the total oxidation rate throughout the year with a minimum daily value in December of 1 x 10^{-6} to 5 x 10^{-6} s^{-1} (daily average in June) with a yearly average of 3 x 10^{-6} s^{-1} (Iversen *et al*., 1991).

Table 6.1 Kinetic data and reaction rates for sulphur compounds used in the model

Parameter	Used in relation [a]	Remarks	Value	Ref.[b]	Units
c_r	$[OH] = c_r Q_r$	Summer (Apr.-Oct.)	7345	(1),(7)	cm^{-3} molec W^{-1} m^2
		Winter (Oct.- Apr.)	3540		
SOx:					
k_{ho}	$SO_2 + OH \rightarrow$ sulphate	gas phase	1.1 x 10^{-12}	(2)[c]	cm^3 $molec^{-1}$ s^{-1}
k_{he}	$SO_2 \rightarrow$ sulphate	Particle phase	1.7 x 10^{-6}	(3)	s^{-1}
k_{aq}	$SO_2 \rightarrow$ sulphate	Aqueous phase	4.0 x 10^{-5}	(9)	s^{-1}

a) All concentrations in molec cm^{-3}; global radiation Q_r in W m^{-2}

b) (1) Van Egmond and Kesseboom (1985); (2) Calvert *et al*. (1978); (3) de Leeuw *et al*. (1985; (7) Hewitt and Harrison (1985); (9) Möller (1980)

c) Value shown here is the rate given by Calvert *et al*. (1978). The actual rate used in the model is 3.2 x 10^{-12}

6.1.2 Nitrogen oxides

As stated earlier, this model was not set up to simulate complex chemistry. All relations between chemical components must be described as first-order or pseudo first-order relations. However, the structure of the model allows for easy inclusion of empirical or semi-empirical parameterisations. A brief overview of the most important reaction paths and their parameterisation follows.

The relation between concentrations of NO, NO_2 and O_3 is to a large extent explained by the photo-stationary equilibrium:

$$NO + O_3 \overset{h\nu}{\leftrightarrow} NO_2 + O_2 \tag{6.8}$$

where the equilibrium constant is proportional to the UV intensity.

The reaction of NO_2 with OH to form nitric acid is the main chemical loss mechanism for NO_2 during daytime:

$$NO_2 + OH \rightarrow HNO_3 \tag{6.9}$$

At night NO_2 is assumed to be lost by reaction with ozone to form particulate nitrate through the following series of reactions:

$$\begin{aligned} &(i)\ NO_2 + O_3 \rightarrow NO_3 + O_2 \\ &(ii)\ NO_3 + NO_2 \leftrightarrow N_2O_5 \\ &(iii)\ N_2O_5 + H_2O_{(aq)} \rightarrow 2\,NO_3^- + 2\,H^+ \end{aligned} \tag{6.10}$$

Hov *et al*. (1988) suggest that in a night-time situation the first reaction in (6.10) will be the rate-determining step. The net reaction can be written as $2NO_2 + O_3 \rightarrow 2NO_3^- + O$, with a reaction rate k_{O3} of $2.1 \times 10^{-13} \exp(-2450/T)$. This leads to an average night-time $NO_2 > NO^-_3$ conversion rate of $2.4 \times 10^{-5}\ s^{-1}$. Other authors such as Tuazon *et al*. (1983) consider the hydrolysis reaction (6.10iii) as limiting ($k = 1.3 \times 10^{-21}\ cm^3\ molec^{-1}\ s^{-1}$), leading to much lower rates. Van Egmond and Kesseboom (1983) used a first-order rate of $0.55 \times 10^{-5}\ s^{-1}$ for the night-time $NO_2 > NO_3^-$ conversion, the rate adopted in the OPS model.
During daylight hours the NO_3 radical formed in (6.10) will be decomposed due to photolysis reactions of which $NO_3 + h\nu \rightarrow NO_2 + O$ is the most important (Magnotta and Johnston, 1980).

Other (temporary) sinks for NO_2 are the reaction with peroxyacetyl radicals, resulting in formation peroxyacetyl nitrate (PAN):

$$\begin{aligned} &(i)\ NO_2 + CH_3COO_2 \rightarrow PAN \\ &(ii)\ PAN \rightarrow NO_2 + CH_3COO_2 \end{aligned} \tag{6.11}$$

and reactions which form nitrous acid (HNO_2):

$$\begin{aligned} &(i)\ 2\,NO_2 + H_2O \rightarrow HNO_2 + HNO_3 \\ &(ii)\ HNO_2 + h\nu \rightarrow OH + NO \end{aligned} \tag{6.12}$$

The decomposition of PAN is an important function of temperature (Hov *et al*., 1988). Measurements in Delft carried out by TNO indicate a PAN concentration which, on average, is only in the order of 5% of the NO_2 concentration (Ogilvie, 1982). The deposition properties are also uncertain but probably not very

different from those of NO_2; it was therefore decided not to take PAN into account as a separate component for this model but to consider it as a part of NO_x.

Nitrous acid has been studied far less extensively than for example, HNO_3. The build-up of HNO_2 observed during the night-time hours is still not fully explained; heterogeneous pathways have been favoured by Kessler and Platt (1984), for example. Heikes and Thompson (1983) have shown, however, that an aerosol formation mechanism is physically unlikely. The overall reaction (6.12) was postulated on results of smog chamber experiments (Cox and Jenkin, 1987; Lammel *et al*., 1989). Rapid photolytic decomposition takes place during the day. Slanina *et al*. (1990) report average HNO_2 concentrations of 0.64 ppb for a forest site in the Netherlands (the Speulderbos), which is in the order of 4 % of $NO+NO_2$ concentrations. Similar results are reported by Kitto and Harrison, (1992). HNO_2 is water-soluble and efficiently removed by precipitation; dry deposition velocities similar to those of SO_2 have been suggested by Wesely (1989). Erisman (1992) estimated the average dry deposition of HNO_2 in the Netherlands at less than 6 % of the total dry deposition of all oxidised nitrogen components

The gaseous nitric acid may react with ammonia to form ammonium nitrate aerosol:

$$HNO_3\ (g) + NH_3\ (g) \leftrightarrow NH_4NO_3\ (s) \qquad (6.13)$$

Temperature and relative humidity have a great influence on the equilibrium concentration of NH_4NO_3. Stelson and Seinfeld (1982b) indicate equilibrium constants at 80% relative humidity of 0.3 ppb^2 at 10^0C and 10 ppb^2 at 25^0C. Due to the relatively high ammonia concentrations in the Netherlands and other European countries, it may be expected that nitrate aerosol is the dominant form, especially in wintertime.

6.1.2.1 Implementation of NO_y chemistry in the model

Modelling concentrations of NO_2 using the photo-stationary equilibrium reaction (6.8) requires estimates of O_3 (background) concentrations on a local scale. Such O_3 concentrations are strongly influenced by neighbouring NO sources. Making this approach unsuited to this model. Basically, the OPS model calculates contributions of sources independent of each other, so empirical relations between NO and NO_2 concentrations cannot be used unless the 'background' NO_2 concentration is taken into account. An alternative would be an iterative approach, i.e. first calculating total concentrations linearly and then the non-linear relations using the results of the first step as the background levels. The calculated NO_2, PAN and HNO_2 concentrations would not be very accurate anyway. These considerations have led to the choice of modelling the sum of NO, NO_2, PAN and HNO_2 as a single conservative species NO_x. The NO_2 concentration needed in the reactions (6.9) - (6.10) is taken as a fraction of the calculated NO_x concentration. Necessary NO_2/NO_x ratios are derived from observations as a function of atmospheric stability and trajectory length according to the classification of meteorological situations used in the present model (see section 1.2). Furthermore, the model uses maps of (prescribed) annual mean background concentrations of SO_2, NO_2 and NH_3 as a basis for spatial and annual differences in chemistry parameterisations. Because the NO_x species have rather different dry and wet deposition properties, the deposition properties of NO_x are adjusted using the aforementioned NO_2/NO_x ratios and a (fixed) HNO_2/NO_x ratio.

When comparing modelled 'NO_x' concentrations with measurements of NO + NO_2, the 4% contribution of HNO_2 and a possible PAN contribution of 5% of the NO_2 concentration has to be kept in mind.
At an average NO_2/NO_x ratio of 0.65, the modelled NO_x (NO + NO_2 + HNO_2 + PAN) concentration may be systematically 8% higher than measured NO_x (NO + NO_2) concentrations.

Secondary-formed species are much less influenced by local sources. In such cases it is much less of a problem to use empirical, averaged relations between NO, NO_2 and O_3. The production of HNO_3 for a given class, *s,* and a transport distance, *x,* is modelled as:

$$\frac{d\,(HNO_3)}{d\,t} = k_{OH}\,[\,OH(x,s)\,]\,r_n(x,s)\,[\,NO_x\,] \qquad (6.14)$$

similarly to the time averaged nighttime formation of NO_3^-:

$$\frac{d\,(NO_3^-)}{d\,t} = k_{O_3}\,[\,NO_x\,]\,f_n(x,s) \qquad (6.15)$$

where k_{OH} is the second-order reaction rate constant (molec^{-1} cm^3 s^{-1}) of reactions (6.9) and k_{O3} the first-order rate (s^{-1}) of reaction (6.10).

Table 6.2 Kinetic data and reaction rates for NO_y compounds used in the OPS model

Parameter	Used in relation [a]	Remarks	Value	Ref.[b]	Units
k_{OH}	$NO_2 + OH \rightarrow HNO_3$	Daytime	1.035×10^{-11}	(2)	cm^3 molec^{-1} s^{-1}
k_{O3}	$NO_2 \rightarrow$ nitrate	Nighttime	5.6×10^{-6}	(1)	s^{-1}

[a]) All concentrations in molec cm^{-3}; global radiation Q_r in W m^{-2}
b) (1) Van Egmond and Kesseboom (1983); (2) Baulch *et al*. (1982)

Table 6.3 Statistical data on nighttime NO_2/NO_x ratios and relative occurrences of nighttime hours for the meteorological classes used in the OPS model. The data are derived from LML observations at rural stations over the 1980-1985 period.

	Period	Length of	Meteorological classes					
			U1	U2	N1	N2	S1	S2
NO_2/NO_x ratio: $r_n(x,s)$	Summer	10	0.78	0.78	0.78	0.7	0.7	0.78
		100	0.78	0.78	0.78	0.7	0.7	0.78
		300	0.78	0.78	0.78	0.7	0.7	0.78
		1000	0.78	0.78	0.78	0.7	0.7	0.78
	Winter	10	0.47	0.47	0.62	0.6	0.3	0.58
		100	0.47	0.47	0.62	0.6	0.3	0.58
		300	0.47	0.47	0.62	0.6	0.3	0.58
		1000	0.47	0.47	0.62	0.6	0.3	0.58
Relative frequency of	Summer	10	0	0	0.61	0.6	1.0	0.98
nighttime hours: $f_n(x,s)$		100	0.17	0.17	0.68	0.6	0.6	0.83
		300	0.43	0.43	0.44	0.4	0.4	0.44
		1000	0.43	0.43	0.44	0.4	0.4	0.44
	Winter	10	0	0	0.66	0.6	1.0	0.99
		100	0.25	0.25	0.71	0.7	0.7	0.92
		300	0.62	0.64	0.74	0.6	0.6	0.63
		1000	0.62	0.74	0.74	0.6	0.6	0.63

Values for k_{OH} and k_{O3} are given in Table 6.2. [$OH(x,s)$] is the OH radical concentration (molec cm^{-3}) calculated with Eq. (6.7), $r_n(x,s)$ the NO_2/NO_x ratio, and $f_n(x,s)$ the relative frequency of occurrence of night-time hours. All of these represent functions of class s and are averaged over a transport distance x. Table 6.3 presents the data for $r_n(x,s)$ and $f_n(x,s)$ for the different classes for both summer and winter seasons on the basis of five years of measurements. It can be concluded from Table 6.3 that it is more important to include seasonal variations in the parameterisations than variations in stability and/or mixing height.
In the (former) TREND model the expression (6.15) was more elaborated in the relation with O_3 (background) concentrations, while variations in O_3, r_n and f_n data were derived from measurements at the Cabauw meteorological tower (Van Jaarsveld, 1995). This approach is not followed in the OPS model because it did not prove to improve the results very much.

The parameter r_n provides diurnal and seasonal variations in NO_2/NO_x ratios to some extent. In the OPS model also a spatial variation is also introduced. This spatial variation is derived from a map of annual mean (background) NO_2 concentrations in combination with an empirical relation between NO_2 and NO_x concentrations (see Appendix IV). The spatial variation factor, f_{n_space}, is calculated as:

$$f_{n\_space} = \frac{NO2_{bg}}{0.65\left(\exp\frac{NO2_{bg}+12.4}{8.6}\right)} \qquad (6.16)$$

with $NO2_{bg}$ in ppb. The value 0.65 represents the average NO_2/NO_x ratio for the Netherlands, so f_{n_space} has unity value when averaged over the Netherlands. Equation (6.16) is applicable to annual mean $NO2_{bg}$ values greater than 10 ppb, a value exceeded for almost all areas in the Netherlands; fn_space has a range of 0.50 (urban areas) up to 1.2 (coastal area of Friesland). The effective r_n value becomes then:

$$r_n eff(x,s) = r_n(x,s)\ f_{n\_space} \qquad (6.17)$$

The yearly average conversion rates obtained are 4.4 x 10^{-6} s^{-1} for the $NO_2 \rightarrow HNO_3$ reaction and 6.9 x 10^{-6} s^{-1} for the $NO_2 \rightarrow NO_3^-$ reaction. From a model intercomparison (Derwent *et al.*, 1989), it appears that these values are more than a factor of 2-3 lower than the values used in the Harwell (Derwent and Nodop, 1986) and the EMEP (Lagrangian) models. These models also use prescribed O_3 and OH concentrations and are confronted with the effects on the chemistry of non-instantaneous mixing. This could be one of the reasons why these models strongly underestimate NO_x concentrations, while HNO_3 and NO_3^- concentrations are in reasonable agreement with the measurements.

The nitric acid produced is in equilibrium with particulate nitrate through reaction (6.13). Because of the very different dry deposition properties of HNO_3 and NO_3^- it is necessary to make the ratio between the two as realistic as possible, but the set-up of the present model does not allow the explicit description of equilibrium reactions.

In the OPS model the ratio f_{HNO3} between the (gaseous) HNO_3 and the total secondary compound, NO3t (= HNO_3 + NO_3), is modelled solely as a function of the NH_3 concentration in the area according to:

$$f_{HNO3} = \frac{HNO_3}{\left(HNO_3 + NO_3^-\right)} = 0.024\left(\frac{NH3_{bg}}{1000}\right)^{-0.44} \qquad (6.18)$$

in which $NH3_{bg}$ is the local (prescribed) background concentration of NH_3 in ppb (see Appendix IV for method and values). The formulation of f_{HNO3} is determined by a best fit to NH_3 and HNO_3 concentration results of a 1D chemistry model applied for the typical Dutch pollution climate for a period of several months. Because of the relatively high NH_3 concentrations in the Netherlands, we can expect higher nitrate aerosol concentrations than elsewhere in Europe. This is what actually is seen in the EMEP network (Hjellbrekke, 1999)

When comparing modelled 'NO3t' concentrations with measurements of NO_3^- aerosol, the contribution of HNO_3 concentration has to be kept in mind.
At an average NH_3 level of 14 ppb the modelled NO3t ($NO_3^- + HNO_2$) concentration may be systematically 16% higher than the measured NO_3^- aerosol concentration.

6.1.3 Ammonia compounds

Ammonia is predominantly released from low-level agricultural sources. Under European conditions a major part of the gaseous NH_3 will react with H_2SO_4 to yield an NH_4^+-containing aerosol (reactions 6.4 and 6.5).

$$NH_3 + H_2SO_4 \rightarrow (NH_4)_2SO_4 \quad (6.19)$$

and

$$NH_3 + H_2SO_4 \rightarrow (NH_4)HSO_4 \quad (6.20)$$

These are one-way reactions and the aerosol will not evaporate again (Asman and Janssen, 1987). A minor part will react with gaseous HNO_3 through reaction:

$$NH_3 + HNO_3 \leftrightarrow NH_4NO_3 \quad (6.21)$$

and a similar equilibrium reaction with HCl will form NH_4Cl (Pio and Harrison, 1987):

$$NH_3 + HCl \leftrightarrow NH_4Cl \quad (6.22)$$

For Europe as a whole enough acid precursors are released to neutralise (in due time) all emitted NH_3. On a local scale, however, or during intensive spreading of manure, not enough acid may be present to convert all NH_3. Therefore, conversion rates are likely to vary both in space and time. In previous versions of the OPS model, a constant rate of 8 x 10^{-5} s^{-1} (28.8 % h^{-1}) was adopted because not enough information was available to make it a function of the season or other factors (Asman and Van Jaarsveld, 1992). This value was consistent with values derived from measurements (Erisman *et al*., 1988) and, when used in transport models, these values resulted in favourable comparisons with observed ammonium levels[1] (Asman and Janssen, 1987). Nowadays, atmospheric concentration levels of sulphur dioxide have decreased by a factor of 5, while NH_3 concentrations are probably at the same level as ten years ago. The assumption of a fixed conversion rate is therefore no longer justified.

6.1.3.1 Implementation of NHx chemistry in the model

Since SO_2 and NO_2 are the primary pollutants for H_2SO_4 and HNO_3, respectively, they would likely parameterise the conversion rate of $NH_3 \rightarrow NH_4^+$ as function of these concentrations. The formation of ammonium is therefore simulated using a one-dimensional model, including the relevant chemical reactions as applied in the MPA model (De Leeuw *et al*., 1990) and also deposition processes. This model is used on the basis of actual meteorological data and supplied with background concentrations of SO_2, NO_x, NH_3, O_3 and OH radicals. The conversion rate follows from the production of ammonium sulphate and ammonium nitrate over a (long) period, divided by the mean ammonia concentration. The conversion rates are then translated into a parameterisation for this rate using regression analyses. This resulted in the following relation between the $NH_3 > NH_4$ conversion rate k_{NH3}:

$$k_{NH3} = 0.67 + 1.36\,C_1 + 10.7\,C_2 + 3.06\,(C_2)^4 - 0.29\,(C_2)^6 \quad (6.23)$$

where C_1 is the ratio in background concentrations NO_2/NH_3 (ppb/ppb) and C_2 the ratio SO_2/NH_3 (ppb/ppb). The background concentrations, included as gridded maps in the OPS model with a spatial

[1] These ammonium measurements were not corrected for blank filter values.

resolution of 10 x 10 km, encompass a large part of Western Europe. The maps are generated in four steps:

1. Concentration maps are calculated with the OPS model for 1984 and 1994 using specific emission data,
2. The concentrations are compared with observations of the LML network and the maps are multiplied with the average ratio observed/modelled for each of the two years,
3. Trend factors relative to 1984 and 1994 are determined from the observations for each year starting in 1980,
4. The concentration maps for specific years are then calculated by inter- or extrapolation the 1984 and 1994 maps using the trend factors of step 3. In this way the yearly concentrations are available for the 1980 - 2002 period. See Appendix IV for more details.

When averaged over the Netherlands k_{NH3} amounts to approx. 16 % h^{-1} (4.4 x 10^{-5} s^{-1}) in 1980 and approx. 5% h^{-1} (1.4 x 10^{-5} s^{-1}) in 1997.

6.2 Dry deposition

6.2.1 Dry deposition velocities of gaseous substances

The general dry deposition flux model of Eq. (4.1) in combination with the resistance model of Eq (4.2) is schematically given in Figure 6.2a. For gases emitted by sources at the surface level, such as NH_3 and gases which do not react on or within canopies, the resistance analogy can only be used if a non-zero surface concentration C_s is taken into account. Such a concentration, sometimes referred to as the compensation point, is defined as that atmospheric concentration below which no deposition takes place.

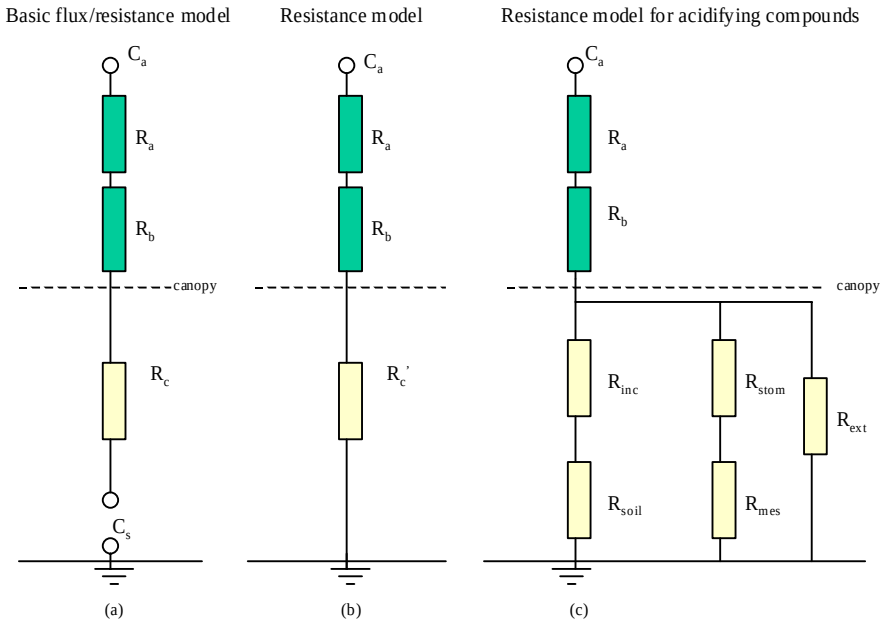

Figure 6.2 Flux/resistance models for dry deposition. Model (b) is applied to non-acidifying substances while model (c) is used in the DEPAC dry deposition module.

Although conceptually simple, the compensation point approach is hampered by the fact that the compensation point concentration may vary strongly with vegetation type and soil properties, and preceding deposition/emission fluxes. Since the effect of these fluxes cannot be directly taken into account in the present transport model, the model in Figure 6.2b with zero surface concentrations is used.

This means that all effects of saturation are effectively included in the surface resistance R_c'. In fact, this is the most commonly used model and also the method by which most experimental results of deposition velocities or surface resistances are presented.
In the case of acidifying compounds, the OPS model uses the DEPAC module for the parameterisation of dry deposition velocities. This module was developed by Erisman *et al*. (1994) on the basis of experimental data such as those derived from the Speulder forest experiments. The resistance model applied in DEPAC is given in Figure 6.2c. In this model, R_{stom} and R_{mes} represent stomatal and mesophyll resistances of leaves, respectively. R_{inc} and R_{soil} are resistances representing in-canopy vertical transport to the soil that bypasses leaves and branches. R_{ext} is an external resistance that represents transport via leave and stem surfaces, especially when these surfaces are wet. The (effective) canopy resistance R_c is calculated as:

$$R_c = \frac{1}{\frac{1}{R_{stom} + R_{mes}} + \frac{1}{R_{inc} + R_{soil}} + \frac{1}{R_{ext}}} \tag{6.24}$$

The DEPAC module contains values or formulae for each of the resistances given in Figure 6.2c and for various land-use types. The module includes the following gaseous components: SO_2, NO, NO_2, and NH_3 and provides a dry deposition velocity and a so-called effective canopy resistance on an hourly basis as a function of meteorological parameters, month of the year and time of the day. Meteorological parameters are: friction velocity, Monin-Obukhov length, global radiation wind speed at canopy height, relative humidity and a surface wetness indicator. Other parameters are land-use class, roughness length and an indicator for the NH_3/SO_2 ratio. The latter is always set to 'high', because of the relatively high NH_3 concentrations in the Netherlands. Another important parameter is the surface wetness indicator because dry deposition velocities of SO_2 and NH_3 are much higher when the surface is wet. Due to the nature of the OPS model it is not straightforward to decide if a certain meteo class is to be labelled 'wet' or 'dry'. The following empirical relation connects the average relative humidity r_h (in %) and precipitation probability P_r to the wetness indicator:

$$nwet = \frac{(0.4 P_r + 0.017 r_h - 0.4)^5}{3.33} \tag{6.25}$$

The surface is assumed 'wet' if $nwet > 0.5$, otherwise it is dry. Expression (6.25) is derived from surface wetness observations in the Speulder forest. The switch point of (6.25) lies around r_h = 87 %. This means that the surface is supposed to be wet in approx. 50% of the time.

At present the DEPAC module contains parameterisations for the nine land-use types given in Table 6.4. Further details on DEPAC are given in Appendix I.

Table 6.4 Land-use classes distinguished in DEPAC

Code	Land-use type	%	Typical roughness length (m)	
			summer	winter
1	Grass land	60	0.03	0.01
2	Arable land	19	0.25	0.10
3	Permanent crops (orchards)	0	-	-
4	Coniferous forest	4	1.08	1.08
5	Deciduous forest	1.2	0.96	0.66
6	Water	7	0.0005	0.00025
7	Urban	5	1	1
8	Other (heather and other nature)	3	0.15	0.10
9	Desert (bare sandy areas)	0	0.001	0.005

The deposition parameterisation works in conjunction with spatial data on (most abundant) land use and roughness length. These data are derived in several resolutions from basic land-use maps with 25 x 25 m detail and more than 25 different land-use types (LGN3). The OPS model selects the required map depending on the chosen output resolution. The highest resolution at present is 250 x 250 m.

6.2.2 Dry deposition of NO_x

In this model NO_x represents the sum of NO, NO_2, PAN and HNO_2. The DEPAC module provides estimates of the canopy resistances of NO and NO_2; for HNO_2, the same parametrisation is used as for SO_2. Dry deposition properties for PAN are assumed to be the same as for NO_2. The canopy resistance for NO_x is now calculated as:

$$R_c\_NOx = \frac{1}{a} - R_a - R_b \tag{6.26}$$

with

$$a = \frac{r_n eff(x,s)}{R_c\_NO2 + R_a + R_b} + \frac{1 - r_n eff(x,s)}{R_c\_NO + R_a + R_b} + \frac{f_{HNO2}}{R_c\_HNO2 + R_a + R_b} \tag{6.27}$$

where f_{HNO2} is the fraction of HNO_2 in NO_x taken at a fixed value of 0.04. R_a is calculated for a height of 4 m. The atmospheric resistances R_a and R_b are included in this calculation only as weighting factors because the calculation of a species weighted R_c has to be carried out on the basis of deposition velocities and not on resistances.

6.2.3 Dry deposition of acidifying aerosols

The route to forming particles containing SO_4^{2-}, NO_3^- and NH_4^+ runs through direct gas-to-particle conversion and evaporation of cloud droplets in which conversion has previously taken place. Newly formed particles are usually smaller than 0.01 μm (Aitken particles). If the gas condenses on existing particles (e.g. heterogeneous processes), the median size of these particles will also be relatively small, because small particles have the highest specific surface area. Through processes such as coagulation, small particles will grow and finally be concentrated in a 0.1– 1 μm range, the so-called accumulation mode. Most theoretical models suggest a v_d between 0.05 - 0.2 cm s^{-1} for this size range and relatively smooth surfaces (z_0 < 0.1 m). Data from the literature suggest that for rough surfaces such as forests the dry deposition velocity will be significantly higher, for example, in the order of 1 cm s^{-1} (Voldner *et al*., 1986; Erisman *et al*., 1994).

A different approach has been followed for acidifying aerosols such as SO_4^-, NO_3^- and NH_4^+ than for aerosols or particles in general. One reason is that there is more experimental data available which makes it possible to distinguish between vegetation types; another reason is that particle-sizes are usually small since the particles have been formed in the atmosphere and are thus independent of industrial processes or cleaning equipment. The parameterisation for the acidifying aerosols is based on the work of Ruijgrok *et al*. (1993), and is also included in the DEPAC module described in Appendix 1.

6.2.4 Dry deposition of NO_3^- + HNO_3

The model describes the transport of only one secondary substance. In the case of nitrogen oxides the secondary substance consists of NO_3t (=NO_3^- + HNO_3) , which has very different dry deposition velocities and therefore very different atmospheric lifetimes. NO_3^- aerosol is the dominant species under European conditions. The model uses a dry deposition velocity adjusted to f_{HNO3}, which is an empirically determined HNO_3/NO_3t ratio (Eq. 6.18). Similar to the dry deposition of NO_x the canopy resistance for NO_3t is determined by:

$$R_c\_NO3t = \frac{1}{b} - R_a - R_b \tag{6.28}$$

with

$$b = \frac{f_{HNO3}}{R_c\_HNO3 + R_a + R_b} + \frac{1 - f_{HNO3}}{R_c\_NO3 + R_a + R_b} \tag{6.29}$$

where R_c_NO3 is derived from the NO_3^- aerosol dry deposition velocity provided by DEPAC. R_c_HNO3 is taken as 10 s m^{-1} under all conditions.

6.3 Wet Deposition

The wet deposition approach for acidifying compounds is identical to what is described in section 4.2, except for the scavenging of SO_2, for which a non-linear semi-empirical parameterisation is used. Two main scavenging processes are distinguished in this model: below-cloud scavenging and in-cloud scavenging. Below-cloud scavenging is important for scavenging from plumes close to sources in situations where there is still no interaction with clouds. An expression for irreversible scavenging of gases is given in Eq. (4.17). This expression is well suited to highly soluble gases such as HNO_3, HNO_2 and NH_3. The rate limiting process is formed by diffusion of the substance through the pseudo-laminar air layer around the falling raindrop (Levine and Schwartz, 1982). In general, however, in-cloud processes are responsible for the highest wet deposition loads (Hales, 1978).

6.3.1 SO_2 scavenging

Below-cloud scavenging
In the case of SO_2, however, the process of uptake is controlled by the (slow) conversion to bisulphite (HSO_3^-) in the falling raindrop, which means that the SO_2 concentration in the drop is in (near) equilibrium with the surrounding air (Barrie, 1978; Ten Brink *et al*., 1988). The approach used in this model for below-cloud equilibrium scavenging (Eq. 4.16), avoids the washout peaks near sources as observed for irreversibly soluble gases (Ten Brink *et al*., 1988) but ignores vertical redistribution of plumes. At larger distances from a source, in-cloud scavenging will dominate the total wet deposition anyway (Hales, 1978). Local below-cloud scavenging of secondary products is ignored because the contribution to total scavenging would be very low.

In-cloud scavenging
Scavenging ratios for SO_2 have been determined from experiments. Haul (1978) derived a ratio of 8×10^4 from hourly measurements of SO_2 and rainfall rates in the UK. Other authors used simultaneous observations of SO_2 and SO_4^{2-} in air and precipitation to estimate scavenging ratios of both SO_2 and SO_4^{2-} (e.g. Misra *et al*., 1985; Chan and Chung, 1986). Chan and Chung report annual scavenging ratios of 4.3×10^5 (SO_4^{2-}), 4.6×10^4 (SO_2), 4.7×10^5 (NO_3^-) and 4.7×10^5 (HNO_3) for rural sites in the province of Ontario, Canada. Barrie (1981) expresses the scavenging ratio of SO_2 on the basis of equilibrium chemistry:

$$\log_{10}(W_{SO_2}) = \log_{10}(K_e) + pH \tag{6.30}$$

where K_e is an equilibrium constant related to the temperature in the following empirical relation: $K_e = 6.22 \times 10^{-8} \exp(4755.5/T)$ (mol l^{-1}). For pH = 4.75 and T = 283 K this results in $W = 7.5 \times 10^4$. A model study carried out by Scire and Venkatram (1985) supports the order of magnitude of these figures. Expression (6.30) was adopted for the first model versions using an average pH of 4.75.
In view of the changing acidity of cloud and precipitation water in the period since 1980, it was felt that a

fixed scavenging ratio was no longer appropriate. For example, pH values of precipitation in the Netherlands have changed from approx. 4.5 in 1980 to approx. 5.25 in 2001. In the same period mean SO_2 concentrations decreased from 22 µg/m^3 to 2.5 µg/m^3. SO_2 may be considered as an important acid forming compound. In contrast, neutralising compounds such as NH_3 have decreased probably not more than 30%. Because background concentration maps of SO_2 and NH_3 are already used for the parameterisation of the $NH_3 \rightarrow NH_4^+$ conversion, it was obvious to base the parameterisation of the SO_2 scavenging ratio on these background concentrations too. An expression using NH_3/SO_2 concentration ratios that approach Eq. (6.30) is to a large extent:

$$W_{SO2} = 50000\ (NH_3c\ /\ SO_2c) \qquad (6.31)$$

where NH_3c and SO_2c are local concentration levels expressed in ppb. Expressions 6.30 and 6.31 are compared using measured data of six LML stations (Figure 6.3). The expressions can be concluded to give similar results, both in space and time.

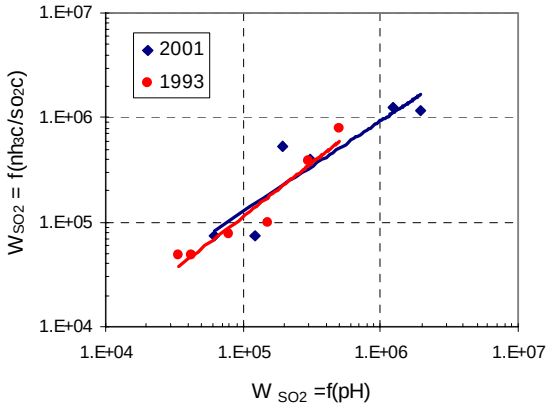

Figure 6.3 Comparison in SO_2 scavenging ratios, one based on pH values and the other on NH_3/SO_2 concentration ratios.

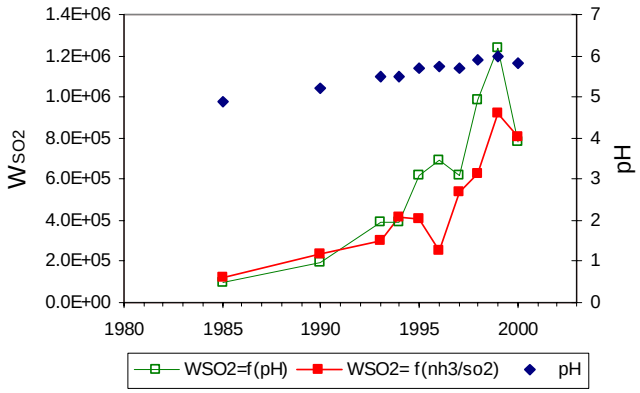

Figure 6.4 Change in the pH values and SO_2 scavenging ratios in time for the Eibergen station

The development of the scavenging ratio in time for the Eibergen station (high NH_3 concentrations in the eastern part of the country,) is illustrated in Figure 6.4. One must realise that increasing *W* values above a value of approx. 5 x 10^5 does not increase wet deposition loads very much.

6.3.2 NO_x scavenging

NO and NO_2 have low water solubilities and their aqueous-phase nitrite and nitrate reactions are expected to be of only minor importance (Seinfeld, 1986). However, nitrogen compounds not explicitly taken into

account in OPS, e.g. nitrous acid, may contribute significantly to nitrate forming in the aqueous phase. These contributions to the wet deposition of NO_x are included in the model by assuming an HNO_2 scavenging ratio of 3.3×10^5 and an average HNO_2 fraction in NO_x of 4%. In this way an effective scavenging ratio of 1.3×10^4 is calculated for NO_x.

6.3.3 NH_3 scavenging

NH_3 is relatively soluble in water. Due to reactions in droplets, the effective uptake of NH_3 is highly improved and, in fact, limited by the diffusivity of NH_3 in air. The OPS model uses a scavenging ratio of 1.4×10^6. Measurements of NH_4^+ concentrations in precipitation confirm the effectiveness of the scavenging process. There is a clear (spatial) correlation between NH_3 concentrations in air and NH_4^+ concentrations in precipitation (Van Jaarsveld *et al*., 2000)

6.3.4 Scavenging of SO_4^{2-}, NO_3^- and NH_4^+ aerosols

Wet scavenging of aerosols is an efficient process (Slinn, 1983). Scott (1982) expresses the scavenging coefficient for soluble particles and for a given distribution of droplet sizes as:
$\Lambda_w = 1.26\ R_i^{0.78}$ (h^{-1}), with R_i the precipitation intensity in mm h^{-1}. A corresponding scavenging ratio W would be $\sim 1 \times 10^6$, which means that within the duration of a single precipitation event most of the particles will be scavenged. Similar high scavenging ratios have been derived from field experiments. The particle size dependency, as noted for below-cloud scavenging, is probably less pronounced for in-cloud scavenging.

6.3.5 Overview of wet scavenging parameters

Table 6.5 Wet scavenging parameters for acidifying components as applied in the model

Component	Local below-cloud scavenging	Scavenging ratio W
Primary:		
SO_2	yes, equilibrium	NH3c/SO2c x 5 $x10^4$ #
NO_x	no	1.3×10^4
NO		0
NO2		0
HNO2	no	3.3×10^5
PAN		0
NH_3	yes, irreversible, $D_g = 0.234\ cm^{-2}\ s^{-1}$	1.4×10^6
Secondary:		
SO_4^{2-} aerosol	yes$	2.0×10^6
NH_4^+ aerosol	yes$	1.4×10^7
NO_3t	yes$	1.4×10^7
NO_3^- aerosol	yes$	1.4×10^7
HNO_3	no	1.4×10^7

SO_2c and NH_3c are average background concentrations (ppb) in the area between source and receptor.
$ Parameterisation from Janssen and Ten Brink (1985).

6.4 Emission processes

Emission and deposition rates of volatile substances applied to the soil or at the soil surface are strongly effected by physicochemical properties of the substance and properties of the soil. Some of these properties depend strongly on meteorological conditions such as wind speed, temperature and precipitation. This category of substances contains ammonia resulting from the spreading of manure but also includes, for example, pesticides applied to soils for agricultural purposes.

6.4.1 NH_3 emissions from land spreading

The DEPASS model (Dynamic Exchange of Pollutants between Air and Soil Surface) is developed in order to describe the vertical transport and diffusion in both soil and atmosphere, and the exchange of pollutants between the compartments in relation to actual meteorological conditions. The model is described in Van Jaarsveld (1996). The following correction factor (relative to the average emission strength) for the NH_3 emission strength of land-spread manure was derived on the basis of this model and using a regression analysis of emissions and meteorological parameters:

$$EC_{spread} = 1 + 1.55\ 10^{-5}\ [\ (100 / R_a\ )^{0.8}\ (\ T + 23\ )^{2.3}\ ]^{1.25} \qquad (6.32)$$

in which T is the ambient temperature in degrees Celsius and R_a the aerodynamic resistance of the lower 4 m of the atmosphere (in s m^{-1}). Basically, the effect of wind speed and atmospheric stability is included in the aerodynamic resistance. The correction factor determined in this way amounts to 1.8 during unstable atmospheric conditions (daytime on sunny days) and 0.07 during very stable conditions (cloudless night under low wind conditions). On average, the factor varies from approx. 0.4 in January to 1.5 in July.

The parameterisation of the relative emission strength of manure applied to the surface is incorporated in the OPS model, first applied in a study on emission–deposition relations in the Netherlands (Van Jaarsveld *et al*., 2000). The most striking result is the difference between the impact of emissions of animal housing systems and emissions due to land-spreading of manure. This is one of the reasons why the effect of emission reduction measures (mainly incorporating manure into the soil top layer) did not show up in measured ammonia concentrations in the Netherlands.

Besides a correction factor for land-spreading emissions describing variations in volatilisation relative to yearly averages, one might consider an activity correction factor. This is of major importance if the model is used on a monthly basis, because there is a distinct seasonal pattern in the application of manure to the field. However, such a correction can be applied afterwards and is therefore not included in the present model.

6.4.2 NH_3 emissions from animal housing systems

For emissions related to animal housing systems a dependency has been chosen on the basis of measurements of Kroodsma *et al*. (1993) and Groot Koerkamp and Elzing (1996). The correction factor is:

$$EC_{house} = 1 + 0.04 * (\ T - T_{avg}\ ) \qquad (6.33)$$

where T is the outdoor temperature and T_{avg} the (long-term) average outdoor temperature (T_{avg}=10). The average correction factor for emissions from animal housing systems is approximately 1.3 in July and 0.7 in January. This kind of emission is clearly less influenced by meteorology than land-spreading emissions. The factor 0.04 in (2) is, in fact, based on relations with indoor temperatures in a mechanically ventilated cattle-housing system. In the present study it is assumed that the temperature variations for

indoor and outdoor are equal, which probably leads to an overestimation of the temperature effect. Moreover, there is also no distinction made between housing systems for cows, pigs or poultry, or between naturally or forced ventilated systems. Neither is a dependency of the ventilation rate on outdoor wind speed included.

6.5 References chapter 6

Asman W.A.H. and Janssen A.J. (1987) A long-range transport model for ammonia and ammonium for Europe. *Atmospheric Environment* **21**, 2099-2119.

Asman W.A.H. and Jaarsveld J.A. van (1992) A variable-resolution transport model applied for NH_x in Europe. *Atmospheric Environment* **26A**, 445-464.

Barrie L.A. (1978) An improved model of reversible SO_2-washout by rain. *Atmospheric Environment* **12**, 407-412.

Barrie L.A. (1981) The prediction of rain acidity and SO_2 scavenging in eastern North America. *Atmospheric Environment* **15**, 31-41.

Baulch D.L., Cox, R.A. Crutzen P.J., Hampson R.F. Jr., Kerr, F.A. Troe, J. and Watson R.P. (1982) Evaluated kinetic and photochemical data for atmospheric chemistry: *J. Phys. Chem. Ref. Data* **11** (Suppl. 1), 327-496.

Behra P., Sigg L. and Stumm W. (1989) Dominating influence of NH_3 on the oxidation of aqueous SO_2: The coupling of NH_3 and SO_2 in atmospheric water. *Atmospheric Environment* **23**, 2691-2707.

Calvert J.G., Su F., Bottenheim J.W. and Strausz O.P. (1978) Mechanism of the homogeneous oxidation of sulfur dioxide in the troposhere. *Amospheric Environment* **12**, 197-226.

Chan W.H. and Chung D.H.S. (1986) Regional-scale precipitation scavenging of SO_2, SO_4, NO_3, and NHO_3. *Atmospheric Environment* **20,** 1397-1402.

Cox R.A. and Jenkin M.E. (1987) Kinetics of the formation of nitrous acid from the thermal reaction of nitrogen dioxide and water vapour. In: Physico-Chemical Behaviour of Atmospheric Pollutants: Proceedings of the 4th European Symposium; Stresa, Italy. D. Reidel, Dordrecht, the Netherlands.

De Leeuw F.A.A.M., Kesseboom H. and Egmond N.D. van (1985) Numerieke verspreidingsmodellen voor de interpretatie van de meetresultaten van het Nationaal Meetnet voor Luchtverontreiniging; ontwikkeling 1982-1985. RIVM, Bilthoven, the Netherlands. Report no. 842017002.

De Leeuw F.A.A.M., Rheineck Leyssius H.J. van and Builtjes P.J.H. (1990) Calculation of long term averaged ground level ozone concentrations. *Atmospheric Environment* **24A**, 185-193.

Derwent R.G. and Nodop K. (1986) Long-range transport deposition of acidic nitrogen species in north-west Europe. *Nature* **324**, 356-358.

Derwent R.G., Hov Ø., Asman W.A.H., Jaarsveld J.A. van and Leeuw F.A.A.M de (1989) An intercomparison of long-term atmospheric transport models; the budgets of acidifying species for the Netherlands. *Atmospheric Environment* **23**, 1893-1909.

Erisman J.W. (1992) Atmospheric deposition of acidifying compounds in the Netherlands. [PhD thesis]. Utrecht University, the Netherlands.

Erisman J.W., Vermetten A.W.M., Asman W.A.H., Waijers-IJpelaan A. and Slanina J. (1988) Vertical distribution of gases and aerosols: The vertical behaviour of ammonia and related components in the lower atmosphere. *Atmospheric Environment* **22**, 1153-1160.

Erisman J.W., Pul W.A.J. van and Wyers G.P (1994b) Parameterization of surface resistance for the quantification of atmospheric deposition of acidifying pollutants and ozone. *Atmospheric Environment* **28**, 2595-2607.

Groot Koerkamp, P.W.G. and Elzing A. (1996) Degradation of nitrogenous components in and volatilization of ammonia from litter in avary housing systems for laying hens. *Transactions of the ASAE*, Vol. 39.

Hales J.M. (1978) Wet removal of sulfur compounds from the atmosphere. *Atmospheric Environment* **12**, 389-399.

Haul P.R. (1978) Preliminary estimates of the washout coefficient for sulphur dioxide using data from an East Midlands ground level monitoring network: Short communication. *Atmospheric Environment* **12**, 2515-2517.

Haury G., Jordan S. and Hofmann C. (1978) Experimental investigation of the aerosol-catalyzed oxidation of SO_2 under atmospheric conditions. *Atmospheric Environment* **12**, 281-287.

Heikes B.G. and Thompson A.M. (1983) Effects of heterogeneous processes on NO_3, HONO and HNO_3 chemistry in the troposphere. *J. Geophys. Res.* **88**, 10883-10895.

Hewitt C.N. and Harrison R.M. (1985) Tropospheric concentrations of the hydroxyl radical - A review. *Atmospheric Environment* **19**, 545-554.

Hjellbrekke A.G. (1999) Data Report 1997; Part 1: Annual summaries. EMEP/CCC-Report 3/99, Norwegian Institute for Air Research, Kjeller, Norway.

Hov Ø., Eliassen A. and Simpson D. (1988) Calculation of distribution of NO_x compounds in Europe. In: Isaksen I.S.A., editor. *Tropospheric Ozone*. D. Reidel, Dordrecht, the Netherlands. p. 239-261.

Hübler G. Perner D., Platt U., Tönnissen A. and Ehhalt D.H. (1984) Groundlevel OH radical concentration: New measurements by optical absorption. *J. Geophys. Res*. **89**, 1309-1320.

Iversen T., Halvorsen N.E., Mylona S. and Sandnes H. (1991) Calculated budgets for airborne acidifying components in Europe; 1985,1987,1988,1989 and 1990. The Norwegian Meteorological Institute, Oslo, Norway. EMEP/MSC-W Report 1/91.

Janssen A.J. and Brink H.M. ten (1985) De samenstelling van neerslag onder een rookgaspluim: modellering, berekening en validatie. Netherlands Energy Research Foundation, Petten, the Netherlands. Report ECN-170.

Kessler C. and Platt U. (1984) Nitrous acid in polluted air masses: sources and formation pathways. In: Versino, B. and Angeletti, editors. Physico-Chemical Behaviour of Atmospheric Pollutants. Proceedings of the European symposium; Varese, Italy. D. Reidel, Dordrecht, the Netherlands.

Kitto A.M.N. and Harrison R.M. (1992) Nitrous and nitric acid measurements at sites in south-east England. *Atmospheric Environment* **26A**, 235-241.

Kroodsma, W., Huis in 't Veld, J.W.H. and Scholtens, R. (1993)Ammonia emission and its reduction from cubicle houses by flushing. *Livestock Production Sci*. **35**:293-302.

Lamb D. Miller D.F., Robinson N.F. and Gertler A.W. (1987) The importance of liquid water concentration in the atmospheric oxidation of SO_2. *Atmospheric Environment* **21**, 2333-2344.

Lammel G., Perner D. and Warneck P. (1989) Nitrous acid at Mainz: observation and implication for its formation mechanism. In: Restelli G. and Angeletti G., editors. Physico-Chemical Behaviour of Atmospheric Pollutants: Proceedings of the 5th European symposium; Varese, Italy. D. Reidel, Dordrecht, the Netherlands.

Levine S.Z. and Schwartz S.E. (1982) In-cloud and below-cloud scavenging of nitric acid vapor. *Atmospheric Environment* **16**, 1725-1734

Liberti A. Brocco D. and Possanzini M. (1978) Absorption and oxidation of sulfur dioxide on particles. *Atmospheric Environment* **12**, 255-261

Magnotta F. and Johnston H.S. (1980) Photodissociation quantum yields for the NO_3 free radical. *Geophys. Res. Lett*. **7**, 769-772.

Misra P.K., Chan W.H., Chung D. and Tang A.J.S. (1985) Scavenging ratios of acidic pollutants and their use in long-range transport models. *Atmospheric Environment* **19**, 1471-1475.

Möller D. (1980) Kinetic model of atmospheric SO_2 oxidation based on published data. *Atmospheric Environment* **14**, 1067-1076.

Ogilvie F.R. (1982) Buitenluchtverontreiniging in Delft in 1980. TNO, Delft, the Netherlands. Report G 980.

Perner D., Platt U., Trainer M., Hübler G., Drummond J., Junkermann W., Rudolph J., Schubert B. and Ehhalt D.H. (1987) Measurements of tropospheric OH concentrations: A comparison of field data with model predictions. *J. Atmos. Chem.* **5**, 185-216.

Pio C.A. and Harrison R.M. (1987) The equilibrium of ammonium chloride aerosol with gaseous hydrochloric acid and ammonia under tropospheric conditions. *Atmospheric Environment* **21**, 1243-1246.

Ruijgrok W., Nicholson K.W., and Davidson C.I. (1993) Dry deposition of particles. In: Lövblad G., Erisman J.W. and Fowler D., editors. Models and methods for the quantification of atmospheric input to ecosystems. Nordic Council of Ministers, Copenhagen.

Scott B.C. (1982) Theoretical estimates of the scavenging coefficient for soluble aerosol particles as a function of precipitation type, rate and altitude. *Atmospheric Environment* **16**, 1753-1762.

Scire J.S. and Venkatram A. (1985) The contribution of in-cloud oxidation of SO_2 to wet scavenging of sulfur in convective clouds. *Atmospheric Environment* **19**, 637-650.

Seinfeld J.H. (1986) *Atmospheric chemistry and physics of air pollution.* John Wiley & Sons, New York.

Slanina J., Keuken M.P., Arends B., Veltkamp A.C. and Wyers G.P. (1990) Acidification research at ECN. Contribution to the Dutch Priority Programme on Acidification. ECN, Petten, the Netherlands.

Slinn W.G.N (1983) Predictions for particle deposition to vegetative surfaces. *Atmospheric Environment* **16**, 1785-1794.

Stelson A.W., Friedlander S.K. and Seinfeld J.H. (1979) A note on the equilibrium relation ship between ammonia and nitric acid and particulate ammonium nitrate. *Atmospheric Environment* **13**, 369-371.

Stelson A.W. and Seinfeld J.H. (1982a) Relative humidity and pH dependence of the vapor pressure of ammonium nitrate-nitric acid solutions at 25 ^{o}C. *Atmospheric Environment* **16**, 993-1000.

Stelson A.W. and Seinfeld J.H. (1982b) Relative humidity and temperature dependence of ammonium nitrate dissociation constant. *Atmospheric Environment* **16**, 983-992.

Stockwell W.R. and Calvert J.G. (1983a) The mechanism of the HO-SO_2 reaction. *Atmospheric Environment* **17**, 2231-2235.

Ten Brink H.M., Janssen A.J. and Slanina J. (1988) Plume wash-out near a coal-fired power plant: measurements and model calculations. *Atmospheric Environment* **22**, 177-187.

Van Egmond N.D. and Kesseboom H. (1983) Mesoscale air pollution dispersion models-II. Lagrangian PUFF-model, and comparison with Eulerian GRID model. *Atmospheric Environment*, **17**, 265-274.

Van Egmond N.D. and Kesseboom H. (1985) A numerical mesoscale model for long- term average NO_x and NO_2-concentration. *Atmospheric Environment* **19**, 587- 595.

Van Jaarsveld J. A. (1995) Modelling the long-term atmospheric behaviour of pollutants on various spatial scales. Ph.D. Thesis, Utrecht University, the Netherlands.

Van Jaarsveld J.A. (1996) The dynamic exchange of pollutants at the air-soil interface and its impact on long range transport In*: Air Pollution Modeling and its application XI,* edited by Sven-Erik Gryning and Francis Schiermayer.

Voldner E.C., Barrie L.A. and Sirois A. (1986) A literature review of dry deposition of oxides of sulphur and nitrogen with emphasis on long-range transport modelling in North America. *Atmospheric Environment* **20**, 2101-2123.

Wesely M.L. (1989) Parameterization of surface resistances to gaseous dry deposition in regional scale numerical models. *Atmospheric Environment* **23**, 1293-1304.

7. Model specification

This chapter defines the application area of the model in terms of chemical characterisation of substances, emission source types, source and receptor domain and time resolution.

7.1 Chemical characterisation of substances

The OPS model works with three groups of substances:

1. Acidifying substances (SO_2, NO_x, NH_3 and secondary products).
   - The properties of acidifying substances are fully defined within the model (see section 6).

2. Non-acidifying (gaseous) substances
   - The group of non-acidifying substances uses a generic approach in which the properties of the substance are expressed in general terms such as:
     - a chemical conversion/degradation rate
     - a dry deposition velocity or a surface resistance
     - a wet scavenging ratio.

   Chapter 5 describes how the model deals with these properties.

3. Particle-bounded substances.
   - A generic approach is followed for substances attached to particles in which the size distribution of the particles fully defines the atmospheric behaviour, see chapter 5).

7.2 Emissions

7.2.1 Source area

The model describes the transport of substances over greater distances, with wind fields generated from the time behaviour of the wind direction, wind speed, atmospheric stability and mixing height averaged over the Netherlands. Despite the rather rough extrapolation, the model was found to describe the large-scale transport of SO_2 satisfactorily (see also section 8). The source area for this model has therefore been set at a circle with a radius of 1000 km, with the Netherlands as the centre. The contribution of sources in this area to concentration and deposition in the Netherlands may be calculated for countries individually. The contribution of sources outside this area, but within Europe, can be estimated, but with less accuracy. The calculation of country-specific contributions from this area is probably not meaningful.

7.2.2 Source types

The OPS model distinguishes the following source types:

a. Point sources:

- source height >= 0 m
- negligible diameter

- with or without heat content
- particle-size distribution (optional)
- diurnal emission variation*

b. Area sources:

- source height >= 0 m
- diameter ca 10 m – 500 km
- square or circular
- with or without (average) heat content
- standard deviation of the source height (from 0 m to average source height)
- particle-size distribution (optional)
- diurnal emission variation*

* The diurnal emission variation has no effect on ammonia because in this case the emission variation is generated internally (see section 6.4), except when an emission continuous in time is specified.

Emissions of either type can be input to the model in any number and in any combination.

7.2.3 Behaviour in time

The time-dependent emission behaviour can only be specified as a daily variation (see section 5.1.1). The options are:

- 0 continuous in time
- 1 according to the (average) industrial activity over a working day
- 2 according to the (average) heating activity for space heating
- 3 dependent on traffic intensity
- -1 to –999 dependent on a daily variation to be specified by the user.

The standard diurnal variations 1,2 and 3 are specified in chapter 5. In the case of user-defined diurnal variations, the code for the diurnal variation in the emission file must be preceded by a minus sign. Codes -1, -2 and -3 are reserved for the user definition of industrial activity, household heating and traffic activity. An example of a file with user defined diurnal variations is given below. The activity is given in 2-hour classes as a percentage of the average emission. The format (in Fortran notation) is (i6,12i6,2x,a). This type of file has a '.dve' extension

```
  Code   0-2   2-4   4-6   6-8  8-10 10-12 12-14 14-16 16-18 18-20 20-22 22-24  Description
     1    73    69    68   100   129   131   124   121   109    97    93    86  ind. emissions
     2    33    33    35    80   150   155   120   116   122   135   145    77  dom. heating
     3    24    16    23   150   175   121   127   154   190   112    60    48  traffic emiss.
    -4     2     2     4     5     6     8    12    20    19    12     5     5  beach life
    -6    12     6     0     0     2     4     8     8    10    12    20    18  cafe life
```

7.2.4 Particle-size distribution

In the case of particulate emissions, the particles are considered to be distributed over five size classes, namely:

Class1	Class2	Class3	Class4	Class5
< 0.95 μm	**0.95 - 4 μm**	**4 - 10 μm**	**10 - 20 μm**	**>20 μm**

The model performs separate calculations for these classes, with specific properties for each size class (see chapter 5). The user can choose from three standard particle-size distributions (see Figure 5.3 and Table 5.1), or can define more specific distributions over the above-mentioned classes. In this way

every emission source can have its own size-distribution, provided that the total number of distributions does not exceed 999. In the case of user-defined size distributions, the code for the size distribution in the emission file must be preceded by a minus sign. Codes -1, -2 and -3 are reserved for user definitions of 'fine', 'medium' and 'course'. An example of a file with user-defined distributions is given below. The emission is given as percentages of the total emission. The format (in Fortran notation) is (i6,5f7.1,2x,a). This type of file has a '.psd' extension

```
 Code  Class1 Class2 Class3 Class4 Class5 Description
     1   70.0   20.0    5.5    2.5    2.0  standard distr. 'fine'
     2   53.0   28.0   11.5    4.2    3.3  standard distr. 'medium'
     3   42.0   33.0   14.5    5.9    4.6  standard distr. 'coarse'
    -4   50.0   20.0    8.0   10.0   12.0  coal fired power plant
    -5   20.0   10.0   10.0   10.0   50.0  waste incinerator
```

In calculating the concentrations and depositions for the heaviest particles (> 20 μm), allowance is made for the fact that the sedimentation rate of these particles is not insignificant, so that plume descent occurs with distance. This plume descent is not influenced by the stratification of the lower boundary layer.

7.2.5 Format of emission data files

The emission data are read from a file. The emission records may be preceded by one header record. Files of this type have the extension '.brn'

```
snr    x(m)    y(m)   q (g/s)   hc(mw)  h(m)  d(m)  s(m)  dv  cat area sd  comp
  1   80100  435000  .100E-01   .000   10.0  2000   3.0   0   1   1    0  SO2
  2  120640  455000  .040E-01   .000   15.0  1000   1.0   1   2   1    0  SO2
  3  110000  472500  .130E-01   .000   20.0  2000   4.0   1   2   1    0  SO2
  4  164000  399500  .220E-01  1.230   10.0 10000   3.0   4   3   1    0  SO2
```

`snr` - source identification number (not essential)
`x` - x-coordinate (m) (or decimal degrees longitude)
`y` - y-coordinate (m) (or decimal degrees latitude)
`q` - source strength (g/s)
`hc` - heat content (MW)
`h` - source height (m)
`d` - source diameter (m)
`s` - vertical spread of source height(s) (m)
`dv` - code for diurnal variation of emission (-999 to 3)
`cat` - source category number (0-9999) (for administrative purposes only)
`area` - country or area number (0-9999) (for administrative purposes only)
`psd` - particle-size distribution code (-999 to 3)
`comp` - name of the substance (not essential)

Source co-ordinates may be specified in the Dutch RDM-system (originating near Paris parallel to 52^{o} 30' longitude) or as geographical co-ordinates (degrees longitude/latitude). The two systems may be inter-mixed.

The format of a source record (in Fortran notation) is:

```
(i4,2i8,e10.3,f6.1,i7,f6.1,4i4,2x,a12)
```

If the co-ordinates are specified in degrees longitude/latitude, the format is:

```
(i4,2f8.3,e10.3,f6.1,i7,f6.1,4i4,2x,a12)
```

7.3 Meteorological statistics

7.3.1 Meteorological time-scale

Basically, the OPS model calculates long-term average concentrations and depositions. In fact, the period for which the calculations are representative is entirely determined by the period for which the meteo-statistics have been made. At present, information is available for the individual years since 1981. The long-term climatological data in the model are based on the 1990-1999 data.

In addition to the standard (multi-year) averages, the OPS model can also calculate concentrations and depositions for shorter periods (specific year, season, month). As for specific areas mentioned in the previous section, special statistics will then have to be compiled for such periods. By way of illustration, the calculated monthly mean concentrations of SO_2, NO_x and NH_3 in the Netherlands show a very good agreement with measurements, see section 8.3.

7.3.2 Meteorological area

In the standard situation the model interpolates the meteorological data of nearby regions to the position of the selected receptor.

Special situations
As an option, the user of the model can disconnect the automatic coupling of meteorological data and receptor position by manually selecting one of the six (standard) meteorological regions in the Netherlands or the Netherlands as a whole, see Figure 7.1. A further option is being able to specify a special climatological data file provided that more specific data for a certain (small) area is available. These files can only be created with the meteorological pre-processor of the model. This pre-processor is, however, currently not available for users.

7.4 Receptor characteristics

Receptor points are characterised by their co-ordinates, height, land-use type and roughness length. The Receptor height is fixed within the OPS model. In terms of the vertical dispersion, the receptor height is set to 0 m. In terms of the influence of dry deposition on the vertical concentration profile, the receptor height is 3.8, in other words, the measuring height of the LML network.

7.4.1 Receptor domain

The area for which concentrations and depositions can be calculated is determined by the size of the area for which meteorological parameters are known. Since the standard climatological data set used for this model is based on observations from the Royal Netherlands Meteorological Institute (KNMI), the maximum size of the receptor area becomes, in effect, the Netherlands and adjoining regions. The land-use and terrain roughness data maps, covering only the Netherlands in great detail, also impose limitations.

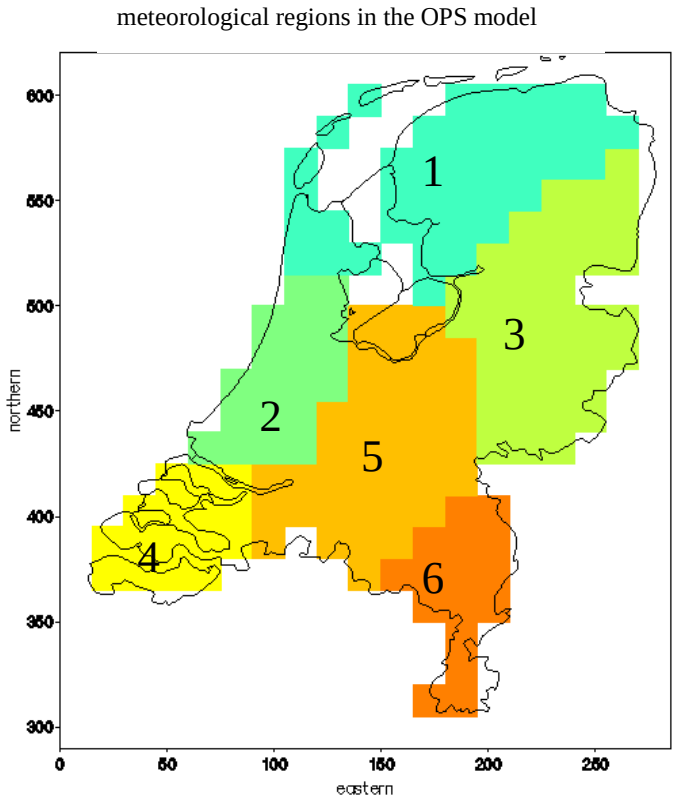

Figure 7.1 Meteorological regions in the OPS model.

7.4.2 Minimum source –receptor distance

This model does not explicitly take into account the direct influence of obstacles (e.g. buildings) on the dispersion. Instead, the general influence of obstacles is expressed in the terrain roughness variable, assuming that obstacles are homogeneously distributed over the emission-receptor area. The shortest distance from a source for which this model may be used is therefore taken as a function of the terrain roughness length.

In flat terrain with no obstacles the minimum distance is in the order of 20 m. For a terrain roughness > 0.1 m, the shortest distance is approx. 200 times the roughness length. When the stack is part of a building, the shortest distance is at least five times the height of the building. The model generates no warnings if these rules are violated.

One should be aware that in the case of gridded receptor points in combination with point sources, the minimum source-receptor distance requirement cannot always be met.

7.4.3 Land-use and roughness characteristics

Since the land-use type and the roughness length are related to the geographical co-ordinates of the point, the model reads the land use and roughness length from maps. For specific receptor locations the model selects the land-use properties from the 250 m resolution map. In the case of gridded receptor points, the model selects a corresponding spatial resolution (250, 500, 1000, 5000 m). It is important to note here is that the calculation of a grid-cell representative roughness length is based on a logarithmic weighing of roughness elements, while the grid cell representative land-use type is defined as the most abundant land-use type within that grid cell.

7.4.4 Selection of receptor points

Receptor points for calculating concentrations and depositions can be chosen:

- on a regular (Cartesian) grid, with a grid distance to be chosen. The domain may be pre-defined (the Netherlands) or defined by the user.
- for a number of specific locations to be defined by the user

The output format differs according to the option chosen. The latter option is especially useful when results have to be compared with observations. The gridded results are formatted in a matrix form, while the results for specific receptor points are formatted as single records for each point.

Although the model permits calculations for a grid, one must realise that:

The OPS model produces, in principle, point information, not grid cell averages!

This should be kept in mind when selecting the position of receptor points in relation to emissions (either point sources or gridded emissions). It is wise - in order to avoid interference- to define a receptor grid in such a way that the receptor points are situated in or near the centre of emission grid cells.

Non-gridded receptor locations are read by the model from a file. A record of the receptor file contains number, name, X co-ordinate in (m) and Y co-ordinate (m). Receptor co-ordinates are specified in the Dutch RDM system (originating near Paris parallel to 52^{o} 30' longitude). In contrast with the old OPS-V1.20E version of the model, co-ordinates must be given as absolute values. The format of receptor files (in Fortran notation) is (i4,1x,a12,2i8). An example is given below:

```
Nr   Name          X-coor  Y-coor
   1 Bilthoven     141900  459100
   2 Rekken        246400  457000
   3 Witteveen     241400  536900
   4 Vredepeel     187300  394700
```

The limitations to the number of receptor points and/or resolution imposed by the model are as follows. For a pre-defined grid covering the Netherlands the maximum resolution (i.e. the minimum grid cell dimension) is 500 m. For a user-defined grid the maximum number of receptorpunts (i.e. grid cells) amounts to 999 times 999 and the maximum resolution is 1 m. There are no limitations when non-gridded receptor locations are read from a file. In practice however, limitations may be imposed by the availability of memory resources, although the memory requirements of OPS are rather low.

7.5 References chapter 7

Van Jaarsveld J. A. (1995) Modelling the long-term atmospheric behaviour of pollutants on various spatial scales. Ph.D. Thesis, Utrecht University, the Netherlands.

8. Model validation and uncertainty

Introduction
Chapter 2 has already presented comparisons on subsections of the model e.g. the prediction of the mixing height (section 2.3.2), a comparison of trajectories (section 2.3.4) and the cross-wind integrated concentration around point sources (section 3.2.1). In this chapter, routine measurements of pollutants in air and precipitation will be used to test model predictions on different time-scales and spatial scales. Sulphur species and oxidised nitrogen species have been selected for these tests because of the abundance of available information, both for measurements and emissions.

This chapter presents the results of the comparisons with measurements. First, the measurement networks are described in terms of density and frequency, followed by a description of the emission data. Comparisons for primary and secondary concentrations in air and wet deposition fluxes are presented on a monthly and annual basis as a test of the influence of meteorological variations. Similarly, the modelled spatial distributions are tested by comparing them with observations at individual stations. The calculated impact of a single (high) source on its direct surroundings is also verified with measurements. Also supplied is an overview of model intercomparisons involving the present model, including several key results.

Finally, an attempt will be made on the basis of the results of the model–measurement comparisons to quantify the uncertainties in the model predictions for the different spatial scales. In the following passages, the terms SO_x, NO_y or NH_x deposition refer to the sum of the deposition of all SO_x, NO_y or NH_x species, respectively. The different SO_x, NO_y and NH_x species are defined in Chapter 6.

8.1 Measurements

Concentrations in air
The concentrations of SO_2 and NO_x ($NO + NO_2$) in air are monitored in the LML on an hourly basis. This network, operational since 1975, first consisted of a total of 226 and 99 sites for monitoring SO_2 and NO_x respectively (RIVM, 1982). In 1986 a newly designed network, consisting of 85 stations for SO_2 and 45 for NO_x went into operation (Elskamp, 1989). With regard to the spatial representativeness, a distinction has been made between so-called gridded, city and street stations. The gridded stations have been set up in the Netherlands to provide a representative image of 'background' concentrations. Up to 1986, concentrations of SO_2 and NO_x were also routinely measured at 4, 100 and 200 m levels on the KNMI meteorological tower at Cabauw. The standard sampling height of the network is 3.5 m.

Concentrations of aerosols (SO_4^{2-}, NO_3^- and NH_4^+) are measured as daily samples using a low-volume filter sampling technique. The number of stations has varied throughout the years between 2 and 6 stations.

Concentrations in precipitation
The concentrations of components in precipitation have since 1983 been routinely monitored on a monthly basis in the National Precipitation Chemistry Monitoring Network (KNMI/RIVM, 1988). In

1988 this network was incorporated in the LML (RIVM, 1989; 1990; 1991). The network consists of 14 stations, located as much as possible at the same sites as the stations for air concentration monitoring. At the beginning of 1988 the so-called bulk samplers were replaced by wet-only samplers. The latter devices exclude dry deposition onto the funnel during dry periods. To obtain comparable results, the concentrations reached with the bulk samplers were corrected with factors derived from parallel measurements with the two samplers (Ridder *et al.*, 1984). These correction factors are 0.75 for SO_4^{2-} and 0.85 for both NH_4^+ and NO_3^-.

Before the measured wet SO_x deposition (measured as SO_4^{2-}) can be used for validation purposes, a correction has to be carried out to exclude sulphate of non-anthropogenic origin. The latter consists mainly of sulphate from sea salt. This correction is accomplished by assuming that the sodium concentration in precipitation completely originates from sea salt, while the molar ratio for sulphate and sodium, amounting to 0.0602, in sea salt is known.

8.2 Emissions

Since the concentration levels measured in ambient air and precipitation constitute contributions of sources (man-made or natural) in a very large area, it will be necessary to take all these contributions into account in the model before a successful comparison can be made with the measurements. With an expected atmospheric residence time for secondarily formed aerosols (SO_4^{2-}, NO_3^- and NH_4^+) of 2-3 days, this means that an emission area as large as Europe will have to be used. From studies on the trans-Atlantic transport of sulphur one can conclude that the contribution from sources in North America to the Netherlands is low (Whelpdale *et al.*, 1988; Tarrason and Iversen, 1992). Furthermore, volcanic and biogenic emissions of sulphur and nitrogen compounds have been considered to have little impact compared to human-induced emissions in this area. It was decided to account for these kinds of emissions by adding fixed 'background' concentrations to the model results (see 8.3.1).

National totals of emissions for SO_2 and NO_x used in the calculations represent the official data submitted by countries participating in EMEP (e.g. Sandnes, 1993). Two different sources of spatial distribution of emissions have been used throughout the years.

1980-1993
The emissions for Eastern European countries are presented in the so-called EMEP grid with a resolution of 150 x 150 km. A 50 x 50 km subgrid distribution in the so-called OECD countries was taken from Lübkert and De Tilly (1988). For an area of approximately 400 x 400 km - including the Netherlands and parts of Belgium, along with former West Germany - emission of SO_2 and NO_x was inventoried by TNO (Veldt, 1981; 1983). The resolution in this area is 5 x 5 km inside and 25 x 25 km outside the Netherlands; data such as position, emission strength, stack height and heat output of a large number of individual point sources are also included. The detailed emissions for the 400 x 400 km area are, however, only available for the year 1980. The relative distribution of emissions is therefore also used for the years following 1980. The SO_2 and NO_x emission density distributions for the Netherlands and Europe as a whole are given in an appendix.

From the gridded emissions, subsets, representing the following emission categories – high-level industrial sources, low-level industrial sources, domestic heating and mobile sources – have been made using estimations of the relative distributions for each country given by Lübkert and De Tilly (1988). In this way it was possible to distinguish source heights and adjust domestic heating emissions to temporal temperature variations. Characteristic diurnal variations for each of the emission categories were also applied (Van Jaarsveld, 1990).

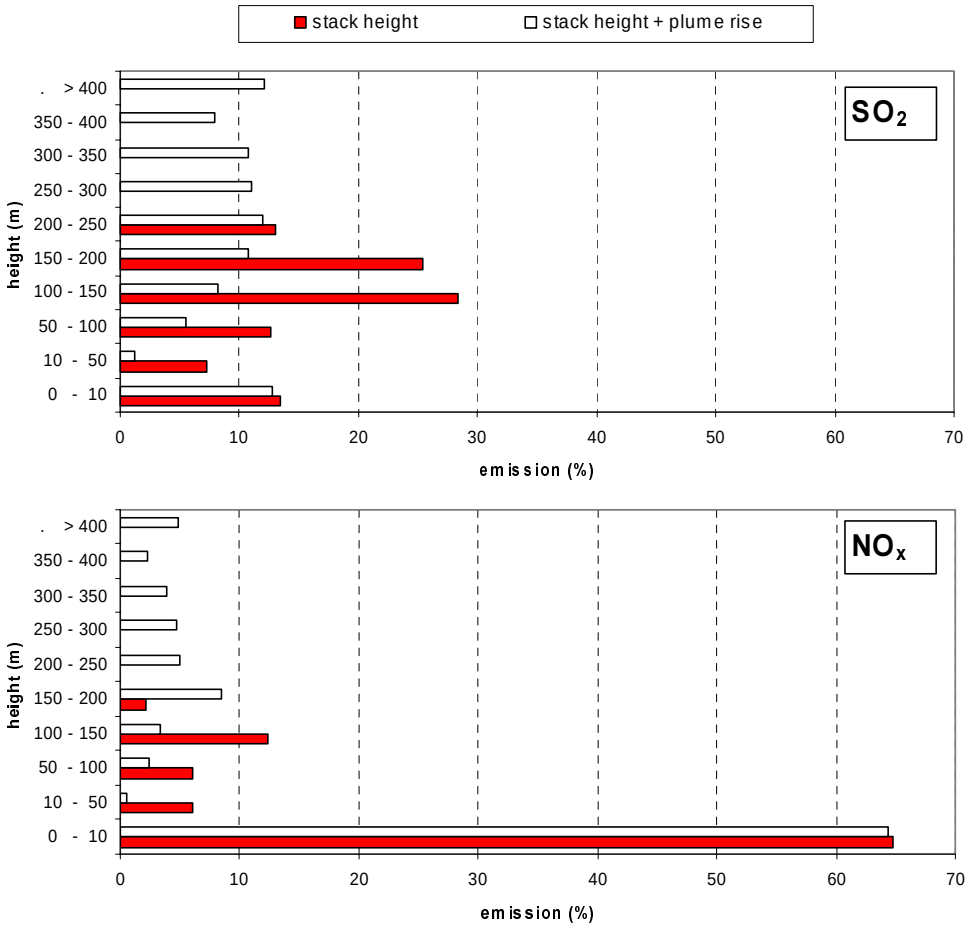

Figure 8.1 *Height distributions of SO_2 and NO_x emissions in the Netherlands in 1980. Solid bars give the stack height distributions, while the open bars represent the plume height distributions, including plume rise.*

The emission-stack height distributions of SO_2 and NO_x, derived from the TNO emission inventory for the Netherlands, are shown in Figure 8.1. This figure clearly reflects the difference between SO_2 and NO_x sources: NO_x dominated by mobile sources and SO_2 by high point sources. If the rise of hot plumes is taken into account, then the difference between SO_2 and NO_x is even more pronounced. In the SO_2 case, the height distribution of emissions may have leaned towards lower emission heights in the 1980-1993 period because the contribution of emission from power plants in the Netherlands decreased from 40% in 1980 to 16% in 1993 (CBS, 1994). The effect of changing contributions of source categories in terms of corresponding changes in spatial distribution of emissions is not taken into account in the calculations.

The NH_3 emissions in Europe (except the Netherlands) are taken from the inventory in Asman (1992). This inventory for the year 1987 has a basic resolution of 75 x 75 km, but for Belgium and the western part of former West Germany the inventory contains emissions for each municipality. The latter emissions are characterised for use in this model by a representative origin and radius. The inventory from Erisman (1989) is used for emissions of NH_3 in the Netherlands. These emissions are given for the years 1987 and 1988 on a 5 x 5 km grid.

1990-2000 Europe. The basis of the SO_2 and NO_x European emission distribution is formed by the CORINAIR 1985 database (CITEPA, 1989; 1991; 1993). This database contains data on individual point sources and aggregated emissions (NUTS level 3) for the so-called EU12 countries. An 11-source sector split has also been . In the RIVM/EUREM model (van der Maas, 1996) the emissions are gridded into a 1^o longitude x 0.5^o latitude grid using GIS procedures. The gridded data are further redistributed in a 5 x 5 km grid covering Belgium and Western Germany in order to fit the Dutch emission grid but also to avoid overlap in emissions near the border. The 11 sectors are translated and redistributed over five sectors: 1. Power plants, 2. Combustion in processes and industry, 3. Processes in industry, 4. Transport and 5. Domestic combustion and combustion in trade. Emission data of non-EU12 European countries were adapted from the LOTOS model (Veldt, 1991) ; these emissions have a 2^o longitudinal x 1^o latitude resolution. A further extension of the data is formed by the emission from ships on the North Sea. These data were taken from the EMEP emission database having a 50 x 50 km resolution in the EMEP co-ordinate system. The result is further documented in Appendix III.

Emissions for the different years are obtained by scaling the base emissions with data reported to EMEP. The sector split has not been changed over the years. A severe limitation of the emission data is that the basic spatial detail in the vicinity of the Dutch border is in fact approx. 50 x 50 km. Considering the position of industrial areas in Belgium close to the Dutch border (Gent, Antwerp), errors in nearby Dutch regions can be expected. The distribution of ammonia emissions over Europe is basically the same as the map produced by Asman (1992). As for SO_2 and NO_x the country emissions are scaled to the official NH_3 emissions reported by EMEP.

1990-2002 Netherlands. The basis of the emissions and the emission distribution is the Dutch Emission Registration (ER) system (Berdowski, 1994). This system consists of two parts: the individually registered emission sources and the collectively registered emissions. Examples of the first category are power plants registered by their co-ordinates, stack height etceteras. Emissions due to mobile sources or emissions due to domestic heating are examples of the collectively registered emissions. The ER systems are regularly updated. All emissions are categorised into a detailed sector split.
The RIVM RIM+ model (Wesselink *et al*., 1998) uses the ER data to produce the emission files required for the usual model calculations. The RIM+ model aggregates the emission data of the detailed sector split into the so-called LLO split, which currently consists of 28 sectors (see Appendix III). The aggregation includes also the weighting of emission characteristics such as source height and heat content. Furthermore the RIM+ model provides the spatial distribution of the (non-point source) emissions and produces the data in the format required by the OPS model. The basic resolution of the diffuse emissions is 5 x 5 km. An overview is given in Appendix III

Agricultural ammonia emissions are calculated by a manure model developed by the Agricultural Economics Research Institute (LEI). The input data for this model are divided into general and specific. General input data are taken from the annual agricultural census. Specific input data concern the nitrogen and phosphate excretion by the different animal categories, the ammonia volatilisation rates from animal housing systems and land application systems for animal manure. The share of systems with a low ammonia volatilisation rate is also taken into account. The yearly sequence of emission calculations is described in van der Hoek (2002). Important for the use of these emissions in the OPS model are the spatial distributions of the emissions (van Jaarsveld and van Pul, 2002). The present data contains emissions from animal housing systems in a 500 x 500 m grid. Other agricultural ammonia emissions (such as those due to the application of manure on grassland) are available on a municipal level and gridded on the basis of 500 x 500m land-use maps. Non-agricultural ammonia emissions, available in the ER system, follow the SO_2 and NO_x approach.

8.3 Comparison with measurements

8.3.1 Estimated concentration and deposition levels due to non-anthropogenic sources

Before a realistic comparison of modelled levels with measured levels can be made, one has to consider the influence of sources not taken into account in the model calculations. These sources include natural emissions but also sources outside the model area such as emissions from North America. In the case presented here, use is made of data from Locht and Van Aalst (1988) who estimated non-anthropogenic fluxes of acidifying components by two methods: a box model in combination with emission estimates of a large area and a method based on measurements carried out at remote (e.g. oceanic) areas. Results are given in Table 8.1. The deposition levels given in Table 8.1 are equal to those used in recent studies (Albers *et al*., 2001) except for the wet deposition of NH_x which is now based on precipitation collected on a weathership in the North Atlantic (Buijsman *et al*., 1991)

Table 8.1 Background concentrations and deposition in the Netherlands

Component	Concentration in air	Wet deposition	Dry deposition	Total deposition
	$\mu g\ m^{-3}$	$mol\ ha^{-1}\ a^{-1}$	$mol\ ha^{-1}\ a^{-1}$	$mol\ ha^{-1}\ a^{-1}$
SO_2	0.20			
SO_4^{2-}	0.30			
SO_x		42	12	54
NO_x #	0.70			
NO_3^-	0.15			
NO_y		36	13	49
NH_3 #	0.20			
NH_4^+ #	0.15			
NH_x		55	48	103

mainly due to natural emissions

8.3.2 Checking the temporal behaviour

In Figures 8.2, 8.2 and 8.3 modelled concentrations and depositions are compared with measurements on a month-to-month basis. Although the model was initially set up to describe long-term averages, it was felt that such a comparison should emphasise the performance of the model with regard to the incorporated meteorological processes. For this comparison meteorological data sets had to be produced by the pre-processor for every single month. For the comparison of SO_2 and NO_x concentrations, only data from so-called gridded stations were selected; for the other species, all available measurements were used. The model calculations were carried out for exactly the same locations.

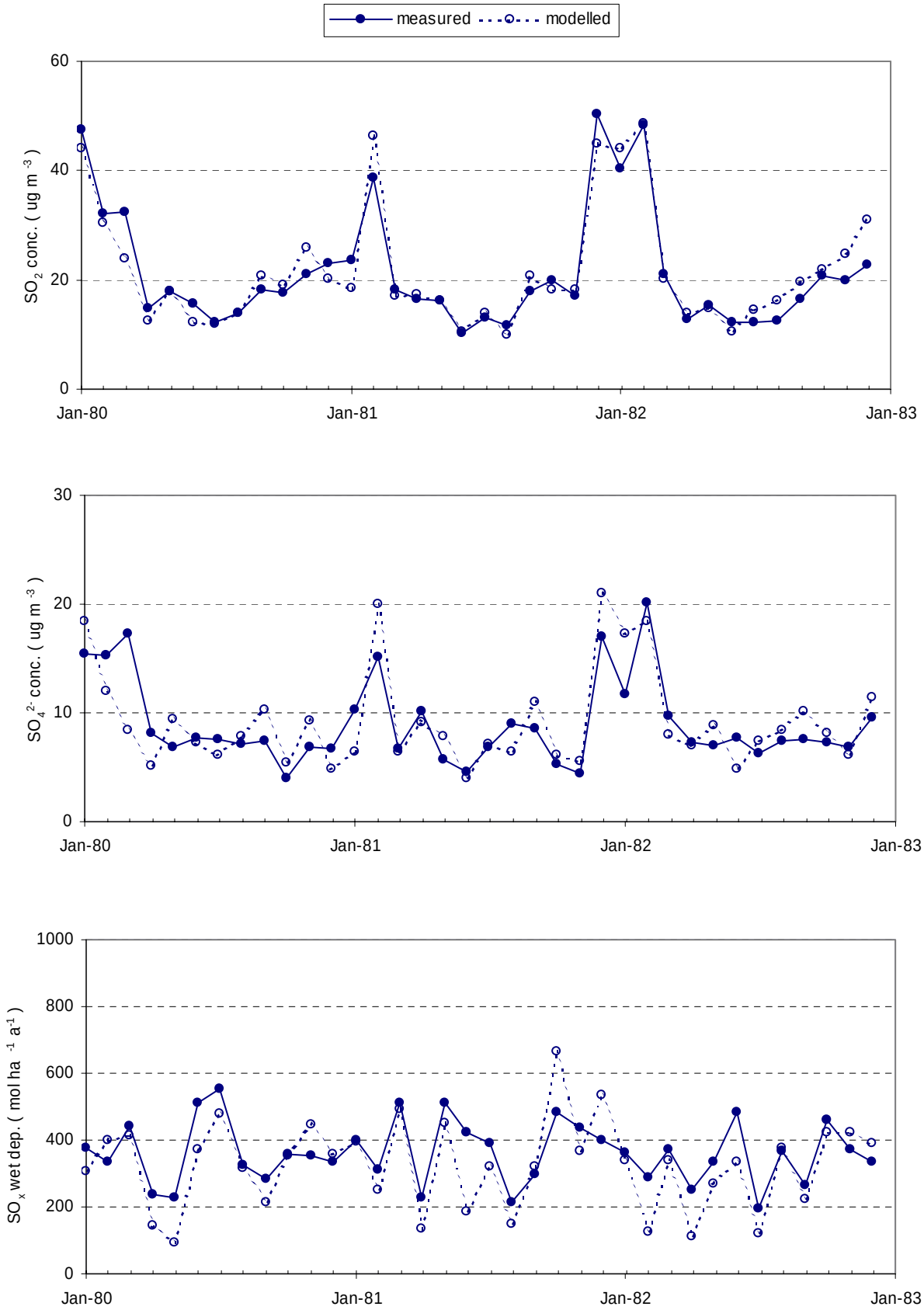

Figure 8.2 *Calculated SO_x species compared with observations. Values represent spatial averages for the Netherlands (SO_2: 97 locations; SO_4^{2-} aerosol: 2-6 locations; SO_x wet deposition: 14 locations).*

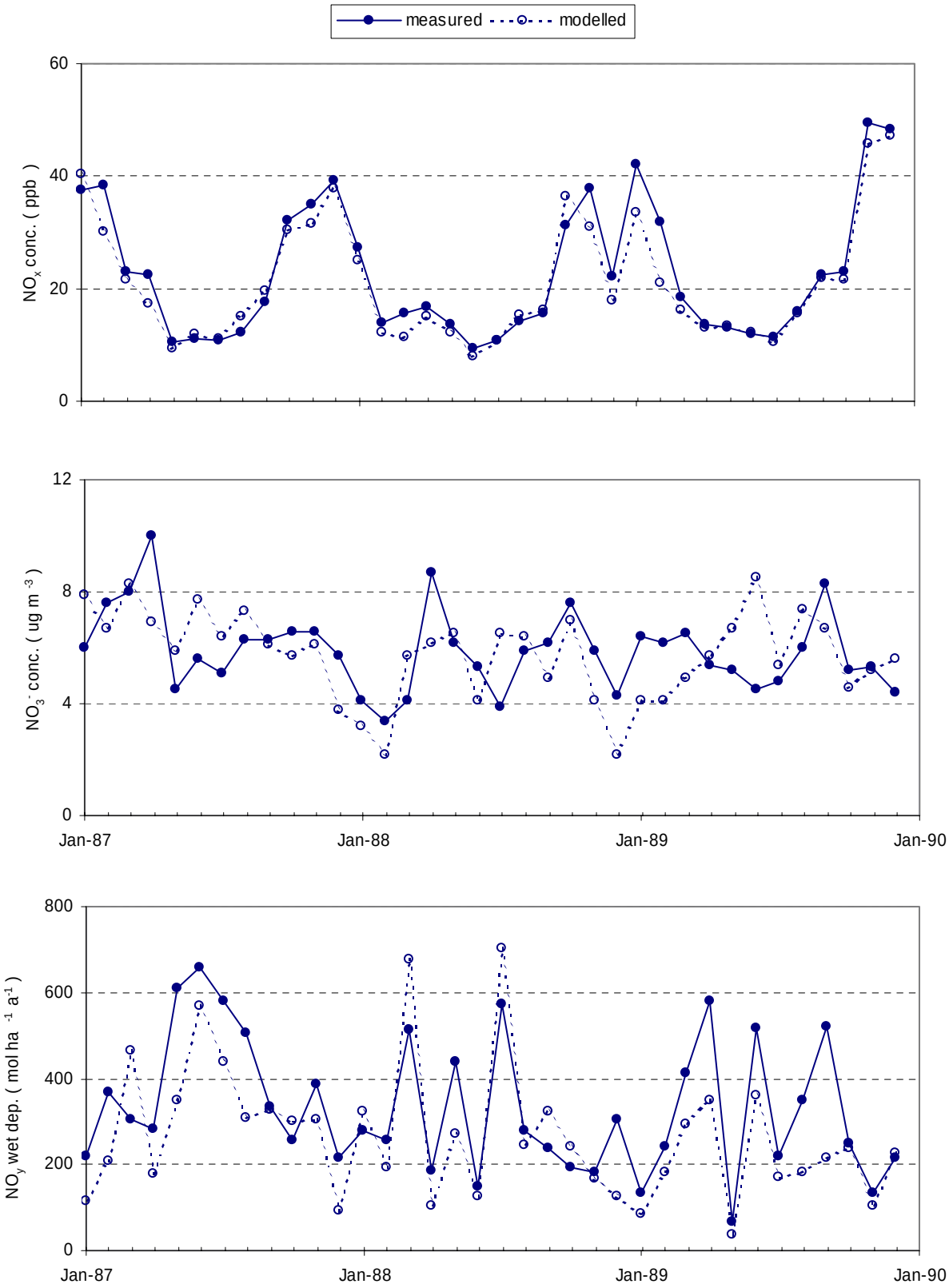

Figure 8.3 *Calculated NO_y species compared with observations. Values represent spatial averages for the Netherlands (NO_x: 33 locations; NO_3^- aerosol: 2-6 locations; NO_y wet deposition: 14 locations).*

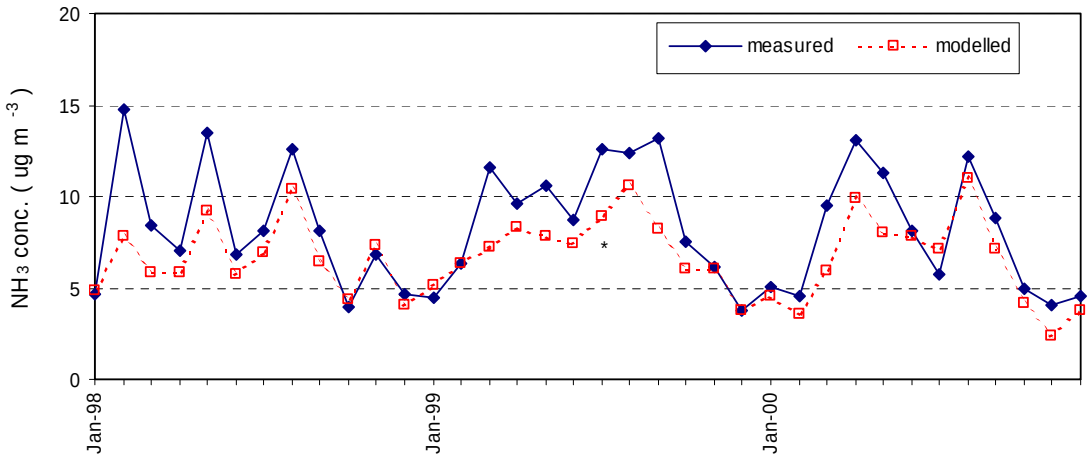

Figure 8.4 *Calculated monthly NH_3 concentrations compared with observations. Values represent spatial averages for the Netherlands (7 locations).*

In order to concentrate on the temporal behaviour of the model, the influence of local circumstances was minimised by averaging over all the stations. The comparison was carried out over a period of three years using the same 1980 emission data for all the individual months and the same meteorological data for all locations.

As can be seen in Figures 8.2 and 8.3 the model follows the month-to-month variations of the primary species SO_2 and NO_x very well. Since spatially averaged concentrations are compared, it can be stated that the observed variations are mainly due to meteorological influences and that the model describes these influences well. A more quantitative investigation, in which parameters are responsible for the temporal variations, is given in section 6.2.

The agreement for the secondarily formed SO_4^{2-} and NO_3^- aerosols is reasonable. High concentrations during several winter months are well simulated. One should keep in mind that the quality of the aerosol measurements is assumed to be less than for measurements of the SO_2 and NO_x data (Erisman, 1992). If one considers that most of the month-to-month variations are caused by variations in precipitation amounts, the performance of the model in simulating monthly wet deposition fluxes is less convincing than for monthly air concentrations. Over the three years shown, there is no indication of systematic over- or underestimation in any season.

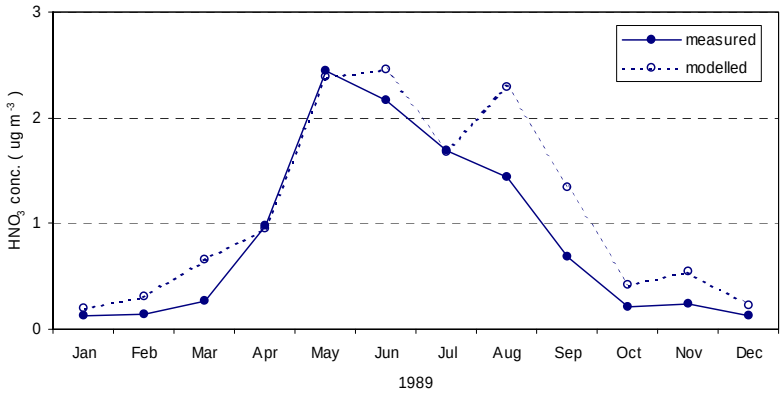

Figure 8.5 *HNO_3 concentrations compared with measurements. Measured monthly values are based on 8-day sampling cycles at three locations in the Netherlands (Mennen et al., 1992).*

Long time-series of measured HNO_3 concentrations are not available. Mennen *et al*. (1992) measured daily HNO_3 concentrations at three locations in the Netherlands at a rate of once in eight days for each location. Their 1989 data are used here to test the performance of the model in simulating monthly HNO_3 concentrations. The results are shown in Figure 8.5. Both measured and modelled concentrations show a distinct diurnal pattern, with the highest concentrations in the summer period.

Quantitative data on the results of this and other comparisons are given in Table 8.2. The results for the 1980-1990 period were taken from Van Jaarsveld (1995). Calculations for more recent years are carried out on the basis of emissions according to the official national data submitted to EMEP by the countries (Vestreng, 2003; updates from http://webdab.emep.int/). Besides a correlation coefficient, the following indices are computed to estimate the goodness of fit between observed and modelled quantities:

$$R_{PO} = \frac{\overline{C_p}}{\overline{C_O}} \tag{8.1}$$

$$RRMSE = \left[\frac{1}{N} \sum \left(\frac{C_P - C_O}{C_O} \right)^2 \right]^{1/2} \tag{8.2}$$

where the C_P and C_O refer to predicted and observed quantities, and N to the number of observations. R_{PO} stands for the ratio predicted/observed and *RRMSE* for the Relative Root-Mean Square Error. This way of normalising the differences with the observed values ensures that all errors in the entire range of possible values will be equally weighted. R_{PO} for the primary components SO_2 and NO_x approaches, both for monthly and yearly averages. For wet deposition of NO_y, the ratio based on monthly averages is lower than the ratio based on yearly averages, while averaging is carried out over the same time period. The reason for this can be found in the way this model classifies meteorological situations (see the discussion in section 4.2 of the previous chapter). In contrast to this, R_{PO} for wet SO_x deposition based on calculations for 10 individual years is lower than for the calculations on a monthly basis for the 1980-1982 period. Here, another aspect plays a role, namely, that measured wet deposition decreased much less in the period 1980-1989 than corresponding SO_2 emissions, which probably points to a non-linearity problem. This phenomenon is further discussed in section 6.2. From Table 8.2 it can also be concluded that the longer the averaging time, the lower the *RRMSE*. Erisman (1992) suggests that on the basis of expert judgement systematic errors in measured yearly average SO_2 and NO_x concentrations are of the order of 15%. The *RRMSEs* for primary concentrations are of the same order, even for monthly averages.

Table 8.2 Comparison of the temporal behaviour of the model, where both model results and measurements are aimed at the representation of spatial averages for the Netherlands. Model results up to 1990, taken from van Jaarsveld (1995), are calculated by OPS-V1.20E, while other results are calculated by OPS-Pro 4.1.

Component	Period	Averaging time	*N*	Pred/obs R_{PO}	Correlation coefficient R^2	*RRMSE* (%)
SO_2 conc.	1980-1982	month	36	1.04	0.94	14
	1980-1989	year	10	1.01	0.86	9
	1999-2002	year	4	1.02	0.97	3
SO_4^{2-} aer. conc.	1980-1982	month	36	0.97	0.57	28
	1980-1989	year	9	0.84	0.85	20
	1999-2002	year	4	0.69	0.78	32
SO_x wet dep.	1980-1982	month	36	0.85	0.56	30
	1980-1989	year	10	0.75	0.76	29
	1999-2002	year	4	1.01	0.92	5
NO_x conc.	1979-1989	month	132	0.94	0.88	15
	1979-1989	year	11	1.05	0.96	7
	1999-2002	year	4	1.11	0.71	11
NO_3^- aer. conc.	1987-1989	month	36	0.97	0.17	30
	1984-1989	year	6	0.96	0.64	8
	1999-2002	year	4	1.03	0.80	2
NO_y wet dep.	1978-1989	month	144	0.75	0.58	36
	1978-1989	year	16	0.98	0.41	12
	1999-2002	year	4	0.89	0.61	12
NH_3 conc.	1995-2002	year	8	0.74	0.92	26
NH_4^-+aer. conc.	1995-2002	year	8	0.78	0.70	25
NH_x wet dep.	1995-2002	year	8	0.68	0.90	32

8.3.3 Checking the trends

In Figures 8.6-8.8 a comparison is made of observed and calculated trends in concentrations and wet deposition. Such a comparison is useful for ascertaining if the model is able to reproduce the (possibly non-linear) changes in the past and, subsequently, to examine the ability of the model to describe the effect of future emission changes. The most dramatic decrease in environmental levels is shown by the SO_x species, for example, the SO_2 concentration decreases more than a factor of 5 in the 1981-2002 period. Wet deposition of SO_x decreases much less, i.e. a factor of 2.5

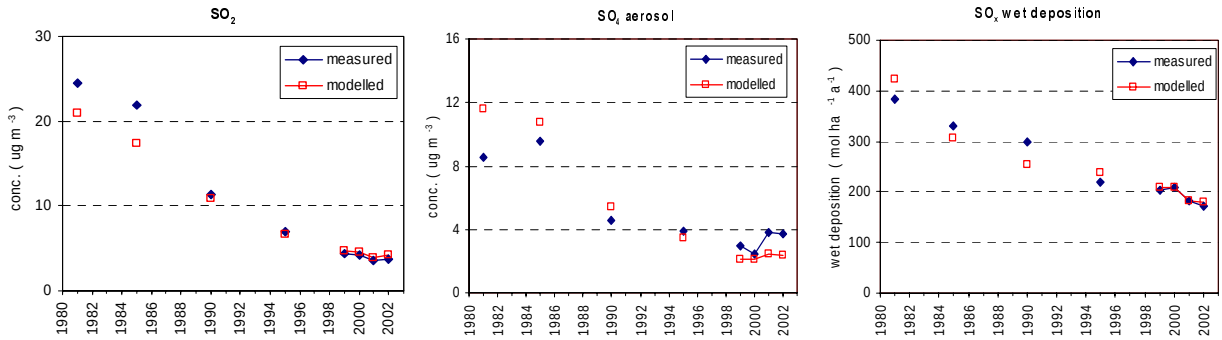

Figure 8.6 Comparison of trends in observations and model results for sulphur compounds.

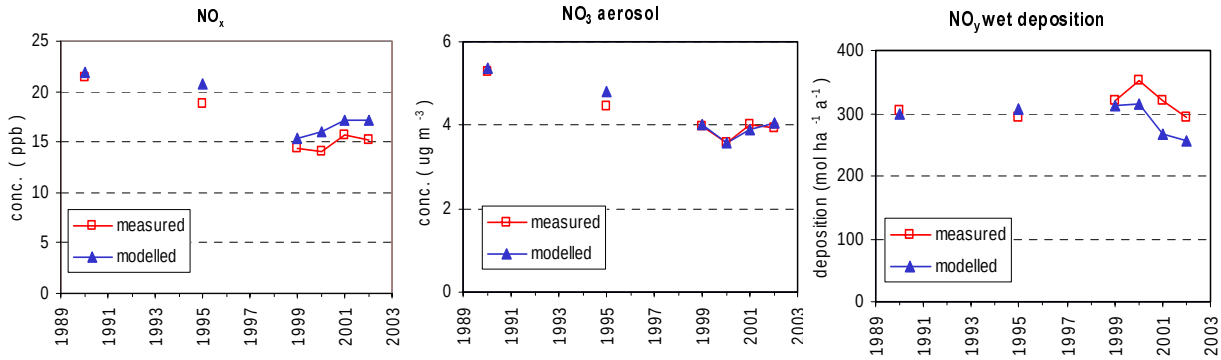

Figure 8.7 Comparison of trends in observations and model results for oxidised nitrogen compounds

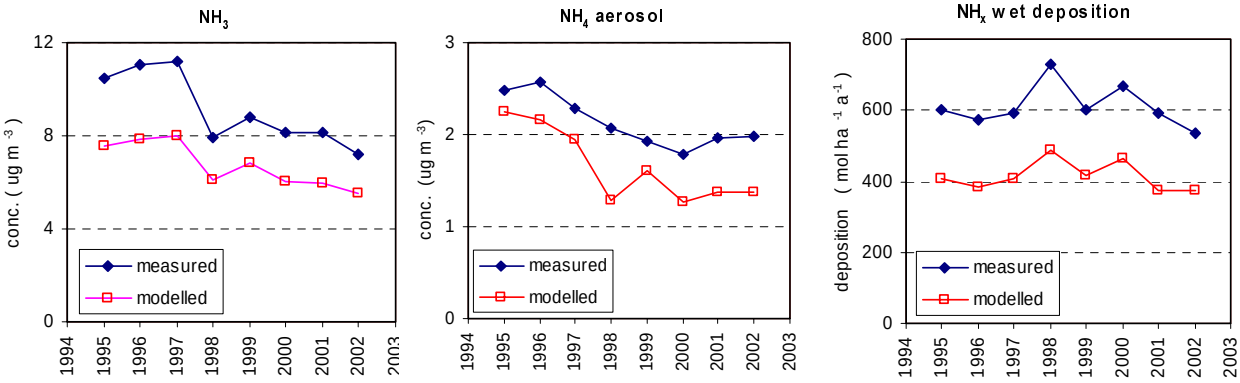

Figure 8.8 Comparison of trends in observations and model results for reduced nitrogen compounds.

The main reason is that the uptake of SO_2 in cloud droplets is limited by other gases such as H_2O_2 and O_3 and therefore is not a linear function of the atmospheric SO_2 concentrations. Most of the non-linear SO_x behaviour is also seen in the model results. This behaviour may be further explained by changes in SO_2 dry deposition throughout the years by changing SO_2-NH_3 co-deposition (lower dry deposition velocities in the early eighties than in more recent years). This effect is still hard to quantify and therefore not taken into account in the present model calculations.

For NO_y species the changes are less dramatic but here too we see a different trend for wet deposition than for NO_x concentrations. The consequence of these differences in trends is that the contribution of dry deposition decreases during the years, while the wet deposition contribution increases. The trends in observations and model results are similar for ammonia compounds. The absolute difference between the model and observations is known as the 'ammonia gap'.

8.3.4 Comparison of time-averaged concentrations on a point-to-point basis

In Figures 8.9-8.11 time-averaged modelled concentrations and wet deposition are compared with measured values of the same for a number of individual locations in the Netherlands. This comparison gives insight into how the model describes the spatial distribution of pollutants. It must be emphasised here that site-specific meteorological data is not used in all cases. From the sensitivity analysis the impact of local meteorology can be shown to be large, especially for low sources. In the case of SO_2 and to a lesser extent also for NO_x, the concentration levels are only partly due to (low-level) local sources, while contributions of remote sources are hardly influenced by local meteorology. So it can be expected that a comparison based on area-averaged meteorology may still give satisfactory results.

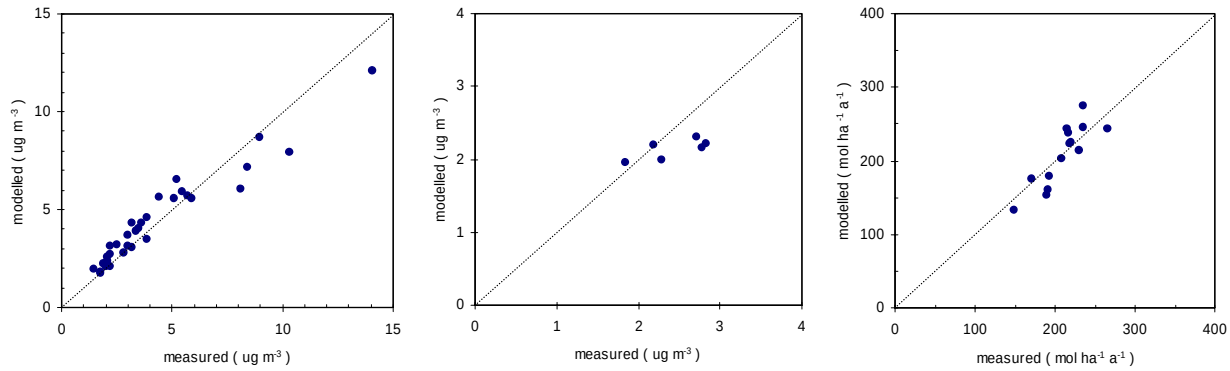

SO_2 concentration 2000 SO_4^{2-} aerosol concentration 2000 SO_x wet deposition 2000

Figure 8.9 Comparison of the spatial distribution of annual mean measured and modelled SO_x concentrations, and wet deposition.

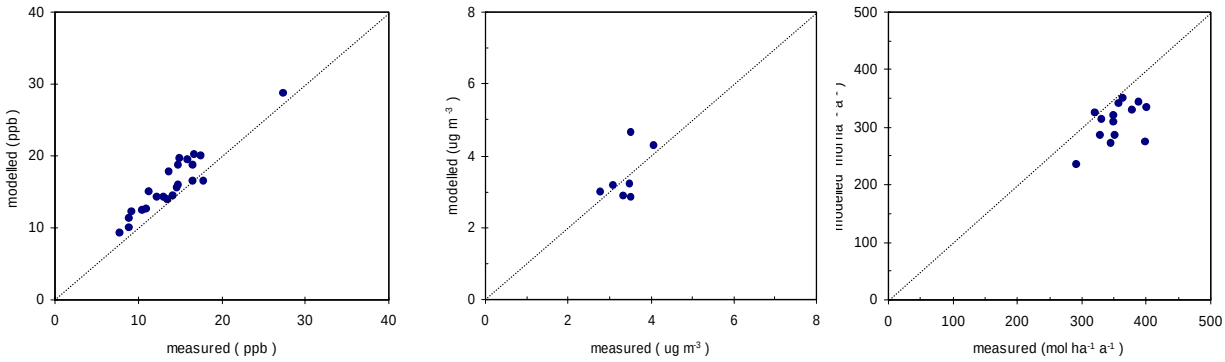

NO_x concentration 2000 NO_3^- aerosol concentration 2000 NO_y wet deposition 2000

Figure 8.10 Comparison of the spatial distribution of annual mean measured and modelled NO_y concentrations, and wet deposition.

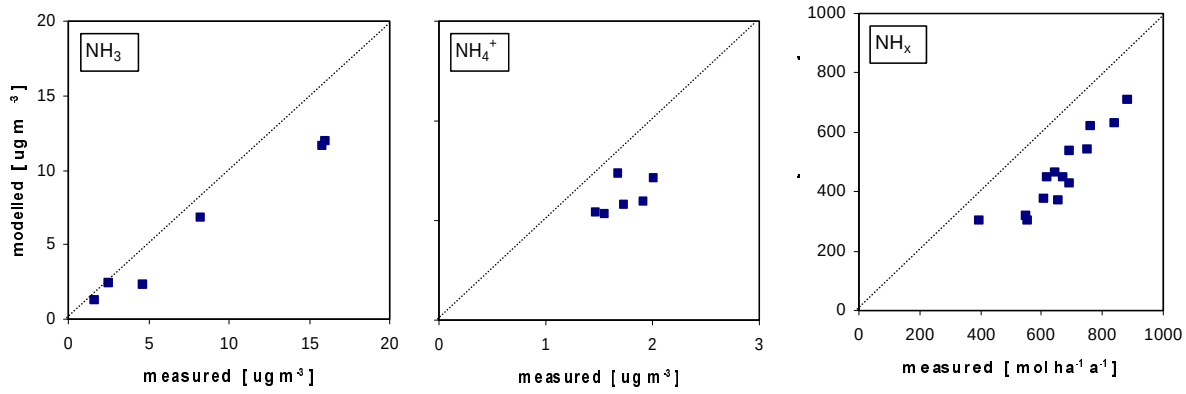

NH_3 concentration 2000 NH_4^+ aerosol concentration 2000 NH_x wet deposition 2000

Figure 8.11 Comparison of the spatial distribution of annual mean measured and modelled NH_x concentrations, and wet deposition.

A comparison on a point-to-point basis will, to a large extent, reflect the spatial resolution and the quality of the emission used. In this case 5 x 5 km resolution emission data for the Netherlands is used, extended with a few hundred individual point sources. Table 8.3 overviews the results of a large number of comparisons. The spatial correlation between modelled SO_2 and NO_x concentrations and measurements was determined for a large number of individual months, together with the *RRMSE*. The results of an investigation on the effect of increasing averaging time is given in Table 8.2. as well. The agreement between model results and observations appears to increase significantly with increasing averaging time. This indicates that an important number of the differences is due to random influences of meteorology, emissions but are also possibly due to the measurements themselves. The high correlation and small *RRMSE* found when using meteorological data for a long-term period also indicate a good quality in the use of the spatial distribution of the emissions.

Although the spatial distribution of emissions has changed during the years, especially for SO_2, there are no indications that the model performance is worse for the 1990 situation than for the situations in 1980 when the relative distribution of emissions is kept the same for all the years. This is probably due to the fact that mainly high sources, which have a relatively low impact on local concentrations, have been changed.

Table 8.3 Comparison on the spatial distribution of pollutant species in the Netherlands with the influence of the averaging time. Model results up to 1990, taken from van Jaarsveld (1995), are calculated by OPS-V1.20E, other results by OPS-Pro 4.1

Component	Stations *N*	Period	Averaging time	*n*	Correlation coefficient R^2	*RRMSE* (%)
SO_2 conc.	97	1978-1986	Month	36	(0.31-0.88) 0.71	(15-54) 25
		1978-1986	Season	16	(0.59-0.76) 0.74	(13-30) 21
		1978-1986	Year	8	(0.72-0.86) 0.83	(15-31) 18
		1978-1986	Multi-year	1	0.90	11
	26-31	1999-2002	Year	4	(0.66-0.91) 0.79	(16-29) 22
SO_4^{2-} aer. conc.	6	1984-1988	Year	3	(0.59-0.86) 0.68	(11-20) 14
	6	1999-2002	Year	4	(0.00-0.52)0.22	(13-41) 34
SO_x wet dep.	14	1980-1988	Year	8+	(0.34-0.46) 0.41	(19-26) 22
	14	1999-2002	Year	4	(0.73-0.88) 0.79	(9-11) 10
NO_x conc.	30	1979-1986	Month	84	(0.31-0.92) 0.67	(12-38) 23
		1979-1986	Season	14	(0.78-0.91) 0.71	(10-22) 16
		1979-1986	Year	7	(0.77-0.88) 0.85	(12-18) 13
		1978-1989	Multi-year	1	0.90	11
	22-25	1999-2002	Year	4	(0.84-0.91) 0.88	(14-21) 19
NO_3^- aer. conc.	6	1986-1988	Year	3	(0.55-0.74) 0.74	(5-25) 18
	7	1999-2002	Year	4	(0.22-0.43) 0.31	(16-24) 18
NO_y wet dep.	14	1988-1990	Year	3	(0.01-0.24) 0.10	(12-22) 16
		1999-2002	Year	4	(0.10-0.45) 0.25	(11-20) 15
NH_3 conc.	6	1995-2002	Year	8	(0.84-0.98)) 0.95	(26-37) 30
		1995-2002	Multi-year	1	0.98	28
NH_4^+ aer. conc.	6-7	1995-2002	Year	8	(0.10-0.65) 0.26	(17-39) 27
		1995-2002	Multi-year	1	0.37	23
NH_x wet dep.	14	1995-2002	Year	8	(0.57-0.84) 0.72	(31-37) 36
		1995-2002	Multi-year	1	0.90	34

The correlation in the spatial distribution for the secondary components is in some cases much less than for the primary components, but the *RRMSE*s are comparable. This is due to the much smaller gradients over the Netherlands for the secondarily formed species. Maps of the distributions given in section 6.1 illustrate this. Spatial distributions of concentrations in precipitation agree better than distributions of wet deposition. The reason for this is that the precipitation amount in the model is the same for all locations, while, in reality, there are spatial differences, even on a yearly basis. It is unclear whether these differences in precipitation represent more than a local effect.

8.3.5 Other comparisons

Concentrations as a function of stability classes
In Figure 8.12 modelled SO_2 and NO_x concentrations are compared with measured concentrations as a function of the stability/mixing height classes used in the model. The LML station, Cabauw, was selected for this comparison as a location not excessively influenced by local sources. Furthermore, a distinction is made between the summer and winter periods of the randomly selected year 1981.

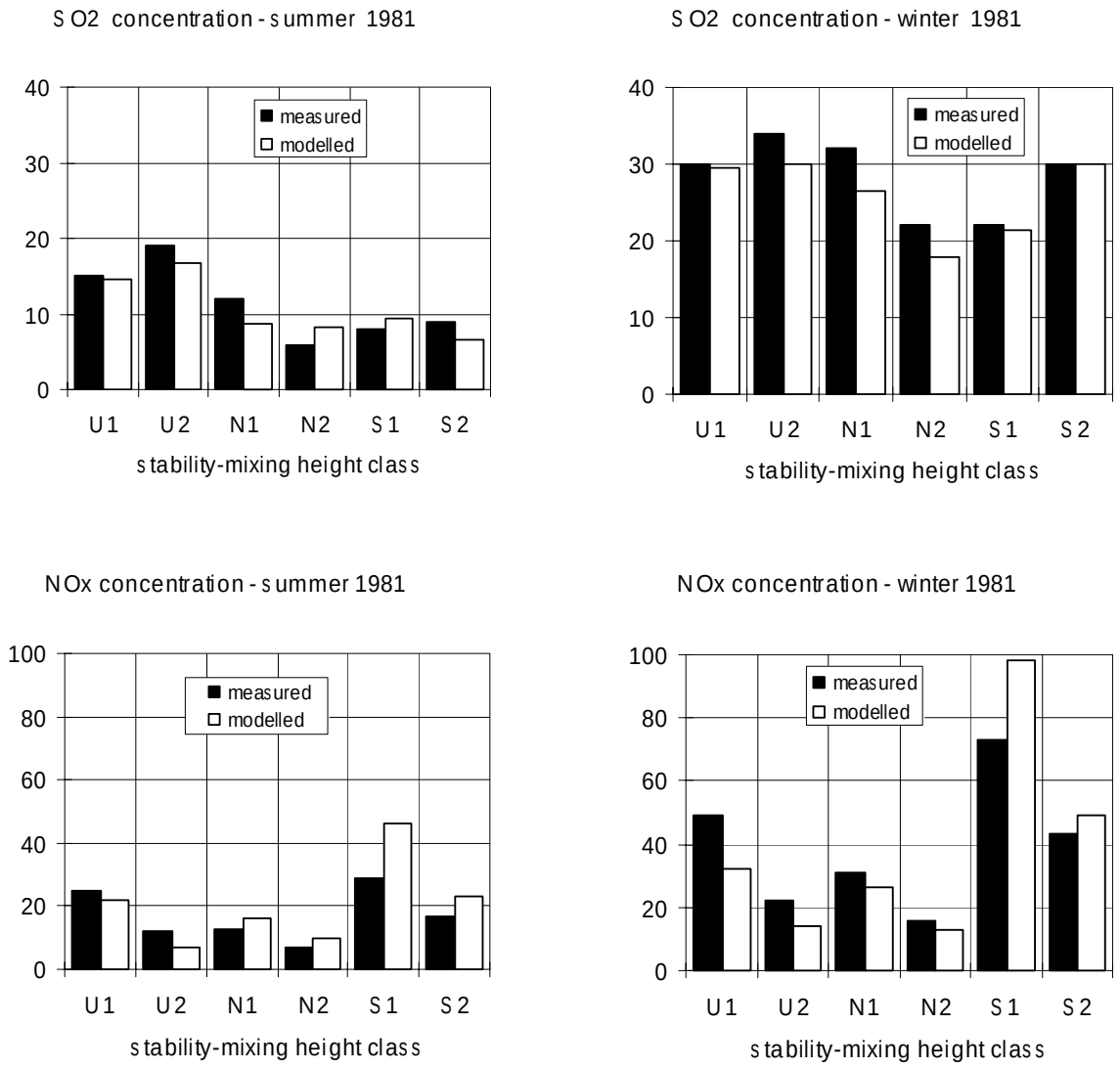

Figure 8.12 Modelled and measured concentration as a function of stability/mixing height class.

A test on the behaviour of the model for different stability cases is to a large extent also representative for the diurnal variation in concentration, since the classes for stable atmospheric conditions, S1 and S2, occur almost only during nighttime, while the classes for unstable conditions, U1 and U2, occur only during daytime. The frequency of occurrence of the classes U1, U2, N1, N2, S1 and S2 is 0.06, 0.07, 0.24, 0.27, 0.12 and 0.23, respectively, during the winter period of 1981, and 0.12, 0.35, 0.15, 0.04, 0.14 and 0.20 during the summer period. There are some remarkable differences in the phenomenology of SO_2 and NO_x when concentrations are categorised with respect to atmospheric stability. For example, under stable conditions, NO_x concentrations are relatively higher than SO_2 concentrations. This is mainly due to the average emission height, which for NO_x (mobile sources) is much lower than for SO_2 (see Figure 8.1).

As can be concluded from the sensitivity analysis carried out by van Jaarsveld (1995), the impact of low sources is highest during the nighttime when stable conditions prevail, while the impact of high sources is highest during daytime, when unstable conditions prevail. Except for the neutral classes, SO_2 concentrations appear to be higher for the classes with the highest mixing height (U2 and S2), while for NO_x the concentrations are highest for the classes with the lowest mixing heights (U1 and S1). Again, this can be explained by the difference in height distributions of SO_2 and NO_x sources. The behaviour of SO_2 and NO_x is similar during neutral conditions: i.e. concentrations are lowest for class N2. This class is characterised by mixing heights greater than 400 m, which occur mainly in high windspeed situations.
It would seem that the model reproduces most of the features present in the measurements. The model underestimates the concentrations for unstable conditions (classes U1 and U2) in almost all cases, while concentrations during stable conditions are overestimated. The latter is most pronounced for the NO_x case. Similar deviations have been found for NH_3 concentrations measured at Vredepeel (not shown here). Therefore it can be generally stated that the model tends to overestimate contributions of low sources during low windspeed situations.

8.3.6 Comparison with single-source short-range dispersion experiments

There is not much field data available to check the performance of a long-term average model such as the one described here against its prediction of concentration and deposition close to a single source. In section 3.1.2 some comparisons have already been presented on the dispersion of pollutants from point sources. One comparison was for a near-surface release (Prairie grass data; Barad, 1958) and another for a passive source release at 115 m (Copenhagen data; Gryning and Lyck, 1984). Both comparisons were carried out for cross-wind integrated concentrations and on the basis of given u^*, L and z_i. Although the agreement can be qualified as good, these tests cannot be considered as a full validation for this range of stack heights.

Essential are field measurements around a single source for at least several months, in which the contribution of this source can be uniquely identified. The model should then predict the average concentration distribution around the source on the basis of its standard meteorological input parameters. These parameters should also be available for the site and for the duration of the experiment. A data set that meets the requirements to a large extent is the so-called Kincaid data set (Bowne and Londergan, 1983). The Kincaid experiment was set up by the Electrical Power Research Institute (EPRI) in Ohio (USA) around the 187-m stack of a coal-fired power plant to serve the development and validation of short-term plume models. The experiment was carried out during the summer of 1980 and 1981. During the experiments there were about 30 SO_2 and NO_x samplers continuously operative at fixed locations within a circle of 12 km around the stack. In addition, there were a number of so-called ‘intensives’ in which a SF_6 tracer was released; SF_6 concentration was measured with samplers, arc-wise positioned at

several distances from the stack. The Kincaid data for the intensive periods is especially suited for testing the behaviour of short-term models for buoyant plumes under unstable conditions.

For the present purpose, only the continuously measured SO_2 data for the first two months of the experiment were used. Background concentrations were determined as the concentration measured by selected upwind stations and subtracted from the measurements every hour. Wind speed and direction measured at 10 m and 100 m was used as meteorological input for the model, together with temperature and global radiation, all on an hourly basis. Neither measured mixing heights nor other special measured parameters, such as vertical wind profiles, were used. The pre-processor was run with the selected data to prepare the climatological data sets for the two periods.

Scatter diagrams are given in Figure 8.13 for the average concentrations measured and modelled for two periods. In both cases more than 90% of the stations were within a factor 2 of the measurements, while the correlation for periods 1 and 2 was 0.7 and 0.6, respectively. It can be seen from the data in Figure 8.14 that the highest concentrations occur under convective conditions. It confirms also that the plume under stable conditions does not touch the ground, giving low concentrations for classes S1 and S2. The measured non-zero concentrations for classes S1 and S2 are, in fact, due to preceding unstable conditions, i.e. parts of the pollutant which have not been advected out of the area.

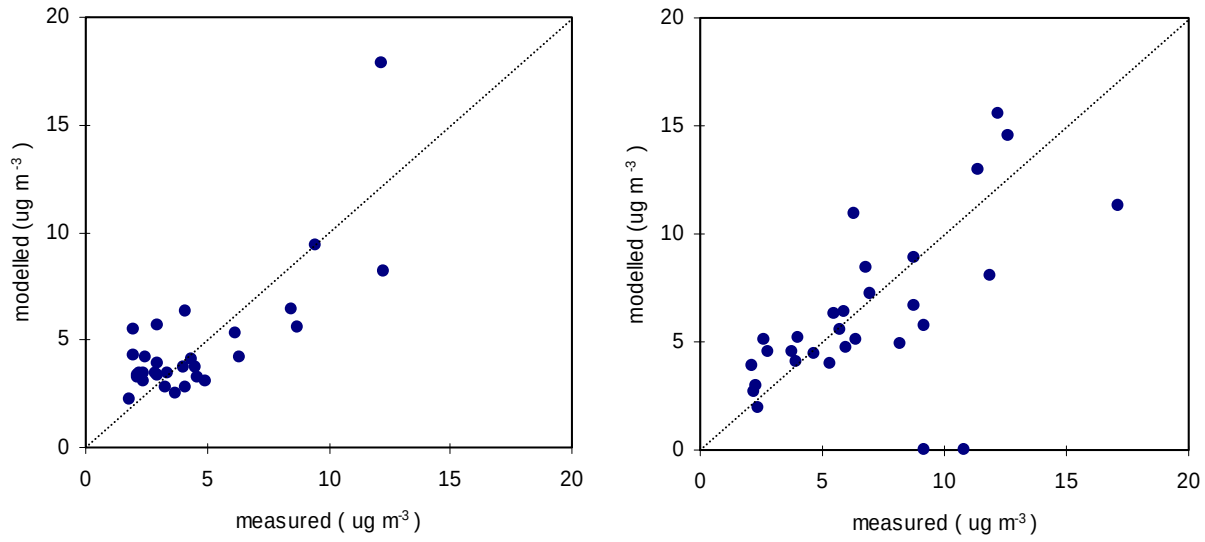

Figure 8.13 *Comparison of measured and modelled SO_2 concentrations around the 187-m Kincaid stack. Left: 26 April-23 May 1980. Right: 23 May-23 June 1980.*

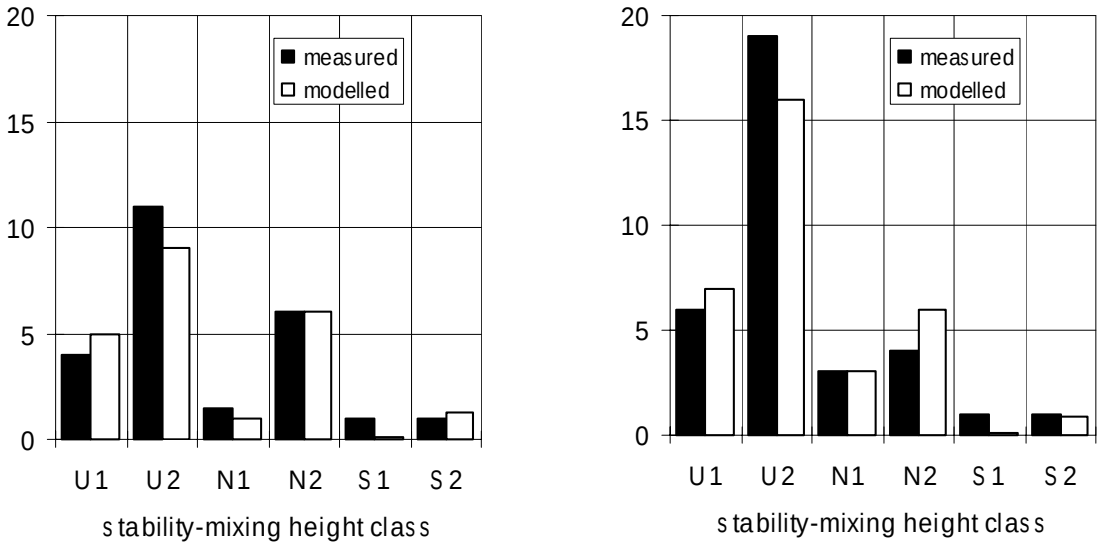

Figure 8.14 *Comparison of measured and modelled concentrations as a function of the stability/mixing height class. Left: 26 April-23 May 1980. Right: 23 May-23 June 1980.*

8.3.7 Comparison with models for the short range

The Kincaid data is also used as a basis for a comparison with other models. The models are compared on the basis of predicting the south-to-north concentration profile through the position of the 187-m stack. Results are given in Figure 8.15.

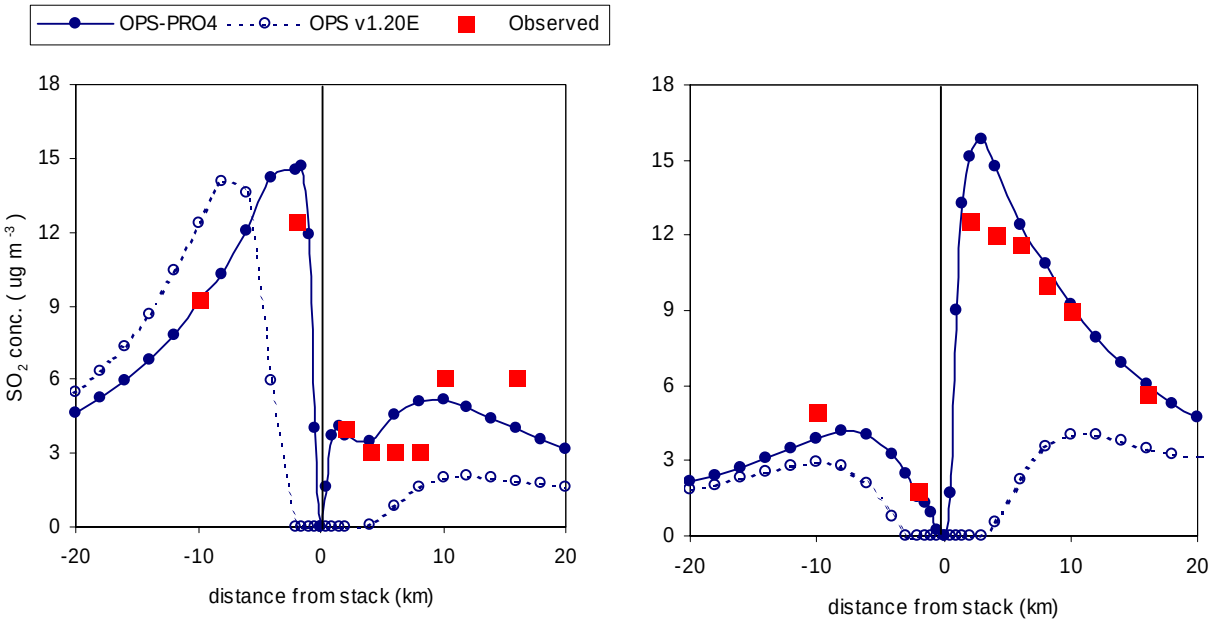

Figure 8.15 *South-to-north concentration profiles measured at the Kincaid power plant versus profiles modelled by several models. Left: 26 April–23 May 1980. Right: 23 May–23 June 1980.*

OPS-V1.20E is the older version of the model using Pasquill dispersion coefficients. It is clear from Figure 8.15 that OPS-V1.20E strongly underestimates concentrations at a distance up to 5 km from the stack. The main cause of the underestimation at short range is the parameterisation of vertical dispersion as a function of atmospheric stability classes. The scheme applied for determining those classes is shown to be strongly biased towards neutral stability (see, for example, Maes *et al*., 1994)

An intercomparison of models for the short range was carried out by Erbrink and Van Jaarsveld (1992). They compared the performance of models on the subject of the description of the yearly average concentration pattern around a 150-m stack with a heat output of 80 MW. The model STACKS is a short-term short-range dispersion model recently developed in the Netherlands (Erbrink, 1994; Erbrink, 1995). OML is a similar model, developed in the early eighties in Denmark (Berkowicz *et al.,* 1986). Both models can be considered as advanced Gaussian models using improved physical descriptions. The concentration profile as a function of distance from the stack is given in Figure 8.16. The OML model is used here on the basis of 1973 (Danish) meteorological data; while the other models use data measured in the Netherlands in different years. For this reason some differences may be expected between the models, but the relation with distance should not be influenced very much. As can be seen, the OPS model shows a performance between the STACKS and the OML models. Recent model intercomparisons, including other models as well, confirm the general picture described here (Maes *et al.*, 1994; Erbrink *et al*., 1994).

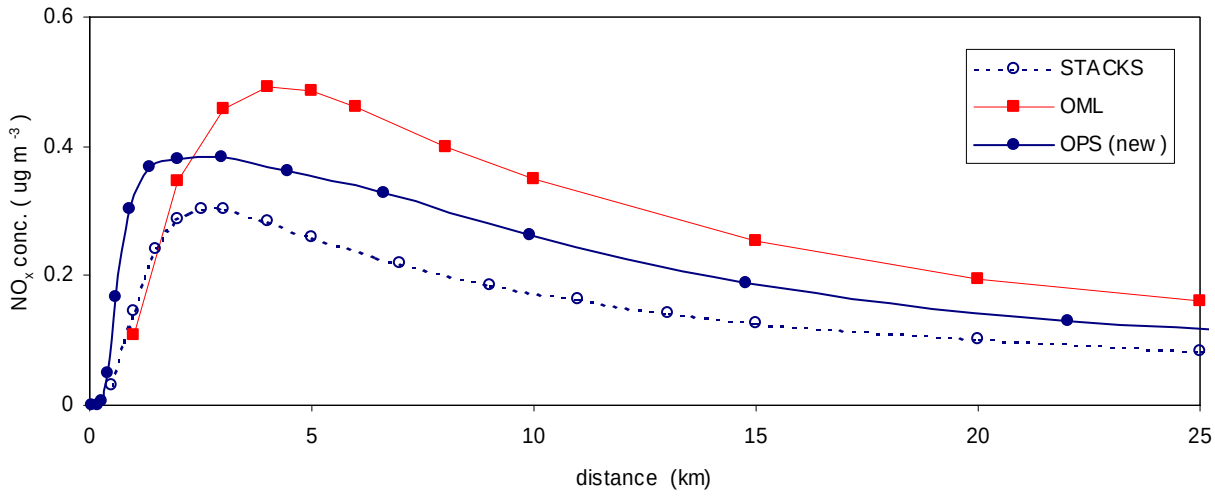

Figure 8.16 *Calculated wind-rose-integrated concentrations versus distance for a 150-m stack (80 MW) according to three models: OML; OPS-Pro 4.1 and STACKS (OML and STACKS, with data from Erbrink, 1995).*

8.3.8 Summary and conclusions on the validation of the model

Both on a local and regional scale, the OPS model has been shown to be able to describe the annually averaged concentrations and wet deposition well. In the case of compounds there is a systematic underestimation of concentrations and wet deposition of 25-35% for NH_x. This discrepancy, analysed in Van Jaarsveld *et al*. (2000), has become known as the so-called 'ammonia gap', due to too low emissions from manure spreading and too high NH_3 dry deposition velocities for grassland.

Although the model is not set up as such, even monthly variations in concentrations of primary-emitted pollutants are described well. Concentrations of secondarily formed products such as sulphate and nitrate aerosols are in reasonable agreement with measurements. It should be noted that much less validation data of this kind is available, while the quality is probably also less than for SO_2 and NO_x. The model is also able to reproduce spatial patterns of concentration and wet deposition very well. This is largely due to the ability of the model to include both area sources of various sizes and individual point sources, all with their specific emission heights. The latter is illustrated by the vertical concentration profiles, which are reproduced very well.

Concentrations in relation to typical atmospheric conditions have also been shown to be in agreement with observations. This means, for example, that in all the cases where diurnal variations in emissions and/or deposition velocities are of importance, the model will still perform well. In its function as a tool for the calculation of long-term average concentrations and depositions in the vicinity of individual point sources, the model is tested with several data sets, including one for buoyant plumes. There are no indications that this model performs worse than more dedicated short-range short-term models.

The *RRMSE* of the measurement and model results combination can be considered as the overall uncertainty (one σ) of the model prediction for a particular component. This *RRMSE* includes, in fact, uncertainties in emissions and measurements. Although the source characteristics, emission distributions and deposition parameters are very different for SO_2 and NO_x, the *RRMSE*s are seen to be very similar. This enhances the confidence that the comparison with measurements carried out can be qualified as a model validation for substances with similar atmospheric residence times and deposition, and removal parameters.

A restriction on the use of the outcome of the comparison exercise may be raised by the question whether the model is 'tuned' in to measurements of the same data set. Although the present model contains no real 'tuning' parameters, it is unavoidable that for certain parameters that value is selected from a range of published data that improves performance best. This is especially true for the chemical conversion parameters used in the model. The validity of the model for situations very different from the present situation in the Netherlands is therefore not certain. On the other hand, the sensitivity analysis carried out in Van Jaarsveld (1995) shows that neither concentrations of primary components (SO_2, NO_x, and NH_3) nor total depositions are very sensitive to variations in conversion rates. The validation of the model carried out here should therefore apply to all substances showing no important chemical degradation such as heavy metals and persistent organic compounds (POPs).

The estimate of model uncertainties for primary species should be valid for all components of the same order of magnitude of deposition and conversion parameter values, provided that the quality of emission data is also comparable.

8.4 Quantification of the uncertainty in model results

Where a model is applied to a problem, it is most desirable to have the uncertainties quantified. It is also desirable to extend such quantification by separating uncertainties in emissions from uncertainties introduced by the model concept, especially if the model is used in conjunction with different emission databases. In the present case an attempt has been made to use the best available measurements of substances, for which also the emissions are the most well-known. However, since accuracy for neither these measurements nor emissions appear to be known, the results of the model validation may not be considered as absolute accuracies but as accuracies relative to the measurements. On the basis of expert judgement, Erisman (1992) suggests systematic errors of 15 %, 20% and 40% in measured SO_2, NO_x and NH_3 concentrations, respectively, averaged over the Netherlands. Tentative guesses for systematic errors in national total SO_2 , NO_x and NH_3 emissions are 15%, 20% and 20%, respectively. The results presented in the Tables 8.2 and 8.3 suggest that uncertainties in model output are of the same order as the uncertainties in both emissions and measurements.

In order to obtain estimates of errors in total deposition fluxes, the errors in the different model output species are combined using the following method of error propagation:

$$E = \sqrt{E_a^{\,2} + E_b^{\,2} + 2\,R\,E_b\,E_b} \qquad (8.25)$$

where E_a and E_b are the errors of the variables a and b and R the correlation between the variables. If a and b are multiplied or divided, E_a and E_b are taken as relative errors; for adding or subtracting they are taken as absolute errors.

8.5 Uncertainties in concentrations and dry deposition velocities

Uncertainties in concentrations ($\Delta C/C$) are derived from the comparison with measurements in this chapter, local uncertainties from the spatial comparison (Table 8.3) and regional averages (the Netherlands) from the temporal comparison (Table 8.2). Note that the comparison with measurements occurs, in fact, on a point-to-point basis, where only the so-called street stations are excluded from the data set. Therefore, in the case of SO_2 and NO_x, the validation also covers city background situations. From a model-measurement comparison for NH_3, mainly the spatial resolution of the emission grid is shown to determine the agreement on a local scale (Van Jaarsveld and Van Pul, 2002). The current emission resolution is 500 x 500m for NH_3 and 5000 x 5000 m for SO_2 and NO_x. The local scale may therefore be interpreted as smaller than 500 x 500m for NH_3 and smaller than 5000 x 5000m for SO_2 and NO_x. Table 8.5 gives the uncertainty estimates for the different components, both for the local and regional scales. The uncertainties in the dry deposition velocities ($\Delta V_d / V_d$) have been mainly adapted from the work of Erisman (1992), who carried out an uncertainty analysis of deposition inferred from measurements only. The deposition fluxes (F), based on calculations for the year 1990, are given to show the relative importance of the different deposition fluxes.

8.5.1 Effect of correlated species on error propagation

Important for the propagation of errors in calculated deposition fluxes is the correlation between the species. The combined error, therefore, may be less than the error in the constituents. From sensitivity analysis it is known that calculated concentrations negatively correlate with dry deposition velocities

(Van Jaarsveld, 1995). This is due to the fact that at high wind velocities, the dry deposition velocity is high, while concentrations are low due to a higher mixing volume. In the case of wet and dry deposition the correlation may be either positive and negative because on the one hand both dry and wet deposition are high when concentrations are high but, on the other, precipitation is related with westerly wind directions when concentrations are usually lower than average. Estimates of *R* are based on an interpretation of the results of the series calculations for the yearly averages for the Netherlands used in section 8.3. The data confirm the strong negative correlation between air concentrations and dry deposition velocities. Dry and wet fluxes appear to be weakly negatively correlated for SO_x and NH_x; for NO_y the correlation is positive. All the correlation given in Table 8.5 must be considered as rough estimates. A large number of sensitivity runs is required to obtain better estimates. Similarly, correlation between the different species on a local scale could not be determined without performing a large number of sensitivity runs. Local deposition is, however, in most cases determined for at least 50% by non-local sources, so mass conservation mechanisms have their effect on this scale too. Therefore half the feedback found for the regional scale is taken for the local scale.

Effect of feedback mechanisms on error propagation

The effect of competitive loss mechanisms is only significant if they take place on a large enough scale. Very local errors in dry deposition velocities have little effect on regional concentrations. It is therefore important to separate the errors into general (and systematic) effects and errors related to specific (and local) ecosystems, mainly of a random nature. Examples of systematic errors are errors in the characterisation of aerodynamic resistances and errors in the canopy resistance due to the modelling of the effect of surface wetness. Examples of random errors are errors in estimating local roughness and errors in the characterisation of small-scale ecosystems.

An example of the way feedback mechanisms work is given in Table 8.4. In this table the effect of a change in the dry deposition velocity of one land-use type (grassland) is given for three locations within the same land-use type and for three locations within a different land-use type (arable land). An approximately 20% decrease in the dry deposition velocity of grassland decreases the dry deposition to grassland by 7-10% but increases the NH_3 concentration and the wet deposition. The sum of dry and wet deposition hardly changes. Here, dry deposition velocity and dry deposition are negatively correlated and the same applies for dry and wet deposition. If locations within a different land-use type are considered, the NH3 concentration will appear to increase but the dry deposition velocity will remain nearly constant.

Table 8.4 Limited sensitivity test showing the effect of a change in the in-canopy resistance for grass

Station	NH_3 conc. value calculated for 2000 ($\mu g\ m^{-3}$)	Roughness length (m)	Change relative to base case				
			Dry deposition velocity	NH_3 conc.	Dry deposition	Wet deposition	Total deposition
Grassland locations:							
Huijbergen	2.4	0.53	0.75	1.17	0.92	1.17	1.0
Zegveld	6.8	0.03	0.83	1.10	0.93	1.15	0.99
Wekerom	11.6	0.08	0.82	1.10	0.90	1.16	0.95
Arable land locations:							
Vredepeel	12.0	0.59	1.01	1.08	1.09	1.17	1.10
Wieringerwerf	2.3	0.26	1.01	1.15	1.16	1.19	1.19
Valthermond	3.3	0.33	1.02	1.15	1.18	1.22	1.18

The change in dry deposition velocity in one of the (large-area) vegetation types is positively related to the change in dry deposition in a different land-use type. This simple sensitivity case indicates that uncertainties in the dry deposition velocity of grassland have the largest impact on the uncertainty of deposition fluxes to other (and smaller) land-use types as arable land but also to natural systems as forest, heathland and small water bodies. This is one of the reasons why dry deposition field research in the Netherlands has been recommended for re-activation but now with emphasis on grass sites (Van Jaarsveld *et al*., 2000). The feedback through mass conservation is a property of an emission-based model approach and forms a major advantage over inference models. It reduces the total uncertainty significantly. In the uncertainty quantification, the effect is only partly taken into account (mainly through the negative correlation (*R*) between dry deposition velocity and concentration). The full impact of feedback on the uncertainty of the model system can only be assessed by performing a sensitivity analysis with dry deposition velocities for different vegetation types as variables.

Table 8.5 Estimated uncertainties (%) in yearly average concentration and deposition where F is the deposition flux, V_d the dry deposition velocity, C the air concentration and R the correlation between constituting parameters

Component	F [&] mol ha^{-1} a^{-1}	Local ecosystem [@]						National ecosystem [@]					
		$\Delta C/C$ [#]		$\Delta V_d/V_d$		R[$]	$\Delta F/F$	$\Delta C/C$ [#]		$\Delta V_d/V_d$		R[$]	$\Delta F/F$
		ran.	*sys.*	*ran.*	*sys.*			*ran.*	*sys.*	*ran.*	*sys.*		
dry SO_2	256	29	15	60	40	-0.35	76	10	15	10	20	-0.7	26
dry SO_4^{2-}	14	30	26	60	50	-0.25	84	10	26	10	30	-0.5	41
dry SO_x	270					0.15	73					0.3	25
wet SO_x	165						20[#]						20[#]
total SO_x	435					0.15	**47**					0.3	**19**
dry NO_x	236	19	15	18	100	-0.40	99	10	15	10	50	-0.8	42
dry NO_3^- $+HNO_3$	184	18	15	120	50	-0.20	130	10	15	10	30	-0.4	31
dry NO_y	420					0.30	91					0.6	33
wet NO_y	264						20[#]						20[#]
total NO_y	684					0.15	**58**					0.3	**24**
dry NH_3	840	25	25	130	50	-0.40	140	10	25	10	50	-0.80	35
dry NH_4^+	32	27	27	80	50	-0.10	100	10	27	10	50	-0.20	56
dry NH_x	872					0.30	136					0.60	33
wet NH_x	384						35[#]						35[#]
total NH_x	1256					0.05	**96**					0.10	**28**

[@] Local ecosystem: e.g. single forest somewhere in the Netherlands; National ecosystem: e.g. all deciduous forest in the Netherlands

[#] Random error derived from comparison with measurements on spatial distribution (Table 8.3), systematic error from comparison on temporal behaviour (R_{po} in Table 8.2). Minimum uncertainty applied to air concentrations: 10% and for wet deposition: 20%

[&] Calculated mean deposition flux for the Netherlands for the year 2000

[$] Applied to systematic errors only

8.5.2 Results

Table 8.5 presents the uncertainty estimates for local and national scales. These estimates include the uncertainty of the current emission data (through the comparison with measured concentrations) for the model and the measurements. The results indicate that uncertainties in dry deposition velocities dominate the overall uncertainty in deposition calculations, both on the local scale and when averaged over the Netherlands. Uncertainties in modelled concentrations are of the same order as uncertainties in the measurements themselves, except for ammonia compounds. Here, all species are 25-35% lower than the measurements. This fact has for sometime been known as the 'ammonia gap'. Small-scale deposition data is still very uncertain, mainly due to the large (random) error in dry deposition velocity of the primary substances (SO_2, NO_x and NH_3). NH_x deposition estimates for small ecosystems may be a factor of 2 incorrect. The uncertainties for calculated total deposition are in close agreement with those obtained by Erisman (1992) for deposition inferred from measurements. Uncertainties in calculated dry deposition are somewhat lower in the present case because of the negatively correlated concentrations and dry deposition velocities. In Erisman's study, no explicit correlation between species was taken into account.

8.6 References chapter 8

Albers R., Beck J., Bleeker A., van Bree L.,van Dam,J., van de Eerden L., Freijer J., van Hinsberg A., Marra M., van der Salm C., Tonneijk A., de Vries W., Wesselink L. and Wortelboer F. (2001) Evaluatie van de verzuringsdoelstellingen: de onderbouwing (in Dutch). RIVM, Bilthoven, the Netherlands. Report no.725501001.

Asman W.A.H. (1992) Ammonia emissions in Europe: Updated emission and emission variations. RIVM, Bilthoven, the Netherlands. Report no. 228471008.

Barad M.L., editor (1958) Project Prairie Grass, a field program in diffusion.Volume 1, Geophysics Research Paper no. 59. Geophysics Research Directorate, Air Force Cambridge Research Center, Cambridge MA, USA.

Berdowski J.J.M. (1994) Emission inventory in the Netherlands. Emissions to air and water in 1990. Publikatiereeks Emissieregistratie, no. 16, Ministry of Housing, Spatal Planning and the Environment, The Hague, the Netherlands

Berkowicz R., Olesen H.R. and Torp U. (1986) The Danish Gaussian Air Pollution Model (OML): description, test and sensitivity analysis in view of regulatory applications. In: De Wispelaere C., Schiermeier F.A. and Gillani N.V., editors. *Air pollution modeling and its application V*. Plenum Press, New York. p. 453-482.

Bowne N.E. and Londergan R.J. (1983) Overview, results and conclusions for EPRI Plume Model Validation and Development Project: Plains site. Available from EPRI, 3412 Hillview Avenue, Palo Alto, California 94304.

Buijsman E., Jonker P.J., Asman W.A.H. and Ridder T.B. (1991) Chemical composition of precipitation collected on a weathership on the North Atlantic. *Atmospheric Environment* **25A**, No. 5/6, pp. 873-883.

CBS (1994) Air pollution. Total emissions caused by human activities, 1980-1993; version 11/94 [in Dutch]. Central Bureau of Statistics, Voorburg, the Netherlands.

CITEPA (1989) CORINAIR; Instructions for use; Version 4.20). CITEPA-21/09/1989

CITEPA (1991) Inventory of emissions of pollutants into the atmosphere. CITEPA-053-14/01/91.

CITEPA (1993) Corinair inventory; Corinair software instructions for use (version 5.13). CITEPA, Paris.

Elskamp H.J. (1989) National Air Quality Monitoring Network, Technical description. RIVM, Bilthoven, the Netherlands. Report no. 228702017.

Erbrink J.J. (1994) The Gaussian model STACKS. In: Cuvelier C., editor. Intercomparison of advanced practical short-range atmospheric dispersion models. Proceedings of the Manno workshop. Joint Research Centre, Ispra, Italy.

Erbrink J.J. (1995) Turbulent diffusion from tall stacks; The use of advanced boundary-layer meteorological parameters in the Gaussian model 'STACKS' [PhD thesis] Free University of Amsterdam, the Netherlands.

Erbrink J.J. and Jaarsveld J.A. van (1992) Het Nationale model vergeleken met andere modellen en metingen. *Lucht* **3**, 86-91.

Erbrink J.J, Tieben H. and Cosemans G. (1994) Application of different dispersion models to a site near the Belgian-Dutch border. In: Kretzschmar J., Maes J. and Cosemans G., editors. Operational short-range atmospheric dispersion models for environmental impact assessment in Europe. Preprints of the 3rd workshop on harmonisation within atmospheric dispersion modelling for regulatory purposes; 21-24 November 1994; Mol, Belgium. p. 357-366.

Erisman J.W. (1989) Ammonia emissions in the Netherlands in 1987 and 1988. RIVM, Bilthoven, the Netherlands. Report no. 228471006.

Erisman J.W. (1992) Atmospheric deposition of acidifying compounds in the Netherlands. [PhD thesis]. Utrecht University, the Netherlands.

Gryning S.E. and Lyck E. (1984) Atmospheric dispersion from elevated sources in an urban area: comparison between tracer experiments and model calculations. *J. Climate Appl. Meteorol*. **23**, 651-660.

KNMI/RIVM (1988) Chemische samenstelling van de neerslag over Nederland: Annual Report 1987 [in Dutch]. De Bilt, the Netherlands. KNMI report no. 156-10; RIVM report no. 228703005.

Locht J.V. and van Aalst R.M. (1988) Depositie van verzurende stoffen op de Nederlandse bodem van niet antropogene herkomst (in Dutch). Report no. R 88/458, TNO, Apeldoorn.

Lübkert B. and Tilly S. de (1988) The OECD-MAP emission inventory for SO_2, NO_x and VOC in Western Europe. *Atmospheric Environment* **23**, 3-17.

Maes G., Cosemans G., Kretzschmar J., Janssen L. and Tongerloo J. van (1994) Comparison of 6 Gaussian dispersion models used for regulatory purposes in the different countries of the EU. In: Kretzschmar J., Maes J. and Cosemans G., editors. Operational short-range atmospheric dispersion models for environmental impact assessment in Europe: Preprints of the 3rd Workshop on Harmonisation within Atmospheric Dispersion Modelling for Regulatory Purposes; 21-24 November 1994; VITO, Mol, Belgium. p. 381-390.

Mennen M.G., Elzakker B.G. van, Hellemond J. van, Eisen I. and Meulen A. van der (1992) Evaluation of a two-and-a-half year study of acidic pollutants using Annular Denuder Systems. RIVM, Bilthoven, the Netherlands. Report no. 222702003.

Ridder T.B., Baard J.H. and Buishand T.A. (1984) The influence of sampling methods and analytical techniques on measured chemical concentrations in precipitation: Technical report [in Dutch]. Royal Netherlands Meteorological Institute, De Bilt, the Netherlands. T.R.-55.

RIVM (1982) Technische gegevens NML. RIVM, Bilthoven, the Netherlands. NML-RIV no. 10.

RIVM (1989) Luchtkwaliteit: Jaarrapport 1988. RIVM, Bilthoven, the Netherlands. Report no. 228702015.

RIVM (1990) Luchtkwaliteit: Jaarrapport 1989. RIVM, Bilthoven, the Netherlands. Report no. 222101006.

RIVM (1991) Luchtkwaliteit: Jaarrapport 1990. RIVM, Bilthoven, the Netherlands. Report no. 222101015.

Sandnes H. (1993) Calculated budgets for airborne acidifying components in Europe; 1985, 1987, 1988, 1989, 1990, 1991 and 1992. DNMI, Oslo, Norway. EMEP/MSC-W Report 1/931.

Tarrason L. and Iversen T. (1992) The influence of north American antropogenic sulphur emissions over western Europe. *Tellus* **44B**, 114-132.

Van der Hoek K.W. (2002) Uitgangspunten voor de mest-en ammoniakberekeningen 1999 tot en met 2001 zoals gebruikt in de Milieubalans 2001 en 2002, inclusief dataset landbouwemissies 1980-2001 (in Dutch). RIVM, Bilthoven, the Netherlands. Report no. 7730040013

Van der Maas C.W.M. (1996) Ontwerp en bouw van EUREM: de Europese Emissie Module in het RIM+ (in Dutch). RIVM, Bilthoven, the Netherlands. Report no. 776001004.

Van Jaarsveld J.A. (1990) An operational atmospheric transport model for priority substances; specification and instructions for use. RIVM, Bilthoven, the Netherlands. Report no. 222501002.

Van Jaarsveld J. A. (1995) Modelling the long-term atmospheric behaviour of pollutants on various spatial scales. Ph.D. Thesis, Utrecht University , the Netherlands.

Van Jaarsveld, J.A., Bleeker, A. and Hoogervorst, N.J.P. (2000) Evaluatie ammoniakredukties met behulp van metingen en modelberekeningen. RIVM, Bilthoven the Netherlands. Report no. 722108025.

Van Jaarsveld J.A. and van Pul W.A.J. (2002) Berekende ammoniakconcentraties in Nederland vergeleken met de intensiveringsmetingen met passieve samplers. RIVM, Bilthoven the Netherlands. Report no. 725501006

Veldt C. (1981) TNO Air quality management system. TNO, Apeldoorn, the Netherlands.

Veldt C. (1983) Nitrogen oxides in the Netherland's ambient air; emissions. TNO, Apeldoorn, the Netherlands. Report 83-01605.

Veldt C. (1991) Emissions of SO_x, NO_x, VOC and CO from East European countries. Atmospheric Environment Vol. 25A, No 0, pp 1-18.

Vestreng V. (2003) Review and Revision. Emission data reported to CLRTAP. EMEP MSC-W Status report 2003. Technical report Note 1/2003, Meteorological Synthesizing Centre – West, Norwegian Meteorological Institute, Oslo, Norway

Wesselink B., v.d.Berg H., Dirkx M., Oostenrijk R., Schilderman C. and Slootweg J. (1998) Achtergronddocument bij emissieleveranties uit RIM+ ten behoeve van het OPS model (in Dutch). RIVM, Bilthoven, the Netherlands. Internal document.

Whelpdale, D. M., Eliassen A., Galloway, J.N. Dovland H. and Miller J.M. (1988) The transatlantic transport of sulphur. *Tellus* **40B**, 1-15.

9. Comparison with previous versions of the model

The first operational version of the model was made available to a wider user group in 1989. The user language was still Dutch at that time. In 1990 an English version was released which also included the calculation of acidifying compounds. These two versions are, to date, the only versions available to the community. The further model development was mainly driven by needs when the model was used in various studies.

The main focus in recent model development has been on ammonia because ammonia is one of the most important environmental issues in the Netherlands. This development has resulted in a few working versions of the model, which have been used in a series of studies and reports. The intention of this chapter is to give a short overview of these working versions, to highlight the main differences and to compare the results for some characteristic situations.

9.1 Model versions

The different stages of development of the OPS model are described below. An overview of the technical differences is given in Table 9.1.

OPS-V1.20E
This version may be considered as the basic version of the OPS model. Over 40 registered copies have been delivered to universities, research groups, engineering companies, environmental departments of provinces and (large) municipalities. The model runs on a PC under DOS and is described in Van Jaarsveld (1990) and Van Jaarsveld and De Leeuw (1993). This version still uses a Pasquill stability classification with fixed coefficients for vertical dispersion. All parameters are spatially homogeneous, including the meteorological ones. Terrain roughness influences the dry deposition velocity but has no effect on dispersion or windspeed profiles. The model already uses different characteristics for surface resistances e.g. dry, wet, frozen and snow cover. Another important issue is that the model uses fixed chemical conversion rates.

OPSEXP6E
This is the version of the model used for the third and final phase of the Dutch Acidification Programme (Heij and Erisman, 1997). The structure of the later versions of the model, in terms of using boundary layer parameterisations for dispersion, as a function of height, is already present is this version. Also introduced here is the spatial variability of meteorological data, roughness and land use. Finally, the DEPAC module was added to the model. This module, as a result of, for example, experimental work within the acidification programme, supplies surface resistances for substances as a function of climatological conditions and land-use class. The OPSEXP6E version is used to calculate time series (1980-1993) of NH_x dry deposition in the Netherlands as well as to predict deposition of acidifying compounds in future years on the basis of emission projections.

OPSEXP8E
The only extension compared to OPSEXP6E is that the R_c parameterisation from DEPAC is now used for all land-use classes other than grassland too (a bug fix).

Table 9.1 Overview of the most important differences among the OPS model versions

		OPS-V1.20E	**OPSEXP6E**	**OPSEXP9E**	**OPSEX12N**
In use since		1991	1996	1997	1999
Meteorological data	observations	Wind data from LML network, precipitation from KNMI network	Wind data from LML network, precipitation from KNMI network	KNMI, LML wind data for 1981-1990	KNMI, LML wind data for 1981-1990
	Spatial differentiation	6 regions, no interpolation	6 regions, inverse distance interpolation	6 regions, roughness corrected observations, inverse distance interpolation	6 regions, roughness corrected observations, inverse distance interpolation
	Long-term statistics	1979-1993	1981-1989	1981-1989	1990-1999
Secondary meteorological parameters	Stability classification	Pasquill, 6 classes to Golder(1978)	6 classes based on Monin-Obukhov length and mixing height	6 classes based on Monin-Obukhov length and mixing height	6 classes based on Monin-Obukhov length and mixing height
	Vertical dispersion	Dispersion coefficients, similar to Dutch National Model	Dispersion based on modern boundary layer parameters.	Dispersion based on modern boundary layer parameters	Dispersion based on modern boundary layer parameters
Roughness & land-use map		No roughness or land-use maps	Based on LGN2; 5 x 5 km	Based on LGN2; 5 x 5 km or 1x1 km	Based on LGN3; 5 x 5 km down to 250 x 250 m
'Background' concentration time series SO_2, NO_2, NH_3		No	No	Yes	Yes
$NH_3 > NH_4$ conversion rate		Fixed at $8.x\ 10^{-5}\ s^{-1}$	Fixed at $2.78.x\ 10^{-5}\ s^{-1}$	Depends on SO_2, NO_2 and NH_3 background conc.	Depends on SO_2, NO_2 and NH_3 background conc.
Emission variation of NH3 depending on meteorological parameters		No	No	Yes	Yes
Dry deposition parameterisation based on DEPAC		No	Partly [&]	Yes	Yes
HNO_3/NO_3 ratio depending on background conc.		No	No	No	Yes
HNO_2 in NO_x		No	No	No	Yes
Wet scavenging ratio of SO_2.		Fixed	Fixed	Fixed	Depends on SO_2 and NH_3 background conc.

[&] For grassland only. This is the main difference with OPSEXP8E, where parameterisations of all land-use types are based on DEPAC.

OPSEXP9E

The treatment of raw meteorological data is an important difference compared with previous versions. Initially, all the wind data came from observations carried out within the LML network. When these observations were stopped at the end of 1993 it became necessary to use data from the KNMI network. The latter is set up with a different philosophy towards wind speed. Stations are located on terrain showing basic differences (more open, e.g. airports). A site and direction-dependent roughness correction was introduced together with a spatial interpolation procedure. In this way, LML data and KNMI data became more comparable and, consequently, so did the model results.

The discovery of the so-called ammonia gap has led to further investigation of ammonia-related processes. The most important change to the previous version is the introduction of conversion rates in dependence of (background) concentration levels.

OPSEX12N
This is the latest (experimental) version. It uses improved land-use and roughness data. A number of minor improvements have been made for NH_x, such as introducing a temperature-dependent variation of emissions from animal housing systems and an improved estimation of the surface wetness indicator. For NO_x the NO/NO_2 and HNO_3/NO_3, ratios are made dependent on the background concentration of NO_2 and NH_3. Furthermore, an estimate of the HNO_2 fraction in NO_x concentrations was introduced, and the dry and wet deposition parameters of NO_X (= $NO + NO_2 + HNO_2$) were adjusted accordingly. For SO_x the wet scavenging ratio is made dependent on the acidity of precipitation, which, in turn, is estimated from (background) NH_3/SO_2 ratios. Through the changing NH_3/SO_2 and NH_3/NO_2 ratios in Western Europe a pseudo non-linear behaviour is introduced for SO_x, NO_x and for NH_x.

The OPSEX12N model version forms the basis of the operational version **OPS-Pro 4.1,** so the results obtained here apply to OPS-Pro 4.1 too.

9.2 Comparison in the case of ammonia in the Netherlands

Probably the most important application of the OPS model is within the field of modelling ammonia deposition. This is because the ammonia issue is a severe problem in the Netherlands. It is therefore likely to focus on ammonia, also in terms of model validation.

Dispersion of ammonia emitted by animal housing systems or evaporated from field-applied manure is very sensitive to local meteorological conditions such as wind velocity (Van Jaarsveld *et al*., 2000). The OPS model has been used as a tool to translate ammonia emissions to air concentrations and subsequent dry and wet deposition since the late eighties (Asman and van Jaarsveld, 1992). Since then the knowledge on NH_3 emissions and atmospheric processes involving ammonia has increased significantly. Moreover, the phenomenology of NH_3 and NH_4 concentrations in air has been understood much better, since many measurements have been carried out. The ongoing focus on ammonia has led to a focus in the model development geared to typical ammonia demands. One item to mention is the incorporation of new insights in ammonia dry deposition parameterisation as a result of the Dutch Acidification Program (Heij and Erisman, 1997). Another is related to the so-called ‘ammonia gap’, which originally indicated a difference in trends in measured atmospheric ammonia levels and ammonia emissions.

A comparison has been carried out on the basis of concentration and deposition at 30 measuring stations (former and present sites for wet NH_x deposition and/or NH_3 concentration measurements) scattered over the Netherlands. All model versions use meteorological data for the year 1995. The emission data is also for the year 1995, with a resolution of 5 x 5 km in the Netherlands and a variable resolution in other countries. The emission data was originally produced in the framework of the Dutch State of the Environment, 1997.

The results are given in Table 9.2 in the form of ratios to the OPSEX12N model version. The standard deviation of the ratios is also included in order to give an impression of the fit between the different model versions. In interpreting the results of the intercomparison one must realise that the models use different land-use data and consequently also different roughness data. The resolution of this data is 1 x 1 km for OPSEX9E and OPSEX12N, and 5 x 5 km for OPSEXP6E and OPSEXP8E, while OPS-V1.20E makes no distinction between roughness and land use at the stations. In general, one may conclude that the average values of calculated NH_3 concentrations do not deviate much from each other. The difference in wet deposition is larger, especially for the original OPS version (OPS-

V1.20E). The differences for dry and total deposition are remarkably small: less than 10%. The latter is probably due to a conservation of mass mechanism between atmospheric concentration and dry deposition but also between wet and dry deposition. Some individual stations deviate much more. This is mainly due to the different land-use and roughness characteristics applied by the models.

Table 9.2 Comparison of model results for ammonia and ammonium distribution in the Netherlands. All values are relative to the OPSEX12N version of the model.

Model version	Eff. NH_3 dry dep. velocity	Eff. NH_3 > NH_4 conv. rate	NH_3 conc.		NH_4 conc.		Dry deposition		Wet deposition		Total deposition	
	ratio[#]	ratio[#]	ratio[#]	std[$]	ratio[#]	std[$]	ratio[#]	std[$]	ratio[#]	std[$]	ratio[#]	std[$]
OPS-V1.20E	1.14	3..94	0.87	0.20	2.14	0.49	1.04	0.30	1.40	0.11	1.12	0.26
OPSEXP6E	0.98	1..37	1.17	0.25	1.43	0.42	1.12	0.27	1.20	0.07	1.12	0.21
OPSEXP8E	1.03	1..37	1.16	0.25	1.43	0.42	1.18	0.32	1.20	0.07	1.17	0.24
OPSEXP9E	1.11	1.02	0.92	0.09	1.00	0.09	1.04	0.23	0.96	0.04	1.02	0.18

[#] Mean of 30 locations in the Netherlands relative to the OPSEX12N model version
[$] Standard deviation of 30 individual ratios

The oldest version of the OPS model deviates most from the latest version, both in terms of processes included and results. These results are compared in more detail in Figure 9.1. This figure shows that the older model underestimates especially the higher NH_3 concentrations. In all cases the OPSEX12N model version performs better when compared with observations. For NH_3 compared with measurements at 8 stations, R^2 = 0.77, 0,76, 0.76, 0.89 and 0.89 for OPS-V1.20E, OPSEXP6E, OPSEXP8E, OPSEXP9E and OPSEX12N, respectively.

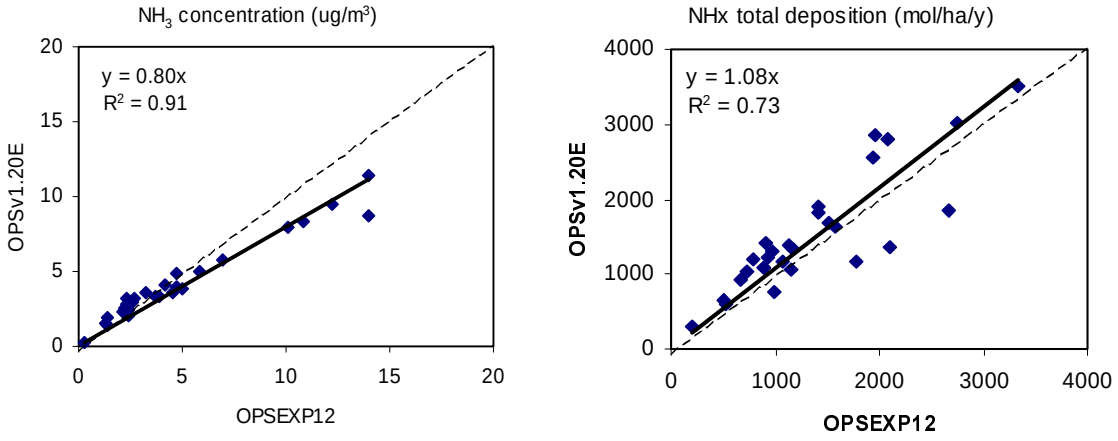

Figure 9.1 Comparison of the results of the present model and the first operational version of the OPS model for the case of ammonia air concentrations and total deposition at 30 locations in the Netherlands.

9.3 Comparison for the case of maximum concentrations near point sources

An important feature of the OPS model is the calculation of concentrations and deposition near point sources. Although most of the model applications are on a national scale, it is important to describe local influences as well, because the set of all local source contributions form the total concentration or deposition on a local scale. Examples are situations in industrial areas, hot spots near roadways or nitrogen deposition on nature reserves.

The model intercomparison is carried out for some source types typical for SO_2, NO_x and NH_3. In this case only the oldest and the newest versions are compared. In all cases, a standard roughness length of 0.15 m is used, along with long-term meteorological data. In all cases the concentration and deposition eastwards of the sources are compared. This means that the highest concentration in the area is probably not presented here because this concentration is usually found in a north-east direction.

Dispersion from high stacks

In Figures 9.2 and 9.3 the concentration and deposition is given for a 150 m stack emitting 1 g s^{-1} SO_2 or NO_x (as NO_2), while the flue gases have a heat content of 80 megawatt. This situation may be representative for modern power plants with no flue gas washing. Typical differences between the two models is that in the new model, the maximum concentration is approximately 20% higher while the location of the maximum is closer to the stack (approximately 3 km vs. 10 km). The maximum deposition is found by both models at the same distance as the maximum concentration or slightly farther away. For an explanation of the differences in total deposition levels, one must realise that the role of wet deposition varies between SO_x and NO_y, but also that wet deposition levels are significantly higher in the new model for both SO_x and NO_y (see Table 9.3). In the case of SO_x, the differences between the models are also due to the differences in (local) dry deposition velocities: 0.90 cm s^{-1} for the new model and 1.40 cm s^{-1} for OPS-V1.20E.

Table 9.3 Fraction of wet deposition in total deposition

Source characteristics	Distance from stack	OPS-V1.20E		OPSEX12N	
		SO_x	NO_y	SO_x	NO_y
150 m, 80 MW	10000	0.28	0.31	0.49	0.64
10 m high	100	0.008		0.015	
3 m high	20		1.4×10^{-6}		1.4×10^{-6}

Dispersion from low sources

A comparison of model results for low emission sources is given in Figures 9.4 and 9.5 for SO_x and NO_y, respectively. For low source heights the wet deposition plays hardly a role close to the source (see Table 9.3). For a 10 m source, the new model gives a slightly lower maximum concentration and deposition than the old model (Figure 9.4). For a 3-m emitting height, representative for dispersion of mobile sources, the difference between the model versions is opposite to the 10-m case. Obviously, the new model calculates higher concentrations for very low source heights and lower concentrations for the medium range. This is illustrated in Figures 9.6 and 9.7 for a wide range of source heights. Although Figure 9.6 is calculated for SO_2, it is applicable for NH_3 too. One may therefore conclude, for example, that the new model calculates significantly higher concentrations for ammonia from manure spreading (emitting height < 1m) than the old version.

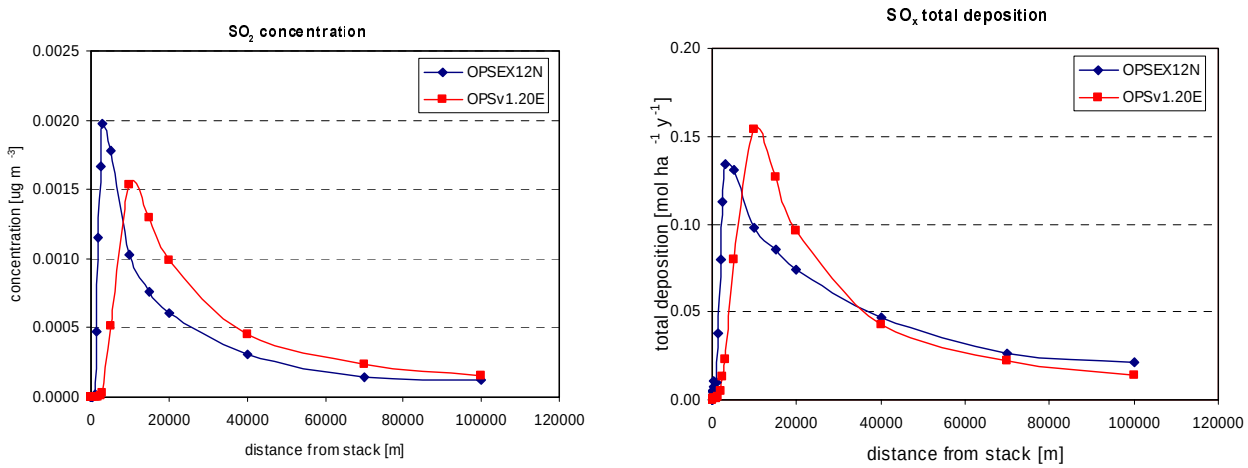

Figure 9.2 *Comparison of SO_2 concentrations and SO_x deposition near a 150-m stack emitting 1 g s^{-1} SO_2 with a heat content of 80 MW.*

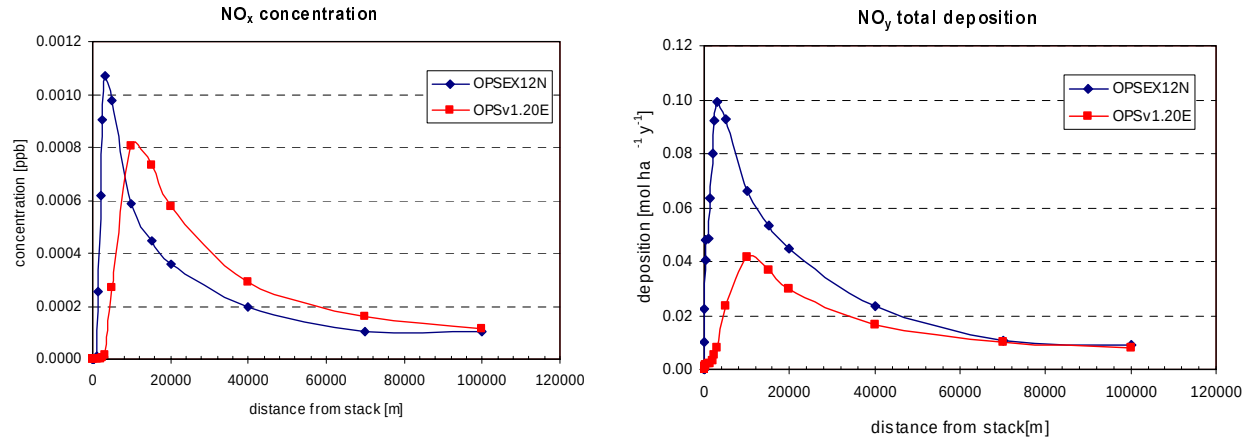

Figure 9.3 *Comparison of NO_x concentrations and NO_y deposition near a 150 m stack emitting 1 g s^{-1} NO_x with a heat content of 80 MW*

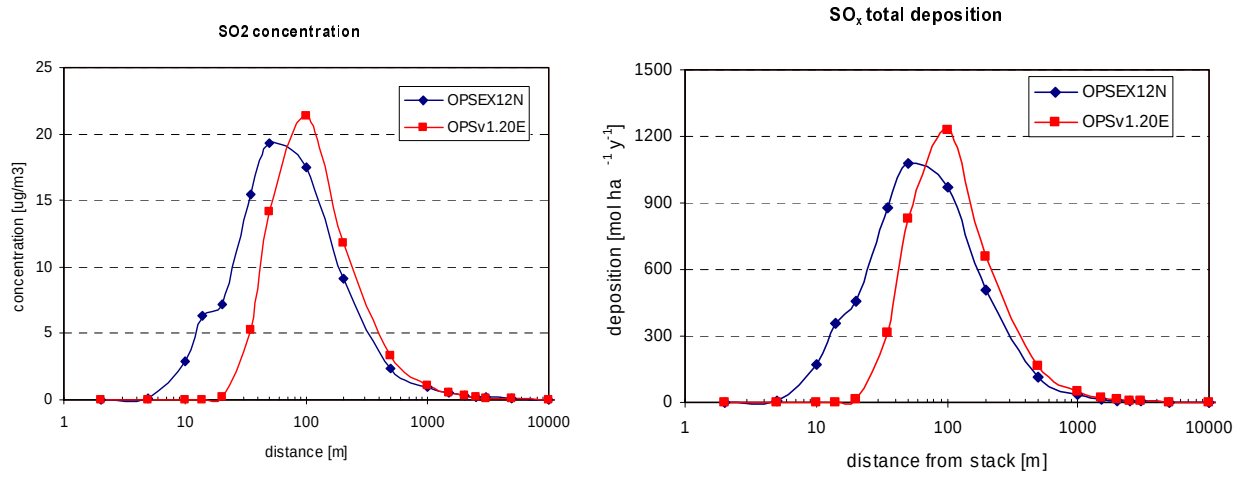

Figure 9.4 *Comparison of SO_2 concentrations and SO_x deposition near a 10 m stack emitting 1 g s^{-1} SO_2 with no heat content.*

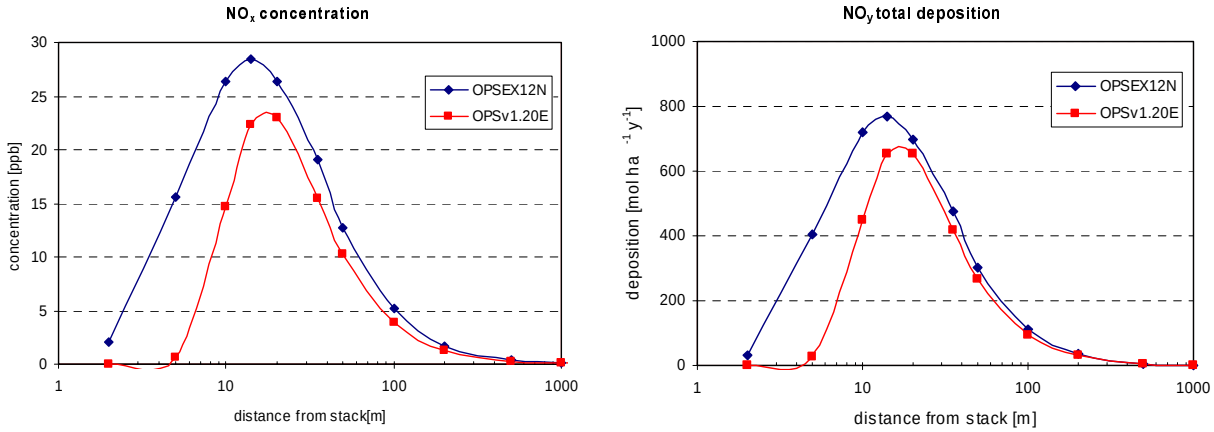

Figure 9.5 *Comparison of NO_x concentrations and NO_y deposition near a 3-m stack emitting 0.1 g s^{-1} NO_x with no heat content.*

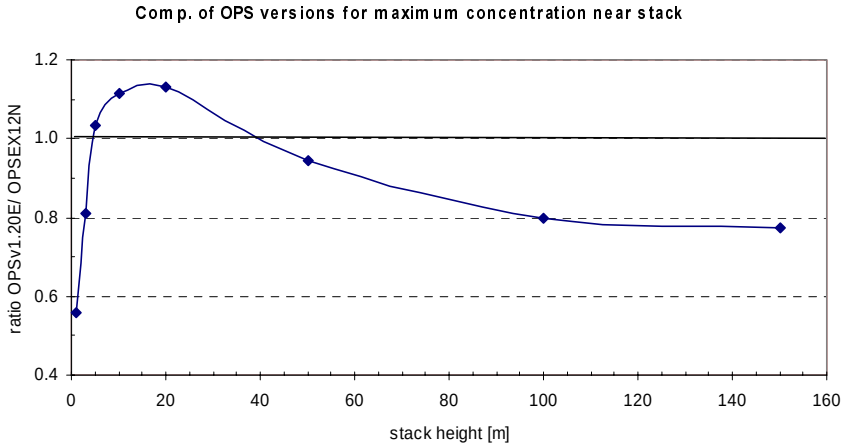

Figure 9.6 *Comparison of maximum concentration (eastward direction) for different source heights.*

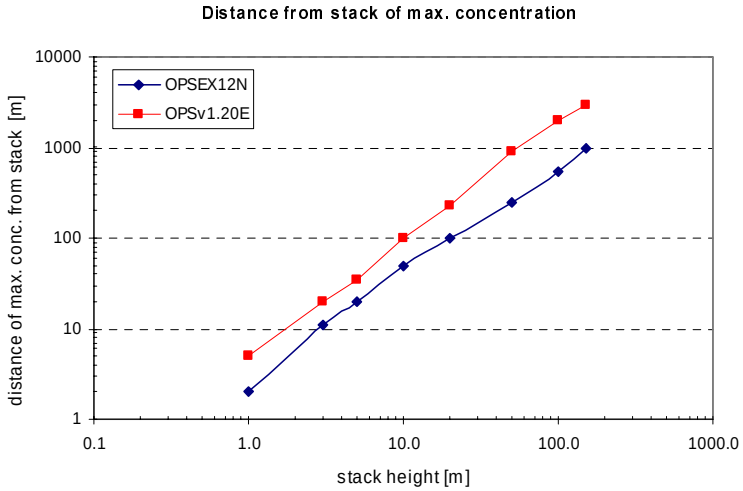

Figure 9.7 *Comparison of the location of the maximum concentration (eastward direction) for different source heights.*

Summary of the comparison with previous versions

The difference in model results for the various versions is ,in general, small as long as the national scale is considered and the same emission data is taken. This is mainly due to the conservation of mass principle. The total deposition above the Netherlands, calculated with the 1990 version of the model, is for ammonia 12% higher than when calculated with the latest version. For deposition on the local scale (5 x 5 km) the difference may be in the order of +/-25%. The overall conclusion is that for the national scale the subsequent versions of the OPS model have given consistent results.

The largest differences between the models are found for very high (point) sources, for which the new model predicts higher maximum concentrations (approx. 25%), located closer to the source (typically 1-2 km versus 8-12 km).

Another important difference is found for very low sources (0-3m). Here the new model calculates higher concentrations (factor 1-1.8). This is relevant for calculating the dispersion of ammonia from field-applied manure but also for traffic-related compounds as NO_x in cities.

The overall conclusion is that the subsequent versions of the OPS model have, over the years, given consistent results.

References chapter 9

Asman W.A.H. and Jaarsveld J.A. van (1992) A variable-resolution transport model applied for NH_x in Europe. *Atmospheric Environment* **26A**, 445-464.

Heij G.J. and Erisman J.W., editors (1997) Acid atmospheric deposition and its effects on terrestrial ecosystems in the Netherlands; Studies in Environmental Science 69, Elsevier, Amsterdam, the Netherlands.

RIVM (1997) State of the Environment 1997 (in Dutch). Samson H.D Tjeenk Willink, Alphen aan den Rijn, ISBN 90 42200995

Van Jaarsveld J.A. (1990) An operational atmospheric transport model for priority substances; specification and instructions for use. RIVM, Bilthoven, the Netherlands. Report no. 222501002.

Van Jaarsveld J. A. and de Leeuw F. A. A. M. (1993) An operational atmospheric transport model for priority substances. *Environmental Software*, **8**, 91-100.

Van Jaarsveld, J.A., A. Bleeker, J.W. Erisman, G.J. Monteny, J. Duyzer and D. Oudendag. (2000) Ammoniak emissie-concentratie-depositie relaties op lokale schaal. RIVM, Bilthoven, the Netherlands. Report no. 725601001.

Appendix I The DEPAC dry deposition module in OPS

Dry deposition velocities in the OPS model are calculated using the submodel DEPAC (DEPosition And Concentration). This model is also used in other RIVM models such as DEADM, EDACS and EUROS but also - in an adaptive form – in the UNECE-EMEP model. Core of the model is the so-called resistance model in which the dry deposition velocity is described with a number of resistances. The most recent overview of the knowledge of the modelling of the dry deposition velocity can be found in Wesely and Hicks (2000). This overview reveals that the so-called canopy resistance R_c is the most difficult one to model. R_c strongly depends on the gas in question and on the properties of the receiving surface, and is therefore very location dependent. Parameterisations derived from measurements elsewhere are not always applicable to the situation in the Netherlands because of this location dependency.

The current status of the modelling of the canopy resistance in the Netherlands is given in Erisman *et al*. (1994). That publication forms the basis of the current DEPAC model. This appendix describes the DEPAC module and gives the current parameterisations. Unfortunately, versions of DEPAC in models such as DEADM and EDACS appear to be slightly different. These models are currently no longer in use.

DEPAC description

The DEPAC module provides a dry deposition velocity and a so-called effective canopy resistance on an hourly basis as a function of meteorological parameters, month of the year and time of the day. Meteorological parameters are: Friction velocity, Monin-Obukhov length, global radiation wind speed at canopy height, relative humidity and a surface wetness indicator. Other parameters are: land-use class, substance code, and roughness length. The module contains dry deposition parameterisations for the following acidifying substances (Table AI.1):

Table AI.1 Substances in DEPAC

Code	Substance	Gas or aerosol
1	SO_2	Gas
2	NO_2	Gas
3	NO	Gas
4	NH_3	Gas
5	HNO_3	Gas
11	SO_4^{2-}	Aerosol
12	NO_3^-	Aerosol
13	NH_4^+	Aerosol

In addition, 9 classes of land use are defined in Table AI.2).

Table AI.2. Land-use classes in DEPAC

Code	Land-use type
1	Grass land
2	Arable land
3	Permanent crops
4	Coniferous forest
5	Deciduous forest
6	Water
7	Urban
8	Other i.e. short grassy areas
9	Desert (dunes, sandy areas)

Dry deposition of gases

The dry deposition flux F is calculated as:

$$F = v_d(z) \cdot c(z) \qquad \text{(AI.1)}$$

where $v_d(z)$ is the dry deposition velocity in $\mathrm{m\,s^{-1}}$ at height z in m, $c(z)$ the concentration in $\mu\mathrm{g\,m^{-3}}$ and F the deposition flux in $\mu\mathrm{g\,m^{-2}}$.

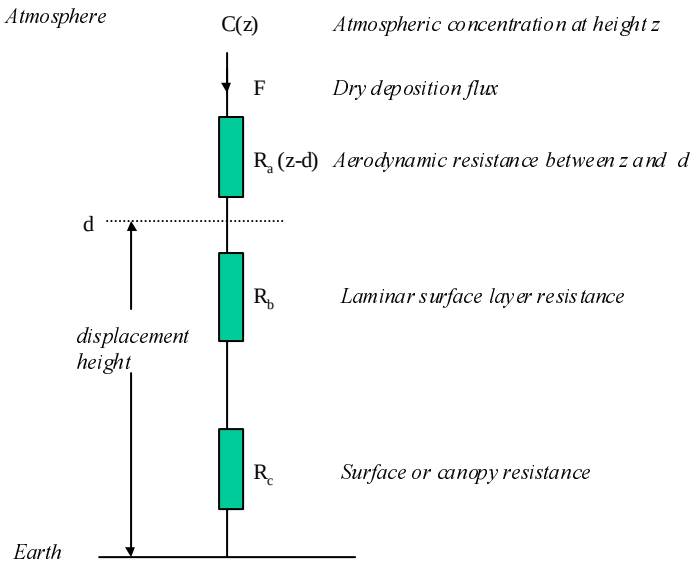

Figure AI.1. The resistance analogy of the dry deposition process of gases.

The resistance model

The dry deposition velocity is simulated using an electrical resistance analogy (see Figure AI.1):

$$v_d(z) = \frac{1}{R_a(z-d) + R_b + R_c} \qquad \text{(AI.2)}$$

with the aerodynamic resistance R_a, the laminar surface layer resistance R_b and the canopy resistance R in $\mathrm{s\,m^{-1}}$.

R_a as a function of height z and displacement height d can be calculated from:

$$R_a(z-d) = \frac{1}{\kappa \cdot u_*}\left[\ln\left(\frac{z-d}{z_0}\right) - \psi_h\left(\frac{z-d}{L}\right) + \psi_h\left(\frac{z_0}{L}\right)\right] \qquad \text{(AI.3)}$$

with κ the Von Karman constant (0.4), u_* the friction velocity in $\mathrm{m\,s^{-1}}$, L the Monin-Obukhov length in m and z_0 the roughness length in m. The roughness length can be determined by using, for example, the classification of Wieringa (1981). The integrated stability function of heat ψ_h can be calculated according to Beljaars and Holtslag (1990). A more simplified approach for R_a is included in DEPAC:

$$R_a(z) = \frac{U(z)}{u_*^2} \qquad \text{(AI.4)}$$

with *U(z)* the wind speed at height z. The OPS model uses Equation (AI.3). Order of magnitude for R_a is 50 $\mathrm{s\,m^{-1}}$. R_b is calculated according to Hicks *et al*. (1987):

$$R_b = \frac{2}{\kappa \cdot u_*}\left(\frac{\mathrm{Sc}}{\mathrm{Pr}}\right)^{2/3} \qquad \text{(AI.5)}$$

with *Pr* the Prandtl number: $\mathrm{Pr} = \frac{\upsilon_{air}}{\gamma_{air}} = 0.7$, υ_{air} de kinematic viscosity of air ($1.461 \cdot 10^{-6}$ $\mathrm{m^2\,s^{-1}}$) and γ_{air} the molecular heat diffusivity of air ($2.06 \cdot 10^{-5}$ $\mathrm{m^2\,s^{-1}}$), both at standard temperature and pressure. Sc is the Schmidt number, which depends on the gas in question: $\mathrm{Sc} = \frac{\upsilon_{air}}{D_x}$, with D_x the molecular diffusivity of the gas in $\mathrm{m^2\,s^{-1}}$. Equation (AI.5) can also be written as:

$$R_b = \frac{2}{\kappa \cdot u_*}\left(\frac{\gamma_{\mathrm{air}}}{D_x}\right)^{2/3} \qquad \text{(AI.5a)}$$

D_x depends on temperature, pressure and the composition of the gas mixture. Several values for D_x are reported in the literature. Table AI.1 shows the selected values for D_x. A pressure or temperature correction is not applied in DEPAC.

Table AI.3 Molecular diffusivity for the different gases used in DEPAC

Code	Gas	D_x in $m^2\ s^{-1}$
1	SO_2	1.1×10^{-5}
2	NO_2	1.3×10^{-5}
3	NO	1.6×10^{-5}
4	NH_3	2.1×10^{-5}
5	NHO_3	1.1×10^{-5}

The order of magnitude for R_b is 10 to 20 $s\ m^{-1}$.

The canopy resistance

The canopy resistance R_c may be considered as the result of a number of sub-resistances representing different processes in and at the canopy. The general model with the canopy resistance split up in sub-resistances is given in Figure 2.

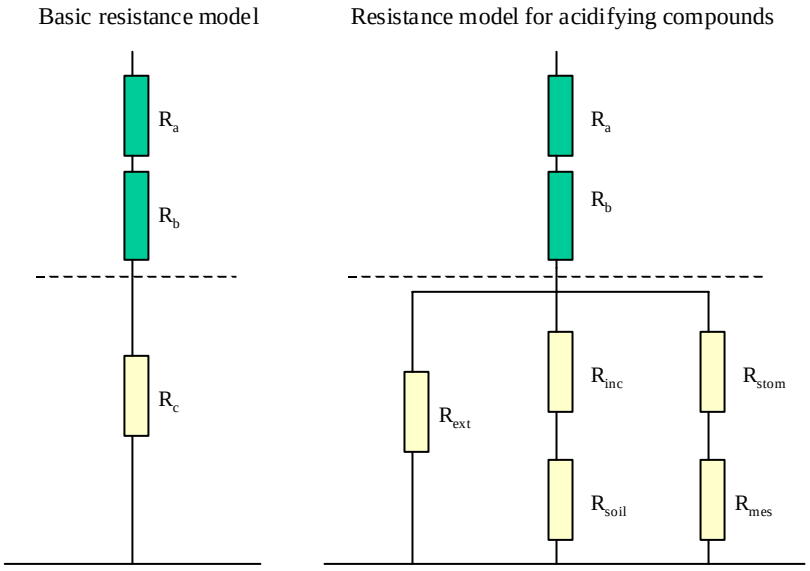

Figure AI.2. Resistance model with sub-resistances for the canopy resistance R_c.

In this model R_{stom} and R_{mes} represent the stomatal and mesophyll resistances of leaves respectively. R_{inc} and R_{soil} are resistances representing in-canopy vertical transport to the soil, which bypasses leaves and branches. R_{ext} is an external resistance, which represents transport via leaf and stem surfaces, especially when these surfaces are wet. The (effective) canopy resistance R_c can be calculated as:

$$R_c = \frac{1}{\frac{1}{R_{stom} + R_{mes}} + \frac{1}{R_{inc} + R_{soil}} + \frac{1}{R_{ext}}} \qquad \text{(AI.6)}$$

The DEPAC module contains parameters for each of the resistances given in Figure 2 for various land-use types (Table AI.2) and for each of the gaseous components of Table AI.1. Furthermore, a seasonal distinction is made in the values of some of the resistances. In a number of cases the general resistance model reduces to its most basic form, that is, when detailed information is lacking (e.g. for HNO_3) or when the surface is non-vegetative such as for bare soil, water surfaces, buildings or when there is a snow-cover. In these cases only Rsoil determines the effective canopy resistance, because R_{ext}, and R_{stom} are set to (near) infinity.

Water surface: $R_c = R_{soil} = R_{water}$
Bare soil: $R_c = R_{soil}$
Snow cover: $R_c = R_{soil} = R_{snow}$
HNO_3 $R_c = R_{soil}$

Stomatal resistance

R_{stom} is calculated according to Wesely (1989):

$$R_{stom,H_2O} = R_i \cdot \left[1 + \left(\frac{200}{Q + 0.1}\right)^2\right] \cdot \frac{400}{T_s \cdot (40 - T_s)} \qquad \text{(AI.7)}$$

and

$$R_{stom,x} = R_{stom,H_2O} \cdot \frac{D_{H_2O}}{D_x} \qquad \text{(AI.8)}$$

where Q is the global radiation in $\mathrm{W\,m^{-2}}$, T_s the surface temperature in °C, D_{H_2O} the molecular heat diffusivity of water vapour and D_x the molecular heat diffusivity of the substance, both in $\mathrm{m^2\,s^{-1}}$. R_i values are given in Table AI.4. Values of -999 in this and further tables indicate that the resistance is near infinity and plays no role under the given conditions.

Table AI.4 R_i values at different conditions according to Wesely (1989) (in s m^{-1})

Season	Grass land	Arable land	Permanent crops	Coniferous forest	Deciduous forest	Water	Urban	Other grassy area	Desert
Summer	60	60	60	130	70	-999	-999	60	-999
Autumn	-999	-999	-999	250	-999	-999	-999	-999	-999
Winter	-999	-999	-999	400	-999	-999	-999	-999	-999
Spring	120	120	120	250	140	-999	-999	120	-999

Mesophyll resistance

The mesophyll resistance R_m is set at $0\ \mathrm{s\,m^{-1}}$ for all circumstances because there are indications that it is low for substances as SO_2, O_3 and NH_3 and because of lack of relevant data to justify other values (Wesely, 1989).

In-canopy resistance

R_{inc} represents the resistance against turbulent transport within the canopy and is calculated according to Van Pul and Jacobs (1993):

$$R_{inc} = \frac{b \cdot LAI \cdot h}{u_*} \qquad \text{(AI.9)}$$

where b as an empirical constant (14 m^{-1}), h the height of the vegetation in m (1 m for arable land and 20 m for forests) and LAI the Leaf Area Index (dimension less). The authors themselves qualify Equation (AI.9) as still preliminary. DEPAC uses LAI as a function of the time of the year according to Table AI.5. The calculation of R_{inc} according to Eq. (AI.9) is only carried out for arable land and forest. For all other land-use classes R_{inc} is set at 0.

Table AI.5 Leaf Area Indexes for some land-use classes

	Grass	Arable land	Perm. crops	Conif. forest	Decid. Forest	Water	Urban	Other grassy area	Desert
May and October	6	1.25	N/A	5	1.25	N/A	N/A	N/A	N/A
June and September	6	2.5	N/A	5	2.5	N/A	N/A	N/A	N/A
July and August	6	5	N/A	5	5	N/A	N/A	N/A	N/A
November - April	6	0.5	N/A	5	0.5	N/A	N/A	N/A	N/A

Soil resistance

DEPAC uses R_{soil} values as given in Table AI.6. The general effect is that wet surfaces enhance the uptake of (soluble) gases. If the soil is frozen and/or covered with snow then the uptake is much less.

Table AI.6. Soil resistances in s m^{-1} for various substances. The values apply to all land-use types including urban areas.

	Rsoil_wet	Rsoil_dry	R soil_frozen[&]	Rwater	Rsnow
SO_2	10	1000	500	10	70(2-T)[$]
NO_2	2000	1000	2000	2000	2000
NO	-999	-999	-999	2000	2000
HNO_3	10	10	10	10	50[#]
NH3	10	100	1000	10	70(2-T)[$]

[&] if T < -1°C
[#] only if T < -5°C, otherwise Rsnow = 10
[$] minimal value = 70; if T< -1°C, Rsnow = 500

External resistance

The external resistance R_{ext} represents a sink for gases through external leaf uptake and is especially important for soluble gases at wet surfaces. Under some conditions the external leaf sink can be much larger than the stomatal uptake. R_{ext} is only calculated for grass, arable land and forest land-use types.

SO_2

The following empirical expressions from Erisman *et al*. (1994) are used for SO_2:

During or just after precipitation (wet = true):

$$R_{ext} = 1$$

In all other cases:

if $T > -1$ °C

$$R_{ext} = 25000 \cdot e^{-0.0693\,rh} \qquad \text{if } rh < 81{,}3\ \%$$

$$R_{ext} = 10 + 0.58 \cdot 10^{12} \cdot e^{-0.278\,rh} \qquad \text{if } rh > 81{,}3\ \%$$

if $-1 > T > -5$ °C

$$R_{ext} = 200$$

if $T < -5$ °C:

$$R_{ext} = 500$$

Here, *rh* expresses the relative humidity in %.

NO_2

Under all conditions $R_{ext} = 2000$

NO

Under all conditions $R_{ext} = 10000$

HNO_3

The basic resistance model is applied and thus R_{ext} is not required

NH_3

The parameterisation of R_{ext} for NH_3 is more complicated. First of all, there is a distinction made in pollution climates represented by NH_3/SO_2 ratios classified as low, high and very low. The corresponding NH_3/SO_2 ratios are, however, not defined. In the present implementation of the OPS model the 'high' definition is applicable under all circumstances. Only this part of the parameterisation is described here.

- For temperatures below 0 °C: $R_{ext} = 200$
- For the land-use classes, water, urban and desert: $R_{ext} = 5 + 19257 \cdot e^{-0.094\,rh}$
- For coniferous and deciduous forests:
  - dry conditions: $R_{ext} = 25 + 19257 \cdot e^{-0.094\,rh}$
  - global radiation > 300 W m^{-2}: $R_{ext} = -500$ #
  - wet conditions: $R_{ext} = 20$
- For grassland, arable land and other grassy areas:

Daytime:	Spring and summer (dry):	$R_{ext} = 100$
	Spring and summer (wet):	$R_{ext} = 20$
	Autumn and winter (dry):	$R_{ext} = 50$
	Autumn and winter (wet):	$R_{ext} = 20$
Nighttime:	Spring and summer (dry):	$R_{ext} = 50$

Spring and summer (wet):	R_{ext} = 20
Autumn and winter (dry):	R_{ext} = 100
Autumn and winter (wet):	R_{ext} = 20

This condition suggests that there is an upward (emission) flux.

Dry deposition of acidifying aerosols

Basically, the dry deposition of particles is modelled using empirical relations. These relations describe the vertical movement of small particles at or within the canopy. The empirical relations can be fitted into a common resistance approach according to Figure AI.3. In this model the effects of all canopy-related processes are included in R_{part}. Together with the aerodynamic resistance it can be included in a dispersion model just as the resistance model for gases. The dry deposition velocity for small particles is then calculated as:

$$V_{d\_part}(z) = \frac{1}{R_a(z-d) + R_{part}} \qquad \text{(AI.11)}$$

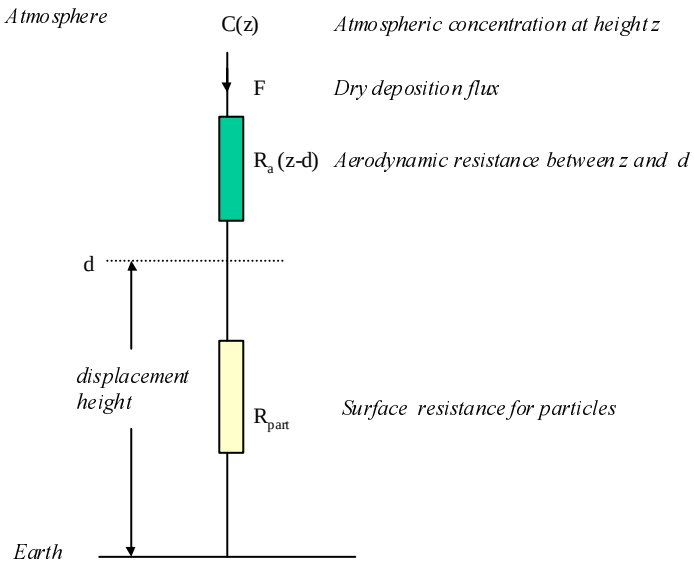

Figure AI.3. Resistance model for small particles.

For roughness lengths below 0.5 m, the particle 'canopy' resistance is modelled according to Wesely *et al*. (1985):

$$R_{part}^{-1} = \frac{u*}{500}\left(1 + \left(\frac{300}{-OL}\right)^{\frac{2}{3}}\right) \qquad if \quad OL < 0 \qquad \text{(AI.12)}$$

$$R_{part}^{-1} = \frac{u*}{500} \qquad if \quad OL > 0 \qquad \text{(AI.13)}$$

For forested areas and areas with roughness lengths above 0.5 m, R_{part} is parameterised according to Ruygrok *et al*. (199x):

$$R_{part}^{-1} = \frac{(u*)^2}{U_h \; E} \qquad \text{(AI.14)}$$

where U_h represents the wind speed at canopy height (m s^{-1}) and E a particle collection efficiency:

$$E = a \; (u*)^b \left(1 + c \; \exp^{\left(\frac{rh-80}{20}\right)} \right) \qquad \text{(AI.15)}$$

with *a, b, c* coefficients defined in Table AI.7

Table AI.7 Coefficients of the collection efficiency parameterisation (Equation AI.15).

	A		*b*		*c*	
	Dry	Wet	Dry	Wet	Dry	Wet
SO_4	0.05	0.08	0.28	0.45	0.18	0.37
NO_3	0.063	0.10	0.25	0.43	0.18	0.37
NH_4	0.05	0.066	0.23	0.41	0.18	0.37

References Appendix I

Beljaars A.C.M. and Holtslag A.A.M. (1990) A software library for the calculation of surface fluxes over land and sea. *Environ. Software* **5**, 60-68.

Erisman J.W., van Pul W.A.J. and Wyers P (1994) Parametrization of surface resistance for the quantification of atmospheric deposition of acidifying pollutants and ozone. Atmospheric Environment **28** (16) 2595-2607.

Hicks B.B., Baldocchi D.D. Meyers T.P., Hosker Jr. R.P. and Matt D.R. (1987) A preliminary multiple resistance routine for deriving dry deposition velocities from measured quantities. *Water Air Soil Pollut.* **36**, 311-330.

Van Pul W.A.J. and Jacobs A.F.G. (1993) the conductance of a maize crop and the underlying soil to ozone under various environmental conditions. *Boundary Layer Met.*

Wesely M.L., Cook D.R., Hart R.L. and Speer R.E. (1985) Measurements and parameterization of particulate sulfur dry deposition over grass. J.Geophys. Res., **90**(D1):2131-2143.

Wesely M.L. (1989) Parameterization of surface resistances to gaseous dry deposition in regional scale numerical models. *Atmospheric Environment* **23**, 1293-1304.

Wesely M.L. and Hicks B.B. (2000) A review of the current status of knowledge on dry deposition. *Atmospheric Environment* **34** (2000) 2261-2282.

Wieringa J. (1981) Estimation of mesoscale and local-scale roughness for atmospheric transport modelling. In: Wispelaere, C., editor. The 11th Int. Tech. Meeting on air pollution modelling and its application. Plenum Press, New York, 279-295.

Appendix II Suggestions for substance-specific parameter values

The OPS model offers a generic approach for the modelling of transport and deposition of substances. The parameters that define the atmospheric behaviour of substances in a generic way are described in Chapter 5. This section deals with the choice of parameter values for such substances. In the case of the acidifying substances SO_x, NO_y and NH_x a more specific approach is chosen, not only for their important role in a major environmental issue but also because the availability of a large amount of research data. The parameter values of the acidifying substances cannot be altered by the model user. These substances and their properties are discussed in Chapter 6.

Table AII.1 Parameter values for pre defined substances as included in 'defcomp.ops'

component name	g_p	mol	R_c	scav.rat.	d_c	rev	conv(a)	conv(b)	ref*)
SO2 - gas. #)	0	64.1	68	80000	.136	1	.5000	.0070	
NOx - gas. #)	0	46.0	300	10000	.160	0	2.0000	.0065	
NH3 - gas. #)	0	17.0	23	1000000	.240	0	5.0000	.0000	
PM10	1	1.0	0	0	.0	0	.0	.0	
CO - gas.	0	28.0	2860	0	.18	0	.0	.0004	
Pb(lead)-aer.	1	207.2	0	0	.0	0	.0	.0	[2]
Cd(cadmium)-aer.	1	112.4	0	0	.0	0	.0	.0	[2]
As(arsenic)-aer.	1	74.9	0	0	.0	0	.0	.0	[2]
Cr(chromium)-aer.	1	52.0	0	0	.0	0	.0	.0	[2]
Cu(copper)-aer.	1	63.7	0	0	.0	0	.0	.0	[2]
Zn(zinc)-aer.	1	65.4	0	0	.0	0	.0	.0	[2]
C6H6(benzene)-gas	0	78.0	9999	17	.113	0	.5400	.0000	[3]
C7H8(toluene)-gas	0	92.0	9999	8	.104	0	2.8000	.0000	[3]
B(a)P(benzo-)-aer.	1	252.0	0	0	.0	0	.0	.0	[6]
HF(fluorine)-gas.	0	20.0	13	1000000	.230	0	.0000	.0000	[1,2]
F(fluorine)-aer.	1	19.0	0	0	.0	0	.0	.0	[2]
HCl(chlorine)-gas.	0	36.5	13	1000000	.190	0	.0000	.0000	[1,2]
Cl(chlorine)-aer.	1	35.5	0	0	.0	0	.0	.0	[2]
HBr(bromine)-gas.	0	80.9	13	1000000	.11	0	.00	.0000	[1,2]
Br(bromine)-aer.	1	79.9	0	0	.0	0	.0	.0	[2]
B(boron)-gas.	0	10.8	49	50000	.150	0	.0000	.0000	[1,2]
B(boron)-aer.	1	10.8	0	0	.0	0	.0	.0	[2]
Se(selenium)-gas.	0	79.0	49	120000	.11	0	.0000	.0000	[2]
Se(selenium)-aer.	1	79.0	0	0	.0	0	.0	.0	[2]
Hg^0(mercury)@)gas.	0	200.6	7000	5000	.071	0	.0000	.0000	[5]
Hg^{II}(mercury)@)gas	0	200.6	150	200000	.071	0	.0000	.0000	[5]
Hg^{II}(mercury)@)aer.	1	200.6	0	0	.0	0	.0	.0	[5]

#) These compounds are fully defined inside the OPS model; parameter values are indications only.
@) See remarks in this chapter

*) References:
[1]: Janssen and Ten Brink, 1985
[2]: van Jaarsveld and Onderdelinden, 1986
[3]: van Jaarsveld, 1989
[5]: EMEP, 2000
[6]: Baart *et al*., 1995

Recommended parameters for standard substances

The contents of the file 'defcomp3.ops' is shown in Table AII.1. This file contains the specific values of the parameters for a number of substances. Most of the substances that have been included in this list are derived from earlier applications of this model.

Parameters on the substances list

g_p: gas-particle switch. 1 = substance is gaseous, 0 =: substance is on particles. The actual size distributions are determined by the emission process, which may vary from source to source. See Chapter 5.1.2 for recommended particle size distributions.

mol: molecular weight of the element or compound. If the compound has no chemical meaning such as is the case for PM10, the molecular weight is set at 1. In the case of particles, the molecular weight is only used as a parameter to convert deposition units e.g. from g m^{-1} s^{-1} into mol ha^{-1} $year^{-1}$.

If the substance is particulate (g_p = 1), then all other deposition parameters are related to the particle size and as such implicitly present in the model. The deposition parameters have been marked "0" on the list for practical reasons.

R_c: the surface resistance (s.m^{-1}). See sections 4.1 and 5.2.1. The surface resistances selected apply to grass vegetation. A value of 9999 means that the dry deposition process is insignificant. The calculated dry deposition flux must be interpreted as an upper limit.

scav.rat.: scavenging ratio (average ratio of water concentration to air concentration at the onset of a shower). See sections 4.2 and 5.2.2. A scavenging ratio of 10^6 means that the wet deposition process is so efficient that the atmosphere is 'washed clean' after every shower. The factor controlling the wet deposition is then the number of showers falling during a certain period.

d_c: diffusion coefficient in air of the element or compound concerned (cm^2.s^{-1}). This parameter governs the washout velocity of a substance. See section 5.2.2.

rev: reversible washout or not (0 = no). This parameter indicates whether material disappears again from a raindrop when this drop comes into cleaner ambient air (e.g. below a smoke plume). See sections 4.2.2 and 5.2.2

conv(a): rate at which the substance is converted into a daughter product or disappears in a way other than by dry or wet deposition (%.h^{-1}); the constant fraction of this in time. See section 5.2.3.

conv(b): as above, but the fraction of the conversion rate which can be related to the solar radiation occurring in the Netherlands. See section 5.2.3 for the use of this parameter.

Remarks concerning the list of recommended parameters

SO_2, NO_x and NH_3

The deposition and conversion processes for SO_2, NO_x and NH_3 are fully defined within the OPS model and also include the production and fate of secondary products such as SO_4^{2-}, NO_3- and NH_4^+ Dry deposition parameters for the different compounds are taken from the DEPAC module (Erisman *et al*., 1994), which is based on experimental work within the acid deposition research programme in the Netherlands and elsewhere. The parameter values given in the list for these compounds are indicative approximations only.

NO_x

The emission of NO_x - in chemical terms - is assumed to be as NO but must be expressed in NO_2 equivalents. Calculated NO_x concentrations are in parts per billion (ppb).

PM10

PM10 is defined by the selection of a size distribution. A major assumption is that the size distribution completely cuts off at 10 µm. Below 10 µm the distribution may vary depending on the size distribution of the different emission sources or source categories. The size distributions are specified in the emission file (see sections 7.4.2 and 7.4.4). The (suggested) size distribution of PM 10 is:

<0.95	0.95-4	4-10	10-20	> 20	[µm]
73	21	6	0	0	[%]

Mercury

The parameterisation used for the modelling of mercury is based on the work of Petersen (1992). Three mercury species may be (independently) modelled:

a. elemental or metallic mercury (Hg^0)
b. divalent mercury (Hg^{II}) such as dimethyl mercury ($(CH_3)_2Hg$)
c. mercury on aerosols (Hg^{II}_{aer}) (e.g. CH_3HgCl)

Although indications exist that different processes produce these mercury species in different ratios, a fixed (emission) ratio between the different species is often assumed. Rjaboshapko and Korolev (1997) use 57% Hg^0, 30% Hg^{II} and 13% Hg_{aer}

The most important atmospheric removal process for Hg^0 is wet deposition through a form of reactive scavenging. Petersen (1992) describes this process as a function of atmospheric ozone and soot concentrations, resulting in relatively high scavenging in Eastern Europe and low scavenging in remote areas. For use in this study a scavenging ratio of 5000 is derived for the North Sea area. In the EMEP model (EMEP, 2000) an average deposition velocity of 0.00015 m s^{-1} is applied for Hg^0, which here is translated in a r_c value of 7000 s/m.

The water solubility of Hg^{II} is high, which leads to effective wet scavenging and to some extent also to effective dry deposition. Following the procedure for determining dry deposition velocities for persistent organics (see this chapter) an effective dry deposition velocity of 0.0045 m s^{-1} for sea surfaces and 0.0035 m/s for land surfaces is derived. Petersen uses a dry deposition velocity of 0.03-0.04 m s^{-1} by assuming that divalent mercury behaves similar to (reactive) HNO_3. The Hg^{II}_{aer} is modelled as all other substances in particle form.

According to Petersen the Hg^0 background concentration in Europe is in the order of 2 ng m^{-3}. Baart *et al*. (1995) estimate that this background concentration is responsible for 33 % of the total mercury deposition in the North Sea and 9 % of the deposition in the Netherlands. A comparison of model results with observations of the OSPAR Comprehensive Atmospheric Monitoring Programme (CAMP) for the years 1990-1991reveals that predicted concentrations in precipitation are in good agreement with measurements. The predicted total deposition load of 8 tons/y for the North Sea area is also in good agreement with the 5-12 tons/y calculated by Petersen.

Estimation of parameter values for non-predefined substances

In many cases one cannot find the substance-specific deposition and/or chemical degradation parameters in literature. The following approach is based on more basic chemical and physical properties of substances as they are to be found in chemical handbooks. Such parameters are vapour pressure, water solubility and the octanol-water partition coefficient. This generic approach leads of course to less accurate results than the situation where parameters can be based on observations.

Gas/particle partitioning

Important for removal and deposition processes is the physical state of pollutants in the atmosphere. Mainly depending on the vapour pressure, pollutants may occur in the gas phase or the particle phase or both. Junge (1977) proposes the following model for the gas-particle partitioning of semi-volatile organic compounds in the atmosphere:

$$\phi = c\ \theta\ (\ \ p^0 L + c\ \theta\ )^{-1} \qquad \text{(AII.1)}$$

where ϕ is the ratio of adsorbed organic vapour on aerosol to the total amount of vapour in air, θ the aerosol surface area ($m^2\ m^{-3}$ air), p^0_L the solute saturation vapour pressure (Pa) and c a constant that depends on heat of condensation and molecular weight. Junge assumed $c \sim 0.17$ Pa m for high molecular weight organics. Since vapour pressures are strongly temperature dependent, the fraction of a substance absorbed to particles will also be temperature dependent. A 10 ^oC increase in ambient temperature will roughly double the vapour pressure. For certain organics this may mean that in tropical regions the organic is mainly in vapour phase while for arctic regions the particle phase is dominant.

The Junge model is widely used in studies on the atmospheric deposition of organics e.g. Eisenreich *et al*., (1981); Mackay *et al*., (1986). Whitby (1978) reports average aerosol total surface areas (θ, $m^2\ m^{-3}$ air) in the range of 4.2×10^{-5} (clean continental background) to 1.1×10^{-3} (urban) with an average background of 1.5×10^{-4}. Considering the range of atmospheric environments, organics having $p^0_L > 10^{-2}$ Pa will exist almost entirely in the vapour phase, while those having $p^0_L < 10^{-6}$ Pa will exist almost entirely in the vapour phase.

Values of (average) particle fractions for various (organic) compounds are given in Table 2. In a number of cases compounds cannot be considered uniquely as gases or as particles. In such cases one can carry out two calculations and see which form dominates concentrations and/or deposition, or one can decide to use a weighted result.

Chemical conversion

Atmospheric reaction rates can be taken, for example, from Atkinson (1986) or Mackay *et al.* (1992). For many compounds, however, no atmospheric reaction rates have been measured experimentally. For organic compounds the reaction with the OH radical is usually the most important loss process. On the basis of the structure of the compound and the reactivity of its functional groups reaction rates can be estimated. See, for example, the work of Atkinson (Atkinson *et al*., 1984, Atkinson , 1987). The accuracy of the method varies from 30% for simple compounds to a factor of 5 for complex molecules (Baart *et al*., 1995).

Aerosols are treated as unreactive in the OPS model. This simplification may lead to an underestimation of the atmospheric lifetime of the compound. For compounds with high degradation rates the particle fraction is therefore also an important parameter.

Wet deposition

When empirical scavenging ratios are not available one can estimate the effectiveness of the wet deposition process on the basis of the water solubility of the substance. For gases the (equilibrium) ratio

of the concentration of a substance in water and air can also be related to the Henry coefficient for a specific substance through:

$$W = \frac{RT}{He} \qquad (W \cong scav.\ rat \text{ in table 1}) \qquad \text{(AII.2)}$$

where R is the gas constant (8.3 Pa m^3 mol^{-1} K^{-1}), T the temperature (K) and He the Henry coefficient (Pa m^3 mol^{-1}). This relation assumes that the gases are reversibly soluble in water, i.e. do not react and/or ionise in the rain droplets and do not attach to particles in the droplets.
The diffusion coefficient D_c (cm^2 s^{-1}) of a substance in air can be approximated using:

$$D_c = k\,[mol]^{-0.5} \qquad \text{(AII.3)}$$

where *mol* is the molecular weight and k a conversion constant (k = 1)

Dry deposition

The dry deposition flux (g m^{-2} s^{-1}) can be calculated from:

$$F_d = v_d(z)\,(\,C_a(z) - C_s\,) \qquad \text{(AII.4)}$$

where $v_d(z)$ is the dry deposition velocity (m s^{-1}) at height z, $C_a(z)$ the average air concentration at height z [g m^{-3}] and C_s the average air concentration at the absorbing surface (soil, vegetation or water). C_s may be considered zero for substances, which immediately react at the surface with other substances, or for substances attached to particles. This is the case for most of the substances considered so far, but not for a group of persistent organic pollutants (POPs). It can be assumed that the initial dry deposition velocity for uncontaminated soil (C_s = 0) will be determined mainly by atmospheric resistances. This assumption leads to deposition velocities in the range of 0.005-0.02 m s^{-1}. Since many organics are not readily degraded in soil or vegetation, C_s will not remain zero and the corresponding dry deposition flux will decrease. If atmospheric concentrations drop to values lower than C_s, the corresponding deposition flux will become negative or in other words there will be a (re-) emission flux.

Flux of gaseous POPs across interfaces; re-emission

Fluxes to soils; air/soil exchange.
Mackay *et al*. (1992) give half-life times in soil for a range of POPs. For many POPs, half-life times are suggested in the order of months or longer. With such half-life times, the concentration in the upper soil layer will soon limit the dry deposition flux because the surface concentration C_s will soon approach C_a. In a steady state situation the time averaged total deposition flux becomes equal to the sum of degradation, uptake by plants and leaching to groundwater. In order to investigate the dynamics of the air-surface exchange of pollutants such as γ-HCH, a numerical one-dimensional model has been developed (Van Jaarsveld, 1996). This model called DEPASS (Dynamic Exchange of Pollutants between Atmosphere and Soil Surface) describes the vertical transport and diffusion in both soil and atmosphere and the exchange of pollutants between the compartments in dependence of actual meteorological conditions. Preliminary calculations reveal that (near) saturation of the upper layer will take place within days. The calculations also show a diurnal cycle of deposition and (re-) emissions, driven mainly by temperature and moist evaporation cycles.

In the current version of the OPS model it is not possible to calculate and maintain soil concentrations dynamically. The effect of saturation and the possible re-emission of previously deposited material is therefore taken into account by introducing an effective dry deposition velocity $v_d\ eff$ such that:

$$F_d = v_d(z)\,(\,C_a(z) - C_s\,) = v_d\ \ eff\ C_a(z) \qquad \text{(AII.5)}$$

It might be clear that such an approach is only valid for steady state situations or for calculating long-term average deposition fluxes. The effective dry deposition velocity is estimated from the DEPASS model results as:

$$v_d \ \ eff = \frac{(\ \overline{F_{net}} - \overline{F_w}\ )}{\overline{C_a(z)}} \qquad \text{(AII.6)}$$

where F_{net} is equal to the sum of the downward deposition fluxes minus the upward (emission) flux averaged over two years. The effective dry deposition velocity may even become negative if much of the wet deposited substance evaporates afterwards. According the calculations with DEPASS this is the case when the organic carbon fraction of the soil is low or if the organic carbon partition coefficient is low. For example, in the case of γ-HCH and an assumed organic carbon fraction in the topsoil of 0.7 % a net emission flux is calculated, and $v_d\ eff$ amounts to -8 x 10^{-4} m s^{-1}. If this fraction is taken at 2.5 %, then $v_d\ eff$ increases to 6 x 10^{-4} m s^{-1}. Calculated $v_d\ eff$ values are given in Table 2, all on the basis of an assumed organic carbon fraction of 2.3 %. In the present calculations the lower limit for $v_d\ eff$ is taken at zero. The effective dry deposition velocities given in Table 2 may be transformed into r_c values by using:

$$R_c = 1 / v_d\ eff - 40 \qquad (\text{s m}^{-1}) \qquad \text{(AII.7)}$$

where $v_d\ eff$ is m s^{-1}. Negative values of $v_d\ eff$ should be translated into a maximum R_c value (R_c = 99999). Although temporal deposition fluxes to vegetation may be quite different from that to soil it is assumed that the half-life of POPs in vegetation is of the same order as that in soil, and that most of the plant-accumulated POPs will finally reach the soil. Some experimental support for this assumption is given by Bacci *et al*. (1990). Their measurements of azalea leaf/air bioconcentration factors suggest that γ-HCH present in the biomass of the plants is comparable to the direct (wet) deposition load to the soil.

Table AII.2 Effective deposition and conversion properties used in a study of deposition of POPs and pesticides to the Netherlands and the North Sea (Baart et al., 1995)

Compound	$\phi^{\&}$	v_d eff soil[#]	v_d sea[$]	Degr. in air	W[#!]
		cm/s	cm/s	%/h	
1,1,1-trichlorethane	0.0001	0.0004	0.01	0.00092	2
2,4-D	10^{-5}	-0.005	0.37	0.71	$9.8x10^{3}$
atrazine	0.20	0.68	0.37	46	$1.9x10^{7}$
azinfos-methyl	0.25	0.046	0.39	69	$1.6x10^{6}$
bentazon	1.0	0.1	0.45	0.069	$1.1x10^{12}$
dichlorvos	10^{-6}	0.043	0.36	0.66	$2.8x10^{4}$
diuron	0.05	0.52	0.45	17	$4.4x10^{6}$
Endosulfan	0.01	0.042	0.40	1.6	$1.7x10^{4}$
fentin-hydroxide	0.18	0.22	0.40	0.50	$3.1x10^{5}$
MCPP	0.05	0.85	0.51	1.25	$7.0x10^{7}$
Mevinfos	0.0006	0.97	0.54	0.45	$1.6x10^{10}$
Lindane	0.0036	0.026	0.19	0.034	$4.2x10^{4}$
parathion-ethyl	0.018	0.51	0.51	9.9	$4.4x10^{5}$
Pentachlorophenol	0.0055	0.49	0.45	0.05	$1.2x10^{5}$
Simazine	0.51	0.45	0.47	0.046	$1.6x10^{7}$
Trifluralin	0.0018	-0.0036	0.32	0.67	$1.3x10^{3}$
PCBs (as PCB52)	0.0055	-0.0017	0.07	0.041	113
Fluoranthene	0.0013	0.11	0.43	0.43	5200
Anthracene	0.00014	0.016	0.36	1.25	1400
B(a)P	0.313	-0.18	0.45	0.4	$1.2x10^{5}$
B(a)A	0.018	0.41	0.47	0.41	$9.4x10^{3}$
B(b)F	0.313	-0.000015	0.45	1.25	$1.0x10^{5}$
B(ghi)P	0.30	0.68	0.45	1.25	$7.3x10^{4}$
B(k)F	0.67	0.38	0.45	0.41	$3.4x10^{5}$
Chrysene	0.087	-0.28	0.42	0.41	$8.4x10^{4}$
Phenantrene	0.0001	0.024	0.38	1.25	1700
indeno(123)pyrene	1.0	0.10	0.45	0.41	$3.7x10^{5}$
Naphtalene	0.0000003	0.0006	0.14	4.1	125

[&] time-averaged solid fraction calculated with the model of Junge (1977)
[#] calculated with the DEPASS model (Van Jaarsveld, 1996)
[&] time-averaged values for the gas-phase fraction, calculated with the model of Liss and Slater (1974)
[!] time and air concentration weighted scavenging ratio based on Henry Constant

Dry deposition of particles
For pollutants in particle phase, the removal rates can be described as a function of the physical parameters of the (carrier) particle, of which particle size is the most important. Small particles tend to behave like gases with the deposition velocity depending on the Schmidt number of the particles (Slinn and Slinn, 1980). Large particles (>2 μm) are efficiently removed from the atmosphere by sedimentation under the influence of gravity. Inertial impaction is of importance for particles with a diameter of between 0.1 and 10 μm. This process is highly dependent on the velocity of the air and the intensity of turbulence in combination with the presence of roughness elements.

Since the lifetime of atmospheric particles is a function of particle size, it is important to know the sizes of the particles as they leave the stack and to take into account the evolution of the distribution. The latter holds especially for substances which are in particle phase at higher temperatures such as heavy metals and some PAHs. It is less important for substances that attach only temporarily to particles during their atmospheric cycle, because these substances distribute over 'aged' atmospheric particles proportional to the surface area of the particles and therefore preferentially adhere to smaller particles.

In the OPS model particles are distributed over 5 size classes, each having a specific particle diameter and specific deposition properties. The dry deposition parameters are taken from the model of Williams (1982) for water surfaces and the model of Sehmel & Hodgson (1980) for land surfaces. The particle-size classes and corresponding (average) deposition parameters are given in Table 1.

Table AII.3. Properties of the particle size classes with respect to dry and wet deposition. Dry deposition velocities are representative for land surfaces with a roughness length of 0.15 m.

Size class	Median aerodyn. diam.	Iinitial mass distributions used		Scavenging ratio W [a]	Mean scavenging rate Λ_{eff}	Mean dry dep. velocity v_d [b]
		I [c]	II [d]			
μm	μm	%	%		s^{-1}	$m\ s^{-1}$
< 0.95	0.2	70	42	1.2×10^5	2.0×10^{-6}	0.00065
0.95 - 4	1.5	20	33	10^6	1.5×10^{-5}	0.0025
4 - 10	6	5	14	10^6	1.5×10^{-5}	0.0071
10 - 20	14	3	6	10^6	1.5×10^{-5}	0.0132
> 20	40	2	5	10^6	1.5×10^{-5}	0.067

[a] scavenging ratio during precipitation
[b] dry deposition velocity for z = 50 m
[c] size distribution used in the calculations for semi-volatile POPs except PAHs
[d] size distribution used in the calculations for metals and PAHs

Water surfaces
An often used approach to the quantification of fluxes across the air-sea interface is the two-layer model of Liss and Slater (1974). In this model the main body of each fluid is assumed to be well-mixed, the main resistance to gas transport coming from the gas and liquid phase interfacial layers, across which the exchanging gases transfer by molecular processes. For gases that obey Henry's law the exchange flux in a steady state situation is given by:

$$F_d = K_a \left(C_a - \frac{H}{RT} C_l \right) \qquad \text{(AII.8)}$$

where

$$\frac{1}{K_a} = \frac{1}{k_a} + \frac{H}{RT}\frac{1}{k_l} \qquad \text{(AII.9)}$$

k_a and k_l are the exchange constants for the gas and the liquid phases, respectively, and c_l the concentration in the liquid phase. The authors of this model indicate k_a = 0.83 cm s_{-1} for water vapour and $k_l = 5.5 \times 10^{-3}$ cm s^{-1} for CO_2. Moreover, they suggest that other gases can be calculated by correcting the given exchange rates with the ratio of the square roots of the molecular weights of the gases.
Although the two-layer model basically contains no resistance for transport in the turbulent layer, the model can be made equivalent to the resistance model given in Equation (AI.7) by equating:

$$K_a = v_d\,; \qquad k_a = \frac{1}{R_a + R_b}\,; \qquad k_l = \frac{1}{R_c}\,\frac{H}{R\ T} \qquad \text{(AII.10)}$$

The practical solution in the OPS model is to use the standard resistance model on the basis of roughness characteristics of the water surface and to estimate R_c from the Liss and Slater model.

For most of the gaseous substances the relatively high water solubility and the relatively rapid mixing in surface waters will lead to negligible resistances in water layers compared to resistances in the atmosphere. For these substances the concentration-weighted yearly average dry deposition velocities are of the order of 0.004 m s^{-1}.

References Appendix II

Atkinson R. (1986) Kinetics and mechanisms of the gas-phase reactions of the hydroxyl radical with organic compounds under atmospheric conditions. Chemical Reviews **86**, 69-202.

Atkinson R. (1987) Estimation of OH radical reaction rate constants and atmospheric lifetimes for polychlorobifenyls, dibenzo-p-dioxins and dibenzofurans. Environmental Science and Technology **21**, 305-307.

Atkinson R. Aschman S.M. and Pitts jr. J.N. (1984) Kinetics of reactions of naphtalene and biphenyl with OH radicals with O3 a4 294 K. Environmental Science and Technology **18**, 110-113.

Baart A.C. Berdowski J.J.M. and van Jaarsveld J.A. (1995) Calculation of atmospheric deposition of contaminants on the North Sea. TNO report TNO-MEP-R95/138.

Bacci E., Cerejeira M. J. Gaggi C. Chemello G., Calamari D. and Vighi M. (1990) Bioconcentration of organic chemical vapours in plant leaves: The Azalea model. *Chemosphere* **21**, 525-535.

Eisenreich, S.J., Looney, B.B. and Thornton, J.D. (1981) Airborne organic contaminants in the Great Lakes ecosystem. *Envir. Sci. Technol.*, **15**, 30-38.

EMEP (2000) Heavy metal transboundary pollution in Europe: Monitoring and Modelling results for 1997 and 1998. EMEP Report 3/2000 MSC_E Moscow and CCC Kjeller, Norway.

Janssen A.J. and Brink H.M. ten (1985) De samenstelling van neerslag onder een rookgaspluim: modellering, berekening en validatie (in Dutch) . Netherlands Energy Research Foundation, Petten, the Netherlands. Report ECN-170.

Junge C. E. (1977) Basic considerations about trace constituents in the atmosphere is related to the fate of global pollutants. In: *Fate of pollutants in the air and water environment*. Part I, I.H. Suffet (ed.) (Advances in environmental science and technology, Vol. 8), Wiley-Interscience, New York.

Mackay D., Paterson S., Schroeder W.H. (1986) Model describing the rates of transfer processes of organic chemicals between atmosphere and water. *Envir. Sci. Technol.*, **20**, 810-816.

Mackay D., Shiu W. Y. and Ma K. C. (1992) Illustrated handbook of physical-chemical properties and environmental fate for chemicals. Volumes I, II and III, Lewis Publishers, Chelsea, Michigan, USA

Liss P. S. and Slater P. G. (1974) Fluxes of gases across the air-sea interface. *Nature* **247**, 181.

Petersen G. (1992) Belastung von Nord- und Ostsee durch ökologisch gefährliche Stoffe am Beispiel atmosphärischer Quecksilberverbindungen. GKSS-Forschungszentrum Geesthacht GMBH.

Ryaboshapko A. and Korolev V. (1997) Mercury in the atmosphere: estimates of model parameters. EMEP/MSC-E Report 7/97, Moscow, 60p.

Sehmel G. A. and Hodgson W. J. (1979) A model for predicting dry deposition of particles and gases to environmental surfaces. *A. I. Ch. E. Symposium Series* **76**, 196.

Slinn S. A. and Slinn W. G. N. (1980) Predictions for particle deposition on natural waters. *Atmospheric Environment* **16**, 1785-1794.

Van Jaarsveld J.A. and Onderdelinden D. (1986) Modelmatige beschrijving van concentratie en depositie van kolenrelevante componenten in Nederland, veroorzaakt door emissies in Europa (in Dutch). RIVM, Bilthoven, the Netherlands. Report no. 228202002.

Van Jaarsveld J.A. (1989) Berekening van concentraties in de Nederlandse buitenlucht met behulp van het OPS-model; Benzeen en Tolueen (in Dutch). RIVM report 228475010.

Van Jaarsveld J.A. (1996) The dynamic exchange of pollutants at the air-soil interface and its impact on long range transport In*: Air Pollution Modeling and its application XI,* edited by Sven-Erik Gryning and Francis Schiermayer.

Whitby K. T., (1978) The physical characteristics of sulphur aerosols. *Atmospheric Environment* **12**, 135-159.

Williams R. M. (1982) A model for the dry deposition of particles to natural water surfaces. *Atmospheric Environment* **16**, 1933-1938.

Appendix III SO_2, NO_x and NH_3 emission data

This appendix specifies the emission data as used for the calculation of acidifying deposition in the Netherlands. The same data is used for the model validation exercise as described in Chapter 8. It is usual to separate emissions into national emissions and foreign emissions. Due to the nature of the OPS model, the impact of remote sources can be calculated with spatially less detailed emission data. Also source properties such as stack height are less critical for remote emissions.

The emission data files consist of a combination of specific point sources and diffuse sources. The latter are usually distributed according to general information such as population density, traffic density and agricultural land use. By relating emissions to human activities it is also logical to harmonise the source characteristics for these emissions between pollutants. The standardised properties of some diffuse emission sectors is given in Table AIII.1. Actual ranges of properties are also given in Tables AIII.2-AIII.7

Table AIII.1 Source properties of some emission sectors

Emission sector	Source height	Std. dev. of source heights	Heat content	Diurnal variation code
	m	m	MW	
Mobile sources	2.5[#]	2.5[#]	0	3
Sea-going ships	15	7.5	6	3
Inland shipping	4	2	0.5	3
Pleasure cruising	1	0.5	0	3
Domestic heating	10	5	0	2
Animal housing systems (NH_3 only)	5	2.5	0	*
Manure application (NH_3 only)	0.5	0.3	0	[$]

[#] This includes the initial mixing due to speed induced turbulence
*: emission variation for animal housing systems, see section 6.4.2;
[$]: emission variation for land spreading, see section 6.4.1

The format of the emission data files is given in section 7.4.2.

NO_x emissions

Table AIII.2. NO_x emissions and source characteristics for the Netherlands. Data from the 1995 base emission file

		Emissions		Number of sources		Heat content		Source height		St. dev. of source heights	Diurnal variation code[1])	Grid size
code	Category	Point sources	Gridded sources	Point sources	Gridded sources	Point sources	Gridded sources	Point sources	Gridded sources	Gridded sources	All emissions	Gridded sources
		tonnes/a	tonnes/a			MW	MW	m	m	m		m
110	Food beverages and tobacco	4038	3045	300	1021	0-17.5	1	5-100	30	0	1	5000
120	Oil refineries	17535	798	118	8	0-53.4	0	3-213	3	0	1	5000
130	Chemical ind	27084	717	374	360	0-60.1	1	3-175	30	0	1	5000
140	Building materials, ceramics and glass industry	5605	3703	108	187	0-9	1.24	8-100	31.7	0	1	5000
150	Iron and steel industry	9656	167	102	157	0-21	0.72	3-100	28.2	0	1	5000
160	Cement industry	1321	0	5	0	0.4-8.6		16-66			1	5000
170	Metallurgical ind.	648	2490	97	1003	0-4.7	0-0.36	3-50	5-14.1	0	1	5000
180	Other industry	2685	1197	151	1396	0-28.2	0-1.49	5-62	5-31.1	0	1	5000
210	Energy: power plants.	54527	2954	239	1602	0-146	0	3-175	3	0	1	5000
220	Energy: diffuse sources (incl. dom. heating)	0	23321	0	1601		0		10	6.7	2	5000
310	Traffic: cars	0	113072	0	1618		0		2.5	2.5	3	5000
320	Traffic: light duty vehicles	0	14235	0	1618		0		2.5	2.5	3	5000
330	Traffic heavy duty vehicles	0	85205	0	1618		0		2.5	2.5	3	5000
340	Traffic: coaches	0	9096	0	1618		0		2.5	2.5	3	5000
370	Rail transport	0	1638	0	545		0		2.5	2.5	3	5000
390	Aircraft	1268	1350	148	1		0	15	457	457	3	7500
430	Agriculture: mobile sources		42175	0	1609		0		2	2	3	5000
460	Agriculture: other sources	0	10281	0	1665		0.05		10	5	2	5000
510	Waste burning	2632	332	31	1601	0-27.7	0	6-110	3	0	1	5000
610	Trade (non-)commercial serv.	0	84	0	1601		0		3	0	0	5000
710	Building industry	4	522	3	1601	0-1.3	0.1	16-35	3.2	2.5	0	5000
810	Consumers (excl. dom. Heating)	0	84	0	1601		0		3	0	0	5000
386	*Inland shipping*	*0*	*32652*	*0*	*4816*		*0.5*		*4*	*2*	*3*	*1000*
387	*Sea-going ships*	*0*	*20749*	*0*	*2863*		*6*		*15*	*7.5*	*1*	*1000*
388	*Pleasure shipping*	*0*	*1320*	*0*	*1459*		*0*		*1*	*0.5*	*3*	*5000*
	Total	127003	364341	1676	31191							

[1]) diurnal variation code: 0 = no variation; 1 = industrial 2 = space heating; 3 = traffic. See chapter 5.1.1 and 7.4.3 for specifications

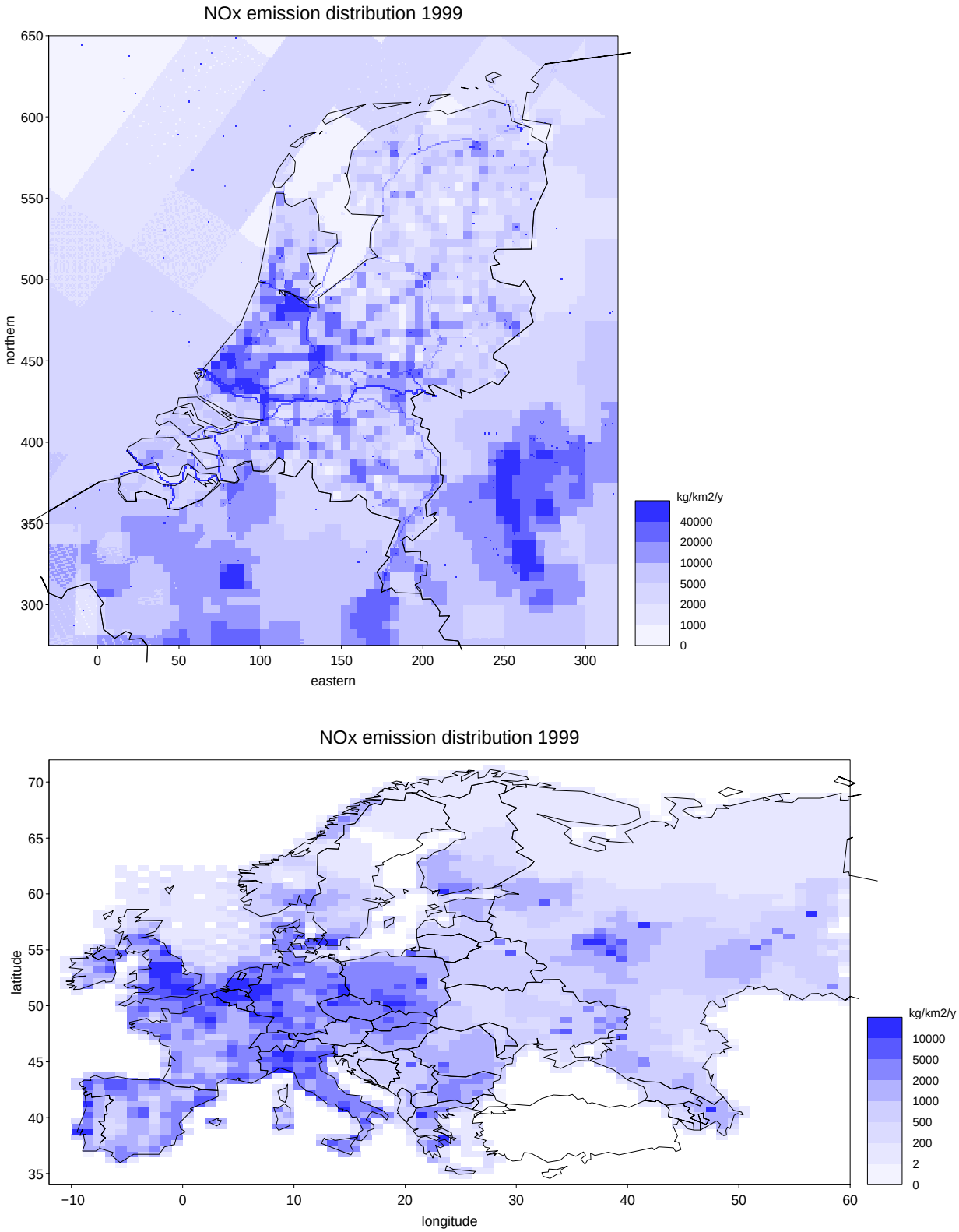

Figure AIII.1 Distribution of NO_x emissions in the Netherlands and Europe.

Other European NO_x emissions

Table AIII.3. Foreign NO_x emissions 1999 as applied to the Environmental Balance 2001 (RIVM, 2001)

			Distribution over sectors*)				
area code	name	Emission (as NO_2) tonnes a^{-1}	100 %	101 %	102 %	104 %	105 %
1	FRG (former)	1420440	21.9	0.8	4.2	65.5	7.6
2	France	1652000	12.67	0.73	4.45	77.2	4.95
3	Italy	1685000	26.44	1.4	6.48	62.98	2.7
4	Netherlands	-	-	-	-	-	-
5	Belgium	301000	29.74	2.28	6.72	56.3	4.96
6	Luxembourg	17000	11.68	0	31.58	52.09	4.65
7	UK	1753000	36.91	2.1	0.4	55.99	4.6
8	Ireland	122000	43.75	0.27	3.42	45.75	6.81
9	Denmark	231000	43.81	0.44	1.28	52.42	2.05
10	Iceland	0	0	0	0	0	0
11	Greece	382000	30.84	1.55	11.75	54.79	1.07
12	Spain	1194000	24.67	1.78	9.24	62.4	1.9
13	Portugal	374000	24.22	0.55	3	70.71	1.52
14	Norway	224000	17.99	0.52	3.94	76.34	1.21
15	Sweden	257000	9.13	0.58	3.05	85.2	2.04
16	Finland	252000	23.09	3.08	6.62	61.65	5.56
17	Russian Fed.	2488000	15	3	5	39	38
18	Estonia	46000	0	0	3	53	44
19	Latvia	42000	0	4	16.99	40	39.01
20	Lithuania	60000	0	1	15.99	41	42
21	Byelorussia	164000	16	3	0	41	40
22	Poland	991000	46.56	0.41	3.91	37.53	11.59
23	Czechoslovakia	543000	57.91	0.95	2.72	26.72	11.7
24	Austria	169000	15.77	3.07	4.85	65.21	11.1
25	Switzerland	123000	8.65	0.91	5	75.54	9.9
26	Liechtenstein	0	0	0	0	0	0
27	Hungary	217000	18.91	0.65	6.86	51.5	22.09
28	Ukraine	455000	22	1	4	37	36
29	Moldavia	21000	29.97	0	1	36.01	33.02
30	Romania	319000	51.28	2.07	9.51	34.55	2.59
31	Bulgaria	223000	44.97	1.54	6.76	43.49	3.24
32	Yugoslavia	212000	46.79	1.04	2.29	48.22	1.66
36	Armenia	10000	0	0	3	49.01	47.99
38	Georgia	54000	0	1	4	48	47
39	Albania	30000	28.21	2.56	0	66.67	2.56
41	Azerbaydzhan	181864	42.66	0.7	2	48.73	5.91
42	GDR (former)	359560	41.88	0.7	1.9	47.82	7.7
	North Sea	647943				100	

*) 100: power plants
101: comb. in processes and industry
102: processes in industry
104: transport
105: domestic comb. and comb. in trade

SO_2 emissions

Table AIII.4 SO_2 emissions and source properties for the Netherlands. Data from the 1995 base emission set.

		Emissions		Number of sources		Heat content		Source height		St. dev. of source heights	Diurnal variation code[1])	Grid size
Code	Category	Point sources	Gridded sources	Point sources	Gridded sources	Point sources	Gridded sources	Point sources	Gridded sources	Gridded sources	All emissions	Gridded sources
		tonnes/a	tonnes/a			MW	MW	m	m	m		m
110	Food beverages and tobacco	617	580	30	1021	0-6.5	1	5-75	30	0	1	5000
120	Oil refineries	61324	64	116	8	0-53.4	0	3-213	3	0	1	5000
130	Chemical industry	10922	290	90	360	0-60.1	1	3-160	30	0	1	5000
140	Building materials, ceramics and glass industry	3538	1083	85	187	0-9	1.24	8-100	31.7	0	1	5000
150	Iron and steel industry	11928	291	48	157	0-21	0.72	3-100	28.2	0	1	5000
160	Cement industry	262	0	2	0	1.5-1.6		16-66			1	5000
170	Metallurgical ind.	356	1795	16	1003	0-0.95	0-0.36	3-50	5-14.1	0	1	5000
180	Other industry	112	75	15	1396	0-1.5	0-1.49	6-62	5-31.1	0	1	5000
210	Energy: power plants.	16481	63	92	1602	0-100	0	3-175	3	0	1	5000
220	Energy: diffuse sources (incl. dom. heating)	0	741	0	1601		0		10	6.7	2	5000
310	Traffic: cars	0	4792	0	1618		0		2.5	2.5	3	5000
320	Traffic: light duty vehicles	0	2303	0	1618		0		2.5	2.5	3	5000
330	Traffic heavy duty vehicles	0	6170	0	1618		0		2.5	2.5	3	5000
340	Traffic: coaches	0	549	0	1618		0		2.5	2.5	3	5000
370	Rail transport	0	99	0	545		0		2.5	2.5	3	5000
390	Traffic: other	0	2616	0	1684		0		2.5	2.5	3	5000
460	Agriculture	0	281	0	1665		0.05		10	5	2	5000
510	Waste burning	519	23	29	1601	0-27.7	0	6-110	3	0	1	5000
610	Trade (non-)commercial serv.	254	3584	25	1608	0.74	0	3-59	3	5.5	1	5000
710	Building industry	2	688	1	1601	0	0.1	16	4.5	2.5	0	5000
810	Consumers (ex. dom. heating)	0	16	0	1601		0	0	3	0	0	5000
386	*Inland shipping*	*0*	*1881*	*0*	*4816*		*0.5*		*4*	*2*	*3*	*1000*
387	*Sea- going ships*	*0*	*12498*	*0*	*2863*		*6*		*15*	*7.5*	*1*	*1000*
388	*Pleasure shipping*	*0*	*73*	*0*	*1459*		*0*		*3*	*0.5*	*3*	*5000*
	Total	106313	40554	549	33250							

1) diurnal variation code: 0 = no variation; 1 = industrial 2 = space heating; 3 = traffic. See chapter 5.1.1 and 7.4.3 for specifications

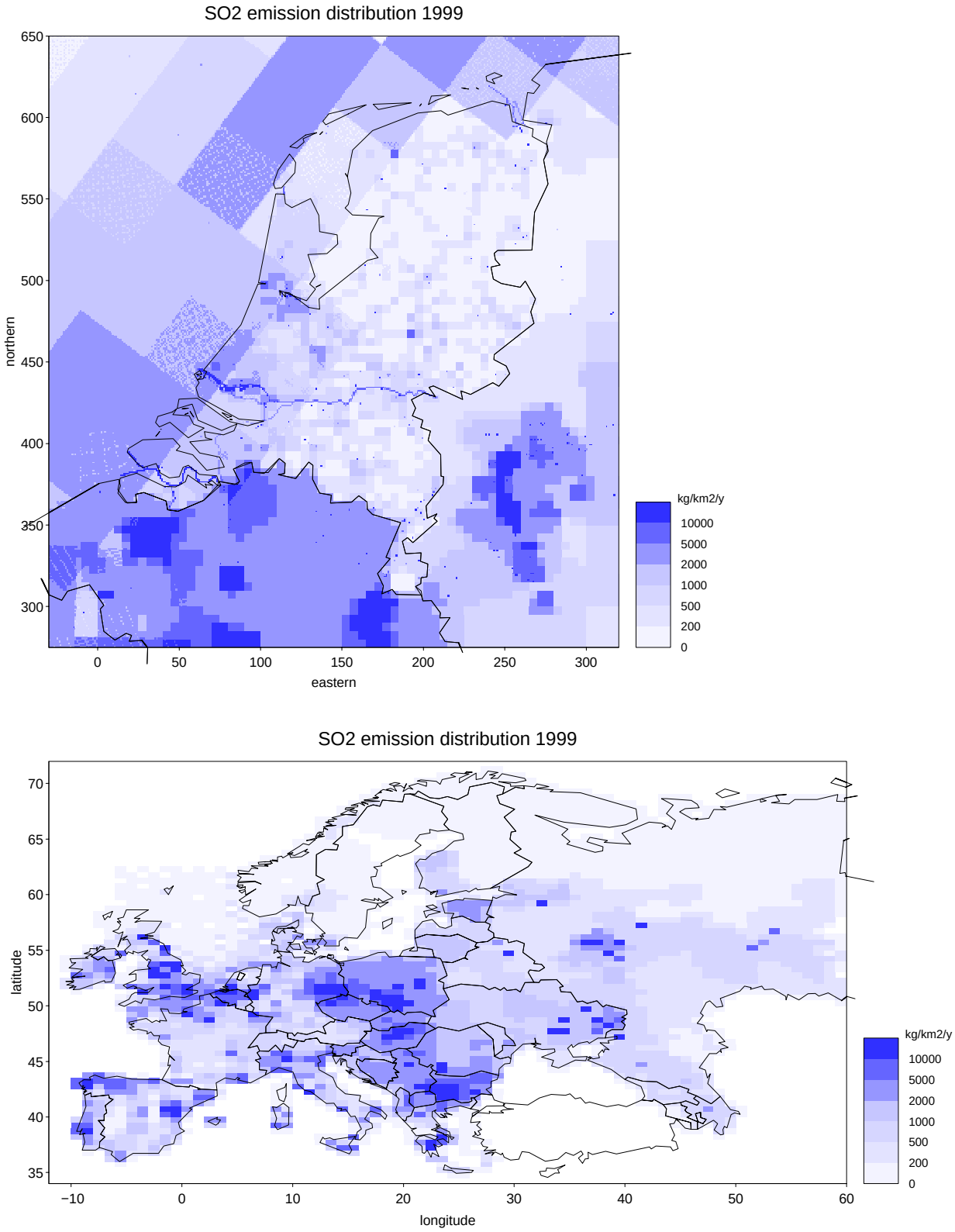

Figure AIII.2 Distribution of SO_2 emissions in the Netherlands and Europe.

Other European SO_2 emissions

Table AIII.5 Foreign SO_2 emissions 1999 as applied for the Environmental Balance 2001, (RIVM, 2001).

			Distribution over sectors*)				
Country code	Name	Emission (as SO_2) tonnes a^{-1}	100 %	101 %	102 %	104 %	105 %
1	FRG (former)	359180	51.8	8.6	8.9	9.1	21.6
2	France	837000	49.62	12.85	6	16.93	14.59
3	Italy	1021000	73.75	6.66	5.89	8.77	4.94
4	Netherlands	-	-	-	-	-	-
5	Belgium	203000	57.7	12.5	12.06	5.71	12.02
6	Luxembourg	4000	32.79	0	52.37	5.47	9.38
7	UK	1616615	79.72	8.69	2.1	4.1	5.39
8	Ireland	176000	76.08	0.24	0.66	5.02	18
9	Denmark	77000	84.43	0.93	3.69	6.19	4.77
10	Iceland	0	0	0	0	0	0
11	Greece	540000	61.42	5.5	3.51	8.8	20.77
12	Spain	1498000	78.12	7.37	4.81	5.97	3.73
13	Portugal	334000	78.97	4.07	7.4	7.72	1.84
14	Norway	30000	35.9	5.27	39.27	14.89	4.67
15	Sweden	49000	44.81	4.09	22.6	19.42	9.08
16	Finland	90000	32.77	27.4	29.35	4.16	6.33
17	Russian Fed.	2208000	32	6	3	1	58
18	Estonia	110000	0	0	9	1	90
19	Latvia	40000	0	11	1	1	87
20	Lithuania	94000	0	4	5	1	90
21	Byelorussia	190000	46	6	0	0	48
22	Poland	1897000	66.96	0.93	2.76	1.83	27.52
23	Czechoslovakia	622000	73.26	1.16	1.24	0.43	23.91
24	Austria	46006	20.39	29.16	4.2	14.87	31.37
25	Switzerland	27000	19.43	18.6	10.01	8.5	43.46
26	Liechtenstein	0	0	0	0	0	0
27	Hungary	591000	41.59	0.86	1.16	1.56	54.83
28	Ukraine	1132000	36	3	2	1	58
29	Moldavia	32000	40	0	1	1	58
30	Romania	912000	84.67	4.12	4.37	3.24	3.6
31	Bulgaria	1251000	84.23	2.44	1.45	1.53	10.35
32	Yugoslavia	1230000	90.5	1.92	1.52	1.52	4.55
36	Armenia	3000	0	0	1	2	97
38	Georgia	33000	0	2	3	1	94.01
39	Albania	120000	75.97	7.15	0.8	2.68	13.4
41	Azerbaydzhan	83054	12.99	7.99	2	1	76.02
42	GDR (former)	931887	86.07	1.14	0.42	0.33	12.04
	North Sea	454000				100	

*) 100: power plants
101: comb. in processes and industry
102: processes in industry
104: transport
105: domestic comb. and comb. in trade

NH_3 emissions

Table AIII.6 Agricultural 1999 NH_3 emissions and source properties for the Netherlands

Code	Category	Emission	Number of sources	Heat content	Mean source height	St.dev. source heights	Emission time-variation[1])	Grid size
		t a^{-1}		MW	m	m		m
111	Animal housing: cattle	42509	14052	0	5	2.5	4	500
112	Animal housing: other	32711	34279	0	5	2.5	4	500
12	Storage of manure	4018	36898	0	5	2.5	4	500
13	Grazing	11256	116130	0	0.5	0.2	5	500
141	Manure applic. on grass land	19544	116132	0	0.5	0.2	5	500
142	Manure applic. on arable land	30985	100562	0	0.5	0.2	5	500
143	Fertiliser use on grassland	8595	116132	0	0.5	0.2	5	500
144	Fertiliser use on arable land	3483	100574	0	0.5	0.2	5	500
	Total	153101	634759					

[1]) 4: emission variation for animal housing systems, see chapter 6.4.2; 5: emission variation for land spreading, see chapter 6.4.1

Table AIII.7. Non-agricultural 1999 NH_3 emissions and source properties for the Netherlands

Code	Category	Emission		Number of sources		Heat content		Source height		St.dev. source height	Diurnal variation [#]	Grid size
		Point sources	Gridded sources	Point sources	Gridded sources	Point sources	Gridded sources	Point sources	Gridded sources	Gridded sources	All emissions	Gridded sources
		t a^{-1}	t a^{-1}			MW	MW	m	m	m		m
110	Food beverages and tobacco	250	2	16	1021	0-3	1	3-49	30	0	1	5000
120	Oil refineries	8		1	0	1.1		44		0	1	5000
130	Chemical ind	2989	119	78	360	0-12	1	3-175	30	0	1	5000
140	Building materials, ceramics and glass industry	567	27	8	187	0.36-1.6	1.24	11-100	31.7	0	1	5000
150	Iron and steel industry	140	2	20	157	0-4.6	0.72	4-39	28.2	0	1	5000
170	Metallurgical ind.	25	126	8	847	0-0.95	0.36	5.5-50	14.1	0	1	5000
180	Other ind.	46	35	7	971	0-4.8	0-1.49	4-30	5-31.1	0	1	5000
300	Mobile sources		2612	0	1618		0		2.5	2.5	3	5000
510	Waste burning	38		3	0	0		3-4		0	1	5000
610[$]	Trade (non-)commercial serv.	13	528	53	1791	0-0.95	0	3-59	3-35	0	0	5000
710[$]	Building industry	1	154	3	1601	0-1.3	0.1	16-35	3.2	2.5	0	5000
810	Consumers		7218	0	1601		0		3	0	0	5000
	Total	4077	10823	197	10154							

[#] diurnal variation code: 0 = no variation; 1 = industrial 2 = space heating; 3 = traffic
[$] spatial distribution taken from NO_x distribution for mobile sources

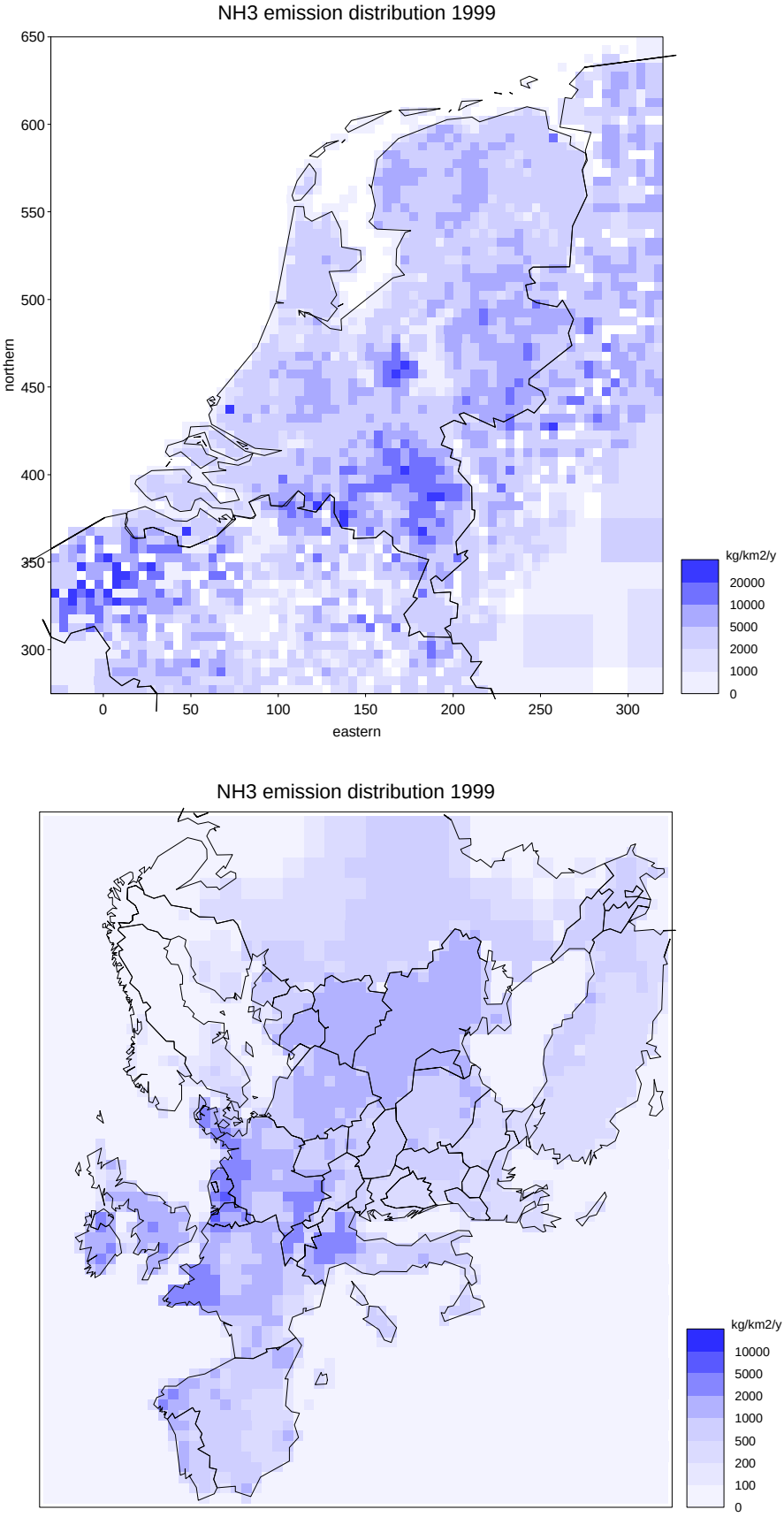

Figure AIII.3 Distribution of NH3 emissions in the Netherlands and Europe

Other European NH_3 emissions

Table AIII.8 European NH_3 emissions 1999 as applied to the Environmental Balance 2001 (RIVM, 2001). No sector split is made. Half of the emission is emitted at a level of 5m, representing emissions from animal housing systems. The other half is considered as manure-spreading emissions and emitted at 0.5 m height.

Area code	Area name	Emission
		t a^{-1}
1	Netherlands	-
2	FRG (former)	500000
3	Belgium	99000
4	France	827000
5	Luxembourg	7000
6	UK	350000
7	Denmark	104000
8	GDR (former)	125000
9	Poland	371000
10	Czechoslovakia (former)	114000
11	USSR (former)	3021267
12	Spain	517000
13	Ireland	127000
14	Sweden	59000
15	Italy	467000
16	Hungary	74000
17	Switzerland	70000
18	Austria	71000
19	Norway	27000
20	Finland	37000
21	Yugoslavia (former)	147077
22	Romania	221000
23	Portugal	97000
24	Bulgaria	66000
25	Greece	74000
26	Turkey	459088
27	Iceland	0
28	Albania	30978

References Appendix III

RIVM (2001) State of the Environment 2001 (in Dutch). Kluwer, Alphen aan den Rijn, the Netherlands.

Appendix IV Prescribed concentration levels

The OPS model cannot take changes in atmospheric composition on chemical reactions or deposition processes directly into account. However, if one can quantify the effect of changing precursor levels on the (bulk) reactions and translate this into simple functions of the absolute precursor levels then such functions can be used in models as OPS. The model then needs maps of precursor concentrations with sufficient spatial and temporal detail. One way to derive such simplified functions is to use a (complex) non-linear model to describe time series of concentration levels of the relevant compounds for a longer period and then fit a mathematical function to relevant model outputs.

For the modelling of transport and deposition of acidifying compounds, (existing) levels of SO_2, NO_2 and NH_3 have been found to be of great importance because of the chemical interactions. The most important is probably the role of NH_3 in the reduction of sulphuric acid to ammonia sulphates and nitric acid to ammonia nitrates. As such, the NH_3 is consumed, depending indirectly on levels of SO_2 and NO_2. A similar interrelation exists for the formation of secondary aerosols. If one considers the dramatic decrease of especially SO_2 in the past 20 years then it is likely to include these levels as input data to the OPS model.

Maps of existing concentration levels are preferably based on measurements; however, current networks are not dense enough to produce maps with sufficient detail. The method selected here is to use the OPS model on the basis of detailed emissions in the Netherlands and other European countries. The spatial detail of the emissions in the Netherlands is 5 x 5 km. Nevertheless, a map resolution of 10x10 km was thought to be sufficient for the present purposes. The resulting maps are given in Figure AIV.1-AIV.3. Because the geographical distribution of emissions does not change very much between years, only maps for 1984 and 1994 have been created. The 1984 map is taken as representative for the period up to 1990 and the 1994 map for 1990 and later years. NH_3 emissions have not changed much between 1984 and 1994 and also reliable measurements are not available for the pre 1993 period, therefore the NH_3 1994 concentration map has been assumed to be representative for all the years. NO_2 concentrations are calculated using a simple empirical relation between NO_x and NO_2 concentrations determined from LML observations. This relation is:

$$NO_2c = 8.6 \ln(NO_x c) - 12.4 \qquad \text{(AIV.1)}$$

where NO_2c and NO_xc concentrations are expressed in ppb. Equation (AIV.1) typically explains more than 90% of measured NO_2 concentrations.

In order to obtain realistic concentration levels, the model results are compared with measurements of the LML, and the average measurement/model ratio is used as a calibration factor for the whole map. The NH_3 calibration factor is taken from a model-measurement evaluation study carried out by Van Jaarsveld *et al*. (2000).

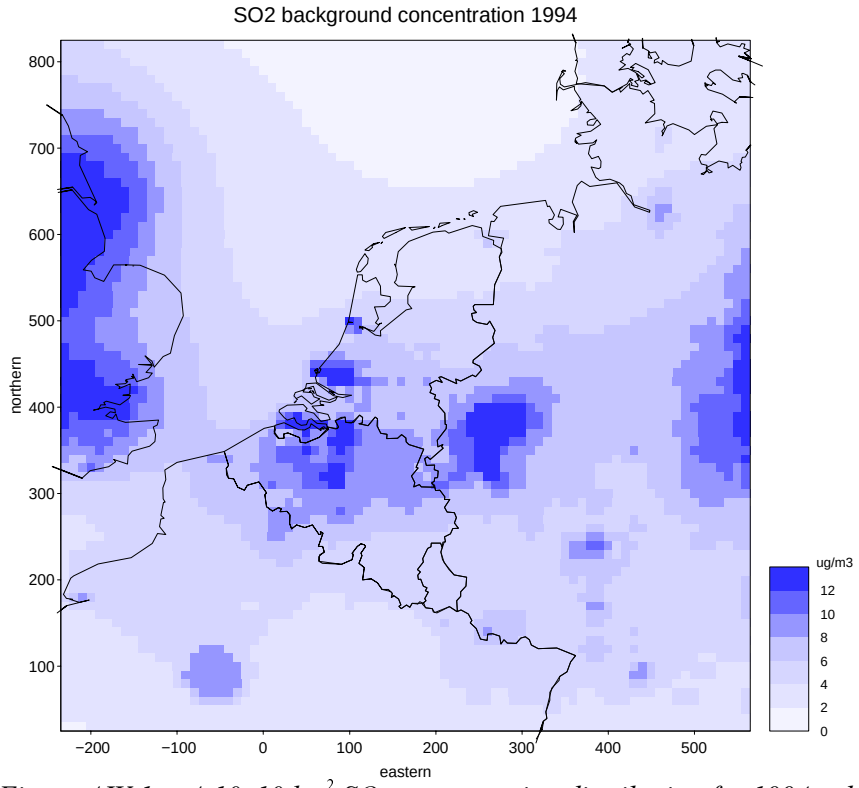

Figure AIV.1 A 10x10 km^2 SO_2 concentration distribution for 1994 calculated with the OPS model on the basis of European emissions (see Appendix III). Emission resolution in the Netherlands, Belgium and Germany: 5 x 5 km^2, other countries: 1^o longitude x 0.5^o latitude.

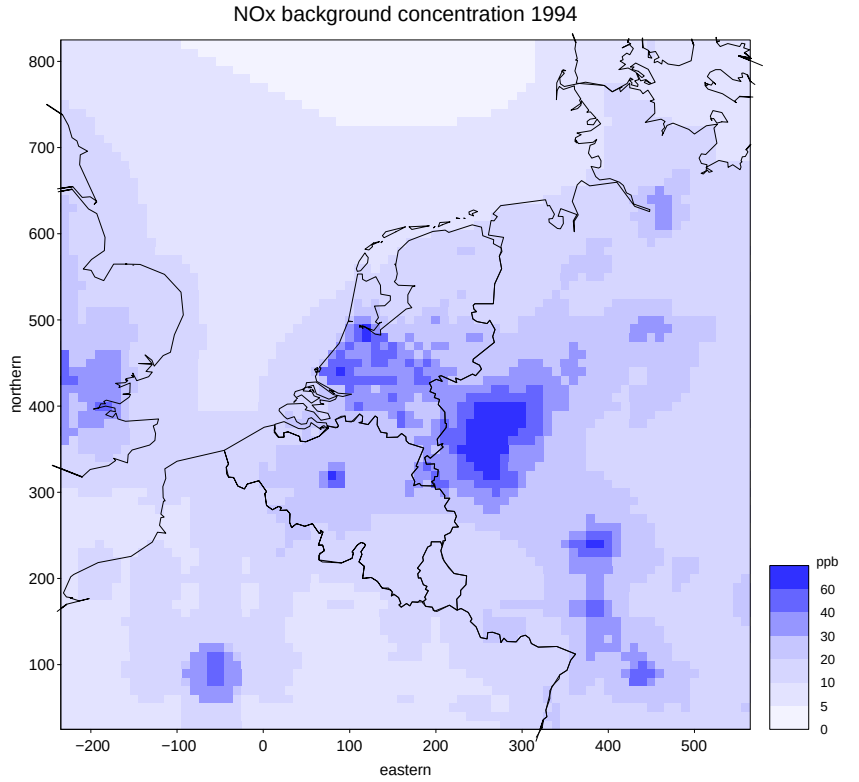

Figure AIV.2 NO_x concentration distribution for 1994; for further details see Figure AIV.1.

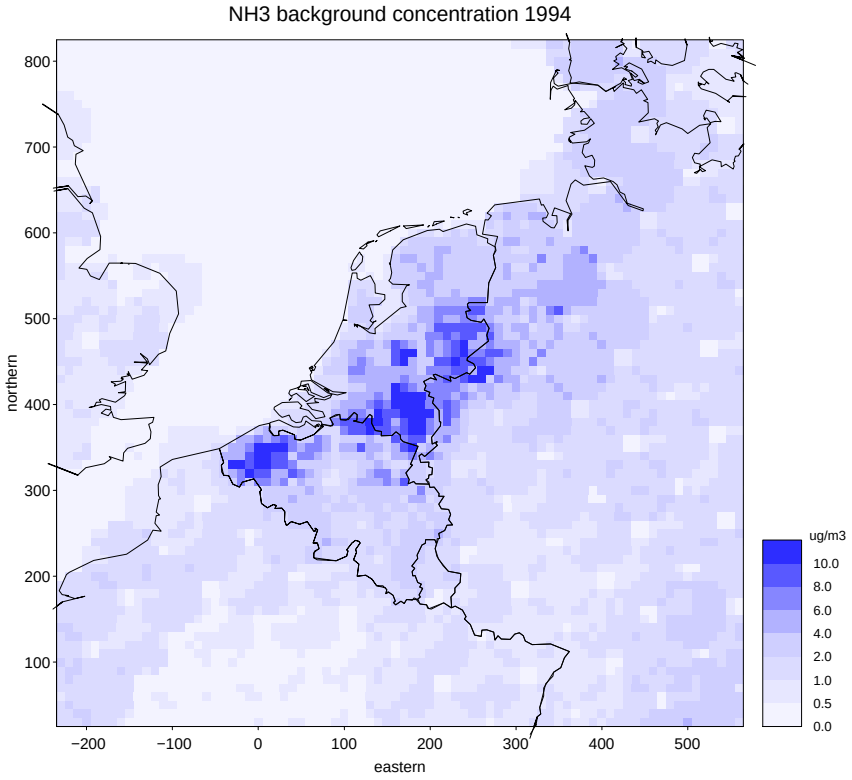

Figure AIV.3 NH_3 concentration distribution for 1994. For further details see Figure AIV.1.

NO_x and NO_2 results were within 15% of the measured concentrations in both 1984 and 1994. The application of a calibration factor was therefore not necessary. In the case of SO_2 the largest discrepancy with measurements was found for 1984: measured/modelled = 1.38. One must realise, however, that no detailed foreign emissions were available for the 1984 situation as they were for 1994. The SO_2 comparison results are plotted in Figure AIV.4. The applied calibration factors are given in Table AIV.1.

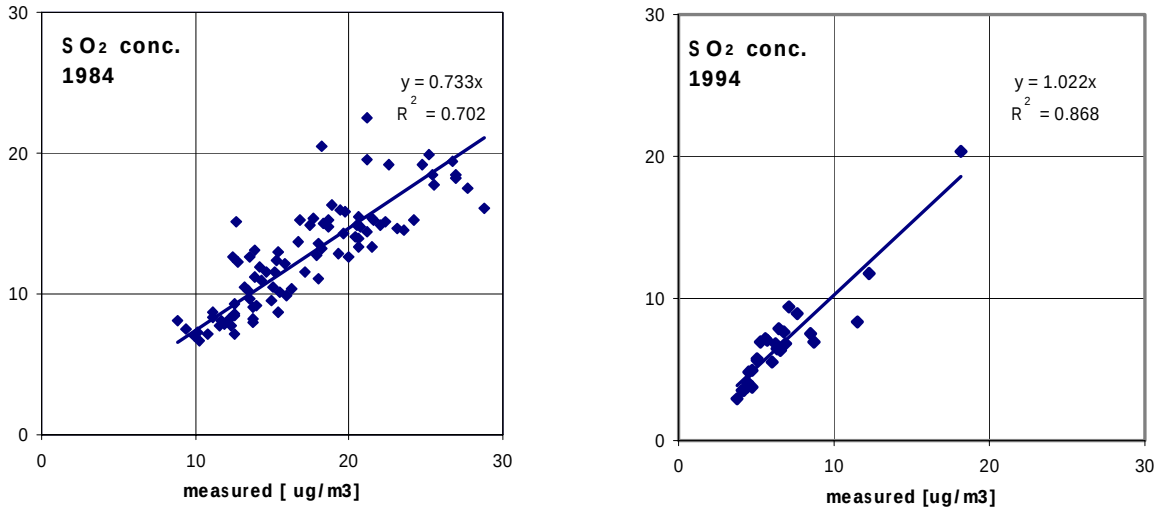

Figure AIV.4 Comparison of measured and modelled SO_2 concentrations for 1984 and 1994.

Table AIV.1 Calibration factors applied to the calculated concentration maps

	1984	1994
SO_2	1.38	1.01
NO_2	1.00	1.00
NH_3	-	1.28

For years other than 1984 and 1994 an inter- or extrapolation is applied on the basis of yearly average concentrations, as measured in the LML network. Figure AIV.5 gives the resulting average concentration levels for the Netherlands together with measured values. In the extrapolated values some smoothing has been applied and compared to the observations. This is done because extremes in year-to year concentrations are usually due to winter episodes, while we need in fact median-like concentration levels. AIV.5 clearly shows the dramatic decrease of SO_2 concentrations since 1979 (~factor 10), but NO_2 levels also decreased clearly since the mid-eighties. Figure AIV.5 also shows that the original assumption of non-changing NH_3 levels is no longer justified for the period after 1997. The selection of existing concentrations is coupled to the selected meteorological period. At present most data are available up to and including the year 2001. If long-term meteorology is chosen then the model assumes a future situation and background concentrations for a recent but fixed year are selected (i.e. 2000). A logical extension in this case is the introduction of future 'background' concentrations, but has not yet been realised.

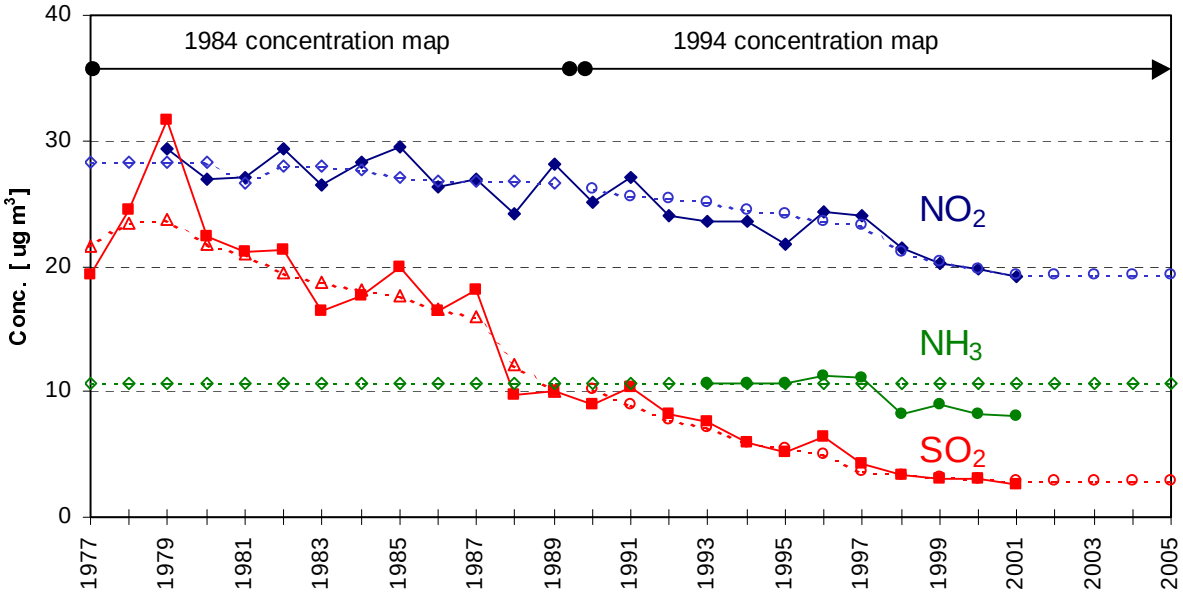

Figure AIV.5 Average concentrations of SO_2, NO_2 and NH_3, measured in the Netherlands (solid lines) and concentrations used as background concentrations in the OPS model (broken lines). The 1984 spatial distribution is used for the period up to 1990, while the 1994 distribution is used for later and future years.

References Appendix IV

Van Jaarsveld, J.A., Bleeker, A. and Hoogervorst, N.J.P. (2000) Evaluatie ammoniakredukties met behulp van metingen en modelberekeningen. RIVM, Bilthoven, the Netherlands. Report no. 722108025.